

**TOWARD CONTEXTUALIZING RECEPTOR-LIGAND
INTERACTIONS IN T CELLS AND MACROPHAGES**

A Dissertation
Presented to
The Academic Faculty

by

Nik Muaz Nik Rushdi

In Partial Fulfillment
of the Requirements for the Degree
Doctor of Philosophy in Biomedical Engineering

Georgia Institute of Technology
Emory University
Peking University

May 2019

Copyright © 2019 Nik Muaz Nik Rushdi

**TOWARD CONTEXTUALIZING RECEPTOR-LIGAND
INTERACTIONS IN T CELLS AND MACROPHAGES**

Approved by:

Dr. Cheng Zhu, Advisor

Department of Biomedical Engineering
Georgia Institute of Technology

Dr. Melissa Kemp

Department of Biomedical Engineering
Georgia Institute of Technology

Dr. Antony Chen, Co-advisor

Department of Biomedical Engineering
Peking University

Dr. Khalid Salaita

Department of Chemistry
Emory University

Dr. Lou Ann Brown

School of Medicine
Emory University

Date Approved: March 21 2019

To my parents, whose sacrifice and love served as inspiration,

ACKNOWLEDGEMENTS

The completion of this dissertation would not be possible without the generous guidance and support from many parties. I wish to thank my thesis committee first and foremost for taking the time and effort to provide me with profound feedback that was instrumental in formulating my projects. I would like to thank Dr. Khalid Salaita for his many collaborations with the Zhu Lab and introducing me to the world of tension probe reporters. The conversations I had with Dr. Salaita regarding molecular biophysics were formative in understanding the physical features of receptor-ligand interactions. From my first interactions with Dr. Salaita through thesis presentations and seminars, I was inspired by how poignant his questions were, which pushed me to improve the way I synthesized information. Interactions with students in his lab were intellectually stimulating and provided a comradery during my graduate tenure. In fact, for a period they were a source of entertaining speculation about the future of T cells and the broader world of immunology. The example is exemplified by their advisor Dr. Salaita, whose curiosity was contagious and a source of great motivation for my projects.

I would like to thank Dr. Melissa Kemp for her direct advice in my early reactive oxygen species work, and her consistent offering of wisdom and encouragement throughout my time at Georgia Tech. Due to my interest in ROS, my advisor Dr. Zhu and I had a meeting with Dr. Kemp and her former student. This meeting is one of my most vivid recollections of being thrilled to be in a research-oriented career. This is because, despite significant overlap in initial interests, the two groups worked together to develop a list of novel experiments, built upon extensive work by the Kemp lab, that harnessed

the strengths of both groups. The meeting taught me the many virtues of conducting collaborative projects and instilled in me excitement for fostering a scientific community. Every subsequent conversation I've had with Dr. Kemp has pushed me to build a comprehensive foundation in literature of the field I am studying which has enabled me to ask better questions and interpret my data in a much more nuanced manner than what I thought was possible from when I began my PhD.

I would like to thank Dr. Lou Ann Brown for introducing me to the vast world of ROS research, for consistently exciting me about any scientific finding, and for being a source of moral support and wisdom in pursuing a career in research. Through the countless times of stress, I would leave every meeting with Dr. Brown reenergized and ready to conduct more experiments. I cannot thank her enough for her kindness and generosity. The entire third aim of this thesis was offered by Dr. Brown as a project to pursue in the case other projects faced challenges. It was an honor and a comfort to work on a project that has established potential based on extensive and profound previous works by Dr. Brown. Both the second and third aims of this thesis have been greatly guided by Dr. Brown. The second aim began as a collaborative grant between the Zhu and Brown labs, which also gave me invaluable first-hand experience in preparing an NIH-type grant. These projects stemmed from my interest in studying asthma, a field of research Dr. Brown is well-versed in. It is without a doubt that the exclusively positive interactions I've had with Dr. Brown, and the knowledge I've gained from the projects she guided, currently drive me to pursue a career in asthma research.

I would like to thank Dr. Antony Chen, my co-advisor in the PKU joint PhD program for his generosity in taking me into his lab in Beijing. Dr. Chen was enthusiastic

about me pursuing international research from the start and generously provided to me all his well-designed resources to ensure a comfortable transition to conducting research in another country. He also went well out of his way to accommodate my limited language abilities and cultural differences during my transition- for example, he made sure I knew where I could find food and was a source of entertaining conversation which reminded me of home. I also would like to thank Dr. Chen for teaching me about super resolution microscopy experimentation and analysis. He allowed me to work with his students to get hand on experience in the imaging field which resulted in a few co-authored publications. Learning about molecular HIV research was particularly instructive in understanding how different fields of research can inform one another.

I would like to thank my PhD advisor, Dr. Cheng Zhu for consistently trusting me and encouraging me to pursue my interests from the first day I met him at graduate recruitment. The opportunities for intellectual growth provided by Dr. Zhu would take up the too many pages of this thesis, so I will highlight my most fond memories. During my first year, Dr. Zhu provided me the opportunity to have lunch with one of the foremost experts in T cell biology, Dr. Anton van der Merwe. This was an experience I could not have fathomed a year prior and it encouraged me to dig much deeper into the surrounding literature. In the same year, Dr. Zhu traveled near and far seeking a collaborator for me to undertake study of the role of T cell in asthma with. This led to several exploratory collaborations and eventually resulted in a successfully funded seed grant with Dr. Brown. Through this experience, I received lessons in writing grants from someone considered a legendary grant writer even by his colleges at Georgia Tech. Dr. Zhu also allowed me complete freedom to shape a scientific project from start to end which is my

most valuable lesson learned in graduate school. The next most valuable lesson I learned was from feedback Dr. Zhu provided about data. He always pushed the boundaries of what I thought was possible in interpreting and dissecting data, as well as what experiments to conduct next. I now perceive data in a way I couldn't imagine before starting my PhD. The same can be said for how I read articles which was previously a weakness for me. The way that Dr. Zhu remembers the most minute detail of a paper even from decades ago pushed me to greatly expand my reading, which has been instrumental in my intellectual growth. Overall, I am deeply honored and grateful for having had the opportunity to study under Dr. Zhu.

The day-to-day struggles of graduate school over the course of almost 6 years were made tolerable through the support of family and friends. I wish to thank my parents who have always been my most ardent supporters. My father always made me out to be smarter than I actually am and would be so enthusiastic about academia banter. Since he is a professor, it was fascinating and a refreshing to hear about the similar excitements and frustrations he experienced despite our fields being extremely unrelated. But perhaps the most valuable lesson I learned from my father through my graduate career was to listen. Both he and my mother would be so excited whenever we would chat on the phone, a thousand miles away, which gave me the comfort knowing that I always had the unconditional love and support to continue my PhD. My mother always made sure I was healthy and happy enough to continue my work. At the same time her positivity always gave me the courage to fight through tough times, and the conversations I had with her over the course of my graduate tenure gave me confidence in my own work. Whenever I would visit exhausted from research, the encouragement from my mother would

reenergize me for months to come. I wish to thank all my 6 siblings. Each one of you has provided me with countless words of encouragement and love which has propelled me forward over 6 years. I am inspired by every single one of you and the diverse professions you are all so passionate about.

I wish to thank my support network of friends in Atlanta and Minnesota. My mentors from Minnesota, James Faghmous and Muneer Karcher-Ramos, played an instrumental role in me getting admitted into graduate school. James introduced me to many aspects of conducting research through his PhD, and Muneer generously took time to read and edit my applications. I would like to thank my Minnesota friends who always provided me with a place to stay when I was visiting and gave me endless words of encouragement to keep fighting through my PhD. The same goes for my friends in Atlanta who always encouraged me to be myself and would be patient and supportive when listening to my many thoughts. Releasing stress and celebrating each other's occasions maintained my physical health necessary to conduct research.

Finally, I would like to thank the many people who provided technical guidance. I wish to thank the Zhu Lab members, who provided invaluable feedback, encouragement, and taught me how to conduct many experiments and interpret data carefully. In particular, I would like to thank Dr. Kaitao Li for his never-ending arsenal of knowledge, wisdom, and kindness which played immense roles in shaping this thesis. I would like to thank Sommer Durham, Nadia Boguslavsky, and Steve Woodard of the Core Facilities for their tireless and selfless hard work to provide a unique resource to the Petit Institute research community. Lastly, I would like to thank my funding sources which included grants from the National Institutes of Health, the National Science Foundation, and the Chinese Scholarship Council.

TABLE OF CONTENTS

ACKNOWLEDGEMENTS	IV
LIST OF TABLES	XII
LIST OF FIGURES	XIII
LIST OF SYMBOLS AND ABBREVIATIONS	XV
SUMMARY	XVI
CHAPTER 1 INTRODUCTION.....	1
1.1 Specific immune response by T cells	1
1.1.1 T cell receptor	2
1.1.2 T cell coreceptors	9
1.1.3 Lck kinase	13
1.2 T cell receptor machinery interactions with oxidative environment	15
1.2.1 Reactive Oxygen Species	16
1.2.2 Effects of ROS specific to TCR triggering.....	18
1.3 Macrophage Immunobiology	21
1.3.1 Macrophage function.....	22
1.3.2 Development of oxidative stress in alcohol exposed macrophages.....	24
1.3.3 TLR4 triggering by LPS.....	25
CHAPTER 2 SPECIFIC AIMS AND HYPOTHESES.....	27
Aim 1	27
Aim 2	27
Aim 3	27
CHAPTER 3 AIM 1	28
3.1 Methods.....	28
3.1.1 Materials	28
3.1.2 Binding Assay	31
3.1.3 Mathematical Characterization.....	39
3.1.4 Calcium Imaging.....	45
3.2 Results	46

3.2.1	TCR-pHLA interactions bind with thousands-fold higher propensity than wild type CD4-HLA interactions.	46
3.2.2	Constraining CD4 and TCR on the same membrane opposed to pHLA results in synergy.....	50
3.2.3	Biomembrane force probe demonstrates a trimolecular species.....	55
3.2.4	Mathematical characterization of synergy	57
3.2.5	Demonstration of synergy in cell system.....	62
3.3	Discussion and Conclusions	68
3.3.1	Synergy between TCR, pHLA and CD4.....	70
3.3.2	Implications for models of T cell triggering	76
3.3.3	T cell machinery signaling loop	81
3.3.4	Implications toward T cell receptor signaling.....	81
CHAPTER 4	AIM 2	84
4.1	Methods.....	84
4.1.1	Materials	84
4.1.2	Optimizing conditions for adhesion frequency	87
4.1.3	Real-time adhesion frequency.....	88
4.1.4	Pharmacologic perturbations	92
4.2	Results	93
4.2.1	Optimization of hydrogen peroxide concentration.....	93
4.2.2	Purified OT1 TCR binding to OVA pMHC is not influenced by H ₂ O ₂ . 96	
4.2.3	OT1 TCR binding to OVA is weakened in the presence of H ₂ O ₂	97
4.2.4	CD8 coreceptor rescues diminished binding between OVA and OT1 TCR	102
4.2.5	Lck activity regulates coreceptor rescue of TCR binding.....	104
4.2.6	Lipid raft oxidation and actin inhibition reduce 2D affinity	105
4.3	Discussion and conclusions	107
4.3.1	Model for oxidation of TCR-pMHC-CD8-Lck signaling loop.....	108
4.3.2	Cholesterol and actin dependencies	113
4.3.3	Role of post-translational modifications in TCR recognition.....	116
4.3.4	Cell- and tissue-scale effects of ROS and antioxidants.....	117
CHAPTER 5	AIM 3	120
5.1	Methods.....	120

5.1.1	Materials	120
5.1.2	Development of Oxidative stress.....	121
5.1.3	Real-time Micropipette Assay.....	122
5.1.4	Intracellular cytokine staining.....	124
5.1.5	Confocal imaging	125
5.2	Results	126
5.2.1	Macrophages secrete less cytokines when supplemented with antioxidants	126
5.2.2	TLR4:LPS bimolecular binding is not a good predictor of ethanol induced derangement.....	127
5.2.3	Cell morphology predicts ethanol induced deficiency	128
5.2.4	Chemotaxis in response to LPS is inhibited upon ethanol treatment ..	129
5.2.5	Actin reorganization influenced by ethanol treatment.....	130
5.3	Discussion and conclusions	131
5.3.1	Novel chemotaxis of macrophages in response to LPS.....	133
5.3.2	Implications for ethanol induced deficiencies	135
5.3.3	Mechanosensitive macrophages.....	137
CHAPTER 6 CONCLUSIONS AND FUTURE DIRECTIONS.....		139
6.1.1	Development of a mathematical model for multi-molecular interactions	139
6.1.2	Reconciliation of oxidative effects on T cell function	142
6.1.3	Toward understanding multi-molecular interactions in macrophages	145
6.1.4	Final Remarks	148
APPENDIX.....		149
A.1.	Binding between mutant TPI and E8 TCR	149
A.2.	Derivation of mathematical model for trimolecular interaction	150
REFERENCES.....		153

LIST OF TABLES

Table 1: Binding kinetics from adhesion frequency	49
Table 2: Parameter fittings describing TCR-pHLA-CD4 cooperativity.....	60
Table 3: Optimization conditions for micropipette experimental chamber buffer	95

LIST OF FIGURES

Figure 1. Micropipette Adhesion Frequency Assay	38
Figure 2. Biomembrane Force Probe assay and analysis.....	40
Figure 3. Reactions between TCR, pHLA, and CD4.....	43
Figure 4. Analytical solutions for bond formations assuming no cooperativity.....	44
Figure 5. Analytical solutions for bond formations with cooperativity.....	45
Figure 6. Micropipette adhesion frequency assay reveals binding of TCR:pHLA, mCD4:HLA, and wtCD4:HLA.....	50
Figure 7. Demonstration of synergy with presence of CD4.....	54
Figure 8. Mobility of molecules dictates degree of synergy.....	55
Figure 9. Single-molecule analysis reveals bond stabilization.....	57
Figure 10. Removing bimolecular interactions reveals synergy.....	61
Figure 11: Dependence of synergy on all bond formation.....	61
Figure 12: Mathematical prediction of cooperativity.....	62
Figure 13. Longer lifetimes when CD4 is present.....	66
Figure 14. Stiffness analysis elucidates trimolecular population.....	67
Figure 15. TCR and CD4 expressing Jurkat cells exhibit synergy.....	68
Figure 16: Optimization of hydrogen peroxide concentration.....	94
Figure 17. TCR affinity to pMHC in response to H ₂ O ₂ exposure.....	97
Figure 18. Hydrogen Peroxide effect on 2D affinity in OT-1 T cells.....	100
Figure 19. Consumption of hydrogen peroxide over time.....	100
Figure 20. Hydrogen peroxide production facilitated by glucose oxidase.....	101
Figure 21. Effect of continuous hydrogen peroxide production on 2D affinity.....	103
Figure 22. The role of Lck activity on 2D effective affinity.....	105
Figure 23. The role of cholesterol in regulating binding.....	106
Figure 24. Effect of cytoskeleton on 2D affinity in the presence of hydrogen peroxide.....	107

Figure 25. Model for effect of H ₂ O ₂ on TCR binding	113
Figure 26. Schematic depicting conditions of macrophage culture in incubator.....	122
Figure 27. Cytokine secretion is inhibited by antioxidants.....	126
Figure 28. Binding assay between macrophages and LPS.	127
Figure 29. Morphological changes in response to LPS	129
Figure 30. Gradient of LPS is sensed by macrophages	130
Figure 31. Extent of actin remodeling for various macrophage conditions.....	131
Figure 32. Mutant TPI binds to E8 TCR with much higher affinity.....	149

LIST OF SYMBOLS AND ABBREVIATIONS

APC	Antigen presenting cell
BFP	Biomembrane Force Probe
CDR	Complementarity Determining Region
Fab	Fragment antigen-binding
Fc	Fragment crystallizable
H ₂ O ₂	Hydrogen peroxide
HLA	Human leukocyte antigen
Ig	Immunoglobulin
ITAM	Immunoreceptor tyrosine-based activation motif
MHC	Major histocompatibility complex
PAMP	Pathogen associated molecular pattern
pHLA	Peptide- human leukocyte antigen
pMHC	Peptide- major histocompatibility complex
ROS	Reactive oxygen species
RBC	Red blood cell
SMAC	Supramolecular activation cluster or complex
SPR	Surface plasmon resonance
TCR	T cell receptor
TLR	Toll-like receptor
A	Area (μm^2)
k_{off}	Off-rate (second^{-1})
k_{on}	On-rate ($\mu\text{m}^4/\text{second}$)
K	Affinity constant (μm^4)
$\langle n \rangle$	Average number of bonds formed, unitless
m	Molecular density per area ($\text{molecules}/\mu\text{m}^2$)
P	Probability of adhesion, unitless

SUMMARY

Immune system response to pathogens is mediated by triggering of receptor-ligand interactions such as the T cell receptor (TCR) engaging with peptide-major histocompatibility complex (pMHC) expressed on infected cells, which can be facilitated by the CD4 coreceptor. However, detecting CD4-pMHC binding has been elusive due to its purported weak affinity. Additionally, there are no models that describe cooperativity between more than two molecules. To address these limitations, the first aim of this thesis was to characterize CD4-pMHC binding and mathematically model trimolecular cooperativity. Using an ultra-sensitive micropipette adhesion frequency assay and biomembrane force probe, the complete set of CD4-pMHC kinetics was experimentally detected for the first time. Surprisingly, when controlled mixtures of TCR and CD4 were probed against pMHC, binding frequency was greatly enhanced clearly demonstrating synergy between TCR, pMHC and CD4. These results were used to develop the first documented analytical solutions for trimolecular cooperativity, which imply a conformational change in TCR-bound pMHC that greatly enhances CD4 binding. A cell system corroborated the model by confirming that the ratio between TCR and CD4 dictates synergy observed in binding kinetics and intracellular signaling, suggesting that CD4 is not a passive facilitator of activation as previously thought.

As T cells travel to sites of inflammation, the trimolecular complex is exposed reactive oxygen species (ROS) generated by other immune cells also seeking to clear pathogen. ROS has been suggested to inhibit T cell function, especially in cancer microenvironments, but in other scenarios, it has been shown to improve T cell function. The dual-role of ROS has long convoluted study of its effect on immune cells which has notoriously limited clinical intervention. Therefore, the second aim of this thesis was to monitor TCR-pMHC binding in response to ROS in real-time using a novel modification of the micropipette assay, in order to deconvolute how the many molecules involved in

binding are each affected. TCR-pMHC binding was reduced by introduction of ROS but could be partially rescued by the coreceptor. The degree of rescue was modulated by the surrounding cholesterol content of the membrane as well as the catalytic activity of proximal kinases. By parsing out molecules in a holistic in situ system, it was concluded that TCR-pMHC binding is weakened due to the disruption of the trimolecular complex by ROS.

Similar to T cells, the macrophage TLR4 receptor requires other surface receptors to robustly recognize its ligand LPS, and the relationship between oxidative stress and macrophage function is mired with conflicting results. Correspondingly, the framework developed in the first two aims of this thesis was applied to a third aim which sought to understand how macrophage function can be both enhanced and impaired by ROS. Unique morphological changes of macrophages induced by LPS engagement were dependent on ROS and correlated well with previously described inhibition of macrophage phagocytosis. At the same time, ROS enhanced cytokine secretion by macrophages and TLR4-LPS binding did not display differences between ROS-treated and untreated cells. Lastly, actin reorganization appeared to be reduced when treated with ROS. These data suggest that unlike T cell activation which is dependent on TCR-pMHC binding, macrophage function is diverse in its regulation as exemplified by ROS improving TLR4 signaling but also inhibiting movement by disrupting actin.

Overall, by introducing biophysical and biochemical contexts to receptor-ligand interactions in tandem, a better understanding of how our immune system sensitively detects pathogens was achieved. The novel results described herein inform rational design of therapeutic interventions including protein engineering enhancement of antigen recognition as well as acute and compartmentalized antioxidant protection.

CHAPTER 1 INTRODUCTION

1.1 Specific immune response by T cells

The human immune system orchestrates robust defenses against pathogens that begin with ‘innate’ responses and can trigger the expansion of a specific ‘adaptive’ response. An innate response is readily available to be exerted upon recognition of an abnormal entity, intracellularly or extracellularly, and is based in recognizing general molecular patterns¹⁻³. An adaptive response recognizes a unique molecular feature but requires a period of priming before it can be executed. Such a response is necessary to overcome pathogens of significant mutational diversity and rapid infection transmission which surpasses the rate at which the innate immune response can maintain resistance¹. A central arm of the adaptive immune response is made up of T cells, which are programmed to specifically recognize the unique molecular features and only act to eliminate the cells they derive from as opposed to features from host cells^{1,3}.

Activation of T cells begins with tissue resident dendritic cells (DCs) scavenging the site of infection and engulfing foreign antigen which leads to DC maturation and involves fragments, or peptides, of the antigen being presented on the surface of the DC, just as they are presented on infected host cells^{3,4}. Upon activation, DCs migrate into peripheral lymph nodes where they encounter antigen inexperienced naïve T cells. DCs and naïve T cells will exchange information through a vast array of physically interacting surface-bound receptors which ultimately serve to mature naïve T cells into ‘effector’ T cells and stimulate their rapid proliferation^{3,5,6}. Vast numbers of effector T cells are attracted to the infection site through action of chemokines and adhesion receptors, extravasate into the tissue space, and recognize infected cells by the peptide matching the one presented on the DC that had previously activated the T cells, affording a specific attack targeted only to infected cells and not to uninfected host cells^{3,7-10}. T cells can

either directly destroy infected cells by means of toxic granules or they can recruit and activate other immune cells to exert the same function³.

As the infection is gradually eliminated, the majority of antigen-specific T cells undergo controlled self-destruction to avoid damaging host cells and tissue, only leaving a small fraction which differentiate into ‘memory T cells’^{3,11}. Upon secondary infection, these memory T cells activate much more rapidly than they previously did as naïve cells and are preferentially localized in non-lymphoid tissues and can therefore more readily respond to the same infection^{11,12}. Recognition of, and response to foreign peptide on DCs and eventually the infected cells, is mediated by the T cell receptor.

1.1.1 T cell receptor

Specific immune responses by T cells are predicated on recognizing molecular features that are not present in the make-up of healthy host cells and tissues. Recognizing host antigen will cause T cells to target self, a disease established as autoimmunity which has deadly consequences¹³. In addition to being programmed to recognize only foreign antigen through processes called positive and negative selection¹⁴, T cell receptor (TCR) recognition is distinct from innate germline encoded receptors such as Toll-like-receptors (TLRs), in that TLRs broadly recognize what are known as ‘pathogen-associated molecular patterns’ (PAMPS) as opposed to a peptide. For example, TLR3 would recognize double-stranded RNA as a pattern as opposed to the nucleotide sequence within the double-stranded RNA³. In contrast, TCR can distinguish even one amino acid difference between otherwise identical peptides anchored within major histocompatibility complexes (MHC)- the combination of which will hereon be referred to as the peptide-major histocompatibility complex, or pMHC- with consequences extending to T cell function and fate^{15,16}. Class-I pMHCs have been reported to anchor peptides between 8 and 15 amino acids long (mostly 9) and can therefore be represented by tremendous number of permutations. Class-II pMHC can yield even greater diversity since the

peptides loaded can vary between 11 and 30 amino acids long. Adding to the diversity are many different alleles of MHC specific to an individual¹⁷. The diversity from pattern recognition of germline encoded receptors would not suffice in recognizing such diverse ligands, and rather relies on recognition by the TCR whose diversity is based in genetic recombination³.

1.1.1.1 T cell receptor diversity

Antibodies, or immunoglobulin (Ig), can recognize virtually any substance by the three-dimensional set of amino acids it binds to on the substance called an epitope³. Diversity of Igs is concentrated in their variable domains which are encoded by separate gene segments in the germline called V, D, and J. The process of randomly joining together different genes from each of these segments is called VDJ recombination and is capable of producing a theoretical limit of 10^{11} antibodies with different recognition³.

1.1.1.1.1 T cell receptor development

Production of TCR diversity uses the same mechanism as Ig diversity. Most TCR are made up of an α chain and a β chain, yielding the $\alpha\beta$ T cell receptor (hereon the $\alpha\beta$ T cell receptor will be referred to as TCR). These chains are encoded in the germline as 52 V segments, 2 D segments, and 13 J segments for the β chain, and about 70 V segments, no D segments, and 61 J segments for the α chain. By randomly joining together these segments for each of the α and β chains, and eventually pairing the α and β chains together, a theoretical diversity of 10^{18} to 10^{20} is estimated³. However, this diversity limited by the number of T cells in one individual, as well as the antigens that the individual encounters in their lifetime yielding a realized diversity of 10^6 to 10^7 different TCR¹⁸. Nevertheless, the TCR is capable of recognizing a large repertoire of pMHC.

The process of expressing a TCR with a specific recognition occurs in the thymus. Progenitor cells from the bone marrow arrive in the thymus without TCR expression and undergo several developmental stages³. Now residing in the thymus, the progenitor is

referred to as a thymocyte, and expresses a functional pre-TCR that is made up of the VDJ-diversified β chain and a pre- α chain. Only thymocytes expressing functional β and pre- α are allowed to survive in a process called positive selection^{3,14}. VJ-diversified α chains are then expressed and paired with the β chains completing the TCR. At this point, cells that express TCR that react strongly to self-antigen are programmed for destruction, in a process termed negative selection, to avoid autoimmunity¹⁴. Upon completion of this stage, T cells are released from the thymus into circulation and can begin to reside in peripheral lymph nodes where they will encounter DCs for activation and effector function³. While each peripheral T cell clone expresses a unique TCR, the TCR can still recognize more than one peptide, a form of cross-reactivity. Therefore, the T cell must be able to discriminate between similar peptides (even with only one amino acid difference) to propagate variable signaling¹⁵. The discriminatory power is present even in thymocytes since the reactivity with self-antigen between positive and negative must be different. If the degree of recognition is the same, T cells that survive through positive selection would all be programmed for death in negative selection³. The discriminatory power between different stages of the TCR development¹⁹ or in the peripheral where T cells discriminate between different foreign antigen^{20,21}, is suggested to be attributed to propagation of conformational changes within the structure of the TCR and proteins associated with it²²⁻²⁴.

1.1.1.1.2 T cell receptor structure

Two polypeptide chains make up the TCR heterodimer, an α and β chain which both span: ectodomains made up of variable and constant regions that are joined by a disulfide bond, transmembrane domains, and cytosolic domains that are too short for signaling^{25,26}. The variable regions of α and β chains are similar to the structure of the fragment antigen-binding (Fab) domains of antibodies which are also known as Immunoglobulin (Ig). The similarities in three-dimensional structures imply similarities

in their functionality of binding antigen. A difference is that Ig Fab binds to antigen in a concave topology while the topology between the $\alpha\beta$ variable domains bind to a relatively flat surface on pMHC^{25,26}. Binding to the peptide is largely mediated by complementarity determining regions (CDR) formed by both variable regions of α and β chains, in particular the hypervariable CDR3^{25,26}. Moving proximally to the membrane from the variable region are the $\alpha\beta$ constant domains. These also have sequence homology to the Ig constant domain especially in the region where the disulfide bond forms between α and β chains^{25,26}. A major difference in the constant β compared to the Ig constant region is a well-structured 12 amino acid insertion termed the FG loop which may have functional importance in amplifying differences in peptides²⁷. Finally, the TCR transmembrane domain is primarily where association with CD3 proteins is driven, by evolutionarily conserved and charged residues²⁸. These CD3 transmembrane proteins are responsible for signal transfer from the TCR variable region to intracellular proteins²⁸.

1.1.1.2 CD3 association with TCR

Upon ligation of a specific pMHC, information is transferred by the TCR through the surface of the T cell, which is a process known as ‘TCR triggering’. However, TCR does not possess an intracellular signaling domain²⁸. Thus, how the TCR is able to transmit signals from the pMHC to intracellular signaling molecules has been a topic of intense investigation for decades. It is well accepted that several CD3 polypeptide chains play a central role in transmitting this signal, due to its constitutive association with TCR²⁸. There are four different CD3 proteins, CD3 γ , CD3 δ , CD3 ϵ , and CD3 ζ . CD3 γ , CD3 δ , and CD3 ϵ each consist of a single Ig ectodomain, a transmembrane domain, and single immunoreceptor tyrosine-based activation motif (ITAM)^{27,28}. CD3 ζ has a short ectodomain, a transmembrane domain, and a relatively longer cytosolic domain with three ITAMS^{27,28}. These proteins present themselves as dimers, more specifically heterodimers of CD3 $\epsilon\gamma$ and CD3 $\epsilon\delta$, and homodimers of CD3 $\zeta\zeta$, and non-covalently

associate with TCR at a 1:1:1:1 ratio forming the TCR-CD3 quaternary complex^{27,28}. Altogether 10 ITAMS are associated with the TCR. These motifs act as molecular switches, whereby upon phosphorylation, they manifest an activation state and can serve as adaptors for signaling molecules which perpetuate a signaling cascade. Phosphorylation is mediated by kinases and dephosphorylation is mediated by phosphatases. A dynamic balance between these actions ensure that signal is only propagated when appropriate²⁹. Another way that CD3 ITAMs phosphorylation can be modulated is due to their positive basic residues that are electrostatically buried in the negatively charged inner leaflet of the cell membrane, rendering the ITAMs inaccessible to phosphorylation by kinases³⁰⁻³³. A body of work theorizes that these chains are released as a physical consequence of TCR-pMHC binding causing the ITAMs to be susceptible to phosphorylation thereby initiating the signaling cascade^{27,34,35}.

1.1.1.3 Measuring T cell receptor binding kinetics

Activation of T cells does not occur without TCR triggering³⁶. Even in their resting state before activation which leads to effector function, TCR are thought to be ‘tickled’ by low affinity self-peptides to maintain a basal level of activation to prevent a state of inactivity^{37,38}. Self-peptides do not fully activate the T cell because this would lead to autoimmunity, but rather remain primed due to cross-reactives that were present in thymocyte development³⁸. One method to quantify the variable effects peptides on T cells through the TCR is to observe T cell effector function. For example, by measuring cytokines secreted by T cells or the extent of proliferation of T cells, ‘potency’ of different peptide can be tested^{39,40}. However, these methods do not directly provide any information about how the pMHC is binding to the TCR, thereby preventing rationale design of peptides to modulate T cell function.

1.1.1.3.1 *3D kinetics*

In circulation, metabolites and proteins are constantly associating and dissociating as part of chemical reactions. For example, enzymes associate with proteins in solution to greatly accelerate chemical reactions. To measure this reaction, isothermal calorimetry can measure thermodynamic changes from gradually titrating one species to another, which can yield the affinity constant for the bimolecular interaction⁴¹. Another scenario is when cells respond to soluble proteins through their surface bound receptors. A well-studied example is receptor tyrosine kinases such as surface bound epidermal growth factor receptor ligated by soluble epidermal growth factor which induces dimerization. Binding between receptor and ligand is a dynamic process, however, which occurs with on- and off-rates of the ligand to and from its receptor and can be modeled by an affinity constant just as with isothermal calorimetry⁴². Quantitative measurements of this type of binding can be mimicked by surface plasmon resonance (SPR).

In this experiment a receptor is anchored in the desired orientation on a surface of a flow chamber. Along the surface is a surface plasmon field which is very sensitive to physical changes along this nanometer-scale thick plane. The ligand is then flowed over the receptor coated surface to allow association which is detected by an increase in plasmon resonance response units. Association is continued until saturation of response units, at which flow is continued without ligand to allow dissociation of bound complexes. This decrease in bound ligand is also detected and finally from all these real time measurements, on- and off-rates as well as an affinity constant can be calculated^{43,44}. SPR has been widely utilized to study various TCR association with their cognate pMHC, and from these studies a positive correlation between peptide potency as measured by cell effector function, and TCR affinity to pMHC have been established^{44,45}. Kinetics such as on- and off-rates are important to detail because their ratio, the affinity constant measured by SPR, do not always predict peptide potency⁴⁶.

1.1.1.3.2 2D kinetics

A third scenario of information transfer exists whereby two membranes that are in sub-micron proximity to each other spatially afford an interaction between two opposing surface bound receptors²⁹. This is the case for the TCR-pMHC interaction along with a large body of molecules between T cells and Antigen Presenting Cell (APC) such as DCs. In fact, within this junction exists an organized supramolecular activation complex (SMAC) between interacting opposing molecules⁶. Since the SMAC was only apparent after minutes of T cell-APC interaction, it is thought that the SMAC represents a climax in the T cell activation state⁶. Therefore, measuring interactions that are physically constrained by membranes are of high relevance to T cell immunobiology. In order to study kinetics between surface bound receptors, micropipette-based 2D binding assay have been developed⁴⁷.

In this experiment, two cells are aspirated onto opposing micropipettes exposing their surfaces to each other. One cell is the live target cell with the receptor of interest expressed on its surface. The other cell is a surrogate APC, a red blood cell (RBC), with the ligand of interest chemically conjugated onto its membrane. The main purpose of using RBCs as surrogate APCs is to magnify binding events. Upon bringing the cells into contact with one another and separating them, a binding event may occur, visualized by deformation of the RBC membrane. Assuming binding events occur at low frequency, the adhesion frequency can be fitted to a probabilistic model that plots adhesion frequency against contact time between cells to extract an effective affinity constant and off-rate for the bimolecular reaction⁴⁷. This assay revealed a much more positive association over a larger range of values between peptide potency and affinity constant between TCR and pMHC²¹. Interestingly, the assay suggested that bimolecular on-rate is a stronger determinant of peptide potency as opposed to what was previously thought to be off-rate²¹. Thus, the micropipette adhesion frequency assay proved to be an effective method to measure of TCR-pMHC binding kinetics.

A refinement of the micropipette adhesion frequency assay was developed to track the fluctuations of the ultrasensitive red blood cell membrane by using what is known as a biomembrane force probe (BFP)⁴⁸. Here, single-molecule scale bond formation and dissociation between TCR and pMHC is visually tracked as the target cell is pulled away from the BFP at a predefined force. A seminal study using this assay found that an accumulation of bonds lasting above a threshold lifetime, occurring within a window of a minute reliably led to intracellular calcium flux in live T cells- a switch-like indicator of T cell activation²⁰. Overall, micropipette-based 2D binding assays have provided a more direct relationship between TCR-pMHC binding kinetics and T cell activation, for specific peptide systems, than the same measurements made using SPR^{19-21,49,50}. Studies using the BFP have also supported the concept of a catch-slip-bond. One type of protein-protein association is a slip-bond which will present shorter interacting bond lifetimes if the molecules are pulled apart by an external force⁵¹. A catch-slip-bond is a counter-intuitive type of association whereby forces on the interacting molecules pulling the bond apart will yield longer bond lifetimes until even higher forces will finally drive the bond to dissociate as in the slip-bond⁵¹. These bonds were first directly observed using atomic force microscopy measuring bonds between P-selectin and P-selectin glycoprotein ligand-1 and were purported to be a mechanism supporting leukocyte surface rolling under shear forces⁵². Using the BFP, various TCR were shown to associate with pMHC through catch-slip bonds. In these studies, catch-slip-bonds were suggested to be a mechanism for amplifying discrimination between pMHC^{19,20,53}, even discriminating between pMHC with similar affinities measured by SPR, but opposite potency effects⁵⁰.

1.1.2 T cell coreceptors

Function of T cells were discovered to vary between targeted killing of infected cells or robust secretion of cytokines⁵⁴. Expressed on the surface of these different

effector cells were also mutually exclusive proteins- CD8 and CD4, respectively^{3,54,55}. These markers were therefore aptly used for identification purposes. Even in the thymus, CD8 and CD4 expression occurred in stages and was useful in understanding stages of T cell development- first double negative thymocytes which express neither CD4 or CD8, then double positive which express both proteins, and finally split between two sets of single positive cells¹⁴. These surface markers were eventually found to serve functional purposes toward TCR triggering based on the two different classes of MHC, class-I and class-II⁵⁴.

1.1.2.1 CD8 coreceptor

CD8-positive T cells were found to be strongly associated with APCs that expressed the class-I MHC. This led to the suggestion that CD8 could bind to MHC-I, which was indeed found to be the case. It was determined that in the class-I interaction, TCR binds to the peptide groove while CD8 binds to MHC⁵⁶. The CD8 coreceptor is encoded by two genes, CD8 α and CD8 β . Both expressed proteins are made up of a single Ig-like domain followed by stalk regions, a transmembrane domain, and a short cytosolic tail²⁷. On T cells, these proteins exist mostly as CD8 $\alpha\beta$ heterodimers but CD8 $\alpha\alpha$ homodimers also exist²⁷. Using SPR, both dimers were found to bind to MHC-I at affinity values ranging from 50-200 μM , which is between one and two orders of magnitude weaker than many TCR-pMHC interactions⁵⁷. Using 2D binding assays, the CD8-MHC interaction was found to have an affinity of $5 \times 10^{-6} \mu\text{m}^4$, which is almost two orders of magnitude weaker than the model OT1 TCR- OVA pMHC interaction^{21,58}. Due to this large difference in binding affinities, the CD8-MHC interaction has been suggested to not play a significant role in stabilizing TCR-pMHC interactions, rather largely to recruit kinases to the TCR-CD3 ITAMs via its cytosolic association with kinases, specifically one called Lck^{27,59}. Despite this consensus, CD8 has been shown to contribute to a 'two-stage binding' represented by an enhanced adhesion frequency after

a delay of 1 second contact time for the OVA system⁶⁰. While the role of CD8 in propagating signal by recruitment of Lck to ITAMs is generally accepted, the role of stabilization of TCR-pMHC by CD8-MHC toward prolonging bond lifetimes has been relatively less explored^{19,61}.

1.1.2.2 CD4 coreceptor

Analogous to the CD8 case, CD4-positive T cells were found to be strongly associated with APCs expressing the class II pMHC^{3,54}. By overexpressing CD4 on cells, previous studies found the cells adhering to B cells expressing class-II MHC after washing, clearly demonstrating binding between CD4 and MHC class II⁶². More recently, it was shown that blocking CD4 can abrogate T cell signaling to a point that would require 30-fold as many TCR-pMHC interactions to recover the same level of signaling⁶³. Peptides in class-II MHC are usually much longer than those anchored in class-I, ranging between 11-30 residues in length^{17,64}. Despite this longer length, the peptide presented in class-I are more amenable to scanning by TCR because the peptide ends are confined by the groove which causes the peptide to bulge out of the groove. Peptides ends in class-II MHC extend out of the groove and are relatively unstructured⁶⁴. The stability of peptides in class-II can also be weaker than in peptides in class-I^{65,66}. To overcome this limitation, previous studies have used a peptide covalently bound to the MHC-II groove when interrogating interactions between TCR and pMHC^{49,67}. Stability of peptide in MHC plays a critical role in TCR recognition because altering anchor residues have shown to greatly modulate binding affinity to TCR, as well as the peptide potency⁶⁸. The measurement that has remained elusive, however, is binding kinetics between CD4 and MHC-II class-II.

1.1.2.2.1 CD4, CD8, and ternary complex structures

In contrast to TCR, CD4 and CD8 are invariant structures and were therefore assumed to interact with conserved regions of polymorphic MHC molecules. Since the

CD8 $\alpha\alpha$ homodimer CD loop binds to the MHC-I $\alpha 3$ membrane proximal domain with a well-structured hydrogen-bond network, it was inferred that CD8-MHC-I binding does not require a conformational change²⁷. CD4 is made up of four Ig-like domains (D1 through D4), a short membrane proximal stalk region, a transmembrane helix, and a cytosolic tail which binds to Lck just like CD8⁶⁹. A distinct feature of CD4 is its angled orientation. When CD4 dimerizes, a ‘butterfly’ profile is observed with an angle at the D1D2 to D3D4 junction of 140°⁶⁹. Unlike CD8-MHC-I binding, CD4-MHC-II binding was not found to be antibody-like and instead occurs CD4 D1 domain wedging between two membrane proximal $\alpha 2$ and $\beta 2$ domains of MHC-II²⁷. Using a superimposition of the CD4-MHC-II complex on TCR-pMHC-II structures, a ternary complex structure was predicted. This technique illustrated a V-shape ternary interaction, with TCR and CD4 binding to MHC-II with their respective membrane proximal regions being clearly distant and not interacting²⁷. The shape of the ternary complex was directly shown by Mariuzza and colleagues using CD4 that possessed much greater affinity to MHC-II, accomplished by yeast display⁷⁰. TCR-pMHC-CD4 displayed the V-shape with approximately 70 Å distance between the membrane proximal C α /C β module of TCR and the CD4 D4 domain⁷⁰. It was suggested that this distance provides ample space for CD3 $\epsilon\gamma/\epsilon\delta/\zeta\zeta$ subunits to organize around TCR along with association with the coreceptor for ITAM phosphorylation^{28,70}. These models likely capture the geometry of the ternary complex but defining the role of CD4 in TCR triggering is incomplete without measuring binding between CD4 and MHC-II.

1.1.2.2 Remarkably low affinity binding of CD4 to pMHC

In contrast to binding between CD8 and MHC-I, measurements for CD4-MHC-II are controversial. The first measurements were made by Reinherz and colleagues using SPR and determined that human CD4 binding to mouse MHC class-II occurred with a K_D of 200 μ M, which is on the same order of magnitude with some CD8-MHC-I

measurements⁷¹. An unsuccessful attempt at recapitulating these results using human CD4 and human MHC class-II interaction concentrations as high as 2 mM was conducted by Davis and colleagues⁷². Further attempts were made by Mariuzza and colleagues who used concentrations as high as 400 μ M with no detectable binding between CD4 and MHC class-II, which is in stark contrast to binding between their mutant CD4 and MHC class-II which occurred with a K_D of 8 μ M and is on the same order of magnitude as many TCR-pMHC interactions⁷³. Instead of SPR, two dimensional assays were also unable to detect a significant difference between bimolecular TCR-pMHC interaction and the trimolecular TCR-pMHC-CD4 interaction^{49,74}. Most recently, Davis and colleagues repeated this experiment using soluble CD4 at concentrations up to 2.5 mM at 4°C without any detectable binding⁷⁵. However, by constraining molecules to two-dimensional interactions, they successfully used the CD4 coated beads to pull down cells expressing MHC-II. To corroborate these findings, cells expressing MHC-II clearly displayed binding to CD4 (400-4,000 molecules/ μ m²) and CD2 (400 molecules/ μ m²) functionalized lipid bilayers, as seen by accumulation of fluorophore conjugated CD4 and CD2 under MHC-II expressing cells⁷⁵. Using the Zhu-Golan approach⁷⁶ they estimate the CD4-MHC-II K_D to be up to three orders of magnitude weaker than TCR-pMHC interactions⁷⁶. These two-dimensional results are reminiscent of seminal work discovering that CD4 can mediate adhesion⁶². However, due to the very low affinity interaction of CD4-MHC-II not contributing significantly to TCR-pMHC interactions based on their calculations, Davis and colleagues concluded that the primary role of CD4 was to deliver Lck to ITAMs, consistent with previous studies^{59,75}. Still, it remains unclear how blocking CD4 could abrogate T cell signaling so significantly⁶³.

1.1.3 Lck kinase

Kinases are enzymes that catalyze the transfer of a phosphate from an ATP to a functional group of a molecule. With the addition of a phosphate group, the functional

group (such as a tyrosine) can be made conformationally accessible for association with specific adaptor molecules and in some cases subsequently phosphorylate other molecules. Such a process is termed a signaling cascade which can be reversible by enzymatic action of phosphatases which catalyze the removal of phosphates. Hematopoietic cells express a family of kinases called Src kinases that are specialized for various roles⁷⁷. T cells primarily express Lck and Fyn from the Src family, but only express Lck consistently throughout their development and lifespan⁷⁷.

1.1.3.1 Lck structure and function

Lck is a 56 kDa protein made up of an N-terminal covalent attachment site for saturated fatty acids, a unique region which mediates association with CD4 and CD8 via a ‘zinc clasp’, a Src-homology 3 (SH3) domain, an SH2 domain, a tyrosine kinase domain, and a C-terminal regulatory domain^{77,78}. Phosphorylation at the C-terminal domain at tyrosine 505 (Y505) of Lck causes intramolecular binding with its own SH2 domain, resulting in an autoinhibited ‘closed’ form⁷⁸. Y505 can be dephosphorylated by the ubiquitous CD45 phosphatase, which will relax Lck into an ‘open’ conformation⁷⁹. Once open, phosphorylation of the catalytic tyrosine kinase domain at tyrosine 394 (Y394) lends the kinase to become ‘active’ and is at that point, capable of phosphorylating the CD3 ITAMs⁷⁹. It is thought that phosphorylation of Y505 is mediated by another kinase, Csk, and phosphorylation of Y394 is mediated by trans-autophosphorylation^{77,79}. Thus, this kinase which is critical for signal propagation from TCR-pMHC interactions exists in a dynamic equilibrium with many other signaling molecules.

1.1.3.2 Lck association with CD4 and CD8

By means of its fatty-acid modified N-terminal end, Lck is anchored in the inner leaflet of T cells. Proximity to the membrane allows for direct imaging of Lck along with other surface bound receptors. Using these methods, it was found that CD4, TCR, and

Lck can colocalize prior to SMAC formation^{80,81}. While Lck propagates signal from TCR-pMHC interactions, there is no direct evidence of TCR directly affecting Lck activation state^{79,82}. In fact, it is estimated that 40% of Lck in T cells are constitutively active and this number does not correlate with TCR or CD4 engagement but does correlate with CD3 ζ phosphorylation⁷⁹, suggesting that Lck exists in a dynamic equilibrium between active and inactive Lck is maintained in resting T cells⁸². More recently, it was shown that the conformational states of Lck can determine their self-clustering capacity with only active Lck inducing clustering⁸². Interestingly, Lck has been found to bind the intracellular portions of CD4 at a higher affinity than CD8⁸³. Using a thymocyte system that expressed a coreceptor chimera with a CD8 ectodomain and a CD4 cytosolic domain, it was determined that increased association with Lck can lead to more efficient TCR triggering⁸⁴. Thus, while there is no evidence for TCR-pMHC influencing Lck activation state, Lck may play a critical role in increasing the efficiency of TCR-pMHC scanning for antigen.

1.2 T cell receptor machinery interactions with oxidative environment

Sites of inflammation are made up of a host of immune cells secreting pro-inflammatory cytokines and chemicals. A major family of chemicals that are secreted by these innate immune cells to destroy pathogens are reactive oxygen species (ROS)^{85,86}. This group of chemicals rapidly and irreversibly oxidize biopolymers such that they disassemble, destroying lipid membranes, nucleic acids, and proteins⁸⁷. Indeed, significant cytotoxic potential in inflammation is attributed to ROS by detecting overly oxidized biomarkers on host cells from scenarios of inflammation^{87,88}. Ubiquitous in cells and tissue, however, are antioxidants which protect the host from damage⁸⁸. The balance between the presence of ROS and antioxidant capacity can be a predictor of severity for various diseases such as asthma^{87,89} and diabetes⁹⁰. When the balance tilts in favor of oxidants over antioxidants, a state of oxidative stress is created confined by defined

spatio-temporal boundaries, which could be organism systemic or localized in specific tissues^{87,91}.

1.2.1 Reactive Oxygen Species

Based in the antimicrobial action of phagocytes and the presence of oxidized biomarkers in various diseases^{85,86}, the consensus was that bursts of extracellular ROS are considered to be harmful to host cells⁸⁸. However, the paradigm of ROS effects in the field of immunology has shifted to one where ROS is also indispensable for many cellular functions as part of intracellular signaling^{91,92}.

1.2.1.1 Chemical action of ROS

Oxidation is defined by a loss of electrons while reduction is defined by a gain of electrons. ROS can be extremely volatile radicals such as the hydroxyl radical which reacts with biopolymers at diffusion-controlled rates and the superoxide anion radical which has a half-life of milliseconds⁸⁷, or non-radicals such as hydrogen peroxide which is a relatively stable molecule⁹¹. DNA oxidation is a major contributor to genome instability and can lead to mutagenesis. Damage can be made to all four bases, as well as the deoxyribose, however the most susceptible to damage is guanine⁹³. A lesion in guanine can cause it to pair with adenine instead of cytosine and can cause transverse mutations after replication^{91,93}. Lipids are easily oxidized by radicals and are commonly used as biomarkers for oxidation⁹¹, while H₂O₂ can freely diffuse through the some membranes due to their uncharged nature⁸⁷ or use aquaporins to transverse less permeable membranes⁹⁴. As for proteins, radicals can damage multiple side-chain and backbone sites⁹⁵. However, less reactive ROS display selectivity in the residues targeted⁹¹. Modification by oxidation can result in increased side-chain hydrophilicity which could result in altered conformations as well as altered interactions with binding partners⁹⁵. In the case of mild H₂O₂, thiols in cysteine residues are oxidized resulting in sulfenic acid. This process of sulfenylation is reversible and can serve as a molecular

switch to change the conformation and interactions of a protein. Formation of a disulfide bond, glutathionylation, S-nitrosylation, S-acylation, and sulfenamide formation are other reversible thiol oxidative modifications and play roles in protein signal transduction akin to and at times associated with tyrosine phosphorylation^{96,97}. This vast array of modifications is exerted by ROS from a variety of sources.

1.2.1.2 Sources of ROS and redox signaling

Recognizing that ROS does not only have detrimental effects was rooted in the fact that mitochondria creates ROS as byproducts of cellular respiration⁹². To produce ATP, oxygen is the terminal electron acceptor for the NAD/NADH redox pair, and oxygen is reduced to water⁸⁷. However, it is estimated that 2% of the oxygen consumed by this process can create byproducts of superoxide and H₂O₂⁹⁸. Superoxide is produced by complex I and II of the mitochondria and released into the mitochondrial matrix. Here it is converted into H₂O₂ which can then freely diffuse into the cytosol⁹⁹. These were thought to be unwanted, but inevitable byproducts of metabolism. This perspective changed when H₂O₂ was found to be critical for processes such proliferation, differentiation, and migration through cysteine modifications^{100,101}. Another major source of intracellular ROS is the NADPH oxidase (Nox) complex which is expressed by many cell types but in particular, is the mode by which neutrophils, monocytes, and macrophages produce millimolar concentrations of ROS for the respiratory burst targeted towards pathogens⁹². In response to recognition of infection by TLRs¹⁰², the integral membrane catalytic subunit joins with regulatory subunits, and produce superoxide in a closed compartment called the phagosome, which protects the rest of the cell from damage^{92,103}. Prior to release toward the pathogen, superoxide is converted to a variety of ROS, such as H₂O₂ or peroxynitrite which is a reactive nitrogen species even more reactive than superoxide^{86,103}. Damage by ROS is largely compartmentalized and along with the action antioxidants, are maintained at tolerable levels at the single-cell scale.

In the event of an infection and recruitment of many inflammatory cells to a site which concomitantly produce ROS, deleterious effects are more likely. While cells will consume ROS using their antioxidants and create a ROS gradient across plasma membranes¹⁰⁴, excess ROS at concentrations produced by NOXs can cause mutations or even lead to apoptosis and necrosis^{105,106}. Homeostasis encapsulates all of the oxidative processes mentioned above through production of antioxidants and action of repair mechanisms, but it also includes equilibrium with oxidative environments external to the organism. A perpetual source of oxidants is in air that is inhaled into the lungs, which is well-suited for such a challenge since alveolus possess the high concentrations of glutathione, the predominant nonprotein thiol in cells⁸⁷. When antioxidants are overwhelmed, an altered equilibrium can develop by various adaptations toward ROS, where the presence of high concentrations of ROS are systemic and chronic. Such altered equilibria exist for airway diseases^{87,89}, alcohol abuse¹⁰⁷, and cancer^{108,109}. In the case of cancer, DNA mutations by ROS can lead activation of oncogenes and further stable production of ROS¹¹⁰. However, some studies have found that antioxidants can contribute to the maintenance and progression of this allostatic state^{110,111}, clearly demonstrating the complex nature of ROS regulation in cancer.

1.2.2 Effects of ROS specific to TCR triggering

In studying effector T cells, which exert their function at sites of inflammation (and therefore oxidation), it is imperative to take into consideration how ROS may influence their efficacy in battling infected cells.

1.2.2.1 T cell receptor redox biology

Despite there being no documented cases of TCR $\alpha\beta$ -chains sensitivity to oxidation by ROS, it is well documented T cell activation is closely related to ROS signaling⁹⁶. Early studies found that introduction of antioxidants inhibited proliferation and cytokine signaling by stimulated T cells¹¹²⁻¹¹⁵. Conflicting studies later found that

ROS stimulated T cell proliferation, in particular conditions^{116,117}. The controversy of whether ROS suppresses or enhances T cell function remains fully understood and likely varies between different T cell developmental stages and the sensitivity of individual molecules of the TCR signaling cascade. A wealth of studies has found that in response to TCR triggering by anti-CD3 crosslinking, T cells generate ROS within 15 minutes^{118,119}, but it was later determined that this ROS burst by Nox is not necessary for expression of activation markers¹²⁰. Another source of ROS in T cells following TCR triggering is the mitochondria. Since studies found that T cells undergo much higher glycolytic flux during T cell activation^{121,122}, Sena and colleagues examined the mitochondrial metabolism. They found that the mitochondria consumed oxygen more rapidly and produced ROS which was sufficient to support T cell activation⁹⁹. Interestingly, it was found that the mitochondria translocates under the TCR¹²³ and localized ROS production enhances phosphorylation of signaling proteins like Lck within 1 minute of TCR triggering¹²⁴. The relationship between ROS and TCR is complex and requires consideration of molecules associated with TCR in order to fully understand its impact on T cell activation.

1.2.2.2 Coreceptor and Lck redox biology

Along with the discovery that CD4 bound to MHC-II was the characterization of relatively higher binding affinity between CD4 and the HIV-1 envelope protein gp120^{125,126}. Once bound to CD4, gp120 undergoes a conformational change which allows interaction with chemokine receptors on the T cell surface, CCR5 and CXCR4¹²⁷. This step causes another conformational change in viral envelope which leads to fusion of the viral membrane with the host plasma membrane and release of viral particle contents into the host cytoplasm¹²⁸. Transmission of HIV-1 infection leads to tremendous loss of CD4+ T cell numbers, and consequently severely impaired immune function. A body of research has found that HIV-positive patients present glutathione antioxidant

deficiency compared to control subjects¹²⁹⁻¹³¹. The redox state of CD4⁺ T cells is important to consider because a disulfide bond in the D4 domain can mediate homodimer formation¹³² which has been reported to be important for TCR-pMHC signaling^{133,134}. However, this cell driven process can also leave the reduced form of CD4 to be susceptible to HIV-1¹³⁵. Indeed, it was shown that the reduced monomeric CD4 is the preferred ligand for HIV-1, as opposed to the oxidized form¹³⁵, and this interferes with formation of CD4 homodimers, which subsequently impairs signaling¹³⁶.

An analogous redox characterization has not been conducted for CD8, but both coreceptors associate with Lck which possesses cysteines critical to their function which are known to be sensitive to oxidation. By mutating cysteines C378, C465, and C476 to alanine, Lck displayed impaired kinase activity including trans-autophosphorylation¹³⁷. In this vein, specifically oxidizing Lck impaired its association with CD4, but this occurred at oxidant concentration greater than what was required to inhibit CD3 ITAM phosphorylation¹³⁸. In contrast, others have found that oxidation of free sulfhydryl groups led to phosphorylation of both the Lck catalytic Y394 and the inhibitory Y505¹³⁹. While the conformation of Lck may be modulated by cysteines, as seen even in HIV-1 patients¹⁴⁰, their activation state is likely indirectly modulated by ROS through phosphatases like CD45 or SHP-1 whose activity has been shown to be reversibly impaired upon oxidation^{141,142}. These large number of possible modifications on Lck and its regulatory phosphatases in response to ROS cause investigation of CD3 ITAMs in an oxidative environment to be convoluted. A more direct measure of ROS influence on TCR triggering could reconcile these seemingly contradictory findings.

1.2.2.3 Membrane cholesterol and actin redox biology

TCR, CD4, CD8, and Lck are anchored in a membrane made up of not only various phospholipids but microdomains of cholesterol. Relatively large aggregates of cholesterol and sphingolipids called lipid rafts have long been part of the ‘fluid mosaic’

model of the cell membrane¹⁴³, and are areas of higher density of surface proteins¹⁴⁴. TCR and its associated proteins were found to be in clusters of cholesterol¹⁴⁵⁻¹⁴⁷, and removal or oxidation of cholesterol would inhibit TCR-mediated signaling¹⁴⁸ and binding^{21,149}. Similarly, inhibition of actin polymerization can inhibit TCR-pMHC binding²¹. While TCR clusters have only been shown to indirectly interact with actin¹⁵⁰, associated signaling molecules further downstream have a direct link¹⁵¹. Oxidation of cofilin, which regulates actin disassembly and assembly is sufficient to cause T cell hyporesponsiveness^{152,153}. Interestingly, lipid rafts and actin seem to regulate each other. Despite actin not linking directly to lipid rafts, disruption of cholesterol will alter actin organization¹⁴⁴. Correspondingly, TCR-stimulated raft clustering depends on the reorganization of actin cytoskeleton¹⁵⁴. This relationship is likely centered on the TCR machinery which can associate with both actin and cholesterol. Recently, disrupting TCR binding to cholesterol using a naturally occurring analog, cholesterol sulfate, inhibited CD3 ITAM phosphorylation¹⁵⁵. Overall, the environment surrounding TCR heavily influences its signaling capacity.

1.3 Macrophage Immunobiology

Macrophages are myeloid derived cells that are present in most tissues throughout the body¹⁵⁶. They are differentiated from monocytes either from circulation, residing in tissues, or in bone marrow. It is imperative to note that macrophages can vary vastly in their functions between different anatomical compartments¹⁵⁶. For example, while lung interstitial macrophages and Kupffer cells in the liver are both highly phagocytic¹⁵⁷, they overexpress different surface markers that may play specialized roles for their local tissue microenvironment¹⁵⁸. Due to their plasticity, macrophages thus represent a model cell system to study how aspects of the environment can have profound effects on cell function.

1.3.1 Macrophage function

Macrophage effector functions span roles across homeostasis, development, and innate and adaptive immunity¹⁵⁹. The large diversity of function is exemplified in the case of alveolar macrophages which is involved in surfactant homeostasis¹⁶⁰, lung injury repair, and even lung tissue development¹⁵⁹. Furthermore, these macrophages serve as both an innate immune cells by phagocytosing particulate¹⁶¹, and an adaptive immune cells by presenting antigen to activate T cells in lung draining lymph nodes¹⁶², albeit at a relatively weaker efficiency^{163,164}. In support of achieving these functions, macrophages undergo activation which is generally defined as antigen-dependent microbicidal activity in response to an infection¹⁶⁵. Early work separated the differentiated states of activated macrophages, or polarizations, into two separate types: M1 and M2.

1.3.1.1 Polarization

The categorization of activated macrophages into M1 and M2 macrophages stemmed from prior work in distinguishing Th1 and Th2 type inflammation responses¹⁶⁵. This dichotomy has enabled comprehensive enumeration of the receptors that can activate macrophages, the intracellular signaling cascades that follow, and ultimately the proteins that are secreted by or expressed on macrophages¹⁶⁶. Briefly, macrophages can polarize to the M1 phenotype in response to LPS (which is a major cell wall component of gram-negative bacteria), IFN- γ , virus internalization, or GM-CSF while, polarization to the M2 phenotype can be induced by IL-4, IgG, IL-10, glucocorticoids, or M-CSF¹⁶⁵. Since the M1/M2 paradigm was studied in prototypical Th1/Th2 diseases, macrophages studied in other pathologies may display a mixed M1/M2 phenotype both in the stimuli they respond to and their effector functions, a finding that underscores the limitation in the current M1/M2 dichotomy paradigm¹⁶⁷.

1.3.1.2 Secretions

Macrophages will secrete various proteins and small molecules after stimulation by LPS. To directly destroy the source of LPS, macrophages can release large amounts of H₂O₂ through superoxide production by NOX complexes¹⁶¹. LPS stimulation can trigger the generation of proinflammatory cytokines like TNF α and IL-6, which increases vascular permeability and activates T and B cells, respectively³. Toward the resolution of clearance, alveolar macrophages can secrete TGF- β which inhibits DC-mediated activation of T cells and can contribute to tissue remodeling^{159,168}. Thus, these cells can play both positive and negative regulatory roles. This central role is exemplified in the airways where alveolar macrophages make up to 90% of the cellular content^{159,164,168}. Upon LPS recognition, macrophages generate chemokines CXCL10, CXCL11, and CCL2, which together recruit other immune cells to exert a more diverse repertoire of defenses^{164,165}. Interestingly, LPS can serve as an auto-chemokine for peritoneal macrophages through production of prostaglandins which would occur on the scale of hours¹⁶⁹. Altogether, these secretions center the macrophage as a proinflammatory hub.

1.3.1.3 Phagocytosis

Macrophages, along with neutrophils, are referred to as professional phagocytes because of their efficiency to engulf objects (cells, pathogens, or debris) larger than 0.5 μ m¹⁷⁰. Unlike receptor mediated endocytosis and pinocytosis, phagocytosis usually functions independent of clathrin and instead relies on actin reorganization. This process can be initiated by both Fc and complement receptors, which recognize particulate that have been opsonized by antibodies and complement, respectively¹⁷⁰. Triggering of these receptors leads to a cascade of phosphorylation events and reorganization of the actin machinery as seen by their enrichment at point contacts with the object¹⁷¹. Furthermore, internalization mediated by Fc-receptors is closely associated with generation of proinflammatory molecules¹⁷⁰. Thus, phagocytosis is a critical mechanism for

macrophages to clear infection. However, this process can be impaired by oxidative environments.

1.3.2 Development of oxidative stress in alcohol exposed macrophages

Excessive alcohol consumption is associated with tremendous clinical complications such as increased risk of acute respiratory distress syndrome (ARDS)^{172,173}. This disease has a mortality rate of 26%¹⁷⁴ and is characterized by the activation of systemic inflammatory cascades due to development of pulmonary edema caused by inflammation, trauma, or severe pneumonia¹⁷⁵. Another example is how alcohol use during pregnancy leads to a 34-fold increase in risk of premature delivery¹⁰⁷ and an increased risk of systemic infection known as sepsis^{176,177}. In a guinea pig model, *in utero* ethanol exposure led to oxidative stress in the developing lungs, as measured by glutathione content, which was associated with impaired alveolar macrophage function and increased risk of pneumonia¹⁷⁸⁻¹⁸⁰. Later in a mouse model of *in utero* ethanol exposure, the same group found that alveolar macrophage displayed not only impaired differentiation, but also impaired phagocytosis and dysfunctional TGF- β secretion¹⁸¹.

1.3.2.1 Upregulation of reactive oxygen species in macrophages

By exposing both primary and cell line macrophages to ethanol, Nox 1, Nox2, Nox4 and associated Phox proteins were expressed at higher levels, which was accompanied by greatly increased production of ROS¹⁸². With continuous exposure to ethanol, the increased in mRNA levels increased up to an apparent saturation point after 72 hours¹⁸². Thus, it is possible that chronic alcohol exposure can shift the immediate macrophage environment into a stable state of oxidative stress. In a later study, concurrent incubation of ethanol-treated alveolar macrophages with the critical antioxidant glutathione downregulated the increase, and this modulation improved phagocytosis. These results were corroborated when ethanol fed mice underwent oral

administration of glutathione. Therefore, there is a clear relationship between oxidative stress and macrophage state and function¹⁸³.

1.3.2.2 Association between oxidative stress and TLR4-LPS axis

To further understand risk factors associated with ARDS, a mouse model was developed which recapitulates the human acute phase^{184,185}. Surprisingly, this mouse model was resistant to LPS challenge and it was discovered that a mutation in the TLR4 receptor was responsible. The impaired TLR4 signaling was also associated with a decrease in oxidized phospholipids, suggestive of reduction in ROS presence¹⁸⁶. Another study found that when production of glutathione was inhibited by gene knockout of Nrf2, causing higher intracellular ROS, LPS-mediated TLR4 signaling improved. This was confirmed when a double knockout mouse model which also prevented ROS generation exhibited similar TLR4 signaling as Nrf2-positive cells¹⁸⁷. Recently, a mutual relationship was discovered whereby TLR4 deficiency abrogated ROS generation, which afforded accumulation of antioxidant capacity, reduced inflammation, decreased TGF- β deposition, and ultimately prevented hypertension-induced kidney injury¹⁸⁸. Supporting studies have found that TLR4 is rapidly shuttled to the membrane upon oxidative stress which may serve as a mechanism to prime macrophages for recognizing pathogens¹⁸⁹. In order to directly determine how oxidative stress influences TLR4 signaling, however, TLR4 binding to LPS must be considered.

1.3.3 TLR4 triggering by LPS

Among all the TLRs, TLR4 is the most well-studied and its signaling is triggered by LPS ligation, but requires a set of additional proteins¹⁹⁰. CD14 was long considered to be a receptor for LPS, because antibody blockade of CD14 abrogated TNF- α secretion¹⁹¹. However, CD14-LPS binding triggered variable signaling cascades than those from TLR4-LPS binding¹⁹². While the receptor for LPS was in the process of being determined, lipid binding protein (LBP) was shown to be critical in the macrophage

response to LPS¹⁹³. Once TLR4 was confirmed to be the primary receptor for LPS, a secreted glycoprotein, MD-2, was shown to associate with TLR4 and confer its sensitivity to LPS^{194,195}. Associations between TLR4, LPS, and MD-2 were corroborated upon determination of the multi-molecular crystal structure. Together, they form an M-shaped multimer made up of two copies of the TLR4-LPS-MD-2 trimolecular complex¹⁹⁶. Dimerization of the two copies creates a platform for adaptor molecules like MyD88¹⁹⁷ and TRIF to initiate a signaling cascade. SPR was conducted to measure the binding affinities between these various molecules. Using soluble mouse proteins, MD-2-LPS interactions had a K_D of 2 μ M; CD14-LPS had a K_D of 9 μ M, and TLR4-LPS had a K_D of 14 μ M¹⁹⁸. Meanwhile, human LBP was shown to have almost 4 nM affinity to LPS¹⁹⁹. Interestingly, progressive association such as LBP-LPS-CD14 from CD14-LPS, or MD-2-LPS-TLR4 from LPS-TLR4, greatly enhanced association to LPS²⁰⁰. These findings support a model where LBP binds to LPS; the LBP-LPS complex binds to CD14 and is extracted from the bacterial membrane; LPS is transferred to TLR4-MD-2; and the TLR4-LPS-MD-2 trimolecular complex undergoes conformational changes to allow the cascade inducing dimerization¹⁹⁶. Thus, binding studies played a critical role in resolving the convoluted complexing of LPS to macrophage receptors. While binding kinetics between the TLR4-MD-2 bimolecular complex and LPS have not been reported, recently it was found that real-time binding between a damage-associated molecular pattern and TLR4 induced macrophage stiffening²⁰¹. Taken together, binding studies conducted on macrophages experiencing oxidative stress could be a powerful approach to more directly understand how TLR4 signaling is modulated by ROS.

CHAPTER 2 SPECIFIC AIMS AND HYPOTHESES

Molecular interactions propagate physical and biochemical signals, ultimately resulting in cellular functions. Often, these interactions involve many molecular species as a means of specializing signal transduction. Furthermore, protein interactions are subject to dynamic soluble extracellular microenvironments. Characterizations of multi-molecular interactions and an investigation of how biochemical perturbations imposed in tandem could influence signal transduction are therefore warranted. To understand this central theme, the model TCR-pMHC-CD4 system was employed to characterize trimolecular interplay. Next, an analogous CD8 coreceptor system was studied to understand how a pathological oxidative environment can influence trimolecular interactions. Lastly, framework from the T cell model was used to study the macrophage TLR4-LPS system whose signal transduction responds with profound plasticity to oxidative environments.

Aim 1: Delineated the role of CD4 co-receptor in T cell receptor triggering

Hypothesis: CD4 binds to TCR-engaged pMHC-II to prolong lifetime of complex

Aim 1a: Detected CD4 coreceptor and trimolecular binding

Aim 1b: Mathematically characterized trimolecular kinetics

Aim 1c: Distinguished purified kinetics to cellular system kinetics

Aim 2: Quantified the effect of H₂O₂ environment on T cell receptor binding

Hypothesis: TCR binding to pMHC-I will be impaired in presence of H₂O₂.

Aim 2a: Developed real-time adhesion frequency assay for ROS study

Aim 2b: Deconvoluted signaling molecules responsible for impaired recognition

Aim 3: Determine the role of TLR4-LPS binding in ROS-impaired function

Hypothesis: TLR4-LPS binding is impaired in an oxidative stress environment

Aim 3a: Conducted real-time micropipette assay for TLR4-LPS binding under ROS

Aim 3b: Imaged movement of macrophages in response to LPS under oxidative stress

CHAPTER 3 Aim 1

Delineating the role of CD4 coreceptor in T cell receptor triggering. A fundamental piece of information missing in the controversy over the role of CD4 in TCR triggering are kinetic measurements of CD4 to MHC-II and an experimentally-determined contribution of CD4 to TCR-pMHC-II association. Since it was found²¹ that constraining the receptor-ligand pair in their respective membranes upon engagement greatly amplifies the difference in on-rates for point mutations within the peptide; affinity and on-rate measurements correlate more closely to peptide potency than the same measurements made by SPR do; and deformations in the ultra-sensitive red blood cell membrane is able to detect lower affinity binding events than capable via SPR, the micropipette adhesion frequency assay was employed to measure CD4 binding to peptide-human leukocyte antigen (pHLA), which is the human analog to pMHC. The same approach was used to measure the trimolecular interaction between TCR-pHLA-CD4, and parameters from these experiments were inputted into a mathematical model to characterize the contribution of CD4 to TCR-pHLA interaction.

3.1 Methods

3.1.1 Materials

Polylink bead coupling kit and 6µm carboxylated polystyrene beads were purchased from Polysciences, Inc. (Warrington, PA). The kit included a polylink coupling buffer, polylink wash/storage buffer, and polylink EDAC. Calbiochem brand Biotin-PEG-NHS for biotinylation of RBCs were purchased from Millipore Sigma (Burlington, MA). Coverslips for micropipette chambers were purchased from Fisher Scientific (Hampton, NH). RPMI1640 + glutamine with no calcium or magnesium, 1X PBS, L15, and 1X HBSS was purchased from Corning Inc. (Corning, NY). PE Quantibrite calibration beads and PE-conjugated antibodies were purchased from BD

Biosciences (San Jose, CA). TCR was stained with PE-conjugated anti-human TCR- β 1 chain clone JOVI.1. CD4 was stained with PE-conjugated anti-human CD4 clone OKT4. pHLA was stained with PE-conjugated anti-human HLA-DR clone L243. Fluo-4 AM was purchased from ThermoFisher (Waltham, MA). Nucleofection kit was purchased from Lonza (Morristown, NJ). Plasmids for full-length TCR and CD4 were purchased and prepared by Genscript (Piscataway, NJ). Peptides were also purchased from Genscript and were loaded onto biotinylated HLA-DR monomers by the Yerkes National Institutes of Health Tetramer Core facility (Atlanta, GA). Completed pHLA were stored at -20°C in 50% glycerol/PBS and a fresh aliquot was used in each experiment. Biotinylated E8 TCR and CD4 were generously gifted by Roy Mariuzza at the University of Maryland. Divalent streptavidin was generously gifted by Baoyu Liu at the University of Utah. All other reagents were purchased from Sigma Aldrich (St. Louis, MO).

3.1.1.1 Acquisition of Cells

For adhesion frequency experiments, whole blood was isolated by phlebotomists from healthy volunteers at the Stamps Health Center at the Georgia Institute of Technology according to a Georgia Institute of Technology IRB-approved protocol. For BFP experiments, human RBCs were isolated from whole blood of healthy volunteers by finger prick according to a Georgia Institute of Technology IRB-approved protocol. TCR β -chain deficient Jurkat J.RT3 cells were purchased from ATCC (Manassas, VA). J.RT3 cells were transfected with the plasmid for full length E8 TCR using retroviral transduction. Briefly, plasmid was amplified using a stable E. Coli and amplified DNA was isolated. Purified DNA was combined with VSV-G envelope protein and psPAX2 in optimum with lipofectamine and cultured with 293T cells. Finally, viral supernatant was incubated with J.RT3 cells, surviving cells were taken for Fluorescence activated cell sorting (FACS) by BD Aria. Cells were sorted three times to ensure narrow and stable surface expression levels of E8 TCR. Subsequently, Jurkat cells with varying surface

expression levels were electroporated with plasmid for full length CD4 within supplemented media using the Amaxa Nucleofector II (Lonza). After a resting period of two days in supplemented media, cells were cultured for one week with periodic passaging before taken for FACS by the BD Aria. Cells were sorted three times to ensure narrow and stable surface expression levels of CD4 that were consistent between all cell lines.

3.1.1.2 Preparation of Cells and Beads

3.1.1.2.1 *Preparation of RBCs for adhesion frequency*

Whole blood was isolated by phlebotomists from healthy volunteers at the Stamps Health Center at the Georgia Institute of Technology according to a Georgia Institute of Technology IRB-approved protocol. Histopaque-1077 was added to the bottom of the tube of RBCs and the suspension was centrifuged. Supernatant containing all cells except for RBCs were discarded and the RBCs were washed and resuspended in ice cold 1X PBS. Following buffer exchange into EAS-45 (2 mM Adenine, 110 mM D-glucose, 55 mM D-Mannitol, 50 mM Sodium Chloride, 20 mM Sodium Phosphate, 10 mM L-glutamine), aliquots of RBCs were mixed with biotin-3400-NHS at a pH of 7.2 for 30 minutes at room temperature. The ratio between RBCs and biotin-3400-NHS were varied to increase the site density of biotin on the surface of RBCs. Controlled biotin sites allowed for defined sites of biotinylated protein when saturating concentrations of proteins were incubated with biotinylated RBCs. 200 $\mu\text{g}/\text{mL}$ divalent streptavidin was incubated with RBCs for 20 minutes at room temperature. Following exhaustive washing of RBCs with ice cold EAS-45, biotinylated OT1-TCR or OVA-MHC-I at a concentration of 20 $\mu\text{g}/\text{mL}$ were incubated with RBCs for 30 minutes at room temperature. RBCs were washed twice with ice cold 1X PBS + 2% BSA and aliquots would be taken for site density measurements by flow cytometry.

3.1.1.2.2 Preparation of RBCs and beads for Biomembrane Force Probe

Freshly isolated human RBCs were biotinylated by covalently linking to biotin-PEG3500-NHS by 30 min incubation at 25°C. Biotinylated RBCs were then incubated with nystatin in N2 buffer (265.2 mM KCl, 38.8 mM NaCl, 0.94 mM KH₂PO₄, 4.74 mM Na₂HPO₄, 27 mM sucrose; pH 7.2 at 588 mOsm) for 30 min at 0°C. Nystatin-loaded biotinylated RBCs were washed twice with and stored in N2 buffer at 4°C for later use in BFP experiments. To coat proteins on beads, borosilicate glass beads were mercapto-propyl silanated and covalently functionalized to monovalent streptavidin-maleimide in phosphate buffer saline (pH 6.8) by overnight incubation at 25°C. Streptavidinylated beads were then incubated with sub-saturating concentrations of biotinylated pHLA, TCR, CD4, or mixtures of protein for 2 hours in HBSS + 2% BSA at 4°C. After coating, beads were stored at 0-4°C to improve stability.

3.1.2 Binding Assay

3.1.2.1 Micropipette Adhesion Frequency

3.1.2.1.1 Coating strategy

Biotinylated RBCs of a specified site density were incubated with 0.2 mg/mL divalent streptavidin for 30 minutes at 4°C, washed exhaustively, then incubated with 20 µg/mL biotinylated TCR, CD4, or pMHC monomers for 30 minutes at 4°C. For mixture coatings, soluble TCR was mixed with CD4 at specified molar ratios and then added to washed streptavidinylated RBCs. Table 3 describes optimized ratios of monomer concentrations in order to achieve specific ratio of coated proteins as quantified by flow cytometry described below.

3.1.2.1.2 Site density determination

Beads or RBCs were incubated with antibodies corresponding to their protein functionalized surfaces for 30 minutes at 25°C using a saturating antibody concentrations. Following three washes and resuspension in 1X PBS + 2% BSA, beads and RBCs were analyzed using the BD Accuri Flow Cytometer FL2 channel for PE excitation and detection. Fluorescence measurements were compared with BD Quantibrite PE calibration beads in order to calculate the number of proteins on the surface of beads. Briefly, fluorescence from beads of four different sizes and with different known number of PE-fluorochromes were used to create a well-fitted ($R^2 > 0.97$) linear regression between the log of mean fluorescence intensity and the log of PE molecule count. The regression was used to back-calculate the fluorescence from PE-stained beads and RBCs.

3.1.2.1.3 Micropipette Adhesion Frequency Assay

This assay used sub-micron scale manipulation to bring into contact a pair of RBCs with ultrasensitive membranes coated with either a receptor or cognate ligand to visually amplify the presence of adhesion at the end of the contact of controlled contact area and contact time. The repeated motions of impingement and retraction were controlled by a piezoelectric actuator. This micropipette apparatus approach is higher throughput than the BFP assay in collecting affinity measurements and was therefore used initially to measure kinetics between purified proteins coated on the RBCs. Upon obtaining kinetic measurements from purified proteins, translating into a cell system required using the BFP assay because human RBCs express CD58 which binds to CD2 which is highly expressed on human derived Jurkat cells.

Pipettes were individually forged to under 1 μm in opening diameter to allow the biotinylated RBC to aspirate and adopt a surface tension that cannot be seen to fluctuate under the microscope. In the field of view were two opposing pipettes- one aspirated an RBC with pHLA while the other aspirated an RBC with TCR alone, wtCD4 alone,

mtCD4 alone, a mixture between TCR and wtCD4, or a mixture between TCR and mtCD4 (Figure 1A). The experiment was conducted under a microscope within a chamber containing a non-CO₂ dependent L15 media supplemented with HEPES to maintain pH and 2% BSA to minimize non-specific adhesions. This media was then sealed with mineral oil to prevent changes in osmolarity during the experiment.

First, the adhesion frequency must be optimized for contact time and site density of interacting proteins. RBCs with various biotin binding sites were used to coat with biotinylated protein, and those with 20-30% adhesion frequency at long contact times (4 seconds was initially assumed to be long because the likelihood of binding 20-30% for most adhesion molecule bonds and strong TCR-pMHC bonds such as OT1 TCR:OVA pMHC would saturate at 2 seconds) were from then on out used as reference site densities. Adhesion frequency was estimated from 50 cyclically repeated contacts of a single pair of RBCs and a mean adhesion frequency would be determined from a stated number of different RBC pairs. Each cycle would consist of 0.5 seconds of approaching over about 10 μ m until the RBCs are in contact (but not visibly impinging), a defined contact time, 0.5 seconds of retraction over 10 μ m back to the 0 μ m baseline, and 0.5 seconds of pausing before the next cycle begins. Adhesion events would be recorded in binary with '1' indicating an adhesive event and '0' indicating no adhesion. An average of values between 50 contacts yields the 'adhesion frequency' for a given contact time. Then, adhesion frequency curves were constructed by measuring adhesion frequency against increasing contact times until saturation would clearly occur (assumed here to not be changing in adhesion frequency for three progressively doubling contact times, (Figure 1B). A Poisson-based probabilistic model for adhesion kinetics mediated by a small number of bonds predicts the average number of bonds formed to be related to the adhesion frequency. $\langle n \rangle$ for a given contact area (assumed to be 3 μ m² between RBCs) is related to the concentration of interacting species, the affinity of the interaction, the off-rate, and the corresponding contact time between cells (Figure 1D). Thus, the 2D

effective affinity can be extracted based on adhesion frequency (Figure 1C). After saturation contact times were determined for all tested interacting species coatings, only the shortest saturating contact times would be used for further experiments comparing 2D affinity or $\langle n \rangle$ values, in order to achieve a higher throughput collection of data.

Non-specific controls were conducted for all sets of species coatings. To do so, RBCs coated with divalent streptavidin anchored irrelevant protein were brought into contact with RBCs coated with proteins of interest. An adhesion frequency curve would be obtained for nonspecific adhesion. Then, for each contact time, the distribution of nonspecific adhesion frequency would be subtracted from the measured distribution of adhesion frequency (Figure 1E).

3.1.2.2 Biomembrane Force Probe

3.1.2.2.1 *Coating*

Sub-saturating concentrations were used to coat proteins on the glass BFP beads to ensure low adhesion frequency ($\leq 20\%$) is achieved for single-molecule measurements, and for there to be sufficient streptavidin site for strong attachment to biotinylated RBC. Proteins were incubated with streptavidinylated beads at a concentration of 4 ng/mL in HBSS + 2% BSA for 2 hours at 4°C, then washed using ice cold HBSS + 2% BSA.

3.1.2.2.2 *Assay*

This assay leverages the ultra-sensitive RBC membrane as in micropipette but instead of only observing the presence of adhesive events, the deformations are quantified by tracking the interface between the RBC membrane and glass bead surface using a high-speed camera. These deformations in distance are converted to force using the spring constant of the nystatin expanded RBC. The derivation and a characterization of spring constant transformation are described elsewhere^{202,203} and depends on the diameter of the micropipette, the size of the RBC, and the size of the interface between

RBC and bead. Accordingly, micropipettes to hold the BFP were forged to be between 1.7 μm and 2.2 μm . Outside this range, the equations used to derive spring constant are not applicable. The BFP would be constructed as follows: A micropipette was calibrated for zero aspiration for every BFP that was constructed. From this baseline, an RBC was firmly aspirated. Then, an opposing pipette aspirating a protein-coated glass bead impinged the bead against the apex of the RBC. Finally, the bead was released from its pipette to complete the BFP (Figure 2 A and B). What was formerly the bead pipette was then free to aspirate the target cell. To calibrate the constant for every BFP used, the opening diameter of the RBC-aspirating micropipette is measured, along with the diameter of the RBC and the diameter of the contact area between the glass bead and the RBC. These values are inserted into a calibration equation described elsewhere²⁰², and an aspirating pressure to obtain an RBC spring constant of 0.3 pN/nm is outputted. The aspirating pressure is accordingly adjusted in relation to the baseline zero pressure, and at this point the BFP assay was ready to be executed.

In the BFP assay, nonspecific adhesions were tested first because higher adhesion frequencies yield a higher probability of multiple bonds forming simultaneously. Thus, the contact time and buffer were optimized to minimize the nonspecific adhesion to below 3%. Jurkat cells were taken directly from incubator at 37°C within RPMI1640 + 10% FBS (hereon abbreviated as R10), concentrated, and then injected into the L15 + 2% BSA supplemented chamber media sealed with mineral oil. The cells were allowed to equilibrate to the new chamber media for 20 minutes before proceeding with the testing of nonspecific adhesions, which was then followed by testing experimental groups.

Typically, 15 minutes of repeated cycles of contact between the Jurkat cell (or bead) against the BFP were conducted. Careful micromanipulation was constantly administered in order to achieve a contact profile that is normal (does not experience shearing forces). Common unsuitable force profiles would involve dragging of the interface, or lack of contact. Additionally, for a majority of Jurkat cells, adhesion was not

detected for the first 30-50 contacts. The 15 minutes of contact included the first 30-50 cycles of no adhesion.

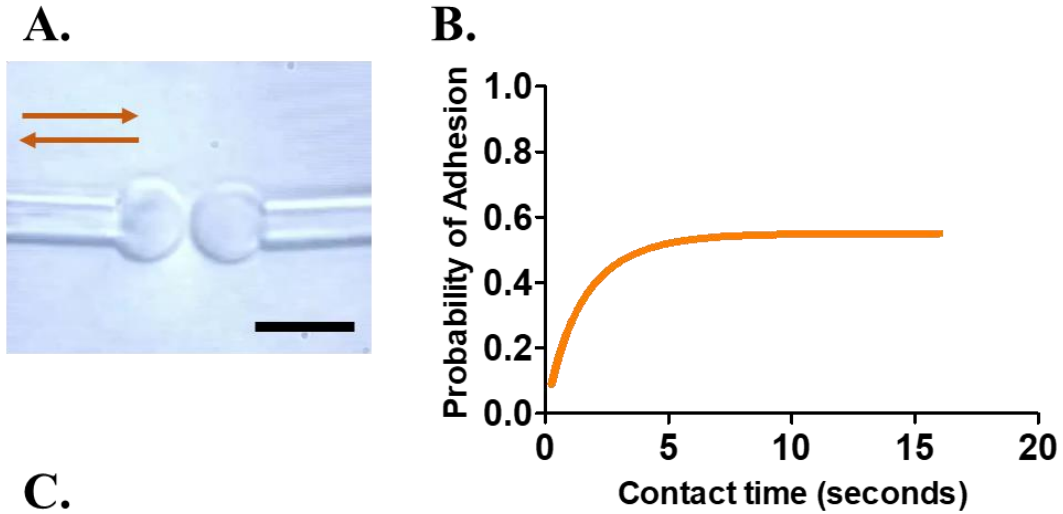
The force spectroscopy mode conducted with BFP was a force-clamp (Figure 2C and D). A force value would be predefined at which the molecular bond was maintained. As the cell impinged the BFP, the force profile read a negative value indicative of force being exerted on the BFP. This force value was maintained at the predefined compression force for the duration of the predefined contact time. At the end of the contact time, the force profile would rapidly ramp increasingly positive until it reached the clamp force, at which it the position of the cell is maintained at until the molecules would reach their bond lifetime and dissociate back to the baseline thermal fluctuation force values of the RBC. Several hundred events would be collected for each clamp force across many different BFP-cell pairs and these values were analyzed.

Every single force profile was analyzed. Adhesion frequency was collected as described in Section 3.1.2.1 between both the presence and absence of bond formation. Successful bond formations were more carefully analyzed using in-house Labview programs. Bond lifetime (from the beginning of force clamp value to the instant the bond dissociates) and bond stiffness (the force experienced by the bond over an extension of the molecular bond) were cataloged. The bond lifetimes are binned by forces and all bond lifetimes within each bin are plotted together as survival curves (log of fraction of bonds lasting longer than a given bond lifetime) fitted to a two-state model for TCR-pHLA bonds and trimolecular bonds, and a one-state model for CD4-HLA bonds. Once a good fit is achieved, all lifetimes within each bin are averaged and plotted against their respective average force.

3.1.2.2.3 Stiffness Assay

The stiffnesses of molecular bonds were modeled as Hookean spring constants which encapsulates the proportionality between the force exerted on a spring and the

distance traveled over the exertion (Figure 2 E and F). Stiffness was measured from the ramping phase of the BFP test cycle. The difference between the displacements of the bead tracking system and the displacements of the piezoelectric actuator-capacitance sensor feedback system yielded the distance at which the molecular springs were experiencing force. Two straight lines were fitted to the piecewise data: One was fitted to the compressive force regime where the bead was slowly ramping away from cell impingement (force < 0). The other was fitted to the tensile force regime where the bead would ramp away from the cell beyond the point of initial contact (force > 0). In this analysis, it is assumed that the magnitude of force on the cell membrane is identical in cell compression as it is in tension. Hooke's law for springs in series is illustrated in Figure 2E and F. The slopes from the two fitted lines provided the spring constants for the cell and the cell-molecule system, respectively. Thus, the spring constant was derived using the equation in Figure 2E and F. An ensemble of molecular spring constant was collected as histograms using similar force bins in the average bond lifetime analyses. Single or double Gaussian distributions were used to fit the histograms. These histograms were then used to estimate the number of molecular bonds that were bimolecular or trimolecular in nature.



C.

$$P_a = 1 - \exp(-\langle n \rangle)$$

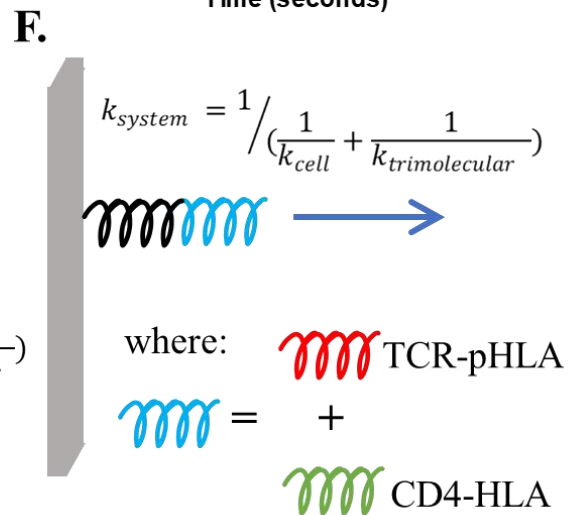
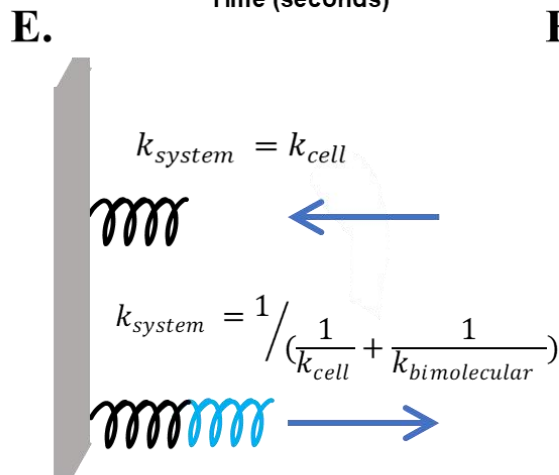
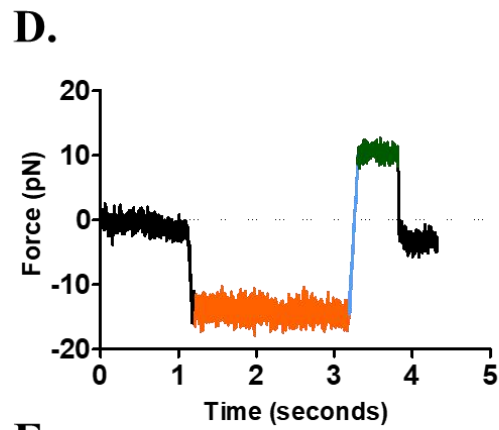
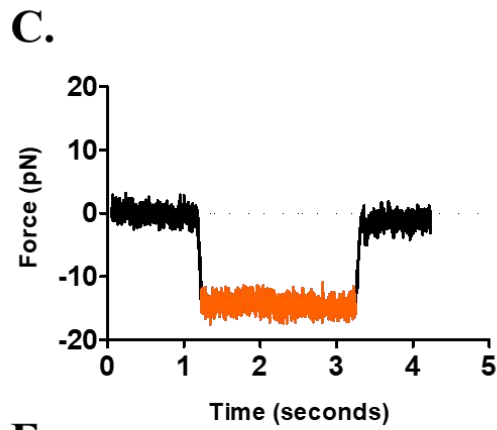
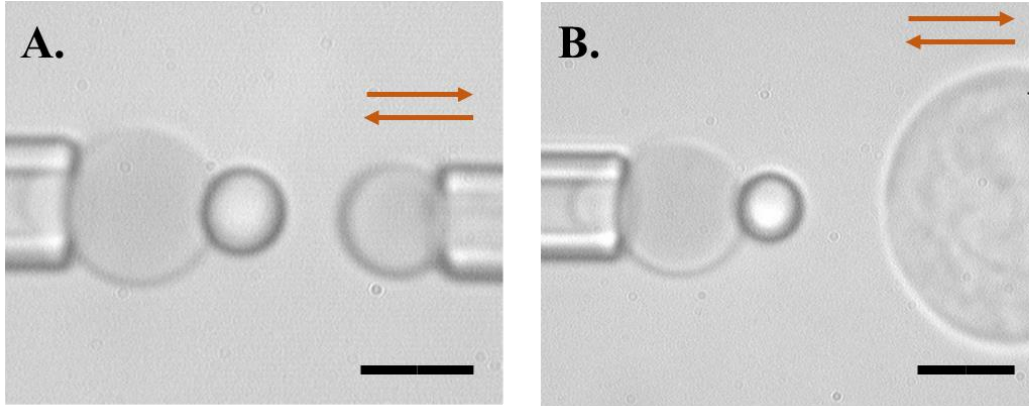
D.

$$\langle n \rangle = m_r m_l A_c K_a [1 - \exp(-k_{\text{off}} t_c)]$$

E.

$$P_a = \frac{P_{\text{measured}} - P_{\text{nonspecific}}}{1 - P_{\text{nonspecific}}}$$

Figure 1. Micropipette Adhesion Frequency Assay (A) Microscopic view of two aspirated RBCs each coated with proteins brought into contact with one another by a piezoelectric actuator attached to the left micropipette. Scale bar 4 μm . (B) Schematic depicting probability of adhesion plotted against varying contact times between cells in A. (C) Poisson distribution describing how the average number of events of a defined scenario is related the probability of the events occurring. (D) Equality describing the parameters constraining the average number of events that can occur. (E) Calculation to subtract nonspecific adhesions from the observed adhesion frequencies to yield the effective probability of adhesions that can be normalized in C.



3.1.3 Mathematical Characterization

The poisson-based model for 2D affinity in adhesion frequency was derived for a bimolecular interaction and does not apply for three interacting species. An extension of

Figure 2. Biomembrane Force Probe assay and analysis.

(A) Microscopic view of BFP opposite from the target cell which was an RBC or a bead. This depicts a scenario where purified pHLA was coated on the glass bead (placed on the apex of an RBC), while TCR and CD4 (either individually or as a mixture) was coated on the target cell. The target cell moved by a piezoelectric actuator which responded to the high-speed tracking of the interface between the RBC and the glass bead on the left. Scale bar is 4 μm . (B) Microscopic view of BFP coated with pHLA opposite from a Jurkat cell expressing TCR, CD4, or a mixture of both at different ratios. The Jurkat cell moved by a piezoelectric actuator which responded to the high-speed tracking of the interface between the RBC and the glass bead on the left. Scale bar is 4 μm . (C) Representative data depicting a BFP assay cycle where no adhesion event occurred. The black trace depicts the thermal fluctuation exhibited by the BFP which was tracked by the interface between the RBC and the glass bead. The orange trace depicts the period when the BFP and the target cell were impinged against one another at a predefined force. (D) Representative data depicting a BFP force clamp assay cycle where an adhesion event occurred. The black trace depicts the thermal fluctuation exhibited by the BFP which was tracked by the interface between the RBC and the glass bead. The orange trace depicts the period when the BFP and the target cell were impinged against one another at a predefined force. The blue trace depicts the ramping phase where the cells remained associated through a single-molecule scale molecular bond which was held at a predefined clamp force. The green trace depicts the bond lifetime duration two molecules remained associated to each other until dissociation which was described by the interaction off-rate. (E) Schematic representing the BFP and target cell as a system of Hookean Springs. The upper spring was experiencing a compressive force and the stiffness described by this system is equivalent to the stiffness of the target cell. The lower system was modeled as two springs in series experiencing a tensile force. The black spring represents the stiffness of the target cell, while the blue spring represents the stiffness of the bimolecular bond. The equation describing the relation between spring constants is displayed. (F) Schematic representing the BFP and target cell as a system of Hookean Springs. The system was modeled as two springs in series experiencing a tensile force. The black spring represents the stiffness of the target cell, while the blue spring represents the stiffness of the trimolecular bond. The trimolecular bond, however, was modeled as two springs in parallel. When exerted in parallel, two spring constants are additive. The equation describing the relation between spring constants is displayed.

the model is derived for the trimolecular case and is described here. The trimolecular association was modeled using mass action kinetics. Depicted in Figure 3, in pathway within a system describes the association of TCR and pHLA and subsequently the association with CD4 to yield the trimolecular complex. The trimolecular complex can be dissociated in the reverse direction or by dissociating TCR first and subsequently CD4.

These two pathways were driven by kinetic on- and corresponding off-rates and exist in equilibrium.

A more simplified view of the above system separated the two pathways into individual ones. Consequently, on- and off-rates describing the first association of the mutually exclusive species did not exist (Figure 4). The resulting average number of bonds formed between two molecules was derived as in section 3.1.2.1.3, and previously²¹. However, the average number of bonds formed between three different species was proportional to the concentration of not two, but all three interacting species, the contact area between cells, and the affinities for two different bimolecular interactions. The total number of bonds observed during an experimental cycle, was therefore described as the sum between trimolecular bonds and any bimolecular bonds from the previous reaction step. When no cooperativity was assumed, that is, the on- and off-rates of TCR to pHLA does not differ from the on- and off-rates of TCR to pHLA-CD4; or the on- and off-rates of CD4 to HLA does not differ from the on- and off-rates of CD4 to TCR-pHLA, the affinities would between these aforementioned steps did not change either. Thus, the trimolecular expressions for average number of bonds formed between the two independent pathways were equivalent. This permitted combining the two pathways (Figure 4), to describe a uniform case of no cooperativity, whereby the total number of bonds observed experimentally was predicted to be the sum of the trimolecular bonds and the two separate bimolecular bonds.

To characterize a scenario of cooperativity, the following assumptions were made (Figure 4). The first was that the on-rate of TCR to pHLA was proportional to the on-rate of TCR to pHLA-CD4 by a scalar 'a'. This scalar encapsulated any influence or conformational change that may occur after the first bimolecular bond. The corresponding off-rates were assumed to be proportional by a scalar 'b'. This scalar encapsulated any change in dissociation from the trimolecular complex compared to dissociation from a bimolecular interaction. Next, the on-rate of CD4 to HLA was

proportional to the on-rate of CD4 to TCR-pHLA by a scalar 'c'. This scalar encapsulated any influence or conformational change that may occur after the first bimolecular bond. Importantly, the fourth assumption was that the off-rate proportionality in this CD4 association pathway, was equivalent to the off-rate proportionality in the TCR association pathway. This assumption was made because any change in bond lifetime is only afforded by the single trimolecular complex. In other words, the branching out into two different pathways which dissociate TCR and CD4 respectively, are reciprocally stabilizing. Additionally, the off-rates between different species measured in this study as well as those measured previously were similar or at least on the same order of magnitude, which were in contrast to measurements made for on-rates which have been shown to vary greatly even with one amino acid difference²¹. These assumptions simplified the construction of mass action expressions for the network of reactions in Figure 3. As detailed further in Appendix A.2, the kinetic equations were constructed by mass action equating the rate of bond formation to associations as positive species and dissociations as negative species. These were then translated into vector form and were solved for an equilibrium solution where bond formation does not change with time. It was determined that the vector describing the difference between the equilibrium set of bond formation and the set of bond formation at any time satisfied a homogenous differential equation. Therefore, analytical solutions for bond formation between the bimolecular species, the trimolecular species, and the total observed bonds was solved. Finally, using the scalar a, b, and c assumptions, the solutions were simplified to yield the expressions in Figure 5.

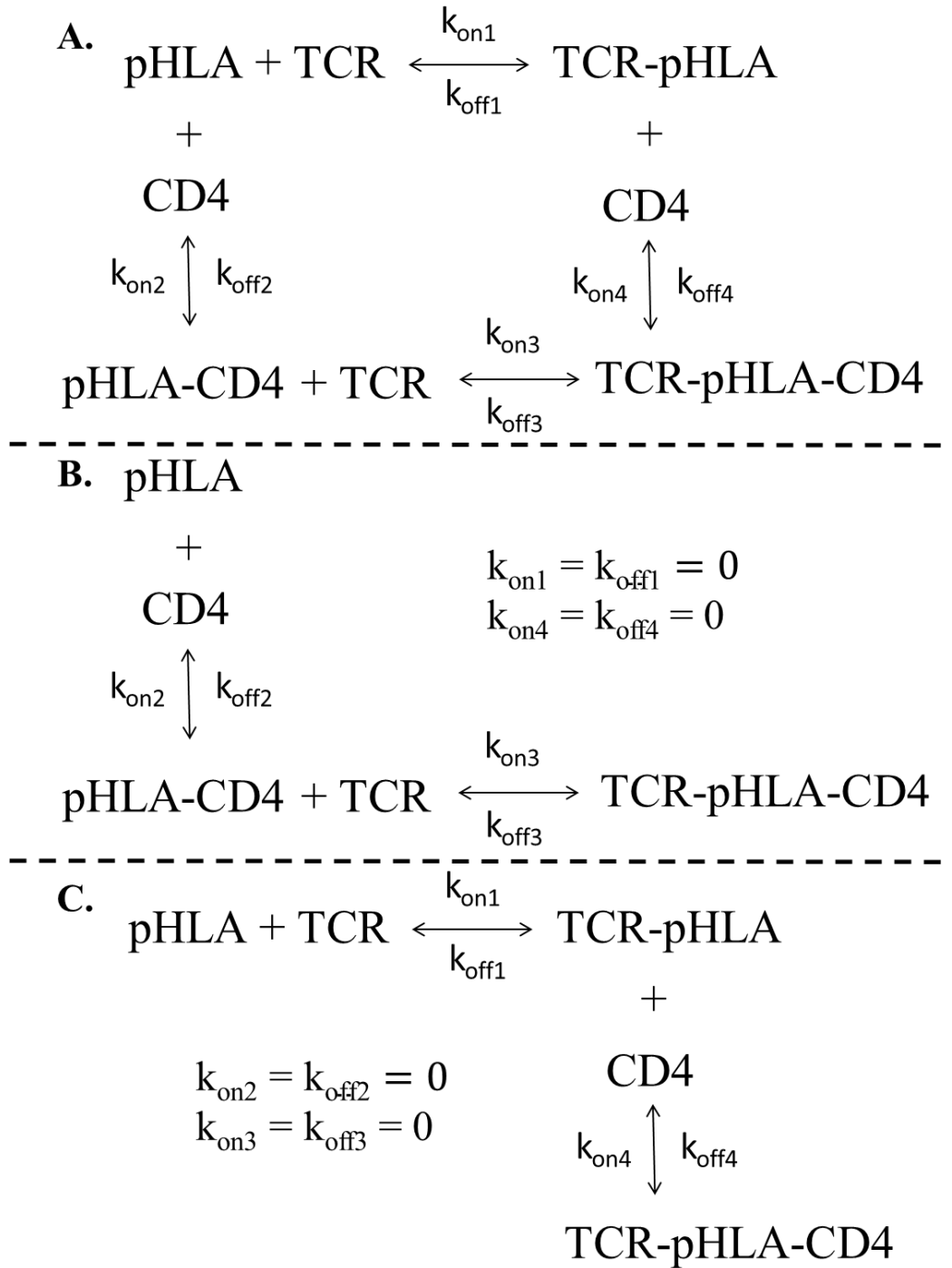


Figure 3. Reactions between TCR, pHLA, and CD4. (A) Diagram depicting the equilibrium chemical reactions between the three species TCR, pHLA, and CD4 along with their respective kinetic rates. (B) Simplified diagram from A depicting CD4 and HLA association first, then associating with TCR. (C) Simplified diagram from A depicting TCR and pHLA associating first then associating with CD4.

$$\mathbf{A.} \quad \begin{aligned} k_{\text{on}2} &= k_{\text{off}2} = 0 \\ k_{\text{on}3} &= k_{\text{off}3} = 0 \end{aligned}$$

$$\begin{aligned} \langle n \rangle_{\text{TCR},\infty} &= m_{\text{TCR}} m_{\text{pHLA}} A_c K_{a1} \\ \langle n \rangle_{\text{tri},\infty} &= m_{\text{TCR}} m_{\text{CD4}} m_{\text{pHLA}} A_c K_{a1} K_{a4} \\ \langle n \rangle_{\text{total},\infty} &= m_{\text{TCR}} m_{\text{pHLA}} A_c K_{a1} (1 + m_{\text{CD4}} K_{a4}) \end{aligned}$$

$$\mathbf{B.} \quad \begin{aligned} k_{\text{on}1} &= k_{\text{off}1} = 0 \\ k_{\text{on}4} &= k_{\text{off}4} = 0 \end{aligned}$$

$$\begin{aligned} \langle n \rangle_{\text{CD4},\infty} &= m_{\text{CD4}} m_{\text{pHLA}} A_c K_{a2} \\ \langle n \rangle_{\text{tri},\infty} &= m_{\text{TCR}} m_{\text{CD4}} m_{\text{pHLA}} A_c K_{a3} K_{a2} \\ \langle n \rangle_{\text{total},\infty} &= m_{\text{CD4}} m_{\text{pHLA}} A_c K_{a2} (1 + m_{\text{TCR}} K_{a3}) \end{aligned}$$

C. The case of no cooperativity:

$$k_{\text{on}1} = k_{\text{on}3}, k_{\text{off}1} = k_{\text{off}3}, k_{\text{on}2} = k_{\text{on}4}, k_{\text{off}2} = k_{\text{off}4}$$

$$\begin{aligned} \langle n \rangle_{\text{TCR},\infty} &= m_{\text{TCR}} m_{\text{pHLA}} A_c K_{a1} \\ \langle n \rangle_{\text{CD4},\infty} &= m_{\text{CD4}} m_{\text{pHLA}} A_c K_{a2} \\ \langle n \rangle_{\text{tri},\infty} &= m_{\text{TCR}} m_{\text{CD4}} m_{\text{pHLA}} A_c K_{a1} K_{a2} \end{aligned}$$

$$\langle n \rangle_{\text{total},\infty} = m_{\text{TCR}} m_{\text{CD4}} m_{\text{pHLA}} A_c K_{a1} K_{a2} + m_{\text{TCR}} m_{\text{pHLA}} A_c K_{a1} + m_{\text{CD4}} m_{\text{pHLA}} A_c K_{a2}$$

Figure 4. Analytical solutions for bond formations assuming no cooperativity. (A) Assumptions and analytical solutions for bond formations depicted in Figure 3A. (B) Assumptions and analytical solutions for bond formations depicted in Figure 3B. (C) Analytical solutions for bond formations when combining the analytical solutions from **A** and **B** using the stated assumptions.

A particular case of cooperativity, where:

$$k_{\text{on}3} = ak_{\text{on}1}, k_{\text{off}3} = bk_{\text{off}1}, k_{\text{on}4} = ck_{\text{on}2}, k_{\text{off}4} = bk_{\text{off}2}$$

$$\langle n \rangle_{\text{TCR},\infty} = \frac{m_{\text{TCR}}m_{\text{pHLA}}A_cK_{a1}}{m_{\text{CD}4}ck_{\text{on}2} + k_{\text{off}1}} [k_{\text{off}1} + m_{\text{CD}4}ck_{\text{on}2} \frac{(m_{\text{TCR}}ak_{\text{on}1} + k_{\text{off}2}) + (a/c)(m_{\text{CD}4}ck_{\text{on}2} + k_{\text{off}1})}{(m_{\text{TCR}}ak_{\text{on}1} + k_{\text{off}2}) + (m_{\text{CD}4}ck_{\text{on}2} + k_{\text{off}1})}]$$

$$\langle n \rangle_{\text{CD}4,\infty} = \frac{m_{\text{CD}4}m_{\text{pHLA}}A_cK_{a2}}{m_{\text{TCR}}ak_{\text{on}1} + k_{\text{off}2}} [k_{\text{off}2} + m_{\text{TCR}}ak_{\text{on}1} \frac{(c/a)(m_{\text{TCR}}ak_{\text{on}1} + k_{\text{off}2}) + (m_{\text{CD}4}ck_{\text{on}2} + k_{\text{off}1})}{(m_{\text{TCR}}ak_{\text{on}1} + k_{\text{off}2}) + (m_{\text{CD}4}ck_{\text{on}2} + k_{\text{off}1})}]$$

$$\langle n \rangle_{\text{tri},\infty} = m_{\text{TCR}}m_{\text{CD}4}m_{\text{pHLA}}A_cK_{a1}K_{a2} \frac{c(m_{\text{TCR}}ak_{\text{on}1} + k_{\text{off}2}) + a(m_{\text{CD}4}ck_{\text{on}2} + k_{\text{off}1})}{b(m_{\text{TCR}}ak_{\text{on}1} + k_{\text{off}2}) + b(m_{\text{CD}4}ck_{\text{on}2} + k_{\text{off}1})}$$

$$\begin{aligned} \langle n \rangle_{\text{total},\infty} = & \frac{m_{\text{TCR}}k_{\text{on}1}}{m_{\text{pHLA}}A_c} + \frac{m_{\text{CD}4}k_{\text{on}2}}{m_{\text{TCR}}ak_{\text{on}1} + k_{\text{off}2}} + m_{\text{TCR}}m_{\text{CD}4}K_{a1}K_{a2}(1/b + \\ & \frac{k_{\text{off}2}}{m_{\text{CD}4}ck_{\text{on}2} + k_{\text{off}1}} + \frac{k_{\text{off}1}}{m_{\text{TCR}}ak_{\text{on}1} + k_{\text{off}2}}) \frac{c(m_{\text{TCR}}ak_{\text{on}1} + k_{\text{off}2}) + a(m_{\text{CD}4}ck_{\text{on}2} + k_{\text{off}1})}{(m_{\text{TCR}}ak_{\text{on}1} + k_{\text{off}2}) + (m_{\text{CD}4}ck_{\text{on}2} + k_{\text{off}1})} \end{aligned}$$

Figure 5. Analytical solutions for bond formations with cooperativity.

Using the stated assumptions, analytical solutions for bimolecular, trimolecular, and total number of bonds were derived.

3.1.4 Calcium Imaging

Cells in R10 were incubated with 5 μM Fluo-4 AM, for 30 minutes in a 37°C incubator with 5% CO₂. Cells were washed with and resuspended in R10, and further incubated for 15 minutes to ensure hydrolysis and activation of dye. Cells were subsequently washed with ice cold 1X PBS + 2% BSA (containing calcium and magnesium) three times and maintained on ice until ready for imaging. Calcium was imaged under an LSM 710 NLO confocal microscope using a 488 nm laser line and a

63X / 1.4 NA oil-immersion Plan Apochromat objective. The main system consisted of a Zeiss 710 confocal scan head mounted on an AxioObserver Z1 inverted microscope stage with motorized stage. For calcium flux studies, glass-bottom wells were cleaned with ethanol and sodium hydroxide. Tetravalent streptavidin was physioadsorbed on the clean surfaces overnight at 4°C, and the surfaces were subsequently passivated with BSA. Biotinylated pHLA was allowed to bind to streptavidin for 30 minutes at 4°C and then the surfaces thoroughly washed. Cells were injected onto the surface and time lapse images were acquired with 30 second intervals over 10 minutes. Images were analyzed for the duration of time a cell required to flux upon reaching a stable plane on the surface.

3.2 Results

3.2.1 TCR-pHLA interactions bind with thousands-fold higher propensity than wild type CD4-HLA interactions.

Both the E8TCR:pHLA and CD4:HLA bimolecular interactions have been undetectable by SPR measurements. However, upon dimerization, E8-pHLA binding was detected by SPR. CD4-HLA binding, in contrast, required immobilization of CD4 on beads at a very high concentration to increase avidity. Thus, the E8TCR:pHLA interaction was examined first because although single-molecule bonds were not achievable by SPR, it is more likely to demonstrate binding than CD4-HLA. Binding between E8 and pHLA was readily detected but required a relatively long contact time of 16 seconds in order to fit data to a plateau regime in contact time compared to the OVA peptide which requires only requires up to 5 seconds (Figure 6A). By repeating this experiment 3 times with different site densities of E8 and pHLA on the RBCs and plotting these values against a poisson transformation of the adhesion frequency, a value of $5.036 \times 10^{-4} \text{ um}^4$ was obtained (Table 1). This value is on the same order of magnitude as those measured for TCR-pHLA interactions between TCR and class-I pHLA. These

results demonstrate that binding between E8 and pHLA can be detected using this method without multimerization

Since interactions between a mutated CD4 and HLA were detectable by SPR, this interaction was next tested as a step closer toward detecting wild-type CD4 binding. Binding was detected between mCD4 and HLA at a comparable adhesion frequency as between E8 and pHLA using a smaller product of receptor-ligand site densities (Figure 6C). When three different experiments using various values of site densities were plotted together, a 2D effective affinity of $2.592 \times 10^{-3} \text{ um}^4$ was estimated (Table 1), which is more than 5-fold the affinity of the TCR-pHLA interaction used in this system and others.

Finally, CD4 and HLA binding was not detected until very high site densities were employed. Using very high site densities requires RBCs that are highly biotinylated, and each biotin site is functionalized with streptavidin. Although streptavidin is subsequently coated with biotinylated protein, the high density of coated streptavidin on one membrane is sufficient to act as a competitor to streptavidin on the opposing membrane thereby resulting in nonspecific binding. To further reduce nonspecific adhesion at high streptavidin site densities, 20 $\mu\text{g/mL}$ soluble streptavidin was present in the chamber during the experiment, and was done within 10 minutes, before soluble streptavidin would replace the coated streptavidin along with the biotinylated protein bound to it, resulting in a loss of adhesion frequency. While conditions were optimized to ensure minimal loss of adhesion frequency over the course of the 10-minute experiment, any value obtained may represent a slight underestimate. Additionally, since the experiment could not occur longer than 10 minutes, longer contact times were not tested in order to prevent a loss of adhesion frequency as well as to not compromise the number of contacts per cell pair. Site densities 3000-times those used in the mCD4 experiment were employed to obtain comparable adhesion frequencies. Thus, albeit the use of several experimental optimizations beyond those required for detecting TCR-pHLA and mCD4-

HLA binding, binding between non-multimerized CD4 and HLA was detected for the first time (Figure 6E).

Several experiments using various site densities were conducted to verify the very weak CD4-HLA interaction. When these site densities were plotted against the average number of bonds formed, a 2D effective affinity of $8.09 \times 10^{-7} \text{ um}^4$ was estimated (Table 1) which is the lowest value ever reported using the micropipette adhesion frequency assay. Using 2D effective affinity as a comparison of strength of binding, the TCR-pHLA interaction is about 622-fold stronger while the mCD4-HLA interaction is about 3203-fold stronger. Considering the micropipette adhesion frequency assay has a larger dynamic range in detecting receptor ligand interactions than SPR, these results support previous studies that report the CD4-HLA interaction is remarkably weaker.

Kinetic rates can be extrapolated from the adhesion frequency. First the fitting is a function of the kinetic off-rate. The order of off rates between these sets of interactions is mCD4:HLA > TCR:pHLA > wtCD4:HLA with values of 0.67, 0.49, and 0.36, respectively. Using the relationship between off-rate and the 2D effective affinity, on-rates for the interactions were calculated as well. The order of on-rates matched that of the off-rates with values of $1.75 \times 10^{-3} \text{ um}^4/\text{s}$, $2.51 \times 10^{-4} \text{ um}^4/\text{s}$, and $2.89 \times 10^{-7} \text{ um}^4/\text{s}$, respectively. Comparing these values to each other, the mCD4:HLA interaction has a roughly 7-fold higher propensity to bind than the TCR-pHLA interaction, which in turn has a roughly 870-fold higher propensity to bind than the wtCD4-HLA interaction. The mCD4:HLA interaction has roughly a 6000-fold higher propensity to bind than its wild-type counterpart. Examining the kinetic rates supports the reasoning that the CD4:HLA interaction is too weak to detect by previous studies which employed SPR.

Table 1: Binding kinetics from adhesion frequency

Relative densities	$A_C K_A$ (μm^4)	k_{off} (s^{-1})	$A_C k_{\text{on}}$ ($\mu\text{m}^4/\text{s}$)
TCR-pHLA	5.036×10^{-4}	0.5	2.518×10^{-4}
wtCD4-HLA	8.09×10^{-7}	0.4	3.236×10^{-7}
mtCD4-HLA	2.592×10^{-3}	0.6	1.556×10^{-3}

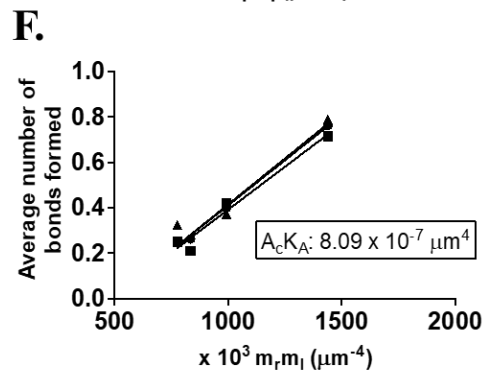
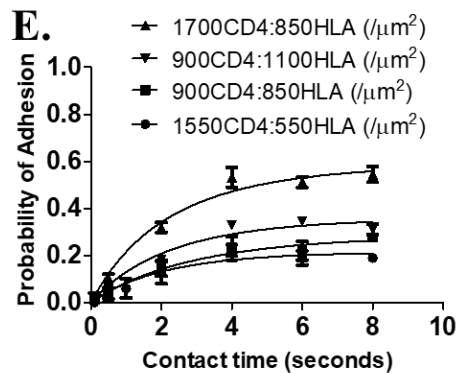
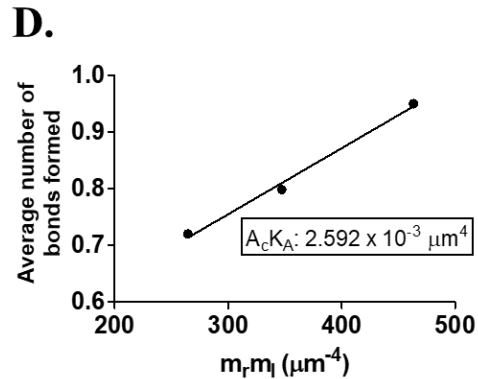
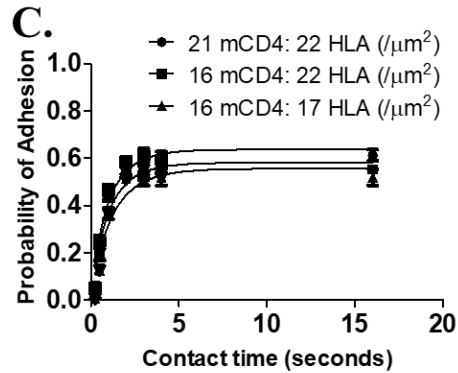
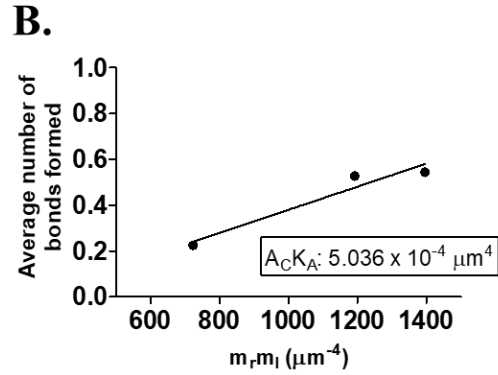
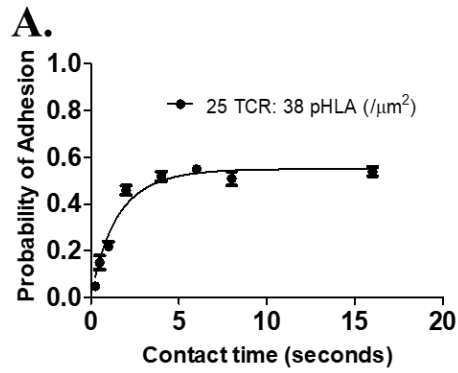


Figure 6. Micropipette adhesion frequency assay reveals binding of TCR:pHLA, mCD4:HLA, and wtCD4:HLA.

(A) Plot of adhesion frequency against contact time between opposing RBCs. The solid curve is a mathematical fitting. (B) Plot of $\langle n \rangle_{\text{obs}}$ against the product of site densities of TCR and pHLA. The solid line is the linear regression between three points plotted and the value of the slope represents the $A_C K_A$ in box. Each point is three different experiments from the plateau region in panel A. (C, E) Adhesion frequency plot for mCD4 and HLA in panel C, and for wtCD4 and HLA in panel E. Each solid curve is a separate fitting using different values for site densities corresponding to those used in experiment. (D, F) Plot between three experiments to estimate $A_C K_A$ of mCD4:HLA in panel D and wtCD4:HLA in panel F. All solid lines are independently conducted linear regression. All points represent experiments repeated in triplicate with error bars representing standard error.

3.2.2 Constraining CD4 and TCR on the same membrane opposed to pHLA results in synergy.

Colocalized on the T cell membrane with TCR are coreceptors to pMHC, CD4 or CD8. By binding the same ligand at different sites, CD8 has been reported to increase the adhesion frequency between cells by 3-fold compared to the bimolecular TCR-pMHC binding. Such a phenomena has not been reported for CD4:MHC due to the inability to distinguish a trimolecular TCR-pMHC-CD4 interaction from the bimolecular TCR-pMHC interaction. To investigate this synergy using the micropipette system used in section 4.2.1, TCR and CD4 were functionalized as a random mixture on the surface of one RBC. To minimize the discrepancies in coating strategies, RBCs with identical biotinylation sites were used. An assumption was made where this coating strategy ensures a constant total number of protein coated on the surface of the RBC, rationalized by streptavidin and biotinylated protein coated at high excess and the interaction between biotin and streptavidin being among the strongest non-covalent interactions reported.

Given a constant total number of proteins, changing the molar ratio between soluble TCR and CD4 within a solution to coat RBCs resulted in different ratios of TCR and CD4 presented on the RBCs. This coating strategy enabled investigation into the contribution of CD4 to TCR binding to pMHC. Beginning at an RBC coating of only

TCR at a site density of 25 TCR molecules per μm^2 , gradually increasing CD4 molecules in the coating mixture resulted in progressively lower adhesion frequency (Figure 7A). Coating with only TCR exhibited roughly 50% adhesion frequency, while coating with a roughly 1.5 TCR/CD4 ratio eventually also matched that adhesion frequency at longer contact times than for only TCR. However, a TCR/CD4 ratio of about 0.5 led to an adhesion frequency to drop to about 40%. Finally, a ratio of about 0.15 yielded frequency of only 20%.

When the number of bonds formed were normalized against site densities of pHLA and TCR as they were in the bimolecular case of only TCR, the trend reversed from that seen in adhesion frequency (Figure 7B). Instead of roughly equivalent curves, the 1.5 TCR/CD4 ratio resulted in about 1.5-fold more bonds formed than only TCR. The trend continued in reverse order until the TCR/CD4 ratio of 0.15 which exhibited about 2.5-fold more bonds formed. These normalizations only utilized pHLA and TCR site densities. To consider the contribution of CD4, a plot of site densities of all three species against the observed number of bonds formed was constructed analogous to those in Figure 6. In stark contrast to the overlapping plots in the bimolecular case when different site densities are used, three plots representing a different TCR/CD4 ratios did not coincide (Figure 7C). Additionally, unlike the bimolecular case which presents the linear dependence of average number of bonds on the product of site densities, these three separate plots did not exhibit linearity. Finally, the slopes of each curve increased with less CD4 mixed on the surface, which is a clear demonstration of increasing synergy since the slopes of these curves yield 2D effective affinity in the bimolecular case. It is worth noting that the curve where $\text{TCR} < \text{CD4}$ is likely an overestimate because only 30 contacts was used to probe RBCs as opposed to 50 contacts in the other panels, resulting in poor resolution despite the experiment conducted in triplicate. This non-linear behavior and lack of alignment underscores the complex relationship between the three interacting species and will be characterized in section 3.2.4. It can also be seen that the bimolecular

case of TCR only results in less observed bonds formed than the case when $TCR > CD4$. Taken together, this TCR-pHLA-CD4 system exhibits synergy in that more bonds are formed when a mixture of TCR and CD4 is coated on RBC probed against pHLA compared to when only TCR and pHLA are probed against each other.

Incorporating a coreceptor to enhance TCR-pMHC binding was previously conducted for the CD8 OT-1 system⁶⁰. The enhancement did not occur until halfway through the saturation curve for the otherwise bimolecular case. To examine if such a two-stage mechanism occurs for the human CD4 system, the resolution of contact times against adhesion frequency was increased. Indeed, an inflection point was observed at what would be about halfway through the saturation curve (2-3 seconds) for the bimolecular case (Figure 8, black curve). The saturation point for the curve normalized by pHLA and TCR site densities occurred at roughly 5 seconds.

The increased resolution in the plot of bonds formed clearly illustrates where synergy is especially pronounced since the values do not deviate greatly from the bimolecular case up to the inflection point. To understand what could be contributing to the development of synergy at later contact time points, the mobilization of proteins on the surface was limited. In the control case, TCR and CD4 are free to diffuse laterally on the RBC surface via their divalent streptavidin linkages to biotinylated cell surface proteins. On the opposing cell surface are freely lateral diffusing pHLA molecules. This exhibited the same number of bonds formed over time as seen in Figure 7 (Figure 8, black curve). In the next experiment, TCR and CD4 were immobilized on the surface of a bead at the same ratio, while pHLA was still free to diffuse on the surface of the opposing RBC. Strikingly, the synergy seen in the black curve was completely abolished and the trimolecular curve coincided with the bimolecular TCR-pHLA curve (Figure 8 red and green curves). In a third experiment, TCR and CD4 were free to diffuse but the pHLA was immobilized on the surface of a bead. In this case, not only was synergy reestablished, but the synergy was greater than in the case where all species were free to

diffuse (Figure 8 blue curve). These data demonstrate that the ability for molecules to diffuse laterally in the junction between interacting cells plays an important role in determining the degree of synergy exhibited by the system.

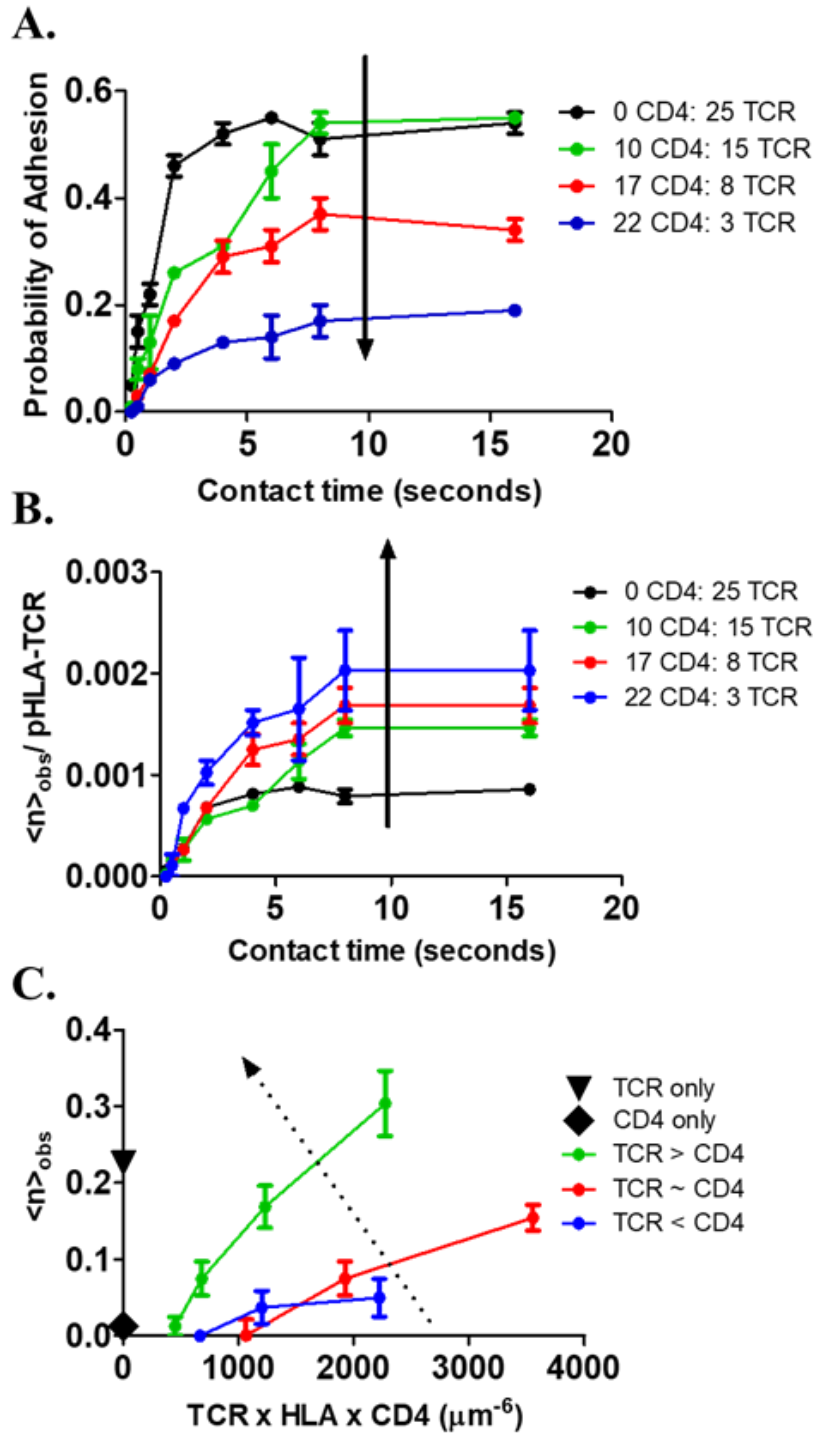
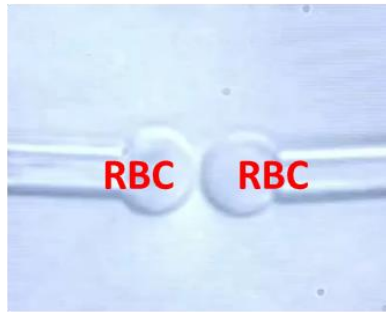


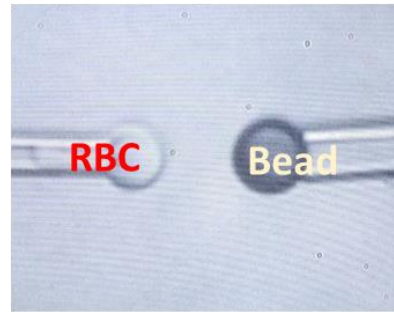
Figure 7. Demonstration of synergy with presence of CD4.

(A) Adhesion frequency experiment where CD4 was gradually displacing TCR on the surface of the RBC. The arrowhead represents the downward trend in adhesion frequency as CD4 was increased with values as seen in the legend per μm^2 . (B) The same experiment in A was poisson normalized against only TCR and pHLA site densities. The arrowhead represents an upward trend in number of bonds as CD4 is added with values seen in the legend per μm^2 . (C) A separate experiment from A and B where the y-axis is the number of bonds formed poisson normalized from adhesion frequency and the x-axis is the product of site densities of three species. The solid lines are connectors (not fittings) between points. The dotted line represents an increasing slope from the three curves. The black symbols are on the axis because of the absence of a third species. All points represent experiments conducted in triplicate. Solid connecting lines are visual connections and not fittings. Error bars represent standard error.

A.



B.



C.

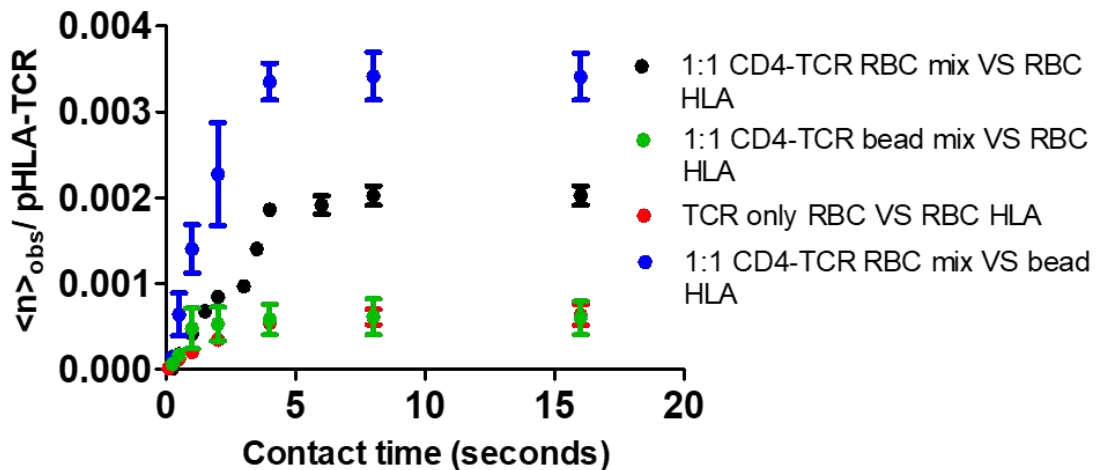


Figure 8. Mobility of molecules dictates degree of synergy.

(C) Plots of number of bonds formed normalized by the TCR and pHLA site densities, against the contact time between cells. The black curve represents the case where all three species, TCR-pHLA-CD4, are freely diffusing laterally. The green curve represents the case where only pHLA is freely diffusing while TCR and CD4 are immobilized on a bead. The red curve plots the case where two species, TCR-CD4, are freely diffusing. The blue curve represents the case where CD4 and TCR are freely diffusing but pHLA is immobilized on a bead. The solid lines are connectors (not fittings) between different points. Error bars represent standard error.

3.2.3 Biomembrane force probe demonstrates a trimolecular species

Adhesion frequency results demonstrated a striking observation of synergy when pHLA interact in trans with TCR and CD4. To pursue the same phenomena in a single-molecule fashion, BFP was utilized. A bead coated with very low densities of pHLA was probed against a bead surface coated with either TCR only or with a mixture of TCR and CD4. In the scenario of bond formation, the pHLA bead will be tracked for displacement relative to its baseline position. Many cycles of this process were recorded and data analyzed for average bond lifetimes against various tensile forces and molecular stiffness. Individual data points were displayed together for the bimolecular interaction between TCR and pHLA in a plot describing the fraction of bonds that survive by a given lifetime (Figure 9A). For very high tensile forces such as 34 pN, it is clear that the survival of bonds exhibits an exponential decay. Similar decays are observed for 27 pN, but upon tensile forces on bonds of 23 pN, a kink in the distribution occurs around the 1-second lifetime bin. A similar kink is observed for the 18 pN distribution. These multi-phase distributions are indicative of prolonged survival of bonds consistent with catch-slip bonds observed in previous studies using BFP. By the 11 pN distribution, the kink is observed to be less pronounced. Averages of these lifetimes were plotted against every force bin to accentuate the kinks observed in the distributions (Figure 9B). In the force-lifetime plots, the prototypical profile for catch-slip bonds were observed for both the bimolecular TCR-pHLA interactions as well as the trimolecular TCR-pHLA-CD4

interaction, consistent with suggestions of an additional bond species suggested by adhesion frequency results. Strikingly, the average bond lifetimes for the trimolecular interaction was almost double the duration for the bimolecular TCR-pHLA interaction. As for the bimolecular CD4-HLA interaction, a prototypical slip bond profile was observed with average lifetimes similar to those at a low force regime as the TCR-pHLA interaction, but much weaker lifetimes at the force bin inducing the peak lifetimes for the two other interactions. These results support the idea that a trimolecular interaction is enhancing kinetics for a more stabilized bond. An additional approach to analyze the data from the BFP assay was to parse out the molecular stiffnesses of each bond by extracting differences in extension under force between the optical bead tracking and the piezo-driven displacements. For the bimolecular TCR-pHLA bonds, a mean stiffness value of about 0.255 pN/nm was extracted (Figure 9C). Upon addition of CD4, however, an additional population emerged with mean stiffnesses of two populations hovering around the same value for the bimolecular interaction, and another at the 0.5 pN/nm bin (Figure 9D). The findings provide supporting evidence for the development of a third molecular species that is stiffer and enhances bond lifetimes beyond the sum of the individual bimolecular interactions.

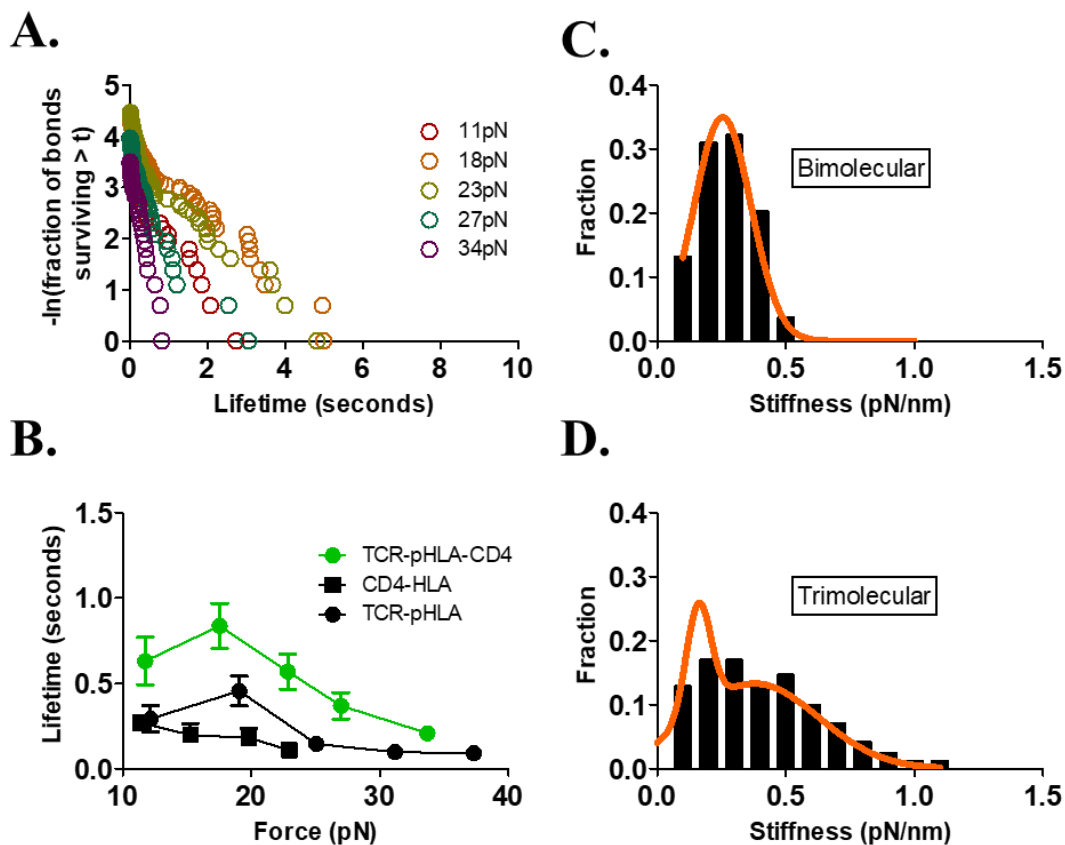


Figure 9. Single-molecule analysis reveals bond stabilization.

(A) Survival curves for the bimolecular TCR-pHLA interaction. Each circle indicates one bond between TCR and pHLA. Different colors indicate the tensile force at which is bond was held to. (B) Average bond lifetimes experienced by a collection of data points within prescribed force bins on the x-axis. Solid lines are visual connectors and not fittings. (C) Histogram depicting molecular stiffnesses of the bimolecular TCR-pHLA interaction. (D) Histogram depicting molecular stiffnesses for bonds formed when TCR, pHLA, and CD4 were present in the system.

drastic increase in number of bonds formed, despite the micropipette measurement showing that CD4-HLA 2D affinity is relatively negligible. To understand the contribution of CD4 to the formation of bonds, a mass-action based model describing trimolecular interactions in the case of no cooperativity was developed (Figure 3). In one pathway, TCR and pHLA are in equilibrium with the bimolecular TCR:pHLA complex. This complex can then be bound to CD4 and is in equilibrium with the TCR-pHLA:CD4 trimolecular complex. In a concurrent pathway, CD4 binds to pHLA first and is in

equilibrium with the bimolecular complex of CD4:pHLA. Correspondingly, this bimolecular complex can then bind to TCR and this reaction is in equilibrium with a TCR-pHLA-CD4 trimolecular complex. Note that the trimolecular complex can dissociate into either of the two bimolecular complexes along two different pathways. In this model, the assumption is that k_{on} and k_{off} values are not different between TCR binding to pHLA and TCR binding to pHLA:CD4. The same assumption applies to when CD4 binds to pHLA or TCR:pHLA. Using this model, bond formation and density values obtained from experiments where only bimolecular interactions occurred were sufficient to model the bond formation prediction if no cooperativity was present. As TCR is gradually displaced by CD4 on a surface with a constant total number of protein, the number of bonds normalized by pHLA decreases completely linearly to the relatively negligible case where only CD4-HLA bond formation is occurring. Plotting the data of from the experiment using TCR/CD4 mixtures of different ratios (Figure 10), the trend is strikingly different (Each column represents the different pHLA density but the same TCR/CD4 ratios). First, the points using same values of pHLA yield different upward trends from only CD4 to only TCR, demonstrating a nonlinear dependence on pHLA density. In other words, all the top points in each column representing one pHLA density show a steeper increase than the trajectory for all the bottom points representing another pHLA density. The squared error between the no cooperativity prediction and the data from mixtures clearly demonstrates that this model does not fit., strongly suggestive of cooperativity contributed by the presence of CD4 (Figure 10C).

These findings are consistent for various degrees of bond formation. Ranging from adhesion frequencies between 1% and 56% which would translate to average bonds formed within the contact area from less than 0.01 to 0.78, clear trends were observed using a linear interpolation (Figure 11). There was a sharp increase from zero bonds formed as soon as TCR is introduced into the system. Extending along one value of TCR, the number of bonds per pHLA much more gradually decrease as CD4 is removed from

the system, suggesting that CD4 is indeed important to form more bonds despite its very weak affinity. Interestingly, there is a clear relationship between bond formation and TCR/CD4 ratio. The highest points are all located toward the $n_{bi} \text{ TCR:pHLA} > n_{bi} \text{ CD4:HLA}$ regime, while the lowest points are toward the $n_{bi} \text{ TCR:pHLA} < n_{bi} \text{ CD4:HLA}$ regime. Thus, if CD4:HLA bimolecular bonds are allowed to dominate, synergy is not likely while if TCR:HLA bonds dominate, the formation of synergy is established.

A mathematical model to predict cooperativity between three different molecules was subsequently developed (Figure 5). Unlike the linear interpolation the mathematical model predicted normalized bond formation as a function of site densities of TCR and CD4 (Figure 12). The prediction (surface) successfully predicted the nonlinearity in bond formation with increasingly large presence of CD4, and fits with the observed data well. The surface is highest at a quadrant where the most CD4 and TCR is present, which is expected, but the shape skews toward the TCR axis, which may reflect the dominance in binding between TCR and CD4. Most importantly, however, are parameters derived from the mathematical model. ‘a’ describes the enhancement of TCR on-rate engagement to pHLA between bimolecular and trimolecular complexes, while ‘c’ describes the same enhancement for CD4. ‘b’ describes the enhancement in off-rate from the trimolecular complex for both TCR and CD4 (Table 2). The value for a was found to be less than unity when TCR and CD4 densities were high which indicates that TCR is less likely to associate with pHLA that is complexed with CD4. This trend was reversed for the case when TCR and CD4 were expressed in comparable densities with pHLA. Meanwhile, the value for b was high for both density scenarios, which indicate that CD4 association with HLA is always enhanced when TCR and pHLA are already engaged. The value for b was always less than unity which indicates that bond lifetimes are always extended when the trimolecular bonds are formed.

Table 2: Parameter fittings describing TCR-pHLA-CD4 cooperativity

Relative densities	a	b	c
TCR ~ pHLA ~ CD4	1.76×10^3	4.39×10^{-1}	2.87×10^7
TCR ~ CD4 > pHLA	1.13×10^{-3}	5.54×10^{-2}	3.33×10^4

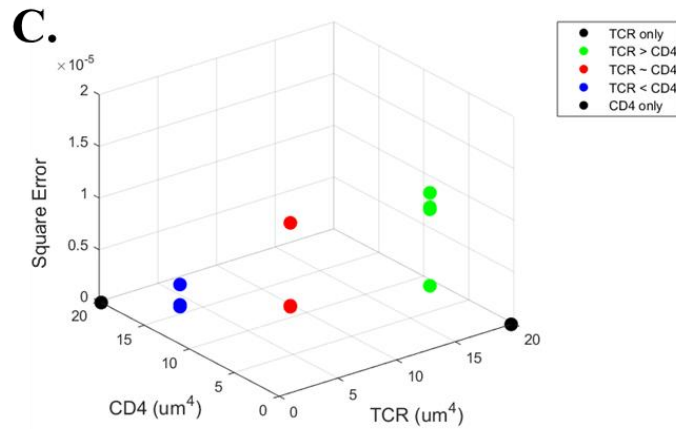
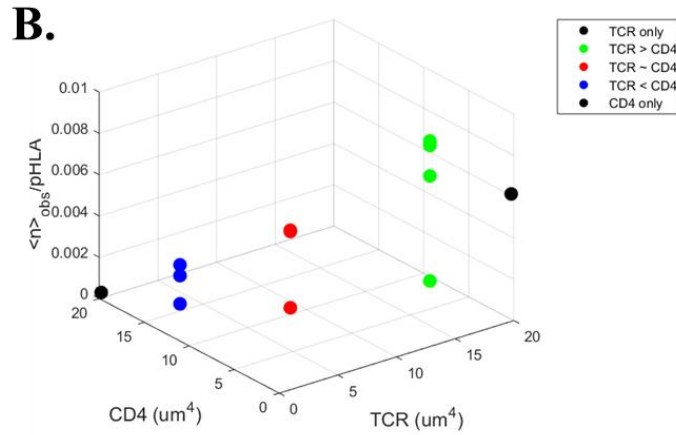
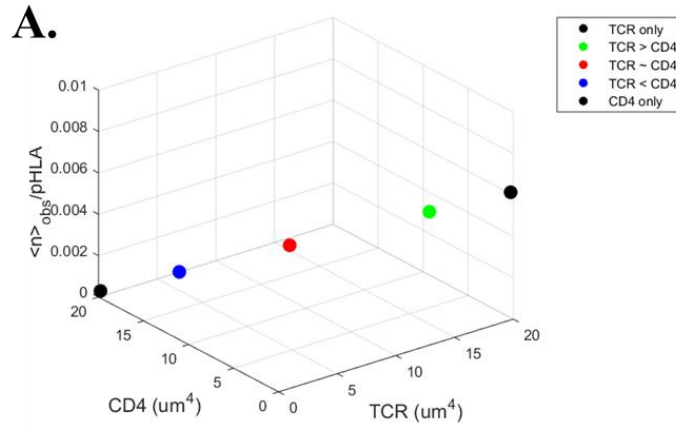


Figure 10. Removing bimolecular interactions reveals synergy.

(A) Simulation of observed bond formation assuming no cooperativity. (B) Plot of data points from micropipette adhesion frequency experiment. (C) Plot depicting the squared error between the prediction in A and the data points in B. Each color represents different TCR/CD4 ratios. The black dots represent an undefined ratio since one species was zero.

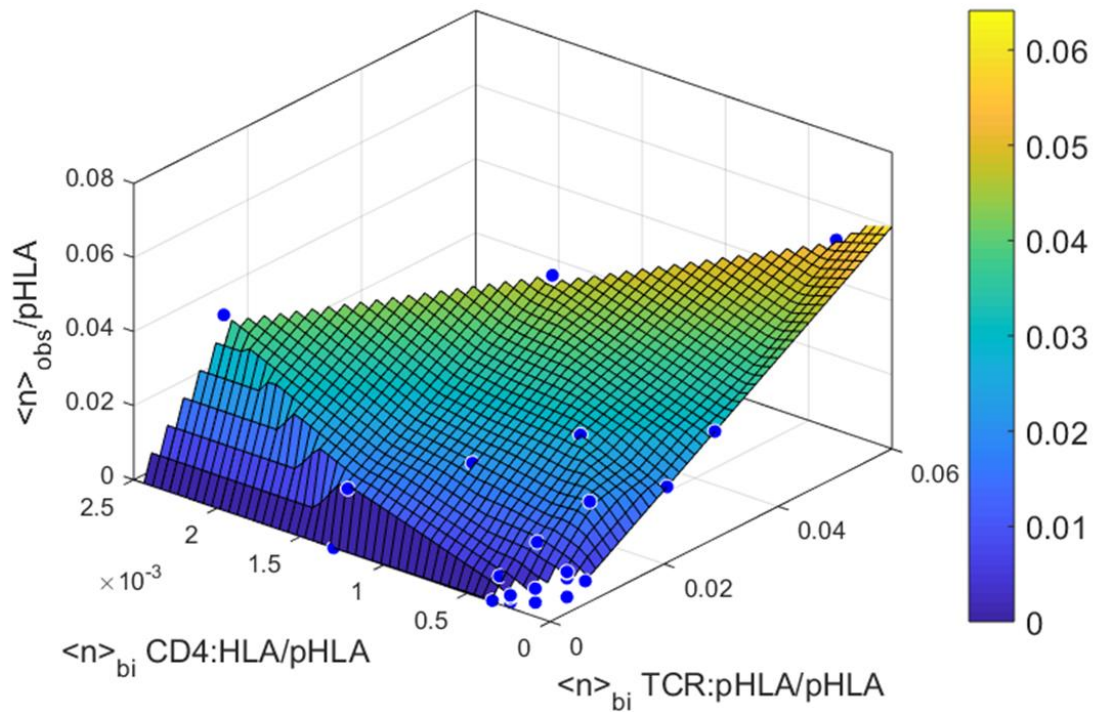


Figure 11: Dependence of synergy on all bond formation.

Plot of experimental data points conducted in triplicate. Surface represents a linear interpolation between data points.

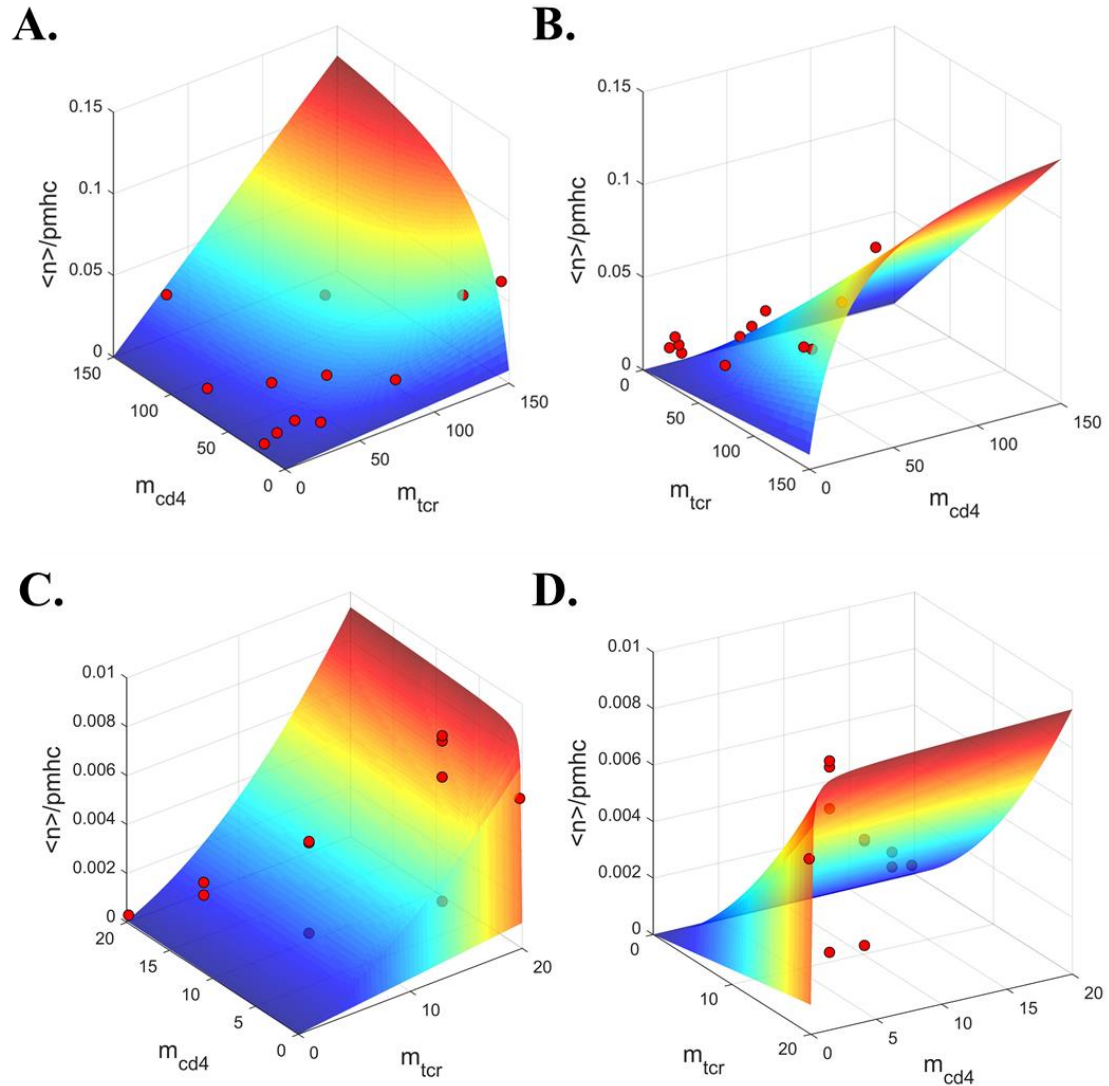


Figure 12: Mathematical prediction of cooperativity.

(A, B) Front and side views of surface predicting the normalized number of bonds based on TCR and CD4 densities. Red points are experimentally determined. (C, D) Front and side views of surface predicting the normalized number of bonds based on TCR and CD4 densities, specifically for TCR and CD4 densities comparable to pHLA. Red points are experimentally determined. These plots were generated in collaboration with Dr. William Rittase and Stefano Travaglini

3.2.5 Demonstration of synergy in cell system

Up to this point, purified proteins have been employed to characterize synergy. To apply this framework to a physiological scenario, Jurkat cells were stably transfected with the full length E8 TCR and subsequently transfected with the full length wtCD4.

The cells were then sorted for surface expression of TCR and CD4 at defined ratios (Figure 13 A-D). Each cell line then underwent BFP testing.

The average lifetime for the cell line which only expresses TCR with no CD4 exhibited a catch-slip bond profile with a peak force of about 0.2 seconds around 15pN (Figure 13E). Lifetimes for the cell line that only expresses CD4 with no TCR demonstrated only a slip-bond profile with a peak force of about 0.3 seconds at the edge of the low-force regime of around 5 pN. When the cell expressed more TCR and CD4 on its surface, the peak average lifetime reaches up to one second and the profile its catch-slip. By comparing the different lifetime profiles, the peak force is in the same force bin across catch-slip-bond profiles. The slip regime for the catch-slip profiles also decrease toward the same low lifetime baseline at high forces. In other words, the profile with the longest lifetimes did not sustain those lifetimes at higher forces compared to profiles with shorter lifetimes. An important caveat to these results is that these bond lifetimes are taken after a contact time of 2 seconds, which is long before the saturation point as seen in Figure 6. Additionally, this contact time is also shorter than the time required to reach the inflection point observed with synergy in Figure 8. Shorter contact times were conducted for these BFP experiments because at longer contact times, adhesion frequency was greater than 10% which increases the likelihood of detecting multiple bonds forming simultaneously, rather than a single-molecule measurement.

Measurements of each single-molecule bond was further dissected to extract information about molecular stiffness as in Section 3.2.5. The bimolecular scenarios exhibited similar stiffnesses as in the bimolecular interactions studied using the purified protein system. Modeled by a single gaussian, the bimolecular TCR-pHLA interaction occurred at a mean stiffness of 0.259 pN/nm with over 92% of bonds having stiffnesses less than 0.5 pN/nm, a standard deviation of 0.104 pN/nm, and an RSDR of 0.0100 (Figure 14A). The CD4-HLA interaction occurred at a mean stiffness of 0.112 pN/nm with 100% of bonds having stiffnesses less than 0.5 pN/nm, a standard deviation of 0.117

pN/nm, and an RSDR of 9.30×10^{-9} (Figure 14C). Histograms of stiffnesses fit well when modeled as a gaussian distribution based on the RSDR values. When examining the trimolecular case, CD4 and TCR are modeled as springs in parallel both interacting with pHLA. When TCR surface expression outnumbered CD4 surface expression on the Jurkat cell, a new population of stiffnesses developed with much higher values of stiffnesses (Figure 14B). A sum of two gaussians were used to model the global population with the overall mean of 0.335 pN/nm, individual means of 0.345 pN/nm and 0.348 pN/nm, standard deviations of 0.118 pN/nm and 0.112 pN/nm, respectively, and an RSDR value of 0.0166. A sum of two gaussians could not be fitted to the case where TCR and CD4 surface expression were comparable (Figure 14D), and therefore a single gaussian was used with a mean of 0.286 pN/nm, which is greater than the mean from the single gaussian modeled for only TCR, a standard deviation of 0.194 pN/nm, and an RSDR of 0.0147. Only 79% of bonds had stiffnesses less than 0.5 pN/nm when TCR outnumbered CD4 while that frequency was 86% for when TCR and CD4 expression were comparable. Despite the inability to fit one scenario to a sum of two gaussians, these data demonstrate that a population with stiffer bonds develops at 2-second contact times when CD4 is expressed along with TCR.

By subtracting the gaussians of the bimolecular cases from the gaussians used to model the trimolecular cases, a difference in populations was approximated which was rationalized to be the formation of trimolecular bonds (Figure 14E). Roughly 20% of bonds were excluded from the bimolecular gaussian for when TCR was greater than CD4, while only about 9% of bonds were excluded when TCR was comparable to CD4. These excluded populations were then used to extrapolate the mean trimolecular stiffnesses. When TCR was greater than CD4, the mean trimolecular stiffness was calculated to be 0.454 pN/nm, while when TCR was comparable to CD4, the mean trimolecular stiffness was 0.373 pN/nm. This difference was not statistically significant by a student t-test. To compare these values to the bimolecular cases, stiffnesses of

TCR:pHLA and CD4:HLA were summed to model springs in parallel. The resulting predicted stiffness from cell lines only expressing TCR or CD4 interacting with pHLA yielded a value of 0.372 pN/nm and was not significantly different from the two calculated trimolecular stiffnesses from interactions by cell lines expressing both TCR and CD4 (Figure 14F).

To determine if these distinguishable biophysical measurements can contribute to functional outcomes, intracellular calcium flux in response to pHLA coated on a glass surface (Figure 15A) was monitored. Cells were loaded with a fluo-4 calcium dye and monitored in 30-second intervals (Figure 15B). Significant increases above baseline fluorescence were concluded to represent calcium flux and cells that underwent this process were further analyzed. Inclusion of CD4 both shortened the time required for cell activation (Figure 15C), and the degree to which cells fluxed calcium (Figure 15D). Taken together, these results suggest that stabilization of TCR-pHLA bonds by CD4 has functional consequences, consistent with previous literature⁶³.

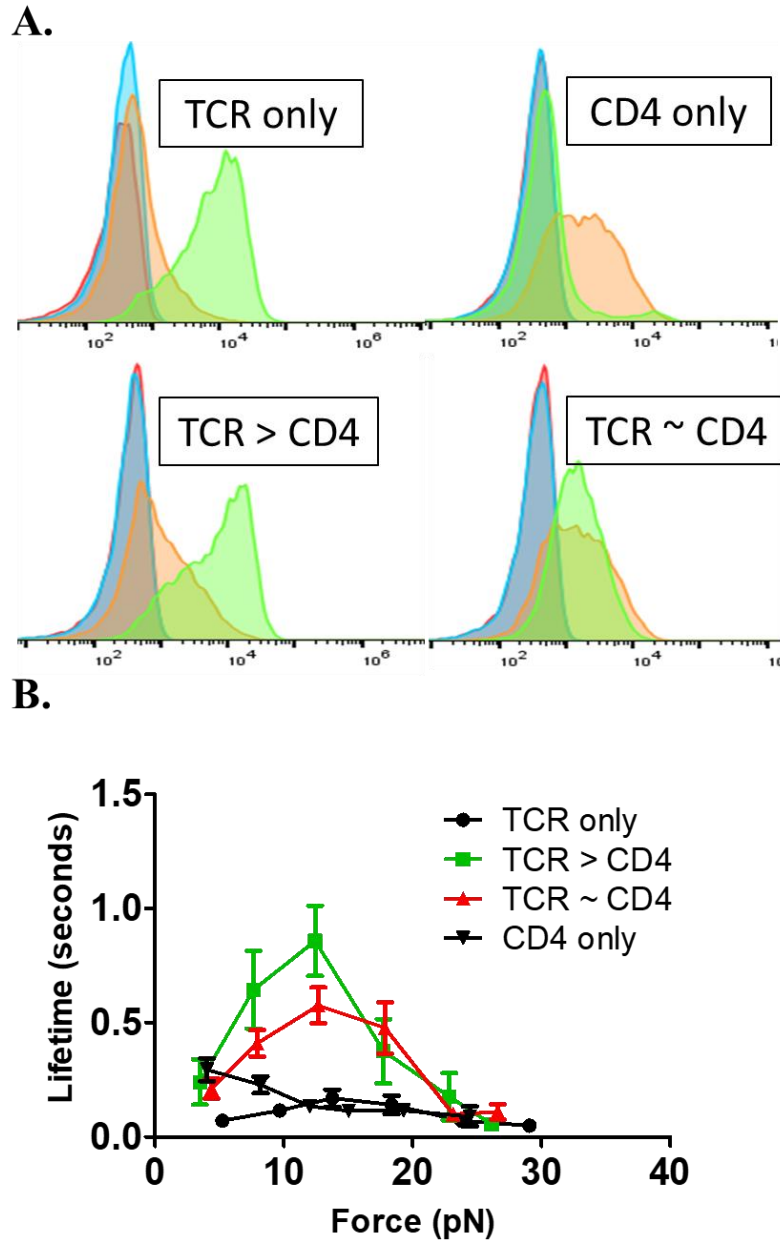


Figure 13. Longer lifetimes when CD4 is present.

(A) Flow cytometry histograms depicting Jurkat cell populations. Red histograms represent a population cells that are unstained. Blue histograms represent a population of cells stained with a PE-conjugated isotype control. Orange histograms represent cells stained with a PE-anti-CD4 antibody. Green histograms represent cells stained with a PE-anti-TCR antibody. (B) Bond lifetime plots for different cell lines conducting using BFP. Solid lines are visual connectors and not fittings. Error bars represent standard error.

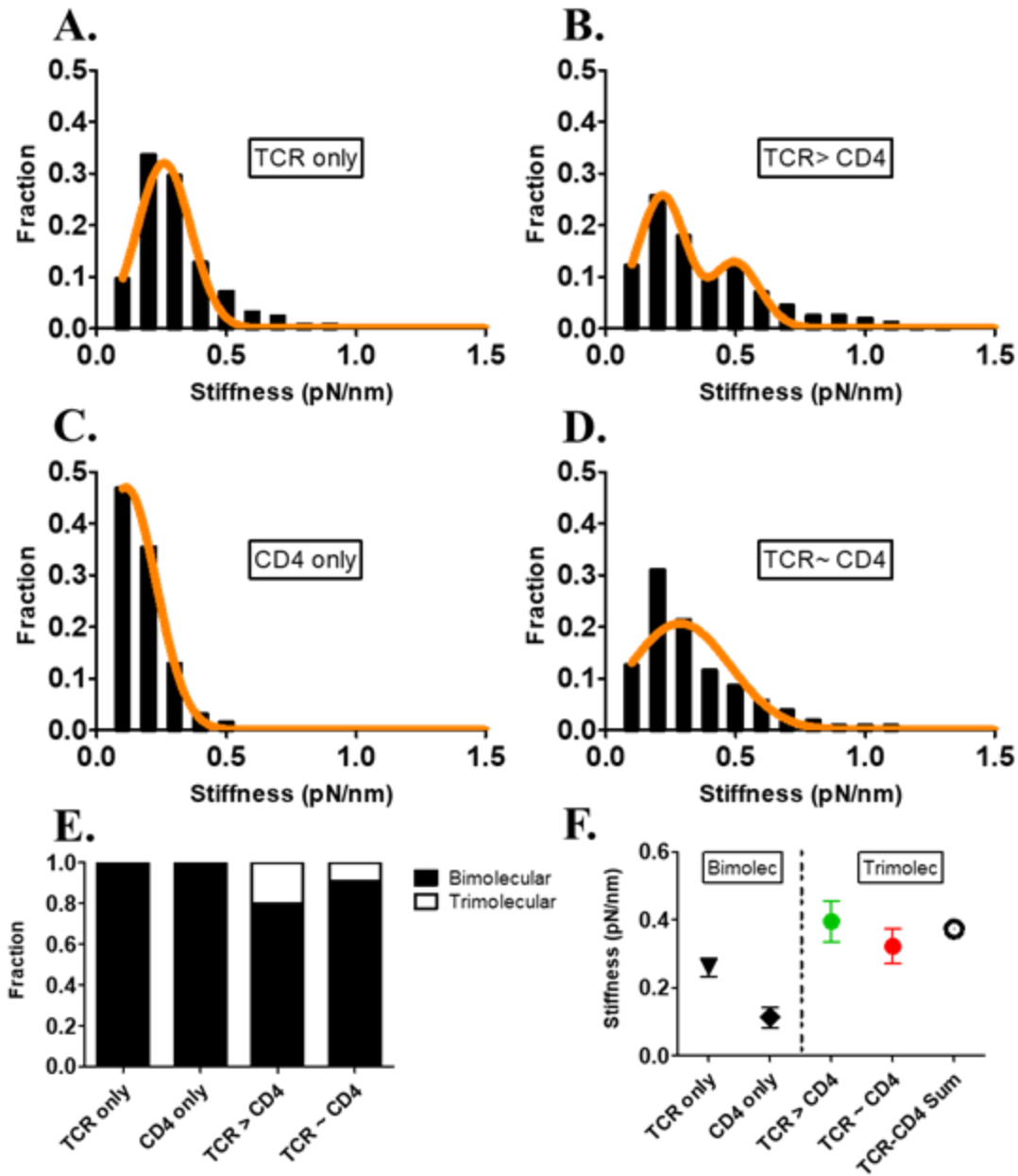


Figure 14. Stiffness analysis elucidates trimolecular population. (A-D) Histograms of bond stiffnesses illustrated by fraction of bonds formed plotted against stiffness values for various cell lines with different TCR/CD4 ratios interacted with pHLA. Orange solid lines represent robust-fitted Gaussians toward the histograms. In the case of panel B, a robust-fitted sum of two Gaussians was used to fit the histogram. (E) Plot depicting the fraction of bonds formed that are bimolecular compared to trimolecular using the different cell lines. (F) Plot depicting the mean stiffness values for both bimolecular and trimolecular cases. The empty point represents a prediction where the two black-filled points were summed to represent two springs in parallel and compared to the stiffnesses for trimolecular bonds extrapolated from data. Error bars represent standard error.

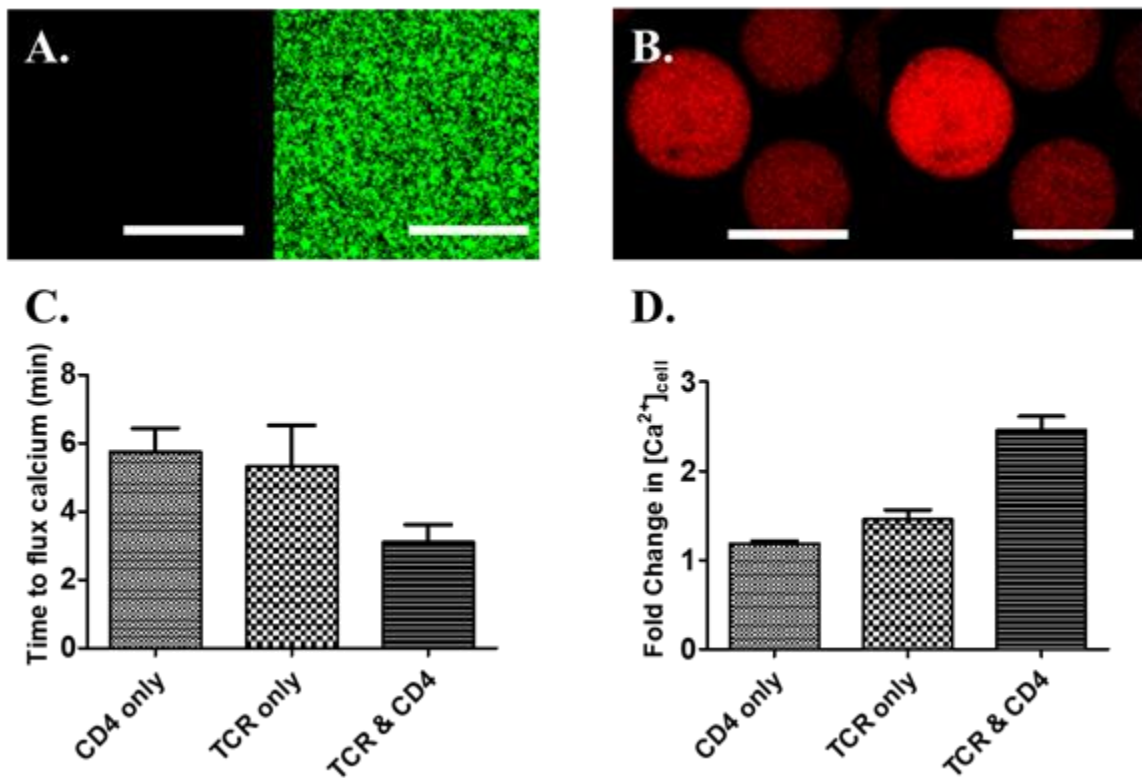


Figure 15. TCR and CD4 expressing Jurkat cells exhibit synergy (A) Confocal images of uncoated surface (left) or surface coated with pHLA (right). Scale bar 10 μm . (B) Pseudocolor images of Jurkat cells loaded with Fluo-4 calcium dye. Left image is frame before calcium flux, right image is first frame of flux. Scale bar 10 μm . (C) Plot depicting time cells on surface required to flux calcium. (D) Plot depicting the degree of calcium flux change compared to baseline fluorescent levels. Error bars represent standard error.

3.3 Discussion and Conclusions

The role of CD4 in TCR triggering is incompletely understood largely due to the undetermined kinetics of CD4 binding to MHC. Attempts at measuring these kinetics conducted with SPR yielded controversial conclusions with some groups not detecting binding^{70,75} while others have measured kinetics similar to those between CD8 and MHC⁷¹. An alternative approach taken by a few groups measured kinetics using in situ methods that analyze the two-dimensional junction between the T cell and the APC. One group used a fluorescence clustering approach to detect accumulation of TCR in response to an antibody blockade for CD4⁷⁴. Interestingly, while the blockade did not alter the

proportion of detectable fluorescence resonance energy transfer (FRET) events which represent TCR-pMHC binding, it did reduce the degree of calcium flux in T cells. A second group used the micropipette adhesion frequency assay and BFP to determine the contribution of CD4 binding to TCR-pMHC two-dimensional kinetics⁴⁹. Adhesion frequency curves that extended to a saturation time of 5 seconds did not differ whether or not there was a CD4 antibody blockade. Additionally, by measuring binding between TCR and MHC loaded with a noncognate peptide, this study aimed to determine the kinetics between CD4 and MHC. However, since binding hovered close to the detection limit of the method, adequate data points were not achievable and therefore a mathematical fitting for on- and off-rates was not possible. Nevertheless, the group estimated that the 2D effective affinity as two orders of magnitude weaker than the interaction between CD8 and MHC measured by the same technique. Finally, a third group plated MHC expressing cells on lipid bilayers functionalized with CD2 and high concentrations of CD4. Measured by accumulation of fluorescently tagged CD4, ratios between bound and free CD4 were used to determine an effective 2D affinity (a different version than one calculated from micropipette adhesion frequency)⁷⁵. Affinity values for the CD4-MHC interaction were calculated to be two to three orders of magnitude weaker than those for typical interactions between T cells and APCs, and was the weakest interaction recorded using their method. The affinity values for CD4-MHC between all these studies were found to be roughly three orders of magnitude weaker than TCR-pMHC interactions and were therefore concluded to be too weak to afford stabilization, especially since no difference in TCR-pMHC binding was found when CD4 was blocked. Nevertheless, the question of how CD4 can contribute so greatly to TCR signaling remains.

In this study, instead of using systems known to signal through TCR-pMHC efficiently, a human TCR-pHLA system known to possess very weak kinetics was employed to amplify any possible contribution of CD4. Reminiscent of seminal studies

examining the role of CD4, binding was detected between CD4 and MHC and surprisingly, the interaction greatly enhanced binding between TCR and pHLA both in on- and off-rates. To quantify the contribution of CD4, mathematical models were developed and found that inclusion of CD4 in TCR-pMHC binding can improve on-rates by up to 6 orders of magnitude and can improve off-rates by up to two-fold. These data provide strong evidence for a synergistic role of CD4 in TCR-pMHC binding in addition to its role in recruiting Lck to phosphorylate CD3 ITAMs, specifically in the case of a weak TCR-pMHC interaction.

3.3.1 Synergy between TCR, pHLA and CD4

To circumvent the outstandingly weak interaction between CD4 and MHC, Mariuzza and colleagues employed a yeast display molecular evolution approach to mutate the binding site toward much stronger association⁷⁰. This approach yielded a mutant CD4 which spontaneously formed a trimolecular complex crystal with TCR and pMHC and provided invaluable structural insights into the potential docking geometries between the three molecules. Of particular interest was the 7 nm gap between the membrane proximal regions of TCR and CD4 which strongly argues against any association between TCR and CD4 and any subsequent model for TCR triggering based on that association. The distance was argued to be maintained by the rigidity of CD4 as opposed to crystal artifacts, justified by the lack of segmental flexibility between the four Ig-like CD4 domains and supported by observations of glycosylation in the D3 and D4 membrane proximal regions. It was suggested that the gap provides ample space for CD3 dimers to organize around the TCR and for Lck to link between the CD3 ITAMs and the coreceptor²⁸. The TCR-pMHC-CD4 system is therefore an effective model to study characterize simultaneous but independent binding events.

The bimolecular mtCD4-MHC interaction was expected to be detected since it was characterized by SPR, whereas the E8 TCR:TPI HLA DR1 and the wtCD4-HLA

DR1 interactions could not be characterized by the same method²⁰⁴. Indeed, binding with mtCD4 was readily observed at a 2D effective affinity magnitude slightly higher than even the OT1 TCR-OVA interaction, with comparable on- and off-rates. Next, using SPR, the TCR-pHLA interaction was not detectable until the TCR was tetramerized to increase avidity and flowed over pHLA. In contrast, adhesion frequency was detected at a modest affinity roughly 5-fold weaker than the mtCD4-HLA interaction, and a comparable off-rate. The on-rate of the TCR-pHLA interaction, however, was almost an order of magnitude lower which could explain how single molecule interactions were not detectable via SPR. Lastly, in contrast to previous studies, CD4-MHC binding was observed without multimerization, albeit with affinity values close to the detection limit of the adhesion frequency approach. Nevertheless, kinetics were determined from adhesion frequency curves and the on-rate was measured to be almost an order of magnitude lower than those measured for CD8-MHC, while the off-rate was comparable. The 2D affinity value is similar to the one estimated using the same micropipette adhesion frequency method⁴⁹. Possible reasons why higher resolution was determined in this study, sufficient for mathematical fitting to attain on- and off-rates, are that highest possible site densities for RBCs was utilized in this study and longer contact times were also employed. In the previous study, the longest contact time used to detect binding was 5 seconds, while 8 seconds was used in the present study. Longer contact times were not employed because they greatly increased nonspecific biotin-streptavidin adhesions. It is expected that higher resolution of the adhesion frequency curves and more accurate mathematical fitting would result from using even longer contact times. The same problem did not present itself for the mtCD4-HLA and TCR-pHLA interactions since nonspecific adhesion were nearly non-existent for relatively much lower biotinylation of RBCs. These data support existing binding studies for mtCD4 and provide an explanation for why other interactions were not detectable.

Upon mixing TCR and CD4 on the same surface to interact with pHLA, higher than expected adhesion frequency resulted. By titrating increasing amount of CD4 to displace TCR on the same biotinylated RBC surface, the adhesion frequency reduced as expected, but normalizing by site densities of TCR and HLA yielded values higher than the case where only TCR was present on the surface. In other words, more bonds were detected between TCR and pHLA once CD4 was included in the system, suggestive of CD4 synergizing with TCR-pHLA. To begin exploring the extent to how CD4 was contributing to higher detection of bonds, another set of adhesion frequency data was plotted against the densities of all three species. Unlike the linear traces presented for the bimolecular cases, the relationship between site densities and bond formation was not linear, indicative of a nonlinear relationship between HLA against TCR and CD4, since for every trace, the values for TCR and CD4 are held constant. This could encapsulate the varying degrees to how TCR and CD4 interact with pHLA, but it could also be a manifestation of a how a trimolecular complex interplays with bimolecular interactions. Additionally, higher bond formation vis a vis the CD4-HLA bimolecular interaction with a tremendously low on-rate is suggestive of a significant enhancement of on-rate or occupancy since CD4-HLA binding should not even be detectable at the low densities of CD4 used in these trimolecular experiments.

An interesting feature was an apparent kink otherwise graded adhesion frequency curves. To validate this feature, a higher resolution adhesion frequency curve was collected and indeed between 2 and 4 seconds was an inflection point in the curve. This observation was reminiscent to two-stage binding observed for the OT1 system when CD8 was included. Consistent with those observations, adhesion frequency doubled, and the kink occurred at the contact time required for roughly half of the maximal adhesion frequency. For the OT1 CD8 system, the inflection point occurred at about 1 second, with a saturation contact time of about 2 seconds⁶⁰. What differs between these two systems is the shape of the cooperativity inflection, with the CD4 system displaying less of a

sinusoidal switch-like inflection as the CD8 system. To understand how this cooperativity could occur, TCR and CD4 were coated either on the fluid membranes of RBCs or immobilized by the same densities and ratios on beads. Cooperativity was abolished when TCR and CD4 were immobilized. One interpretation is that diffusion is required for cooperativity since densities were carefully chosen to ensure CD4 and TCR could be in close enough proximity to synergize on pHLA together at a population level as determined by flow cytometry. However, it is possible that this proximity was not ensured at a single-molecule level despite matching of densities between RBC and bead experiments⁷⁰. Nevertheless, this experiment does suggest that diffusion trapping by bimolecular interactions to enhance distal bimolecular interactions is not occurring. Next, using BFP and very high CD4 densities to surround TCR, longer bond lifetimes were detected when CD4 was included compared to when only TCR and pHLA were interacting, suggestive of an enhanced molecular bond. This was corroborated with molecular stiffness analysis which examined all bonds formed in BFP experiments and found that a stiffer species compared to the TCR-pHLA interaction emerged. Taken together, these data suggest that a trimolecular species forms between TCR, pHLA, and CD4 with kinetics enhanced beyond the sum of any of the bimolecular kinetics.

The data presented here could not be fitted to the adhesion frequency mathematical model previously used since that expression only describes a bimolecular interaction. A system of equations was described in this study to include interaction with a third species. To simplify the model, two separate pathways were considered and a which describes a case of no cooperativity was developed. It is important to highlight that these pathways represent sequential binding in two different hypothesis, where either TCR or CD4 bind to pHLA first. Simultaneous binding is also possible, but this model assumes a sequence. Additionally, given a single pHLA monomer, it is likely that the TCR will bind first since the on-rate for the TCR-pHLA interaction is many orders of magnitude greater than that of the CD4-HLA. Nevertheless, when on-rates are assumed

to not change between bimolecular complexing and trimolecular complexing, the system of equations that describes the trimolecular complex greatly simplifies and should yield a linear relationship between bond formation and the product of the three species' densities. As discussed earlier and represented in Figure 6, the linear relationship is not the case and there is significant deviation from the observed data closer to higher TCR/CD4 density ratios. Fitting data to the trimolecular model yields a closer, albeit not ideal, fit to the observed data. What was captured in the model was the nonlinear trend toward a point where TCR density is greater than CD4, as seen in the observed data. The parameters that were determined from fitting consistently describe tremendous enhancement in CD4 binding to HLA after TCR engagement, and a prolonging in both TCR-pHLA and CD4-HLA bond lifetimes due to trimolecular bond stabilization. What appeared to vary between different sets of data was the nonlinear trend in relation to the density of pHLA, which was also seen with earlier micropipette results plotting against three species. Thus, the mathematical model successfully describes how three species can synergize, but future work must incorporate an additional nonlinear factor encompassing the convoluted relationship between pHLA against TCR and CD4. It is possible that such a fitting could also describe the kink in the adhesion frequency curves representative of a two-stage cooperativity. Indeed, this must be considered because the data points used when plotting the observed bond formations are from the well-established saturation regime of the adhesion frequency curves which follows the inflection point.

Finally, this mathematical framework structured observations of bond formation in a Jurkat cell system. The expression of TCR on Jurkats was consistent between TCR only and TCR > CD4 cell lines. The TCR expression on the TCR ~ CD4 cell line also appeared uniform. However, despite three rounds of sorting, since CD4 was transfected into Jurkats after established TCR expression in three different cells lines separately, CD4 expression was not consistent or broadly uniform between cell lines. This could contribute to the low number of trimolecular bonds formed as determined through

stiffness analysis. For example, in the TCR ~ CD4 cell line, most cells did not express CD4 higher than isotype control levels. If these cells were used for BFP experiments, the data points would be skewed toward a bimolecular TCR-pHLA scenario. A more likely explanation for the low number of trimolecular bonds detected, however, is the short contact time used in the BFP assay. Instead of the 6 to 8 second contact time threshold where adhesion frequency for the trimolecular case appeared to saturate, only 2 seconds was used due to excessive nonspecific adhesions beyond 4 seconds. In the BFP assay, adhesion frequency must be maintained lower than 20% in order to predict the vast majority of bonds formed are single-molecule bonds. At 4 second contact times, the adhesion frequency neared 30% and therefore a significant fraction of bonds recorded were not between single-molecular interactions. Examining bond lifetimes revealed that the bimolecular TCR-pHLA interaction is prolonged under force in the purified system compared to the cell system. The difference between these two systems have been discussed in previous studies. Some have provided evidence that glycosylation of TCR can accelerate dissociation of TCR-pMHC²⁰⁵⁻²⁰⁷, which is consistent with the results seen in this study. In contrast, others have speculated that association between TCR and CD3 in a cell system can contribute to stabilized force-regulated bond lifetimes²¹. Both are viable explanations of the data but likely rely strongly on the TCR-pHLA pair used. In this study, a very weak TCR-pHLA interaction was used with a peak force-regulated bond lifetimes of about 0.2 seconds in a cell system. The doubling in bond lifetime for the purified system could certainly be explained by less glycosylation, and it is possible that the disruption by glycosylation dominated any stabilization by CD3. Comparing the zero-force bond lifetimes measured in BFP demonstrate that even without force-regulation, there was slight stabilization in bond lifetime when CD4 is included with the TCR-pHLA interaction. Strikingly, this stabilization was greatly amplified under force by up to 5 times, where different catch-slip bond profiles were clearly distinguishable. This provided strong evidence that force accelerates trimolecular bond formation. The

acceleration was not as pronounced for the Jurkats where TCR and CD4 expression were comparable. This can also be attributed to the short contact time. By relating these data back to the adhesion frequency curves, a 2 second contact time does not effectively distinguish the bimolecular interactions from the trimolecular interactions and was only in the beginning of the two-stage inflection point for cooperativity. The observation of longest bond lifetimes occurring when TCR expression was greater than CD4 expression suggests that at this short contact time, CD4 is more effectively being included for trimolecular bonds than if there was a higher TCR/CD4 ratio. Importantly, the force at which the bond profiles progress from catch to slip are consistent between all cell lines. This supports the idea that TCR and CD4 bind pHLA and independent sites and that dissociation of any component of the trimolecular complex will lead to dissociation of the TCR-pHLA portion dictates the detection of bonds by BFP. These data are consistent with mathematical modeling that predicted a skewing of greater number of bonds formed toward high TCR/CD4 ratio and supports the model that TCR and pHLA bind first, followed by stabilization by CD4. Synergy was also demonstrated in functional assays where Jurkats were plated on glass surfaces coated with pMHC, where CD4 cooperativity not only led to a faster time to flux calcium, but also a higher degree of calcium flux. Overall, these data present a strong case for synergy between TCR, pHLA, and CD4 to stabilize bond formation between T cell and APC to result in more robust T cell signaling.

3.3.2 Implications for models of T cell triggering

TCR triggering is defined in this thesis as the antigen-specific engagement of TCR with pMHC resulting in phosphorylation of the CD3 ITAMs. This process is the initiating step toward T cell activation and effector functions. Such functions result in targeted destruction of abnormal cells expressing relatively miniscule amounts of foreign antigen compared to the abundance of self-antigen also expressed, highlighting the

exquisite specificity afforded by TCR recognition. This is accomplished despite the observation that TCR-pMHC interactions are generally much weaker than interactions between cell adhesion molecules such as between integrin and its various ligands, which highlights the sensitivity of TCR triggering. To explain these two TCR capabilities, various models for TCR triggering have been proposed. These models consider kinetics between various components of the TCR machinery as well as their static and dynamic physical features²⁰⁸. Processes within the scope of this thesis begin at engagement of TCR to pMHC through the point of Lck phosphorylation of CD3 ITAMs. Therefore, only models discussing those points will be discussed below. A detailed explanation of the receptor-mediated mechanosensing between T cells and APCs that incorporates all other published models for TCR triggering is described elsewhere³⁶.

3.3.2.1 Kinetic proofreading

The original concept of kinetic proofreading or kinetic amplification was proposed independently by John Hopfield in 1974²⁰⁹ and Jacques Nino in 1979²¹⁰ to address the specificity paradox in biochemical reactions, whereby point differences in the makeup of one reactant can be discriminated by the second reactant. This was apparent with the unexpectedly low error rate involved in ribosomes recognizing mRNA codons. The solution, they proposed, was a multi-step ‘ratchet’ process where progressive intermediates ‘proofread’. If the intermediate is proofread to be inappropriate, an exit step occurs at a faster rate than the subsequent correct reaction rate down the overall pathway.

In the case of TCR, avoiding triggering due to nonspecific stimuli is particularly daunting because expressed on the surface of APCs is predominantly self-peptides. Similarities between self- and foreign-peptides could therefore result in T cell activation and autoimmunity if the only distinguishing factor was the binding interface determined by a few amino acids. Therefore, the kinetic proofreading model for TCR triggering²¹¹ relies on the bond lifetime, also known as dwell time, for specific TCR-pMHC

interactions. It was postulated that self-peptides that may bind to TCR through similarities in binding interface would confer a relatively very short lifetime- since all self-reactive TCRs will have been removed by negative selection during thymic development- compared to bond lifetimes with foreign peptides. During the bond lifetime period of proofreading for self-peptides, irreversible exit steps would occur before signal can be transmitted to allow for phosphorylation of CD3 ITAMs, affording specificity of activation only to foreign cognate peptides. This model is well accepted to be involved in TCR triggering and recent unpublished studies using optogenetics demonstrate that the dwell-time of TCR-pMHC interactions is an important determinant for triggering. A complementary study using BFP expanded upon this idea by incorporating force-regulation of bond lifetimes. It was shown by Salaita and colleagues that T cells can exert actin-dependent tensile forces on pMHC through the TCR²¹². This finding is in line with early observations that actin retrograde flow contributes to SMAC formation, and more recently it was shown that actin arcs can translocate TCR¹⁵⁰. Using this strong basis for studying bonds under tension, it was found that 10-15 pN tensile forces can prolong bond lifetimes for many TCR-pMHC interactions²⁰. In fact, it was recently suggested that the induction of catch-bond profiles can predict whether TCR triggering occurs much more effectively than affinity values. It is postulated that force pulling through the TCR is mechanism for kinetic proofreading which can discriminate between foreign-peptides which will exhibit a catch-slip profile when bound to TCR under force, while self-peptides will exhibit a slip profile. Thus, consistent with optogenetic studies, off-rates can be a determining factor to trigger TCR in a kinetic proofreading fashion.

What has not been studied is how coreceptors can contribute to proofreading. This is largely due to neglect since early studies found that TCR triggering can occur without the presence of coreceptors, and that coreceptors alone are insufficient to lead to T cell activation²⁰⁸. Additionally, many studies concluded from the weak CD4-MHC affinity that the coreceptor could not play a role in stabilizing the TCR-pMHC bond

toward more effective triggering⁸⁴. It is important to note that coreceptors are heavily implicated in initiating phosphorylation events via association with Lck and pMHC. These events may represent one step in kinetic proofreading whereby bond lifetimes long enough to reveal CD3 ITAMs to phosphorylation by coreceptor engaged-Lck could select foreign pMHC over self-pMHC, but these steps are extrinsic to the prolonging of the bond lifetime itself. The results in the current study make a case for CD4-mediated enhancement of bond lifetime. Together with functional experiments which showed that inclusion of CD4 promoted the time and degree of calcium flux, coreceptors may play a non-negligible role in kinetic proofreading. This role was especially pronounced when relatively small amounts of CD4 enhanced bond lifetime up to 5-fold. Within the force-regulated enhancement may be kinetic proofreading steps to amplify cognate TCR-pMHC interactions which experience catch-slip bond profiles. A natural question to follow is whether coreceptor-mediated enhancement occurs for self-peptides? Unlike the TCR, CD4 binding to pMHC is conserved for a given MHC allele and could therefore influence both foreign- and self-peptide interactions with TCR. A second model for TCR triggering informs this possibility.

3.3.2.2 Serial triggering and co-agonism

Comparison between relatively strong TCR-pMHC interactions with antibody-antigen interactions reveals that the former is weaker by up to 6 orders of magnitude, which prompts the question of how such a weak interaction can trigger a highly consequential signaling event when many other receptor-ligand interactions rely on much stronger affinities? A serial triggering model that addresses this question of sensitivity posits that TCR with a relatively high dissociation rate compared to other receptor-ligand interactions, rapidly rebind to the same or other pMHC to repeat the process of triggering to the point that enough short signals accumulate to produce a sufficiently strong signal to reach a threshold that initiates T cell activation²⁰⁸. Evidence supporting this model are

delays found between several TCR-pMHC engagements and markers of T cell activation such as calcium flux. The Zhu lab found that accumulation of binding events over a course of a minute resulted in intracellular calcium flux²⁰ and was corroborated by another group who found that T cells require less than 3 minutes to signal after TCR and pMHC were thought to first engage²¹³. Not mutually exclusive from the kinetic proofreading model which focuses on a series of molecular steps under an overall reaction rate, the serial triggering model shifts focus on the population of TCR-pMHC interactions. An entire sequence of kinetic proofreading steps may occur within each unit of bond lifetime followed by dissociation and rebinding. However, rebinding between TCR and pMHC can occur on time-scale so short that they are masked from bulk affinity values and are difficult to discern even for single molecule bond lifetime measurements. Since the present results found stabilization by CD4 cooperativity, the role of both TCR-pMHC and coreceptor rebinding in the accumulation of units toward a threshold is considered in section 3.3.3.

On the surface of APCs are MHC which are loaded mostly with self-peptide²¹⁴. Whereas T cells highly reactive to self-peptide were removed during negative selection, other T cells must be mildly reactive to self-peptides in order to be positively selected in the thymus. Interestingly, when T cells were engaged with an *in-situ* mimicking surface made up of a mixture of both cognate and non-cognate peptide loaded on the same pMHC, T cell activation was found to be enhanced^{214,215}. A possible explanation for this phenomena is proximity of Lck-engaged coreceptors to the cognate TCR-pMHC interaction enables efficient signaling. Based on results from the present study, coreceptors could bind to MHC with or without TCR engagement. It would follow therefore, that even if coreceptor-bound pMHC engaged transiently with a non-cognate TCR, Lck would still be readily available to transfer to association with a TCR bound to a cognate pMHC since TCR were shown to exist in nanoclusters¹⁴⁹. By this model, co-

agonism relies on coreceptor binding to MHC, which was shown in the present study, and could play an important role in the sensitivity of TCR triggering.

3.3.3 T cell machinery signaling loop

Transfer of extracellular information to intracellular signaling is termed outside-in signaling and describe the case of pMHC ligation resulting in signal inside the T cell through the TCR³⁶. The opposite transfer also exists, whereby intracellular signaling events can alter how the molecules behave outside the cell, termed inside-out signaling. Such a process has been documented for the integrins where calcium flux inside the cell will lead to drastic conformational changes of the integrin's ectodomain which modulate its affinity to its ligands. A similar process can be applied to the TCR, CD3, pMHC, and CD4 complex which has been previously described as a pseudo dimer of dimers¹⁹. Recognizing that Lck can associate with CD3 ITAMs, a recent study investigated whether the Lck-ITAM interaction can have a functional role in maintaining association between TCR-pMHC in the ectodomain. To support this idea, they found that preventing association between ITAM and Lck by using an Lck inhibitor, caused the lifetimes between TCR-pMHC to shorten. This may be due to the fact that without the support from Lck-ITAM rebinding between TCR-pMHC is less likely. Conversely, by increasing the association between Lck and the intracellular domain of the coreceptor, they were also able to achieve longer bond lifetime. Results from the present study support similar conclusions by confirming CD4 is indeed stably binding to MHC, thereby opening the possibility that the pseudo-dimer-of-dimers is self-stabilizing especially under tensile force as seen in the present study's BFP bond lifetimes results.

3.3.4 Implications toward T cell receptor signaling

The general consensus prior to the present study was that the predominant role for coreceptors was to recruit Lck into proximity of CD3 ITAMs for phosphorylation by binding to MHC⁸⁴. Without characterizing kinetics of CD4-MHC binding, it is difficult to

understand how the kinetics of phosphorylation of ITAMs by free Lck can differ from phosphorylation by coreceptor-bound Lck. Considering less than 7% of Lck were found to be bound to CD4 coreceptors but up to 40% are constitutively active⁷⁹, the stability of Lck-ITAM association modulated by the coreceptor binding to MHC is pertinent to understanding the role of coreceptors. This question is underscored by studies demonstrating a functional role of CD4 since antibody blockade is sufficient to reduce T cell activation by 30-fold⁶³. The TCR system used in the present study is unique in that the wild type TCR could not be detected to bind to pMHC²⁰⁴. Indeed, the wild type triose isomerase peptide derived from melanoma is not recognized by the E8 TCR, which results in immune evasion. A naturally occurring point residue mutation does not change the affinity with pMHC but resulted in a T cell response 5 orders of magnitude greater. Thus, despite indistinguishable 3D kinetics, the E8 TCR was very sensitive to changes in its interaction with pMHC which was characterized by distinct structural differences from its interaction with the wild type TPI peptide. It is therefore less surprising that this TCR was sensitive to coreceptor cooperativity which was not detected in previous studies, including those using the micropipette adhesion frequency assay. It is possible that the relatively stronger TCR-pMHC interactions used in previous studies masked the contribution of CD4 to stabilization.

While this suggests that CD4 stabilization can occur for all other TCR-pMHC interactions, the contribution of stabilization toward successful TCR triggering remains unanswered. For instance, as shown in previous studies, CD4 stabilization may play a minimal role for strong TCR-pMHC interactions, some of which have been shown to trigger TCR in absence of coreceptor²⁰⁸. However, for other weaker TCR-pMHC interactions such as the E8 TCR-TPI MHC interaction, CD4 stabilization may provide a means for baseline signaling to maintain cell survival. The functional results in this study support such a view. The percentage of cells that fluxed calcium in response to the “cryptic” wild-type TPI pHLA was very low compared to when anti-CD3 was used to

crosslink CD3 and bypass TCR. However, for cells that did flux calcium, the time required for flux and the degree of flux was enhanced with CD4 inclusion. The enhancement in the magnitude of calcium flux correlated well to the prolonging of bond lifetime due to CD4 which demonstrates a direct relation between the synergy experienced at a single molecule scale to cell effector functions. Consistent with previous studies²⁰, an accumulation of these long lifetimes (in this scenario, facilitated by CD4) over a course of a few minutes may have led to calcium flux in only in a small percentage of cells, without the risk of over-activating cells which would lead to autoimmunity. The parameters solved for by the mathematical model suggest that tremendous enhancement is occurring for CD4 association with HLA between the bimolecular and trimolecular scenarios. Enhancement is on the other hand, not observed for the TCR-pHLA interaction. But in both pathways, stabilization by the trimolecular complex is evident. This suggests that a conformational changes occur in the pHLA molecule upon engagement with TCR, which makes CD4 association much more amenable. Although such a conformational change has not been reported, it has been well documented that minor changes in the residues anchoring peptides can have profound impacts on the binding interfaces of pHLA. Thus, it is not unreasonable to speculate that binding with TCR can reciprocate conformational changes. The development of this model represents the first analytical solution for a simultaneous association between three different molecules. It builds on previous models for cooperativity such as the Hill, Koshland-Némethy-Filmer, and Monod-Wyman-Changeux models. These three models rely on logarithmic coefficients that may be related to multiple binding sites of a substrate for one ligand and elegantly encompass allosteric changes. Overall, the results from this aim clearly demonstrate that CD4 synergizes with the TCR-pHLA interaction to yield enhanced on-rates and off-rates resulting in a stabilized trimolecular complex which contributes to TCR triggering toward more efficient T cell activation.

CHAPTER 4 Aim 2

Quantify the effect of H₂O₂ environment on T cell receptor binding. Interactions between TCR, pMHC, and CD4 are constrained by the membranes of their respective cells which migrate through dynamic soluble microenvironments. DC-mediated T cell activation occurs within peripheral lymph nodes which is a distinct microenvironment from where TCR recognition of pMHC on infected cells occur. In such inflamed environments, ROS has been shown to play a convoluted role on T cell function⁹⁶. In some cases, H₂O₂ was determined to be necessary for signal transduction and effector functions¹¹²⁻¹¹⁴, while in other cases, H₂O₂ was suggested to cause impairment in recognition leading to disease progression^{116,216}. Since membrane bound CD4 has been shown to be sensitive to dimerization upon reduction of cysteines in its D2 domain which alters its binding properties¹³², the focus of study in this aim will be on CD8, which has not been reported to be ROS-sensitive. By studying the CD8 coreceptor, influence of ROS on TCR-associated components other than the TCR-pMHC-CD8 interaction can be analyzed. Together, this will inform a model that characterizes TCR recognition in an oxidative environment.

4.1 Methods

4.1.1 Materials

CD8 purification kit was purchased from Stemcell Technologies (Vancouver, Canada). HBSS and PBS was purchased from Corning (Corning, NY). Quantibrite beads and PE-antibodies were purchased from BD Biosciences (San Jose, CA). J.T. Baker brand H₂O₂ was purchased from Avantor (Allentown, Pa). Amplex Red enzymatic kit was purchased from ThermoFisher (Waltham, MA). Calbiochem-brand Latrunculin A and biotin-NHS polymers were purchased from Millipore Sigma (Burlington, MA). Recombinant biotin-tagged OT1-TCR was generously gifted by David Margulies at the

National Institutes of Health. Recombinant CD4 generously gifted by Roy Mariuzza at the University of Maryland. Peptides were synthesized by Genscript (Piscataway, NJ) and loaded onto MHC by the Yerkes National Institutes of Health Tetramer Core facility (Atlanta, GA). All other materials including cholesterol oxidase and the Lck specific ATP-competitive inhibitor, 7-Cyclopentyl-5-(4-phenoxyphenyl)-7H-pyrrolo[2,3-d]pyrimidin-4-ylamine⁵³, were purchased from Sigma Aldrich (St. Louis, MO).

4.1.1.1 T cells

Naïve CD8⁺ T cells were isolated from spleens of OT1 transgenic mice according to a Georgia Institute of Technology IACUC-approved protocol. T cells were purified using a Stemcell Technologies CD8⁺ negative purification kit, according to the manufacturer's protocols. Briefly, spleens isolated from mice were stored in ice cold 1X HBSS no longer than 1 hour until ready for purification. Spleens were physically grinded through a 100µm filter in the presence of ice cold 1X PBS without calcium or magnesium. RBCs were lysed and remaining cells were coated with an antibody cocktail that excludes coating CD8⁺ T cells. Coated cells were magnetically removed using streptavidin magnetic beads leaving only CD8⁺ naïve T cells. Cells were resuspended in R10 and stored in a 37°C incubator with 5% CO₂ until ready for injection in a micropipette experimental chamber.

4.1.1.2 Preparation of RBCs for adhesion frequency

Whole blood was isolated by phlebotomists from healthy volunteers at the Stamps Health Center at the Georgia Institute of Technology according to a Georgia Institute of Technology IRB-approved protocol. Histopaque-1077 was added to the bottom of the tube of RBCs and the suspension was centrifuged. Supernatant containing all cells except for RBCs were discarded and the RBCs were washed and resuspended in ice cold 1X PBS. Following buffer exchange into EAS-45, aliquots of RBCs were mixed with biotin-3400-NHS at a pH of 7.2 for 30 minutes at room temperature. The ratio between RBCs

and biotin-3400-NHS were varied to increase the site density of biotin on the surface of RBCs. Controlled biotin sites allowed for defined sites of biotinylated protein when saturating concentrations of proteins were incubated with biotinylated RBCs. 2 mg/mL tetravalent streptavidin was incubated with RBCs for 20 minutes at room temperature. Following exhaustive washing of RBCs with ice cold EAS-45, biotinylated OT1-TCR or OVA-MHC-I at a concentration of 20 µg/mL were incubated with RBCs for 30 minutes at room temperature. RBCs were washed twice with ice cold 1X PBS + 2% BSA and aliquots would be taken for site density measurements by flow cytometry. Also conjugated with OT1-TCR or OVA-pMHC were glass beads. Beads were etched with NaOH, mercaptopropyl-silanated in an acidic reaction, and covalently conjugated to maleimide-streptavidin in an overnight reaction with phosphate buffer at a pH of 6.5. Beads would be incubated with sub-saturating concentrations of protein (2 ng/mL) for 2 hours at 4°C, washed with 1X HBSS + 2% BSA, and taken for site density measurements by flow cytometry.

4.1.1.3 Measurement of site density by flow cytometry

Beads or RBCs were incubated with antibodies corresponding to their protein functionalized surfaces (PE-conjugated anti-mouse TCR V α chain for OT1-TCR, and PE-conjugated anti-mouse OVA for the pMHC) for 30 minutes at room temperature using a saturating antibody concentration. Following three washes and resuspension in 1X PBS + 2% BSA, beads and RBCs were analyzed using the BD Accuri Flow Cytometer FL2 channel for PE excitation and detection. Fluorescence measurements were compared with BD Quantibrite PE calibration beads in order to calculate the number of proteins on the surface of beads. Briefly, fluorescence from beads of four different sizes and with different known number of PE-fluorochromes were used to create a well-fitted ($R^2 > 0.97$) linear regression between the log of mean fluorescence intensity and the log of PE

molecule count. The regression was used to back-calculate the fluorescence from PE-stained beads and RBCs.

4.1.2 Optimizing conditions for adhesion frequency

H₂O₂ is well-documented to be cytotoxic, dependent on the concentration used. These range from no detectable effects on intracellular proteins when concentrations used are sub-nanomolar, transient and permanent stunting of cell metabolism in the micromolar range, to induction of apoptosis and necrosis of the cell in the millimolar range¹⁰⁶. However, cytotoxic effects also depend on the duration of H₂O₂ exposure¹⁰⁶. A concentration of H₂O₂ representative of an inflamed environment was optimized based on literature values²¹⁷, the timing of experiment, condition of cells, and quality of adhesion frequency.

4.1.2.1 Consumption of hydrogen peroxide

To measure H₂O₂ concentrations in cell suspensions, an Amplex Red enzyme-based fluorescence indicator of H₂O₂ was employed according to manufacturer's protocols. Briefly, Amplex Red was dissolved in DMSO and mixed with a horse radish peroxidase solution and the manufacturer's reaction buffer. Cells were allowed to react with H₂O₂ at various times in a solution representative of the experimental micropipette chamber which was made up of cells at a specific density, RBCs, and 2% BSA in 1X PBS. Following the completion of reaction time, supernatant removed from cells by centrifugation was collected and mixed with the Amplex Red reaction solution for 30 minutes at room temperature away from light. The 96 well plate was inserted into a BioTek Synergy H4 microplate reader plate reader to measure fluorescence signal using 560 nm excitation and detecting 590 nm emission. Fluorescence intensities were normalized against a calibration curve using four different known concentrations of manufacturer-provided H₂O₂.

4.1.2.2 Production of hydrogen peroxide by glucose oxidase

After testing several different concentrations, 0.135 U/mL of glucose oxidase (GOx) was used in all experiments. First, the production of H₂O₂ by this amount of GOx was characterized by absorbance monitoring at the 240-280 nm wavelength using a Thermofisher nanodrop spectrophotometer. Solutions of the same concentration of GOx and varying concentration of glucose were monitored for increased amplitude of the peak at 240-280 nm over the course of 1 hour. This rate of change in absorbance was assumed to be the rate of H₂O₂ production and plotted against glucose concentration to yield a linear regression. An optimized glucose concentration was determined by matching the integrated H₂O₂ produced with the integrated H₂O₂ consumed. A representative experimental solution of cells, glucose, H₂O₂, GOx, and 2% BSA in 1X PBS was tested for pH changes using a calibrated Thermofisher pH meter over the course of 30 minutes.

4.1.3 Real-time adhesion frequency

Beyond the closer correlation between TCR-pMHC affinity and peptide potency compared to SPR measurements²¹, the micropipette adhesion frequency assay is advantageous for the ability to measure binding between molecules on live, functional cells. This was clearly demonstrated in a study that imaged calcium flux in T cells concurrently with cycles of pMHC contact²⁰. Typically, affinity values would be obtained from 30-50 contacts and averaged between tens of cell pairs. Since changes in adhesion frequency have been documented to occur in a temporal fashion during this period of repeated contacts²¹⁸, quantifying the TCR-pMHC 2D affinity in real-time would describe the propensity of the T cell to recognize antigen at a given time in response to an external perturbation. Herein, a modification to the protocol described in section 3.1.2 to be conducted in real time is described.

The micropipette chamber was prepared as follows: four well-separated droplets of 35 μ L of 1X PBS + 2% BSA were placed on a coverslip. Another coverslip was used

as a top which held droplets in place, and the droplets were sealed with mineral oil to prevent osmotic changes. Before the experiment, T cells and RBCs were stained with their respective antibodies and analyzed on flow cytometry as described in section 3.1.1. This ensured the presence of molecules to be tested. Additionally, site density measurements will later be used to calculate 2D affinity values as described in section 3.1.2.

Injected into each media droplet within the chamber was 1 μL of T cell suspension directly from the 37°C incubator at a concentration of 4×10^5 cells/mL to ultimately provide a final cell concentration of 1×10^5 cells/mL (after addition of ROS for a final volume of 40 μL). In the field of view under the microscope, the right pipette forged to specifically hold a bead (2 μm diameter bead was aspirated by a 1.5 μm diameter pipette) or a T cell (6 μm diameter naïve T cell was aspirated by a 3 μm diameter pipette and aspirated until the tail of the T cell within the pipette was no longer than 1 μm). The pipette on the left, forged to 1 μm in diameter was used to aspirate the RBC and was programmed to approach the target cell over a distance of 10 μm in 0.5 seconds, remain in contact with the target cell for 2 seconds, retract 10 μm in 0.5 seconds, and remain at the 0 μm reference point for 0.5 seconds, before the next cycle begins. This was repeated for 30 cycles for each cell pair aspirated.

One cell pair was used to confirm binding occurred between cell pairs. Accounting for cell-to-cell variability, this first cell pair was used to optimize an appropriate adhesion frequency (10-50%) by optimizing the site densities on the RBC, and this procedure was conducted for all experiments. For experiments that were found to decrease gradually in adhesion frequency, a higher baseline frequency was used such as 60%, to ensure the lowest level of adhesion frequency was still captured by the experiment.

Following the first cell pair, 4 μL of freshly diluted 100 μM H_2O_2 in PBS was injected into the experimental droplet for a final concentration of 10 μM and a timer was

initiated. Adhesion events would be collected in a Microsoft Excel file in correspondence with the time by recording the time at which the first contact was made, and the last contact. When a new cell pair was aspirated, the 30-contact cycle was repeated but the timer continued through the course of about a 30-minute experiment. This process was repeated with new cell pairs until 30 minutes was reached, at which point the experiment ended with the 30th contact of the cell pair tested at that point. Through the entire process, data for one time-course was collected. This experiment was repeated at least 8 times to calculate mean values between cell pairs at corresponding time courses. Nine cell pairs were tested across a time course.

4.1.3.1 Caveats

Probability of adhesion is a function of the contact time between two surfaces expressing a receptor-ligand pair. A saturation of contact time can be reached at which point probability of adhesion no longer increases with longer contact times. However, this saturation value varies greatly between different ligands.

A set of adhesion frequency collection per cell for real-time experiments included 30 cycles of contact and retraction. Given previous studies that have predicted TCR triggering by pMHC can occur within 1-3 minutes of pMHC engagement^{20,213}, durations of 2-6 seconds per cycle would be appropriate for the total number of cycles within the window. A receptor-ligand pair with relatively fast on-rates and long bond lifetimes is the OT1 TCR-OVA pMHC. Previous studies have found saturation contact times to be achieved within 2 seconds²¹, suitable for the requirement of this assay. Altogether, each cycle consisted of 0.5 seconds of approaching, 2 seconds of contact, 0.5 seconds of retraction, and 0.5 seconds of delay before the next cycle, totaling 3.5 seconds for 30 cycles. A combined time of 1 minute and 45 seconds for the total test duration between one cell pair fits well within the few minutes of TCR triggering, at which point downstream signaling may convolute measurements.

This real-time adhesion frequency assay is not conducive to studying receptor-ligand interactions with low on-rates and fast off-rates, such as the E8 TCR-TPI MHC pair used in aim 1. The saturation contact time was measured to be more than 4 seconds and therefore, a total cycle of 30 contacts between cell pairs may extend beyond the time T cell signaling will remain untriggered.

Capturing binding within early stages of TCR triggering is desired because the signaling cascade that ensues may influence the degree of binding²¹³. The goal of this aim is to capture effects of extracellular soluble environment on receptor-ligand binding constrained by a membrane anchored microenvironment. Recently, the Zhu lab has shown that kinase activity can influence binding at a bond-to-bond basis⁵³. Unlike BFP which measures single bond lifetimes, the micropipette adhesion frequency assay captures affinities at an overall cellular scale (which can be used to calculate bulk values of on- and off-rates but are not necessarily single molecule measurements). Thus, even if kinase activity is changing, this assay will lump those changes into cellular-scale measurements of affinity between receptor-ligand species.

4.1.3.2 Statistics

In purified TCR-pMHC experiments, each time-binned affinity distribution (conducted in at least triplicate) was tested against the distribution of all time-binned values using parametric one-way ANOVA tests. The null-hypothesis in these tests was that the TCR-pMHC interaction is not sensitive to ROS as it is exposed to H₂O₂ over the one variable of time. Significant differences between distributions of each time point would indicate that the null-hypothesis is proven false. Unless specified otherwise, the remainder of experiments in this aim were analyzed using non-parametric two-way ANOVA tests for significant differences between experimental groups. Specific null-hypotheses varied between experiments, but generally they were testing whether the TCR-pMHC interaction is sensitive to ROS and if that difference depended on time,

coreceptor binding, or a pharmacologic perturbation. To analyze the dynamics of affinity changes, other statistical approaches were used. For results that displayed a decrease and increase of affinity values, separate linear regressions were taken for descending and ascending portions of data¹⁹. These slopes were compared to a zero slope and tested for significance. The null-hypothesis for these tests were that the slopes did not deviate significantly from zero-slope. For results using glucose oxidase, only one linear regression for each experimental group was used and those slopes were compared were tested for significance against zero slope. To test for statistical significance in the delay of time to decrease in affinity between the experimental groups upon injection of glucose oxidase cocktail, distributions of time were tested against each other using a parametric one-tailed student's t-test. The null-hypothesis for this test was that the time point at which the mtOVA plot significantly decreased (as tested by a student's t-test from its baseline values) did not differ from the time point at which the wtOVA plot significantly decreased. *, **, and *** described statistically significant differences with p-values smaller than 0.05, 0.005, and 0.0005, respectively. T-tests were not conducted on individual affinity value points along the time axis because, although these points are experimentally matched, they occurred at different time points and could not be directly statistically compared. Therefore, one- and two- way ANOVA tests were opted to test for significant differences between affinity values across experimental groups. All statistics were performed using GraphPad Prism 5.

4.1.4 Pharmacologic perturbations

For Lck inhibition experiments, OT1 T cells in R10 were incubated with 5 μ M Lck inhibitor for 30 minutes at 37°C in a 5% CO₂ incubator⁵³. Cells were injected into the micropipette chamber supplemented with 5 μ M Lck inhibitor. For actin inhibition experiments, OT1 T cells in R10 were incubated with 1 μ M latrunculin A for 30 minutes at 25°C^{21,219}. Adhesion frequencies were noticeably changing over the course of the

experiment. Therefore, they were divided between ‘early’ events which were calculated from cell pairs during the first 15 minutes of the experiment, and ‘later’ events which were calculated from cell pairs during the last 15 minutes of the experiment. Mean values between groups were tested using unpaired student’s t-tests with ** and *** representing significant differences between groups with p-values smaller than 0.005 and 0.0005, respectively. To robustly oxidize membrane cholesterol, OT1 T cells in R10 were incubated with 5 U/mL of cholesterol oxidase for 30 minutes at 37°C in a 5% CO₂ incubator²¹. Cells were then injected into the micropipette chamber media, with no further supplemented cholesterol oxidase. Mean values across the entire time course were compared between cholesterol oxidized and non-cholesterol oxidized groups using a two-way ANOVA with a null-hypothesis that the two groups did not statistically differ in affinity values.

4.2 Results

4.2.1 Optimization of hydrogen peroxide concentration

Literature values for H₂O₂ concentrations used to incubate T cell range from sub-micromolar to 1 mM. To begin optimizing the concentration of H₂O₂ to use for these experiments, cells were incubated with H₂O₂ at various concentration within a solution representative of the experimental micropipette chamber. After 30 minutes of suspension in PBS supplemented with 2% BSA (to minimize nonspecific adhesion) at 25°C, the vast majority of cells in the chamber (86%) did not experience apoptosis or necrosis (Figure 16). When treated with a 10 µM of H₂O₂ bolus for 30 minutes, the distribution of cells was very similar, with 85.2% of cells not experiencing cell death. However, when treated with a 100 µM bolus for the same duration, roughly 16% of cells underwent apoptosis as indicated by positive Annexin V staining. Finally, with treatment of 1 mM of H₂O₂ for 30 minutes, almost half of the cells underwent apoptosis, and up to 16% of the cells exhibited markers for both apoptosis and necrosis which was indicated by positive

propidium iodide staining. The bolus concentration of 10 μM of H_2O_2 was used for subsequent experiments since it exhibited negligible differences in cell viability from the control group.

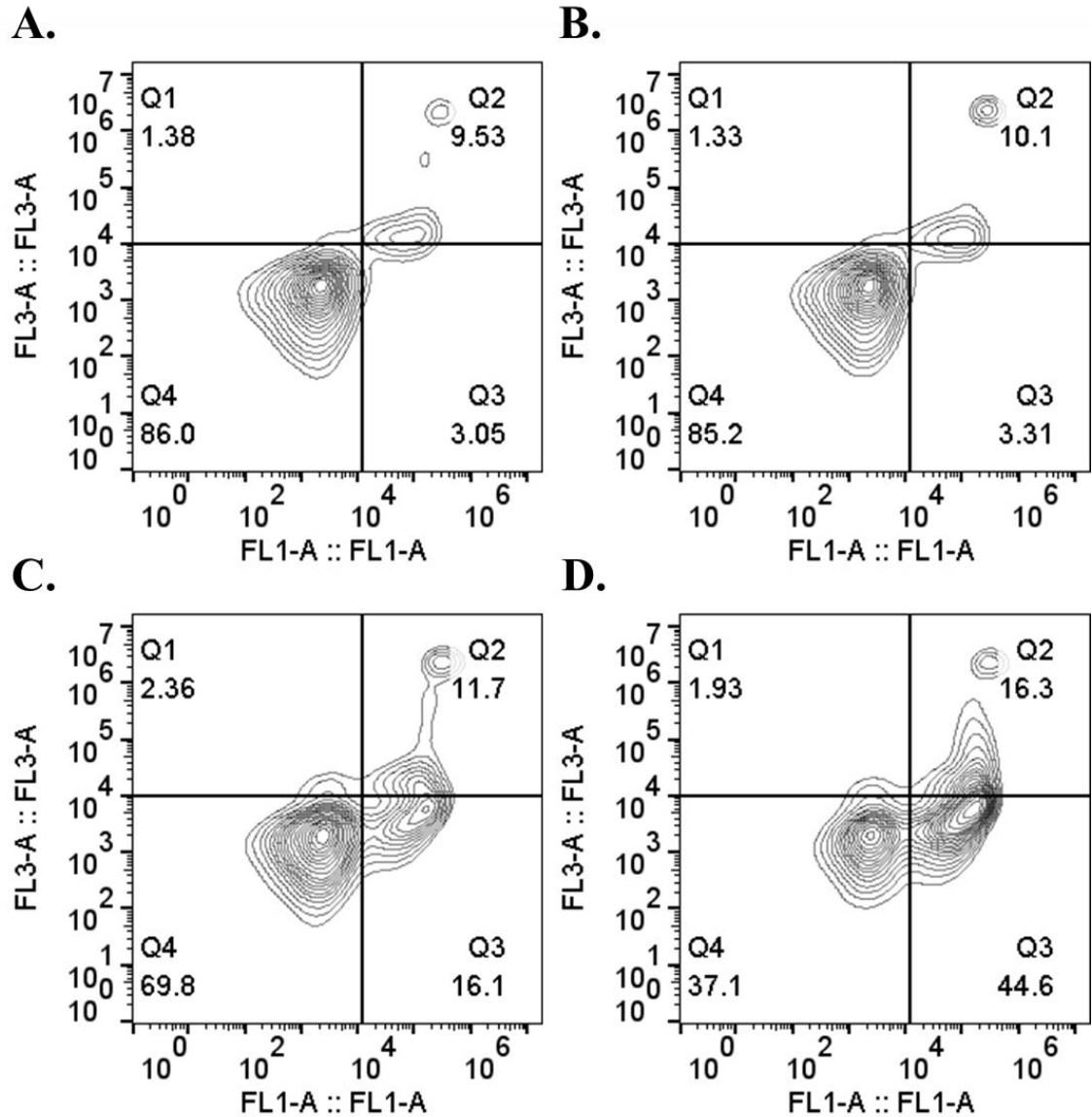


Figure 16: Optimization of hydrogen peroxide concentration.

(A-D) Contour plots from flow cytometry depicting cells undergoing apoptosis (x-axis as measured by Annexin V staining) or necrosis (as measured by propidium iodide staining) after 30 minutes incubation at 25°C in the stated concentrations of H_2O_2 in PBS supplemented with 2% BSA. (A) No H_2O_2 . (B) 10 μM H_2O_2 . (C) 100 μM H_2O_2 . (D) 1 mM H_2O_2 .

Table 3: Optimization conditions for micropipette experimental chamber buffer

Component	Optimized	Experimentally
H ₂ O ₂ Concentration	10 μ M	10-fold lower exhibited no changes in affinity for TCR-mtOVA, while 10-fold higher yielded poor cell quality
Chamber media	PBS + 2% BSA, with or without glucose oxidase	2% BSA yields negligible change in H ₂ O ₂ concentration but is necessary to minimize nonspecific adhesion
Cell concentration	100,000/mL	When 1 million cells/mL was used no significant change in affinity was observed
Amount of RBC inside chamber	< 0.5 μ L	Does not yield any changes in H ₂ O ₂ concentration at volumes used
Receptor-Ligand density	Combined \sim 2000/ μ m ⁴ for TCR and pMHC	Provides enough adhesion frequency resolution in the case of a decrease
Duration of treatment with H ₂ O ₂	30 minutes	Observed drop and recovery in this time frame, viability, TCR surface expression
Cell type	Naïve CD8+ T cells	Activated CD8 T cells were attempted with less prominent effect
Type of micropipette test	Many cells in one 30-minute test as opposed to one cell for 30 minutes	Examines "early" recognition, larger number of cells tested
Nonspecific	Negligible	No nonspecific adhesion between

Adhesion		RBC and cells were detected over 30 contacts
Glucose Oxidase Treatment	0.135 units/mL	Highest concentration where no change in RBC stiffness was detected
pH	No change	Buffer prevents changes in pH

4.2.2 Purified OT1 TCR binding to OVA pMHC is not influenced by H₂O₂

There are no documented cases of CD8 restricted TCR losing binding affinity to pMHC in response to H₂O₂. To confirm this is the case, a mutant variation of pMHC-I was employed that prevents binding between CD8 and MHC-I, thereby only testing the interaction between TCR and the binding region where peptide is loaded onto MHC-I. Recombinant OT-1 TCR was coated on a bead and probed against mutant OVA pMHC coated on an RBC yielding 2D effective affinity values that are consistent with values from previous studies²¹ (Figure 17). Upon injection of H₂O₂, no changes in 2D affinity were observed over the course of 30 minutes. By calculating the 2D affinity values for each cell-pair over the time course of the experiment, each cell pair acted as time bins in real-time, thereby affording the observation of affinity in real-time on live cells. The lack of change in 2D affinity over time supports the concept that the bimolecular interaction between the TCR molecule and pMHC molecule are not influenced by oxidation by H₂O₂.

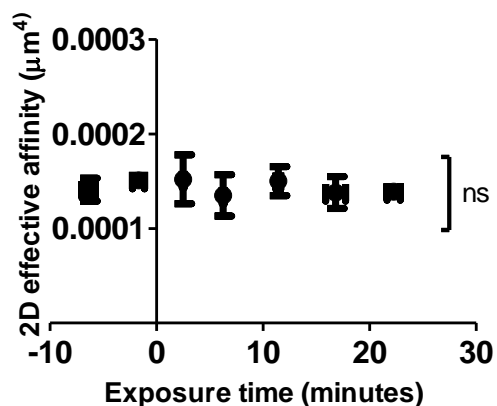


Figure 17. TCR affinity to pMHC in response to H₂O₂ exposure.

Each point represents affinity values between TCR coated on beads and pMHC coated on RBCs, in triplicate. Error bars represent standard error. An unpaired student's t-test was conducted between distributions for every point against distributions of the trace.

4.2.3 OT1 TCR binding to OVA is weakened in the presence of H₂O₂

Translating the lack of change in binding affinity into a cell system where TCR is expressed on OT1 transgenic T cells, the same micropipette adhesion frequency experiment was conducted with live cells instead of beads. In stark contrast to the purified system, 2D affinity values dropped within a minute of H₂O₂ introduction, reached a minimum at about 10 minutes, and gradually increased back to baseline levels attained before the introduction of H₂O₂ (Figure 18). Affinity values are normalized against the site densities of mutant pMHC on RBCs and TCR on T cells, and these values did not change over the time course of the experiment. Thus, despite TCR being monoclonal and the T cells being genetically identical, the 2D affinity can change in response to H₂O₂.

Injection of H₂O₂ into the chamber was administered as a bolus at 0 seconds. One explanation for the rebound in 2D affinity after about 10 minutes was that the effect of H₂O₂ diminished over time due to a loss in concentration. H₂O₂ was reported to consume H₂O₂ in fibroblasts¹⁰⁶, and therefore consumption was investigated for the OT1 T cells used in this system. Using different cell densities in solution, H₂O₂ concentration was monitored by fluorescence using the Amplex Red enzyme-facilitated conversion into

resorufin in response to H_2O_2 (Figure 19). These consumption profiles were fitted to a first order decay rate, and these functions were integrated to determine the dependence of rate of consumption on cell concentration. With an increase in concentration, molar amount of H_2O_2 consumed increased proportionally, as indicated by a well-fitting linear regression. Therefore, OT1 T cells were indeed consuming H_2O_2 and the loss in concentration may be responsible for the rebound in 2D affinity after 10 minutes.

To prevent the loss of H_2O_2 , a solution of glucose oxidase and glucose was developed to balance the depletion of H_2O_2 by T cells with generation of H_2O_2 from glucose. This was conducted within the experimental buffer which would prevent small changes in pH due to the glucose oxidase reaction and resulted in an experimental chamber predicted to be a constant concentration of H_2O_2 (Figure 20). Using this system, the 2D affinity values between TCR and mutant OVA gradually decreased and appeared to remain at a lower 2D affinity value (Figure 21). For the mtOVA trace, affinity values decreased upon injection to the same levels as in the bolus scenario. The wtOVA trace did not follow the same trend as the bolus scenario as discussed in section 4.2.4. These results suggests that continuous production of H_2O_2 by glucose oxidase can different effects on TCR-pMHC binding than a bolus injection.

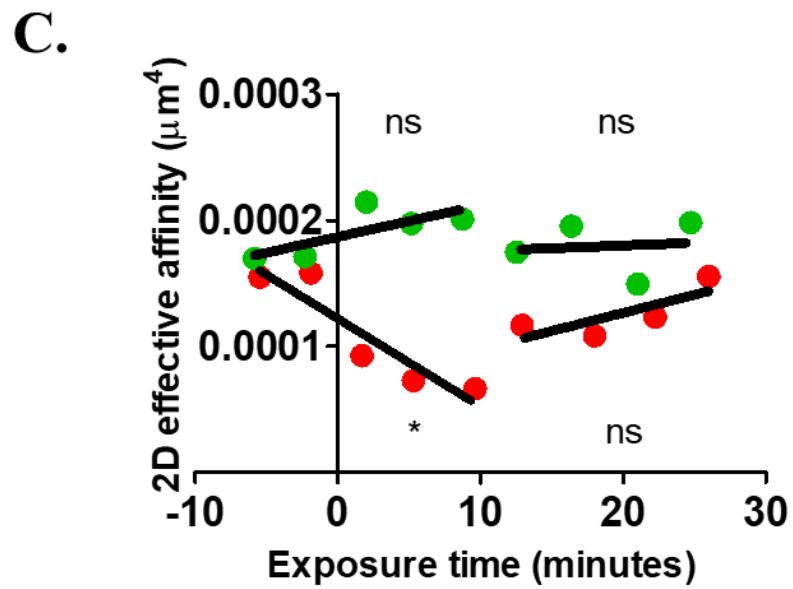
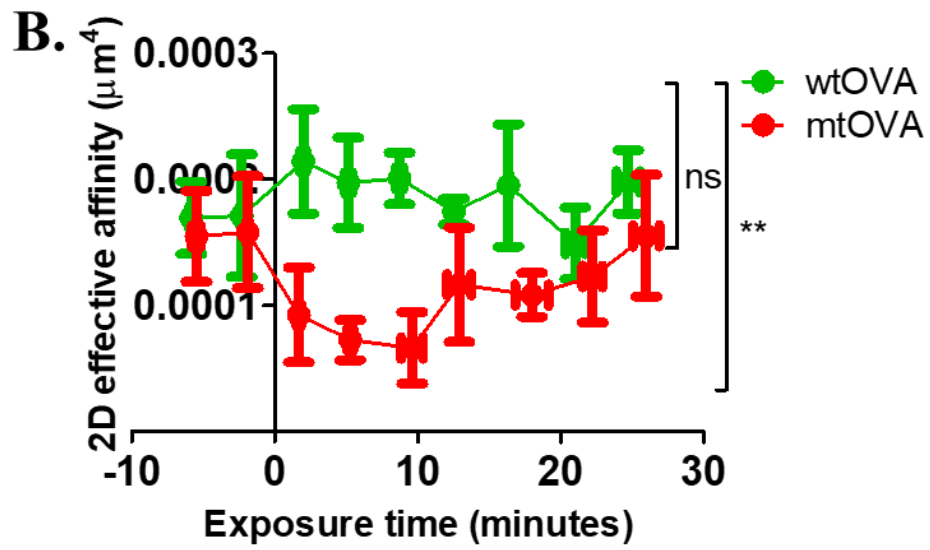
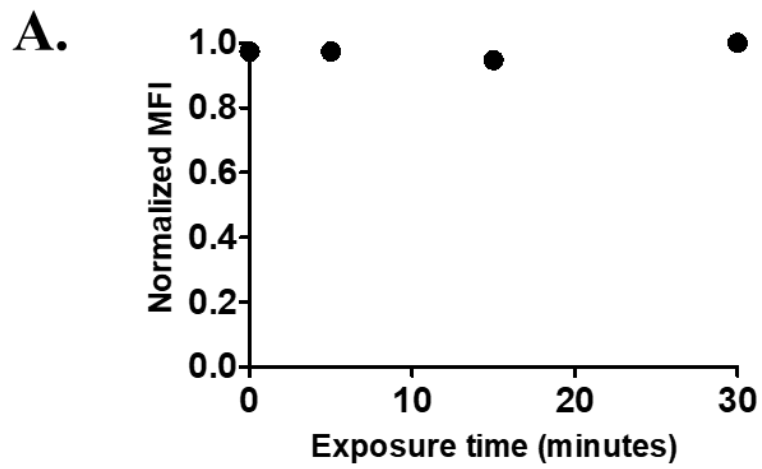


Figure 18. Hydrogen Peroxide effect on 2D affinity in OT-1 T cells.

(A) Surface expression of OT-1 TCR measured by flow cytometry over the time course of the experiment in the presence of H_2O_2 . (B) Plot of 2D affinity over time for wtOVA (green) and mtOVA (red) against OT1-TCR on live cells. Lines between points are visual connectors and not fittings. (C) Plot of same points from B but with overlaid linear regressions depicting significant differences from zero-slope. Error bars represent standard error. ** represents $p < 0.005$ using a two-way ANOVA test between red and green groups.

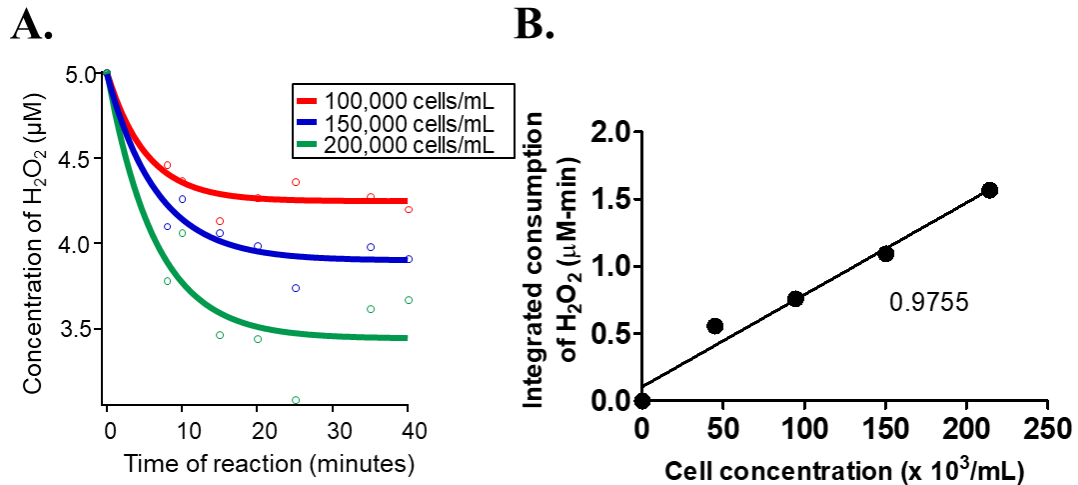
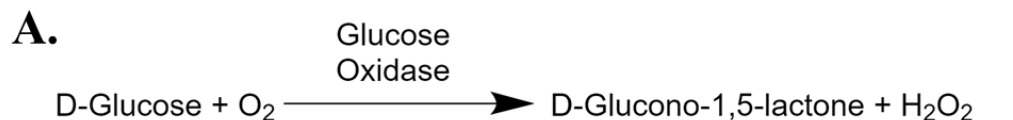
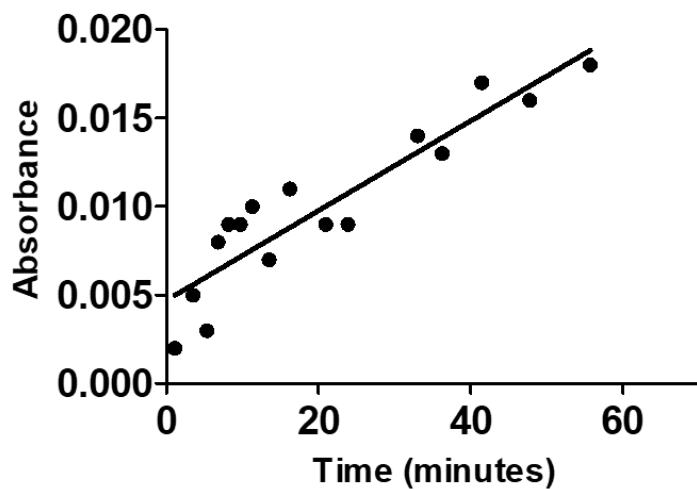


Figure 19. Consumption of hydrogen peroxide over time.

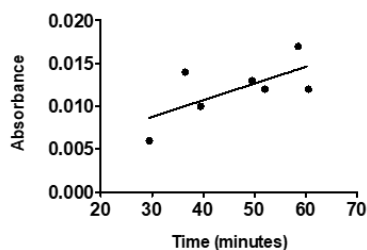
(A) Concentration of H_2O_2 over time in the presence of a specified cell density. Solid curved are first order decay functions fitted to the data with a starting point of 5 μM of H_2O_2 . (B) Plot of area under the curve from panel B against cell concentration. Solid line is a linear regression between the points with R^2 value displayed.



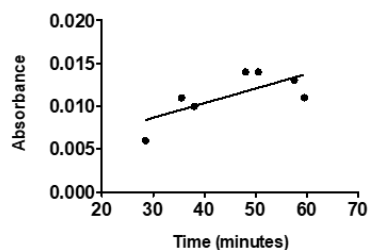
B.



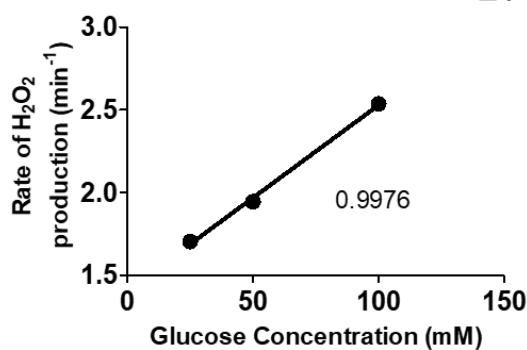
C.



D.



E.



F.

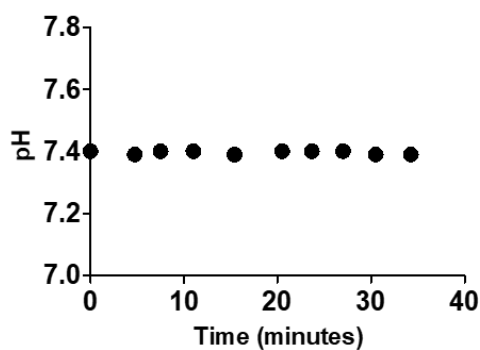


Figure 20. Hydrogen peroxide production facilitated by glucose oxidase. (A) Diagram depicting chemical reaction indicating stoichiometry between glucose, oxygen, and H₂O₂. (B-D) Plots representing absorbance readout by spectrophotometer at 240 nm peak fitted to linear regression. (E) Linear regression between slopes of lines from **B-D** to indicate the relationship with glucose concentration. The R² value is displayed. (F) pH monitoring of the optimized experimental chamber buffer.

4.2.4 CD8 coreceptor rescues diminished binding between OVA and OT1 TCR

To understand the extent of this reduced affinity towards pMHC, the wild-type pMHC was employed which allows binding to the CD8 coreceptor also expressed on the T cell. Therefore, in this experiment, both TCR and CD8 can bind to the pMHC on the surface of the RBC. By allowing CD8 binding, the reduction was completely abrogated, where the 2D affinity values between TCR and pMHC did not decrease over the course of 30 minutes of H₂O₂ bolus exposure (Figure 18). Interestingly, the affinity appeared to increase slightly immediately following bolus injection of H₂O₂. Since the only difference between experimental set-ups was the molecular make-up of the MHC molecule, it was concluded that CD8 binding was responsible for rescuing otherwise diminished binding in response to ROS.

When glucose oxidase was employed to generate a constant concentration of H₂O₂, the 2D affinity values between TCR and wtOVA persisted longer at the same value than the mtOVA, but eventually began to decrease to a level almost as low as the case for mtOVA (Figure 21). The 2D affinity values also appeared to increase after 20 minutes, but not to baseline levels before injection and was not monitored after 30 minutes. Linear regressions fitted to both traces reveal negative slopes for both data sets unlike the case of bolus injections. These results suggest that continuous production of H₂O₂ by glucose oxidase can influence CD8 incorporated TCR-pMHC binding in a fashion that a bolus injection is not capable of exerting.

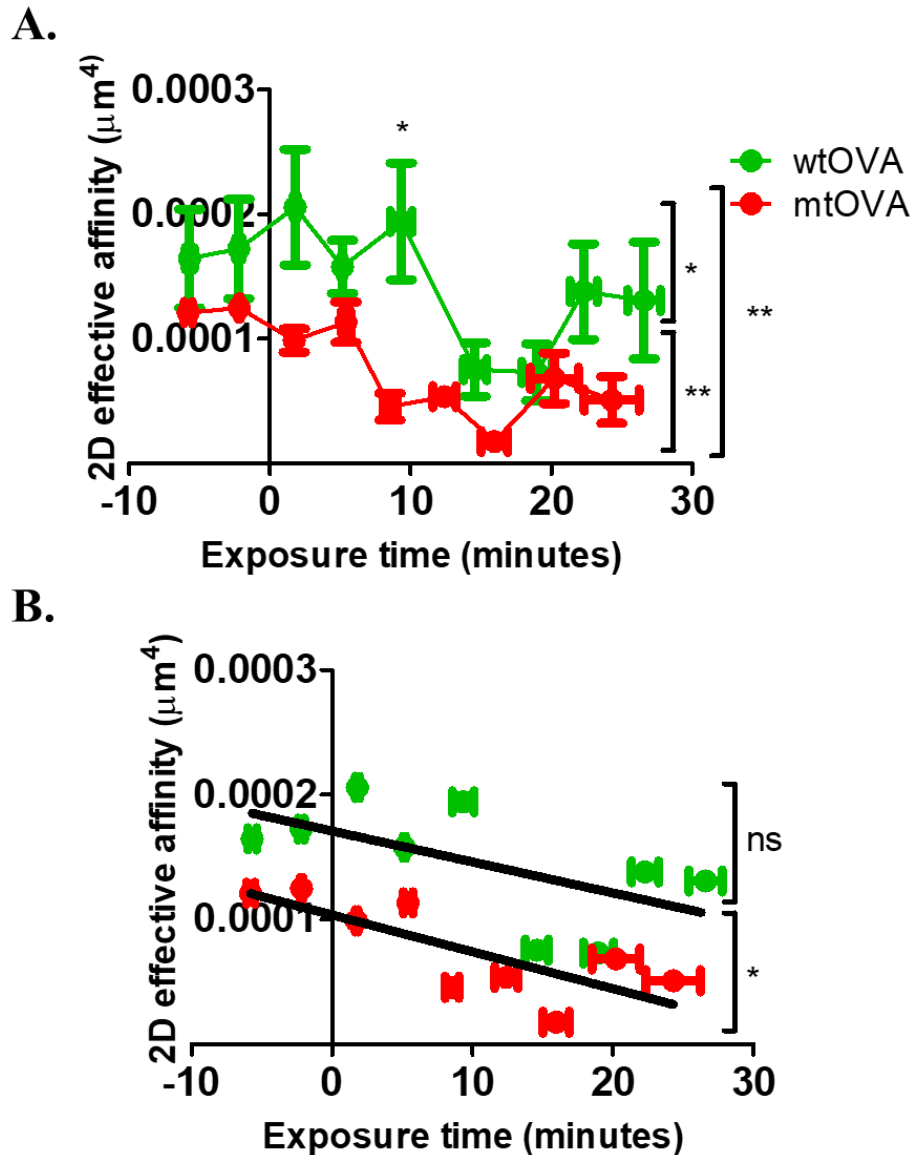


Figure 21. Effect of continuous hydrogen peroxide production on 2D affinity. (A) Plot depicting 2D affinity between TCR and wtOVA or mtOVA over time. * above the green trace represents $p < 0.05$ using an unpaired student's t-test to test for significant differences between the time point at which the affinities significantly decrease (described in more detail in the statistics section 4.1.3.2). * to the immediate right of the traces represents $p < 0.05$ using an unpaired t-test between the lowest and baseline point distributions on the green trace, ** represents $p < 0.005$ tested in the red trace. ** to the far right of the traces represent $p < 0.005$ using a two-way ANOVA between traces. Solid lines between points are visual connectors and not fittings. (B) the same plots from A but with linear regressions fitted to each trace and statistically compared to a slope of zero. Error bars represent standard error.

4.2.5 Lck activity regulates coreceptor rescue of TCR binding

While the TCR-pMHC interaction was shown here to not be sensitive to oxidation by H₂O₂, other components of the TCR machinery have been documented to be sensitive to ROS. One example that has been widely documented to be ROS-sensitive is the Lck kinase. Since this kinase can act as a bridge between CD3-ITAMs which are associated with TCR and the CD8 coreceptor, we hypothesize that this this kinase may be responsible for stabilizing the wtOVA-TCR interaction in response to ROS.

Cells were incubated with an ATP-competitive Lck inhibitor and underwent binding with wtOVA. Without Lck inhibition (DMSO vehicle treated cells), 2D affinity values remained stable over 30 minutes as shown earlier, as previously shown without DMSO vehicle (Figure 22). However, upon Lck inhibition, the TCR-wtOVA interaction displayed sensitivity to H₂O₂ bolus injection, as indicated by a decrease and increase similarly seen with mtOVA in response to H₂O₂. The value that the affinity reduced to was also similar to values when mtOVA-TCR binding was exposed to a bolus of H₂O₂. Additionally, as observed before, there was a slight increase in affinity for the non-treated wtOVA-TCR interaction upon bolus injection, but this increase was not observed when Lck was inhibited. These data suggest that Lck is regulating the resistance to decrease in 2D affinity in response to ROS exposure.

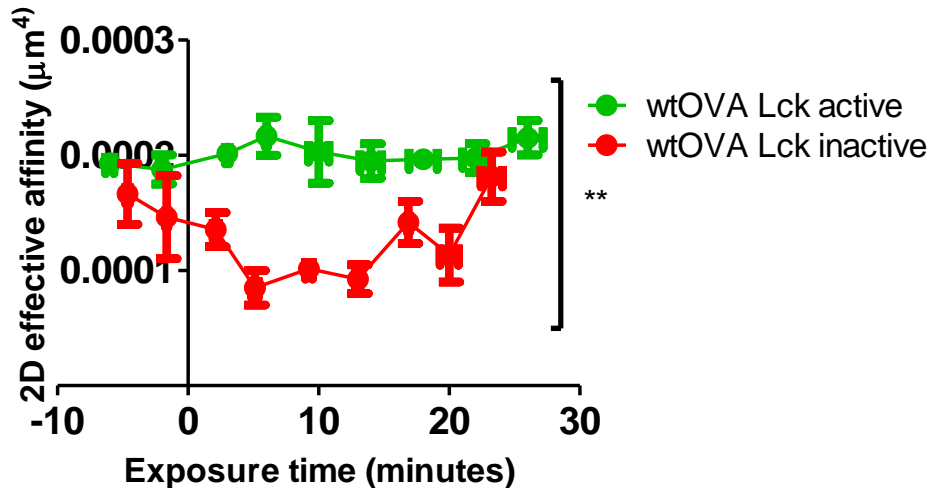


Figure 22. The role of Lck activity on 2D effective affinity.

Plots depicting 2D effective affinity in response to a bolus injection of H_2O_2 when cells were either left untreated (green trace) or pre-treated with an Lck inhibitor (red trace). Lines between points are visual connectors and not fittings. Error bars represent standard error. ** represents $p < 0.005$ using a two-way ANOVA between the red and green traces.

4.2.6 Lipid raft oxidation and actin inhibition reduce 2D affinity

Another species susceptible to ROS is membrane cholesterol. Since it has been suggested recently that TCR associates with cholesterol to present itself in an active and inactive state, cholesterol oxidase was used here to examine the effect on 2D affinity. Cells were preincubated with cholesterol oxidase which oxidizes cholesterol to cholestenone and prevents association with TCR. The progression of cholesterol oxidation was therefore not tested in this experiment. Here, the mtOVA system was used to only observe the interaction between TCR and loaded peptide (without convolution of coreceptor protection effect). Cells treated with a vehicle exhibited the decrease and increase in 2D affinity in response to H_2O_2 injection shown before. Cells that were pretreated with cholesterol oxidase, however, exhibited a much lower 2D affinity to the baseline non-treated mtOVA scenario, and this value did not change over the course of H_2O_2 exposure for 30 minutes (Figure 23). Interestingly, the 2D affinity value shown by

cells here is very similar to the values reached and maintained at when glucose oxidase is continually generating H_2O_2 , for both the mtOVA and wtOVA cases.

The actin cytoskeleton is known to be closely associated with lipid rafts, necessary for robust 2D binding, and responsible for TCR-mediated pMHC pulling. Therefore, binding under H_2O_2 exposure with inhibited actin polymerization was examined to understand the interplay between oxidation and actin remodeling mechanisms. Both wtOVA and mtOVA binding to MHC was greatly inhibited upon pretreatment with latrunculin A while H_2O_2 was injected as a bolus (Figure 24). While the values of affinity did not change from before the bolus injection to after the bolus injection, after 15 minutes of exposure without further inhibition by Latrunculin A, they appeared to show small increases. This experiment displayed potential relationships between oxidation and actin polymerization with regards to TCR binding to pMHC.

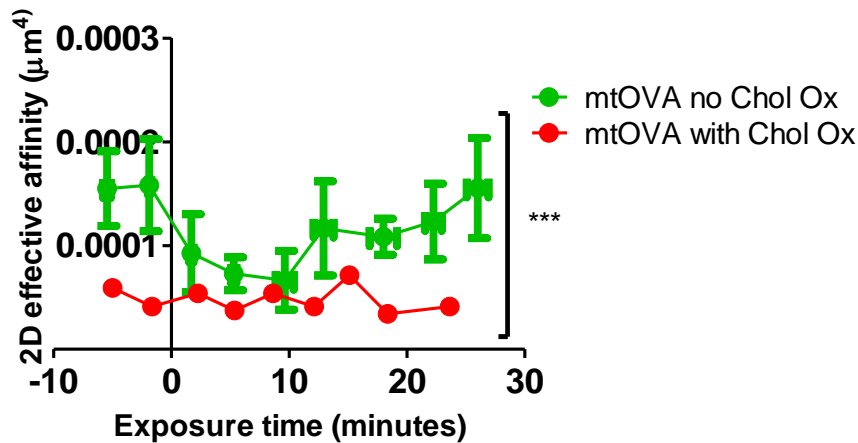


Figure 23. The role of cholesterol in regulating binding.

Plots depicting 2D effective affinity in response to a bolus injection of H_2O_2 when cells were either left untreated (green trace) or treated with cholesterol oxidase (red trace). Lines between points are visual connectors and not fittings. Error bars represent standard error. *** represents $p < 0.0005$ using a two-way ANOVA tested between the green and red traces two test for significant differences between the cholesterol oxidized group and the non-cholesterol oxidized group.

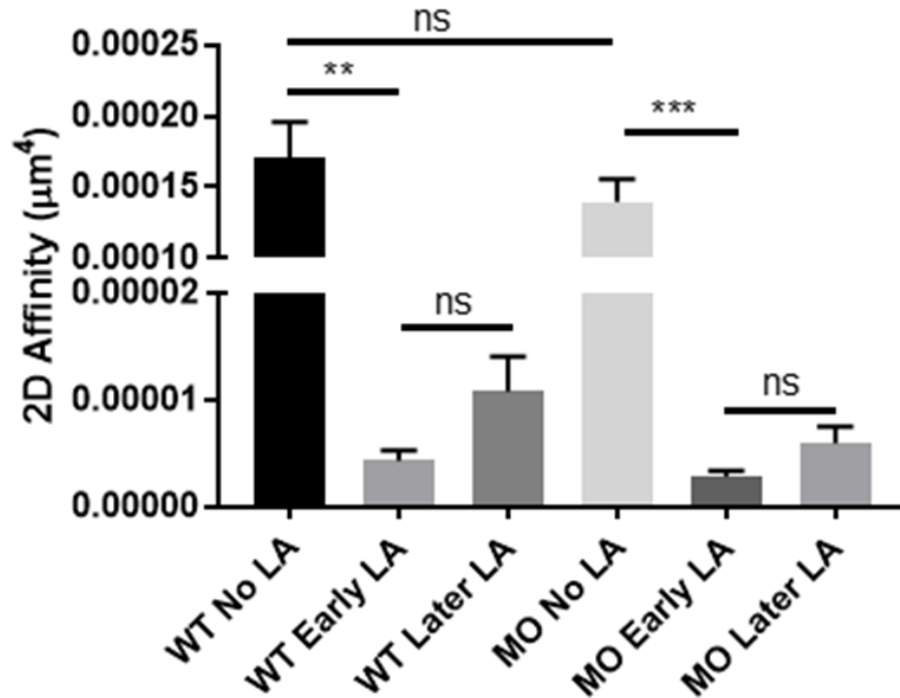


Figure 24. Effect of cytoskeleton on 2D affinity in the presence of hydrogen peroxide. Plot depicting 2D effective affinity between TCR and wild-type OVA (WO) or mutant OVA (MO) under a bolus of H₂O₂ after cells were pre-treated with Latrunculin A. Early plots represent affinity from the first 15 minutes, while later plots represent affinity from the next and last 15 minutes of the experiment. Error bars represent standard error. ** and *** represent p-values less than 0.005 and 0.0005 respectively by an unpaired t-test.

4.3 Discussion and conclusions

Excessive presence of ROS has been well documented in inflammatory environments associated with autoimmunity⁹⁰, cancer²²⁰, and airway diseases⁸⁷. Since T cells play a central role in these pathologies, the effects of ROS on T cell function have also been long well studied, albeit with discrepant conclusions⁹⁶. For instance, T cell proliferation was found to be both inhibited and promoted by ROS. Further complicating investigation was that T cells produce a burst of ROS in response to TCR triggering, which also serves as a mode to release calcium from the mitochondria in a feed-forward fashion. Finally, many (but not all) TCR-associated molecules have been documented to be sensitive to oxidation which can alter the efficiency by which TCR is triggered⁹⁶. The complexities in the interplay between endogenous and exogenous ROS, as well as the specific oxidative sensitivities of kinases, phosphatases, cholesterol, and actin, prompted

treating the T cell as a black box. In this approach, TCR binding to pMHC was monitored in real-time while all the effects of ROS on the T cell were ongoing. The input into the T cell black box (with or without CD8 coreceptor binding) was H₂O₂, and the readout was the degree of TCR-pMHC binding. Through this dissection, it was determined that the degree of binding in response to ROS was regulated by the presence of coreceptor binding, Lck kinase activity, and membrane cholesterol organization. This is the first direct demonstration of how these mechanisms can regulate TCR binding to pMHC on live cells in real-time which provides novel insights into how TCR recognize antigen in pathological environments.

4.3.1 Model for oxidation of TCR-pMHC-CD8-Lck signaling loop

To test whether TCR-pMHC binding is sensitive to oxidation by H₂O₂, a real-time micropipette adhesion frequency assay was developed which monitors the 2D effective affinity of interactions on live cells in real-time. This approach leveraged the observation that TCR is triggered within 1-3 minutes, at which point signaling cascades may occur which could enhance binding through further recruitment of TCR, kinases, and adaptor molecules. The time resolution of this method is therefore the duration of one cell pair interacting for 30 contact which would occur over no longer than 3 minutes. Using this method, recombinant OT1 TCR was probed against mtOVA pMHC which prevents CD8 binding. While, there is no CD8 on the RBC coated with TCR, this condition served as a control for future experiments using primary OT1 T cells which express high levels of CD8. Additionally, this interaction focused the attention only on TCR-pMHC sensitivity to ROS. As expected, the interaction was found to remain at a stable affinity throughout the 30 minutes of ROS exposure, clearly indicating that the TCR-pMHC interaction does not experience binding-altering oxidation to a mild 10 μM treatment of H₂O₂, which was found in pathological environments¹⁰⁶. This was not, however, the case when mtOVA was probed against primary OT1 T cells.

Without contribution of CD8, TCR-pMHC binding underwent a period of diminishing affinity followed by a recovery. While the specific mechanisms by which the changes occurred may differ, they are likely both due to oxidation of a T cell intrinsic factor since no change in affinity was observed before injection of H₂O₂, and no changes in affinity were observed for the purified protein interaction over the same time course. The recombinant TCR-mtOVA interaction displayed roughly the same affinity as those measured in the cell system, as previously shown. For the decreasing regime between the time of H₂O₂ injection and about 10 minutes, oxidation of a variety of TCR-binding-associated molecules may have reduced the on-rate between TCR and pMHC, which will be discussed further later. To rationalize the recovery regime which began around 15 minutes after H₂O₂ injection and ended at the conclusion of the experiment at 30 minutes, two possibilities were proposed: 1) cells consumed H₂O₂ and the TCR-binding-molecules that were sensitive to oxidation returned to their reduced state as H₂O₂ was gradually depleted; or 2) cells underwent an adaptation phase in which the cell exerted compensatory mechanisms to recover binding to baseline levels in response to an unchanging H₂O₂ concentration. Interestingly, using wtOVA abrogated changes in TCR-pMHC binding affinity. Since the only difference in the experimental set-up compared to the mtOVA case was the molecular make-up of the MHC molecules which either allowed or prevented CD8 binding, it was concluded that the coreceptor rescued diminished binding in response to ROS.

To test the two possibilities for why a recovery period was experienced in the case of mtOVA binding, H₂O₂ consumption was measured. Indeed, it was discovered that T cells were consuming H₂O₂ at a cell density dependent rate. However, it was found that consumption of H₂O₂ plateaued for T cells over time, as opposed to a profile exhibiting continual consumption to zero. While it was clear that T cells do indeed consume H₂O₂, a possible explanation for the plateauing profile was that T cells may produce ROS in response to activation by ROS. It was previously suggested that nonphagocytic NADPH

Duox1 produced ROS in response to T cell activation as indicated by calcium flux as means to sustain TCR signaling. This model is consistent with the current data whereby low cell densities are activated by H₂O₂ more readily and may produce ROS as measured by the Amplex Red assay. For the intermediate cell density, cells first consume H₂O₂ by their antioxidants but sufficient H₂O₂ is present to activate H₂O₂ generation which together with exogenous H₂O₂ would eventually deplete antioxidants preventing any further consumption. In contrast, cells in the highest density tested may have consumed most of the H₂O₂ before generating activation-mediated ROS. Altogether, these findings clearly demonstrate H₂O₂ consumption which precludes the second possibility for the affinity recovery, which was based on the assumption that H₂O₂ concentration was not changing. Therefore, it was assumed that the effects of H₂O₂ were wearing off on TCR-binding-associated molecules. To test this assumption, an optimized solution with constant production of H₂O₂ by GOx was developed and it was found that the reduction of affinity was prolonged for the mtOVA and strikingly, a reduction in affinity was observed for the wtOVA case as well. This supports a model where any rescuing capacity of the CD8 coreceptor could only sustain an extent and duration of H₂O₂ oxidation, before itself being prone oxidation.

As discussed earlier, several TCR-binding-associated molecules are sensitive to oxidation. The difference in binding profiles between mtOVA and wtOVA in response to H₂O₂ bolus provided a first speculation into what could be important for TCR binding in an oxidative environment. Since Lck associates with the coreceptor, testing its role was a logical progression. By maintaining Lck in an inactivated state, TCR-wtOVA binding was found to resemble TCR-mtOVA binding in response to a H₂O₂ bolus. These data are consistent with a model described by a recent study discussed in Section 3.3.3, which proposed a TCR signaling loop between the TCR-CD3 complex, the Lck-CD8 coreceptor complex, and the pMHC on the APC. In the referenced study, the coupled trans-cis heterodimeric interactions were proposed to amplify discrimination between positive-

and negative-selecting ligands¹⁹. Association between CD8-bound Lck and the CD3 ITAMs played a central role in this discrimination. The same Lck inhibitor used in that study was used in the present study and it appeared to play a similar role in stabilizing TCR-pMHC interactions in the presence of H₂O₂, although direct measurements of bond lifetimes were not measured in the present study. This is due to observations made during optimization of the present study where H₂O₂ induced stiffening of the RBC. This phenomena occurs due to oxidation of Fe²⁺ in the hemoglobin prosthetic group to Fe³⁺ which creates methemoglobin. Such an alteration is incompatible with the BFP assay which is centered around the stiffnesses of carefully modified and calibrated RBCs. Using RBCs in the micropipette adhesion assay in the presence of H₂O₂ was carefully optimized, however, the requirement of stiffness is far less important. The only necessary feature for RBCs was qualitative deformability that could be observed with 40X magnification and did not change quantitatively in response to H₂O₂. This was confirmed to be the case when the purified protein system was tested. No reduction in affinity was found in this case which is in support of both no change in the receptor-ligand interaction and no change in RBC deformability monitoring. Had bond lifetimes been measured, it was hypothesized that H₂O₂ bolus would reduce bond lifetimes in a similar fashion to how Lck inactivation altered select catch-bonds into slip bonds. It was concluded that exposure to H₂O₂ (continuously produced by GOx) resulted in inactivation of Lck and reduced affinity which mirrored the effect seen when the coreceptor was not engaged to mtOVA. These findings underscore the importance of the Lck-engaged coreceptor in stabilizing TCR-pMHC interactions.

Whether H₂O₂ directly or indirectly inactivates Lck could not be directly determined from the available data. Previous studies suggest that critical cysteines mediate the association between Lck and the coreceptor¹³⁷. Under H₂O₂ exposure of the present study, these cysteines could undergo oxidation and association to the coreceptor could be prevented. This would abrogate the mechanotransduction loop which could

result in reduced binding in response to H₂O₂ even if the CD8 coreceptor was present to interact with pMHC. It is important to note that Lck would still be bound to the membrane, and this scenario does not reveal anything about the activation state of Lck. However, without its association to CD8, Lck would not serve as a bridge between TCR-CD3 and CD8 regardless of its activation state and therefore it is reasonable to posit that oxidation-modified Lck would effectively serve equivalent roles in the context of TCR-pMHC binding.

An alternative possibility to the importance of Lck in TCR-pMHC binding is that H₂O₂ is indirectly influencing Lck by inactivating phosphatases which are known to be sensitive to oxidation. Both CD45 and Shp1 have been shown to be critical in the regulation of TCR proximal signaling⁹⁶. CD45 has been shown to be able to dephosphorylate both the activating Y394 and the inhibitory Y505, thereby deactivating and activating Lck, respectively. Additionally, CD45 has been extensively studied for its role in the kinetic segregation model for TCR triggering²⁹. Accordingly, it is thought that CD45 is largely excluded from sites of TCR-pMHC-CD8 binding, therefore implying that CD45 must exert its effects on Lck away from these sites. In contrast, it is clear that Shp1 is a negative regulator for TCR signaling because Shp1 deficiency has been shown to lead to T cell hyperresponsiveness. Accordingly, it was found that Shp1 dephosphorylates the inhibitory tyrosines for both Lck and Zap-70. Both these phosphatases were shown to be inactivated by H₂O₂. Interestingly, the ROS burst resulting from TCR triggering was sufficient to cause sulfenylation in Shp1 and Shp2 phosphatases. This suggests that even transient oxidation was capable of inactivation, which would consequently lead to prolonged activation of Lck. However, an enhancement in activation of Lck due to phosphatase inactivation should result in higher affinity interactions, assuming the converse effect of the mechanotransduction loop, and was therefore concluded to not play a role in the reduction in affinity. Upon closer inspection of the data however, a small increase in affinity was observed for all the

wtOVA cases. While not significantly different from the baseline, the increase does indeed consistently coincide with a response to a transient change in ROS concentration. Taken together, both direct and indirect oxidation effects on Lck by H₂O₂ are plausible based on observations of real-time data.

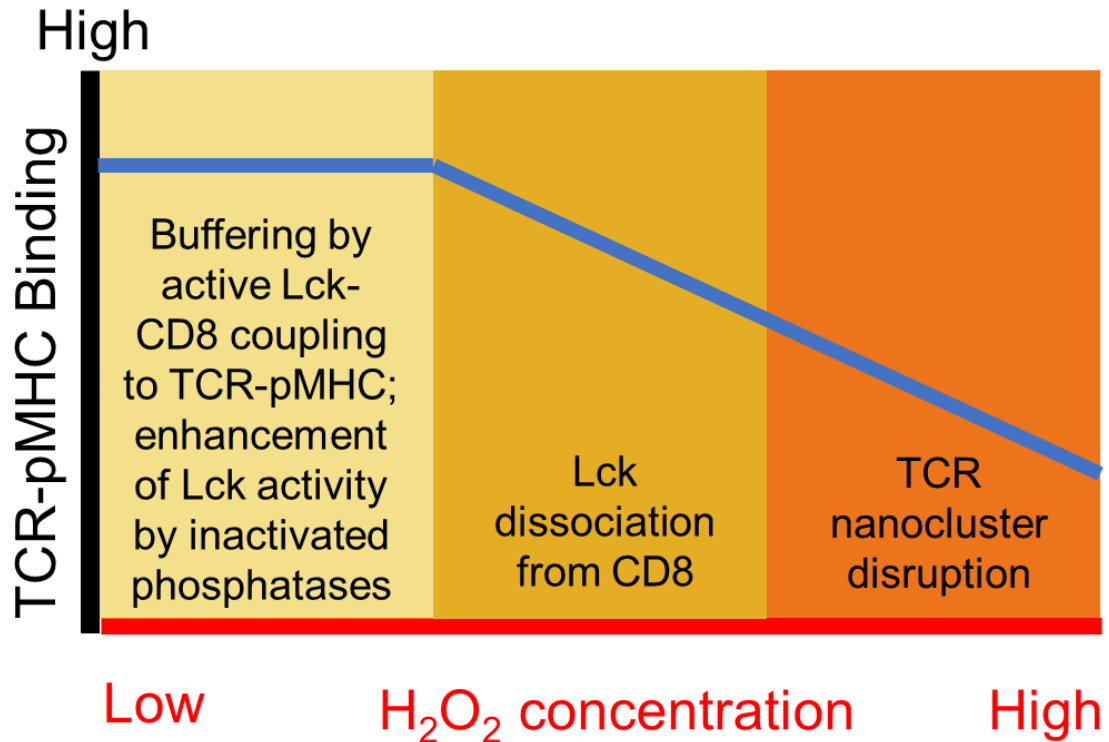


Figure 25. Model for effect of H₂O₂ on TCR binding

4.3.2 Cholesterol and actin dependencies

All of the aforementioned proteins are anchored in the plasma membrane which contains microdomains rich in cholesterol¹⁴⁴. Referred to as lipid rafts, these microdomains are also densely populated with surface proteins. TCR has long been associated with lipid rafts and it has been suggested to play role in TCR triggering by multimerizing TCR and increasing its avidity. More recently, cholesterol that associates with the TCR β -chain transmembrane region has been suggested to lock the TCR into a resting state which prevents phosphorylation of the CD3 ITAMs by active kinases²²¹.

Upon dissociation with cholesterol, the TCR is in a primed active state which can be stabilized by binding to pMHC. This allosteric model, however, does not encompass binding kinetics between TCR and pMHC when influenced by cholesterol association. In fact, a previous study by the same group provided evidence that cholesterol association with TCR did not influence the affinity between TCR and pMHC, however it did play a role in increasing the avidity of the interaction¹⁴⁹. Another study determined that displacement of cholesterol by its naturally occurring derivative, cholesterol sulfate (which does not bind to the TCR β -chain transmembrane region), reduced CD3 ITAM phosphorylation¹⁵⁵. By disrupting TCR nanoclusters, analogously to how cholesterol oxidase can disrupt nanoclusters, TCR triggering was inhibited. These studies underscore the importance of cholesterol in CD3 ITAM phosphorylation and provide insight into how a drastic reduction in TCR-pMHC affinity were observed in cell systems using micropipette assays. One possibility is that TCR adopt organizations or conformations that are stabilized by pMHC interaction which is a model consistent with aforementioned literature positing a TCR primed state. Monte Carlo simulations support this concept by demonstrating that once a single TCR is primed, it can propagate the same conformation to the surrounding TCR within the nanocluster²¹⁸. The phenomena of propagating increased binding to other TCR could be quantified using a memory index, which examines enhancement of bond formation relative to prior bond formations. In the present study, a positive memory index would be expected for the unperturbed interactions between OT1 TCR and mtOVA due to the presence of TCR nanoclusters. However, upon oxidation by H₂O₂ or by cholesterol oxidase, the memory index would be expected to be closer to zero since the nanoclusters would be more dispersed, thereby preventing the TCR-pMHC bond to serve as a scaffold for future bond formations. The degree of reduction in affinity due to cholesterol oxidase, coincides closely with the trough experienced by the TCR-mtOVA interaction in response to the H₂O₂ bolus, as well as for both mtOVA and wtOVA interactions when treated with continuous H₂O₂.

These data support a model whereby oxidation of cholesterol by H₂O₂ disrupts nanoclusters, altering the primed state of TCR which preferentially binds to pMHC, resulting in reduced 2D effective affinity to pMHC.

A similar response was imagined for the influence of actin polymerization on affinity values. Previous studies have shown that preventing actin polymerization by latrunculin A results in a drastic reduction of affinity between OT1 TCR and OVA pMHC²¹. Interestingly in this study, it was found that regardless of the incorporation of CD8 binding to pMHC, affinity values were still greatly reduced upon treatment with latrunculin A. Since exposure of H₂O₂ did not decrease either of the affinity values between TCR and mtOVA and wtOVA, it was concluded that the ability for actin to reorganization played the most dominant role in TCR binding regardless of the oxidative state. Nevertheless, actin components have been previously shown to be sensitive to oxidation¹⁵³. Cofilin is kept in an inactive form in the plasma membrane by binding to phosphatidylinositol 4,5-bisphosphate. Upon Ras-dependent dephosphorylation, cofilin adopts an activated state which can mediate actin polymerization which was shown to be important for SMAC formation. This activated state was also shown to be sensitive to its redox environment, whereby oxidation keeps cofilin insensitive to dephosphorylation. Another study using DNA force probes have shown that inhibition of actin reorganization prevents TCR-mediated pulling on pMHC^{212,222}, thereby clearly demonstrating that the T cell is capable of generating force through the TCR and that the force is actin-dependent. These forces have been previously shown to play a central role in amplifying the discriminatory power of the TCR when scanning pMHC. These studies indicate that actin plays a central role in TCR recognition of pMHC, and inhibition by oxidation could abrogate its dominance. The results in the present study do not support this concept, however. The main piece of data that argues against oxidation of cofilin and prevention of membrane proximal actin reorganization is the unchanging affinity values of TCR-wtOVA in response to H₂O₂ bolus exposure. Supporting this are affinity values that did

diminish never reaching the remarkably low affinity values seen when actin polymerization was inhibited by latrunculin A. Thus, both membrane proximal oxidation of cofilin and global oxidation-mediated inhibition of actin reorganization, respectively, were unlikely. In conclusion, as depicted in Figure 25, oxidation of cholesterol nanoclusters rapidly reduces affinity of TCR-pMHC but can be rescued by the quaternary molecular signaling loop between TCR, CD3, Lck, and CD8. However, after a threshold of H₂O₂ concentration is reached without counter from antioxidants, the quaternary-signaling loop stabilization is disrupted possibly due to critical cysteine mediated dissociation of Lck from CD8. These conclusions derived from the real-time analysis afforded by the micropipette adhesion frequency assay.

4.3.3 Role of post-translational modifications in TCR recognition

The cancer microenvironment contains a soluble milieu of proinflammatory cytokines, chemokines, ROS, and reactive nitrogen species. It is incompletely understood how these various soluble species can modulate one another, but it has long been appreciated that together, they can have an inhibitory effect on infiltrating T cells recognizing tumor antigen. Myeloid derived suppressor cells (MSDCs) were suggested to be the predominant cell type in the microenvironment to promote tumor-associated CD8+ T cell tolerance²²³⁻²²⁵ by directly contacting CD8+ T cells^{220,223,226}. It was reported that MSDC-upregulated superoxide reacted with constitutive levels of nitric oxide to yield peroxynitrite which could induce structural modification of TCR and CD8 molecules²¹⁶. Based on molecular modeling, the relatively stable²²⁷ and disruptive²²⁸ nitrotyrosine resulted in an impaired TCR-pMHC-CD8 interaction which explained their observed induction of antigen-specific non-responsiveness of peripheral CD8 T cells and could be reversed by prophylactic treatment of peroxynitrite-neutralizing uric acid²¹⁶. This study clearly demonstrated how post- translational modifications on TCR and CD8 could lead to impaired TCR recognition of antigen ultimately resulting in tumor tolerance. However,

the study relied on adoptive transfer of large amounts of MSDCs which may induce exaggerated levels of peroxynitrite, as suggested by further results in their studies with very limited levels of nitrotyrosine in CD8⁺ T cells, far from enough to reflect tumor tolerance. Instead, present in much higher levels than effects of nitrotyrosine are oxidative effects due to ROS generated from a variety of inflammatory cells, including MSDCs²²⁶. Due to the ubiquitous nature of oxidation sensitive kinases and phosphatases in inflammatory cells, it is reasonable to speculate that ROS may play a more significant role in tumor tolerance than nitrotyrosine. Thus, this study provides a complementary mechanism to altered recognition of antigen by CD8⁺ T cells.

4.3.4 Cell- and tissue-scale effects of ROS and antioxidants

The role of ROS in T cell function is convoluted, with many signaling molecules important for T cell activation being sensitive to oxidation in both positive and negative regulatory fashions, and functions such as cytokine secretion and proliferation reflecting the same discrepancies. These conflicting conclusions could be a result of different antioxidant capacities of T cells at its various developmental and activation stages, as well as the presence of antioxidants in different anatomical compartments. For example, activated CD8⁺ T cells were shown to have a higher antioxidant capacity than naïve CD8⁺ T cells; and in asthma studies investigating the role of oxidative stress on T cell function, T cells in peripheral blood experienced no deficiencies while those in the oxidative environment of the lung exhibited impaired effector function. Additionally, regulation of TCR binding and signaling itself can be dynamic based on its location in the body, as previously shown during viral infections.

Nevertheless, there is a wealth of studies that suggest that ROS plays a central role in tumor initiation and progression. To protect against these purported deficiencies in immune surveillance due to ROS, Ando and colleagues²²⁹ transduced catalase into CD4⁺ and CD8⁺ T cells. Indeed, expression of catalase were concluded to improve function

and proliferation of CD4⁺ T cells, rescue CD8⁺ T cells from cell death, and improve CD8⁺ T cell capacity to recognize antigen all in excessive presence of H₂O₂ (between 100 and 200 μ M bolus administration). An alternative possibility, consistent with results in the present study, is that catalase improved the viability of T cells, affording them their baseline effector functions. In a subsequent study²³⁰, they co-expressed catalase with a chimeric antigen receptor (CAR) and that the bicistronic expression was found to improve targeted killing compared to only CAR expressed T cells, mainly at the 12.5 μ M which is a more reasonable H₂O₂ concentration to model a pathological microenvironment without convoluting effects of apoptosis or necrosis. Interestingly, the improved killing was more pronounced with bystander T- and natural killer cells. Thus, the protection mediated by antioxidants appeared to play a more important role in T cells where the mechanisms for TCR specific recognition were not bypassed by the CAR. Those findings are consistent with conclusions from the present study whereby signaling molecules important for TCR recognition of antigen may be impaired by H₂O₂.

Administration of antioxidants for the goal of preventing cancer has demonstrated conflicting clinical outcomes. Some studies have provided evidence of antioxidants as an effective strategy to prevent the initiation or progression of some cancers²³¹⁻²³³, while others have found that they increase the likelihood of initiation for other contexts of cancer²³⁴⁻²³⁶. Generally, dietary antioxidants did not reduce the incidence of cancer and in fact there is experimental evidence that they increased the incidence and death from lung and prostate cancers²³⁷. Supporting these clinical data were two recent complementary studies that showed oxidative stress in fact plays a role in limiting metastasis of melanomas^{238,239}. They found systemic antioxidants directly improved the migratory properties of cancer cells and enabled prolonged survival through circulation that otherwise would have been detrimentally oxidative. Therefore, administration of antioxidants leading to a systemic reduced environment must be considered with caution for cancer therapy. It is important to note, however, that neither of these studies examined

the role of antioxidants in the initiation of cancer. Rather, they relied on examining fully developed cancers of a highly tumorigenic mouse melanoma model. The results of the present study are focused on immune surveillance prior to the point where metastases occur but following the generation of an oxidative microenvironment which may impair TCR recognition. It was shown for the first time herein, that continuous presence of H₂O₂ does indeed reduce binding between TCR and its cognate pMHC which would impair its activation and effector function in killing target cells. This dysfunction was likely accomplished by oxidation of membrane cholesterol and Lck cysteines. Genetically modifying CD8⁺ T cells to express catalase may be a viable system to improve recognition of tumor antigen.

CHAPTER 5 Aim 3

Determine the role of TLR4-LPS binding in ROS-impaired function. ROS generation by NOX proteins and TLR4-LPS signaling interact in a positive feedback fashion^{187,188}. Meanwhile, upregulation of ROS generation induced by ethanol exposure impairs macrophage differentiation and phagocytosis¹⁸³. These discrepant findings may be a reflection of the temporal scale of oxidative stress experienced by macrophages, as well as the plasticity in macrophage responses to its immediate microenvironment. Together with the fact that TLR4 ligates LPS in concert with other proteins including soluble MD-2 and membrane bound CD14, formidable questions surrounding the role of oxidative stress in macrophage signaling may be reasonably approached using the framework developed in Aim 1 and 2 of this thesis. Specifically, the real-time adhesion frequency assay allowed for monitoring of binding between TLR4, LPS, and associated proteins in a temporal scale previously not studied. Additionally, these experiments were conducted while macrophages endogenously produced ROS. This method could reciprocally inform the study of T cells in oxidative stress.

5.1 **Methods**

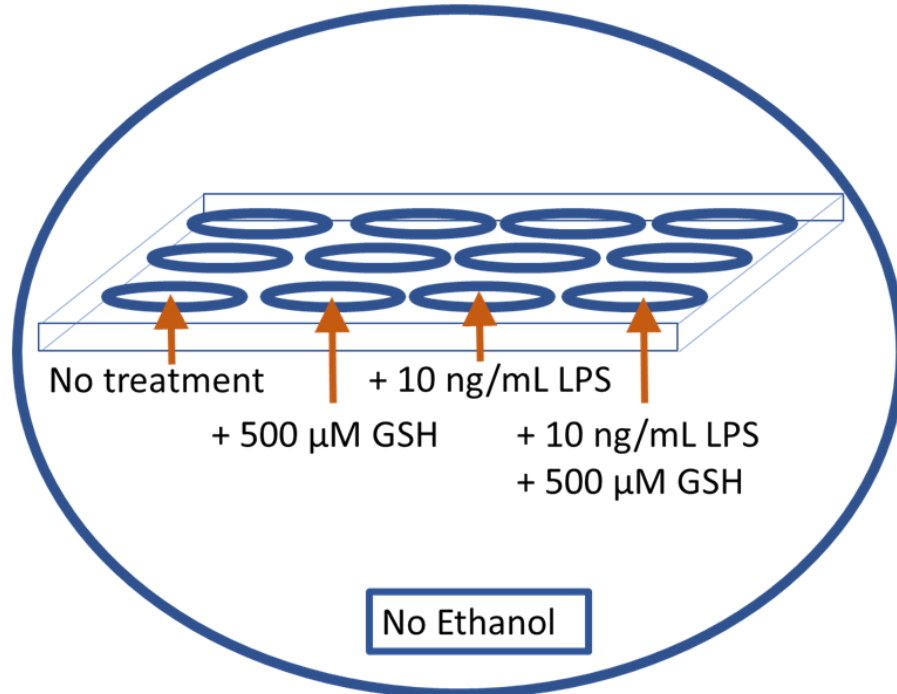
5.1.1 **Materials**

Ultra-pure biotin-LPS from EB was purchased from InvivoGen (San Diego, CA). Antibody for LPS-core was purchased from Hycult Biotech Inc. (Wayne, PA). Fc-block antibody cocktail was purchased from Bio-Rad Technologies (Hercules, CA). All other antibodies were purchased from Biolegend (San Diego, CA). Calibration beads for Alexa488 were purchased from Bangs Laboratories/Polysciences (Warrington, PA). MH-S alveolar macrophage cell line was generously gifted by Lou Ann Brown at Emory University. All other reagents were purchased from Sigma Aldrich.

5.1.2 Development of Oxidative stress

Macrophages were cultured in R10 + penicillin/streptomycin for 24 hours. Afterward, cells were scraped from the flask and added into wells of a 12-well plate at a seeding density of 10^5 cells/mL with or without 0.08% ethanol in RPMI1640 supplemented with 2% FBS. Overall, four conditions were established for the two sets of cells as shown in Figure 26. One group was the control group with no treatments, the second group was treated with 500 μ M reduced glutathione (GSH) for the duration of ethanol exposure, the third group was treated with 10 ng/mL LPS only for the third day of ethanol exposure, and the fourth group was treated with both 500 μ M GSH and 10 ng/mL LPS. For the fourth condition, GSH was present for the duration of ethanol exposure while the LPS was only added on the third day. GSH was added to cells directly from frozen stock solutions of 50 mM which were prepared no longer than one month in advance. Altogether, each 12-well plate was placed inside a modular incubation chamber (Billups, Del Mar, CA) with a water supply of the same ethanol concentration within the cell media to provide an ambient environment matching that immersing cells. Both modular incubation chambers were placed entirely in 37°C incubators with 5% CO₂. These conditions were refreshed, and the modular incubation chamber flushed, every day, for 3 days. On the third day of incubation, 10 ng/mL LPS were added to the appropriate wells. On the fourth day, cells were scraped from wells and replenished against with corresponding media. Fractions of cells were allocated for the micropipette assay, confocal microscopy, or flow cytometry.

A.



B.

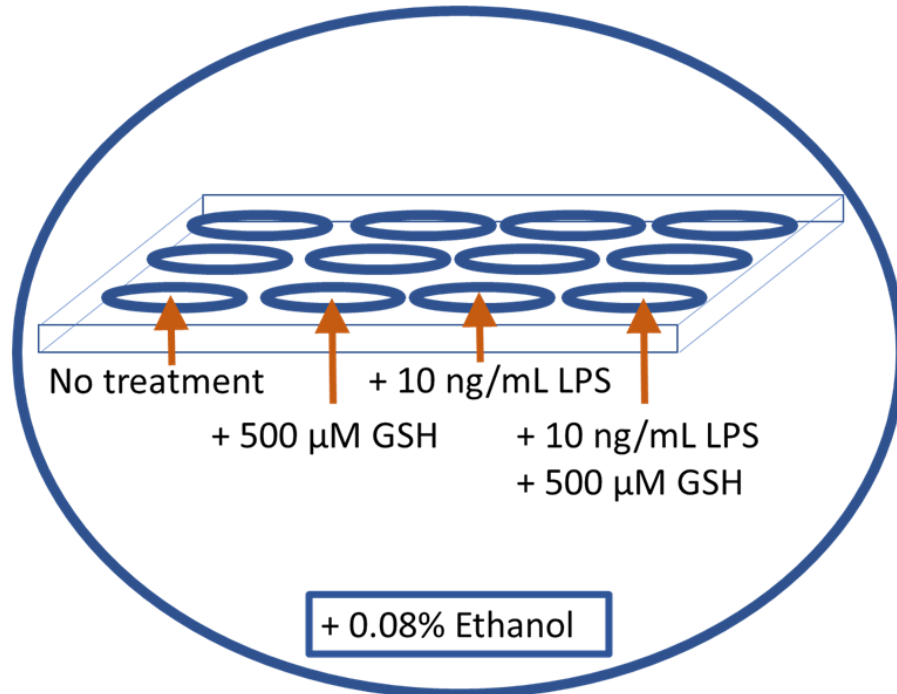


Figure 26. Schematic depicting conditions of macrophage culture in incubator

5.1.3 Real-time Micropipette Assay

A modification of the real-time adhesion frequency method described in section 4.1.3 was employed to observe binding kinetics in real-time. Available SPR data for

interactions between TLR4 and LPS suggested that the method was appropriate since the kinetics were similar to those between OT1 TCR and OVA pMHC. However, upon unsuccessful attempts in obtaining binding data, the method was further modified as follows: RBCs were coated with LPS-biotin using the same method described in section 3.1.2.1.1. Briefly, RBCs with the highest possible biotinylation capacity were coated with tetravalent streptavidin for 30 minutes at 25°C. After extensive washing, LPS-biotin was added to RBCs at a final concentration of 100 µg/mL and incubated 30 minutes at 25°C. The presence of LPS on RBCs and TLR4 on macrophages were confirmed by antibody staining quantified analysis using the BD Accuri flow cytometer as described earlier. Antibody against the LPS conserved core region bound to LPS coated on RBCs, which was further conjugated to an Alexa488 secondary antibody. Following blocking using an Fc-blocking antibody cocktail, TLR4 on macrophages were coated with antibody against mouse TLR4, and a secondary conjugated with an Alexa488 stained the primary. Quantification of the sites was conducted using Alexa488 calibration beads and as described in section 3.1.2.

5.1.3.1 Binding

Protocols for micropipette adhesion frequency from Aim 1 and Aim 2 were combined to investigate binding between TLR4 and LPS. Briefly, macrophages and coated RBCs were placed in the experimental chamber. Pipettes were used to aspirate and probe the cells against each other, and adhesion frequency was monitored over time. The real-time micropipette method requires that the binding interaction achieves a saturation as a function of early contact times (roughly 2 seconds), for sufficient sampling of data. Contact times of 2 seconds were used, but this did not achieve binding distinguishable from nonspecific binding. Longer contact times such as those used in Aim 1 were then used, and even further constant contact time throughout the experiment was tested. Data is presented for 8 second contact times which did not differ from constant contact.

Experiments in all cases occurred over a course of 15 minutes in the micropipette chamber at 25°C.

5.1.3.2 Morphological changes

The pixels on the monitor for micropipette were calibrated to translate measurements on the monitor into the metric scale. Sizes of macrophages were measured before the first contact with LPS-coated RBC. At the end of 15 minutes, the following measurements were made and are depicted in Figure 29: the size of the macrophage from the opening of the pipette as the origin, the distance macrophage reaching onto the pipette from the opening of the pipette as the origin, the size of the macrophage in along the y-axis at the center of the macrophage along the x-axis. Using these measurements, the following normalized morphology changes for the macrophage were measured: The normalized distance macrophages traveled onto the pipette; and the distance traveled by the RBC-facing cell edge. Both of these measurements were normalized by the size of cells and were based on a reference point of the pipette opening.

5.1.4 Intracellular cytokine staining

Following 3-day development of oxidative stress across 4 conditions, cells were replenished in fresh corresponding media supplemented with 10 ng/mL LPS and BD Golgiplug to prevent cytokine secretion. Cell were incubated for 6 hours in a 37°C incubator with 5% CO₂, and then scraped off. Cell were fixed using Biolegend fixation buffer for 20 minutes at room temperature in the dark. After washing, cells were permeabilized using 0.1% triton-X100 in PBS for 5 minutes on ice. For each condition of cells, unstained control, isotype control, blocking control, as well as PE-anti mouse TNF- α and PE-anti-mouse IL-6 antibodies were tested. Permeabilized fixed cells were incubated with Fc-blocking antibody cocktail for 30 minutes, then with fluorophore-conjugated antibody for 30 minutes at 25°C in the dark. For the case of the blocking control, fluorophore-unconjugated anti-mouse IL-6 or anti-mouse TNF- α was incubated

with cells for 30 minutes, and then added with the corresponding fluorophore conjugated antibodies. Staining was analyzed by flow cytometry on the BD Accuri flow cytometer.

5.1.5 Confocal imaging

Coverslips were prepared to present a gradient of LPS on its surface in order to allow macrophages to ‘sense’ changes of concentration of surface bound LPS over cellular size distance scales. Coverslips were sonicated with ethanol for 15 minutes and washed extensively with water. 1 M sodium hydroxide was added to coverslips and allowed to clean surface for 2 hours at room temperature. Coverslips were washed extensively with water and then buffer exchanged with PBS. Tetravalent streptavidin in PBS (100 µg/mL) were added to each coverslip and incubated at room temperature for 1 hour. Coverslips were washed with 1X PBS supplemented with 2% BSA 3 times and then incubated with 1X PBS + 2% BSA for 30 minutes at room temperature. All buffer was aspirated, only leaving a wet surface. At one end of the coverslip, 1 µL of 1 mg/mL LPS-biotin was added slowly. Coverslips were incubated at 4°C for 1 hour. To wash, 1X PBS +2% BSA was added at the opposite end in a direction toward the center of coverslip. Buffer was removed slowly at the same end where the LPS was added. This one directional washing process was repeated two more times. Finally, 200 µL of cells suspended in R10 (cell concentration of 10^4 /mL) would be added to each newly aspirated coverslip, and cells would be incubated at 37°C for 6 hours. At the end of 6 hours, cells would be fixed in 4% PFA for 10 minutes, washed, and then analyzed under confocal microscopy for cell density distributions and LPS distribution. Cell distribution, LPS distribution by Alexa488 staining, and F-actin distributions were imaged under an LSM 710 NLO confocal microscope using 488 and 594 nm laser lines and a 20X / 0.8 NA Plan-Apochromat air objective or a 63X / 1.4 NA oil-immersion Plan Apochromat objective (when imaging F-actin distributions). The main system consisted of a Zeiss 710

confocal scan head mounted on an AxioObserver Z1 inverted microscope stage with motorized stage.

5.2 Results

5.2.1 Macrophages secrete less cytokines when supplemented with antioxidants

Ample evidence exists for the deficiency in macrophage phagocytosis and differentiation upon ethanol exposure. However, there is also evidence for enhancement of macrophage function in an oxidative environment. To draw a more direct comparison between effector functions studied elsewhere, cytokine generation in this ethanol induced oxidative stress model was monitored by Golgi-inhibited intracellular cytokine staining in flow cytometry. Three-day supplementing with antioxidants appeared to reduce generation of both TNF- α (Figure 27A) and IL-6 (Figure 27B), consistent with previous studies that showed that inhibition of antioxidant production led to higher IL-6 generation. Ethanol treatment purported to upregulate ROS generation, appeared to yield larger generation of TNF- α , but was not rescued to baseline levels without antioxidants.

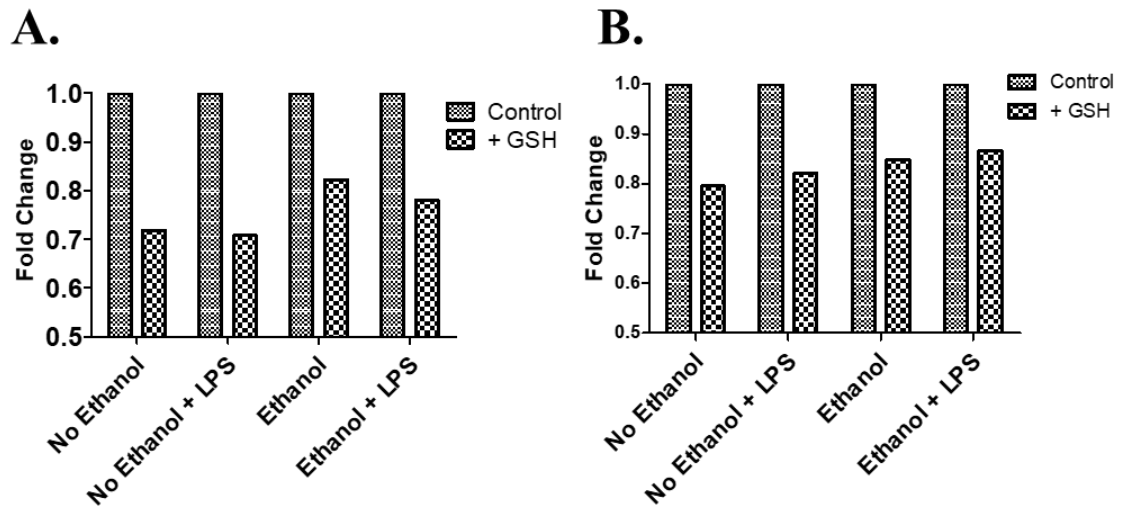


Figure 27. Cytokine secretion is inhibited by antioxidants.

(A) Plots depicting effect of 3-day glutathione supplement on TNF- α generation for various conditions. (B) Plots depicting effect of 3-day glutathione supplement on IL-6 generation for various conditions.

5.2.2 TLR4:LPS bimolecular binding is not a good predictor of ethanol induced derangement

To reconcile the variable macrophage effector functions in response to oxidative stress, the initial trigger for macrophage activation- binding- was tested against its cognate ligand. TLR4 is a toll like receptor that ligates LPS and triggers a signaling cascade ultimately leading to cytokine secretion. To test TLR4 functionality under ethanol exposure, macrophages were probed against a surrogate cell coated with LPS at a high density. Whether or not macrophages experienced ethanol exposure, binding to LPS at high concentrations and for prolonged contact times, yielded about 5% binding (Figure 28). When the cells were pretreated with soluble LPS for 24 hours, the binding frequency increased to almost 15% but there were no differences between the ethanol or no-ethanol treated macrophages. These data indicate that binding frequency of TLR4 to LPS did not correlate with the dysfunctional state of the macrophage.

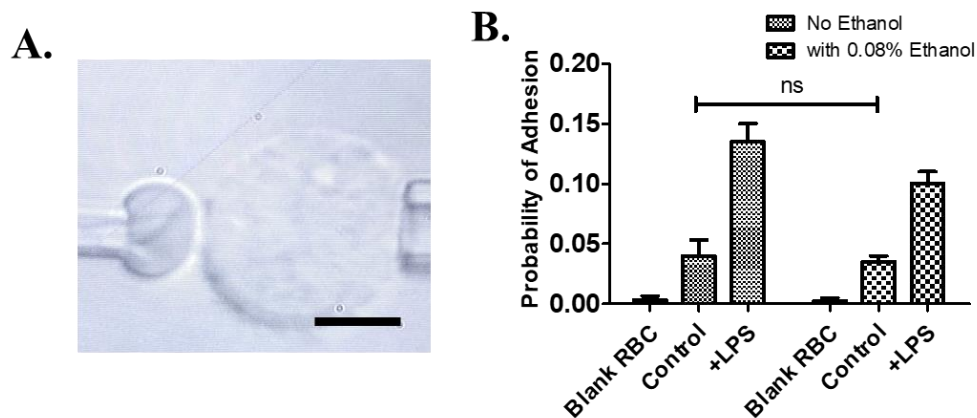


Figure 28. Binding assay between macrophages and LPS.

(A) Microscopic view of RBC coated with LPS (left cell) interacting with macrophage expressing TLR4 (right cell). Scale bar 4 μm. (B) Plot depicting adhesion frequency between RBC and macrophages not conditioned or conditioned with 0.08% ethanol for three days. Control condition was not treated with LPS while + LPS condition was pretreated for 24 hours. Error bars represent standard error and an unpaired t-test was employed for significance.

5.2.3 Cell morphology predicts ethanol induced deficiency

During the binding frequency experiments, cell morphology visibly changed over the course of the 15-minute experiment while the macrophage was repeatedly contacted with the LPS and was therefore monitored and quantified (Figure 29 A and B). Strikingly, by the end of the experiment, macrophage was seen on the pipette distal from the RBC. Cells were observed enveloping the pipette (not on one side or the other of the pipette). This effect was abrogated if the macrophages were treated with ethanol and was partially rescued if the cell experienced concurrent conditioning with the glutathione. Another morphology change observed was movement toward or away from the RBC coated with LPS. While the movements were not as drastic as seen with the movement onto the micropipette, cells that were pretreated with LPS moved toward the RBC, while those that did not experience pretreatment of LPS moved away from the RBC. In contrast to the rescuing nature of the glutathione conditioning for movement onto the pipette, glutathione appeared to prevent movement toward or away from LPS at the cell edge facing LPS, from the frame of reference of the pipette. No morphological changes were seen with control RBCs, which were only coated with streptavidin (Figure 29 C and D). Thus, since LPS was the only molecule presented to the macrophages, these data suggest that LPS can act as a signal to induce cellular morphology changes at a timescale of minutes.

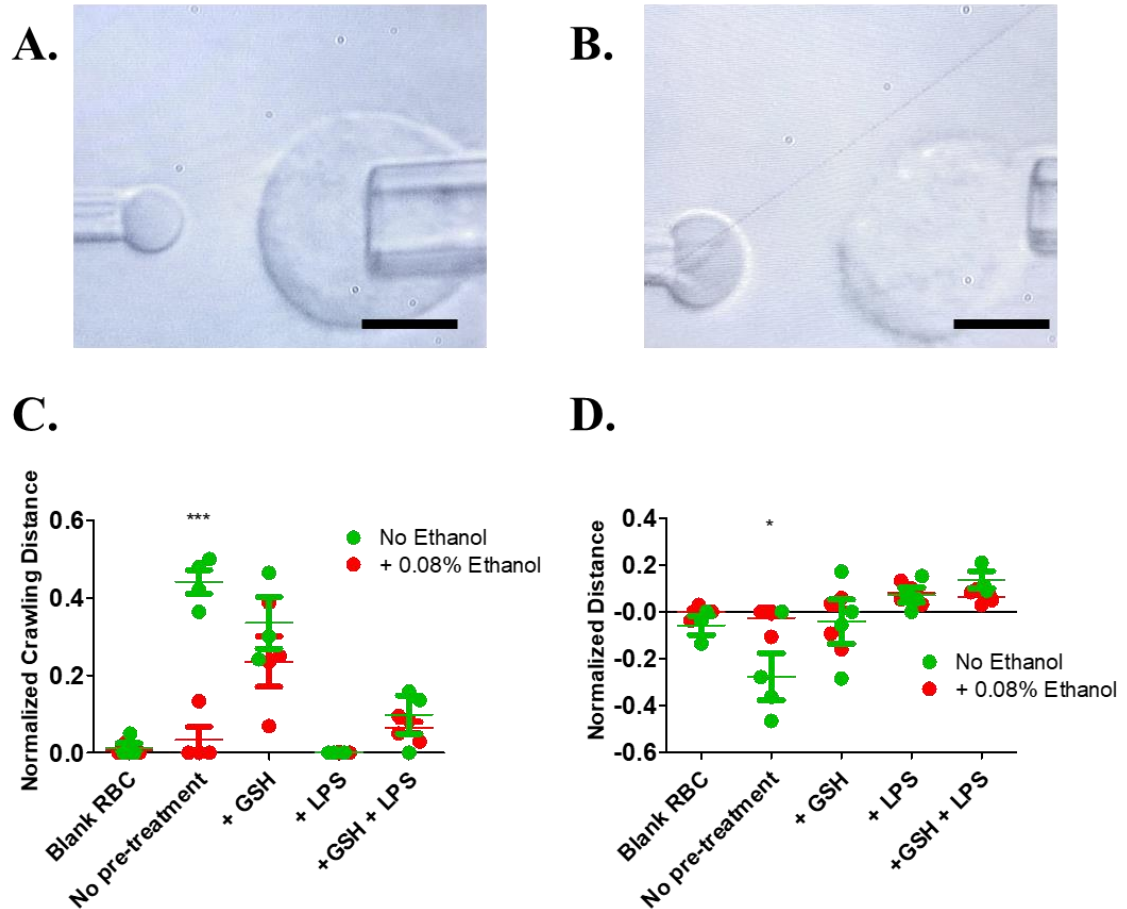


Figure 29. Morphological changes in response to LPS
 (A) Microscopic view of macrophage engulfing aspirating pipette. Scale bar 4 μm . (B) Microscopic view of macrophage elongation toward the LPS-coated RBC. Scale care 4 μm . (C) Plot depicting quantification of morphological changes of crawling on pipette seen in **A**. Error bars represent standard error and *** represents $p < 0.0005$ using a two-tailed t-test. (D) Plot depicting quantification of morphological changes of polarization toward LPS seen in **B**. Error bars represent standard error and * represents $p < 0.05$ using a one-tailed t-test.

5.2.4 Chemotaxis in response to LPS is inhibited upon ethanol treatment

To extend these findings to a more high-throughput fashion and to observe consequences of LPS-induced movements over a longer period of time which is representative of macrophage activation from LPS, macrophages were plated on surface coated with LPS in a gradient fashion. Over the diameter of the coverslip, LPS concentration increased and depleted gradually with concentration changes occurring at

the distance scale of the macrophage size (Figure 30A). After 30 minutes of allowing cells to reach the surface, the fraction of cells across a cross-section of the coverslip relative to corresponding LPS density was determined. By relating these values to the ‘chemotactic’ index of the control setting which was without a surface coating or with any treatment of the macrophages to account for the general distribution of cells on a coverslip, cells pretreated with LPS clearly moved toward greater concentrations of LPS, while those that were not pretreated with LPS moved away from greater concentrations of LPS (Figure 30B). These results suggest that macrophages can undergo chemotaxis in response to LPS at short time scales depending on their activation state.

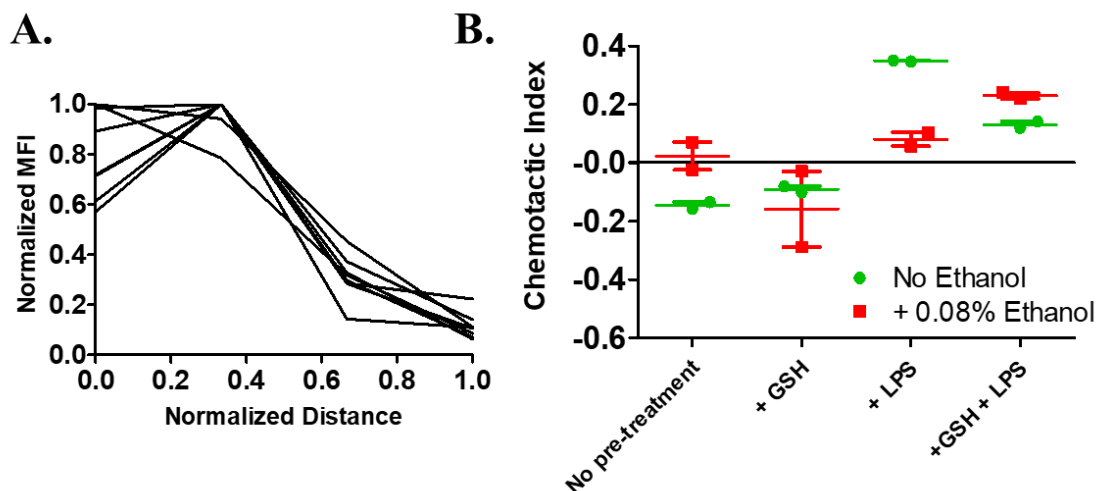


Figure 30. Gradient of LPS is sensed by macrophages
 (A) Traces that depict mean fluorescence intensity of LPS coating on a glass surface over the same distances. (B) Plots displaying the effects of conditioning and pre-treatment of macrophages on their polarization toward LPS. Positive values for the chemotactic index represent skewing of macrophage adhering toward greater LPS concentrations, while negative values represent adhering toward less LPS.

5.2.5 Actin reorganization influenced by ethanol treatment

Since cellular motility is associated with actin reorganization, cells across all conditions were stained with a phalloidin to observe the density of filamentous actin. This was achieved by calculating the ratio of fluorescence intensities between intracellular F-actin staining and the overall cellular actin staining (Figure 31). For the cells not treated

with ethanol, glutathione appeared to reduce the actin ratio, indicative of less actin within the cell. This was rescued by LPS pretreatment but again diminished when LPS pretreatment was supplemented with glutathione. For the cells conditioned with ethanol, glutathione pretreatment appeared to lead to higher intracellular actin. LPS pretreatment did not lead to any changes compared to the control ethanol condition, even when supplemented with ethanol. Importantly, when cells not pretreated with glutathione or LPS were conditioned with ethanol, intracellular actin decreased. Overall, these results mirror those observed in the micropipette assay and indicate that ethanol exposure leads to less actin polymerization in the cell which can also be partially achieved by glutathione supplementing.

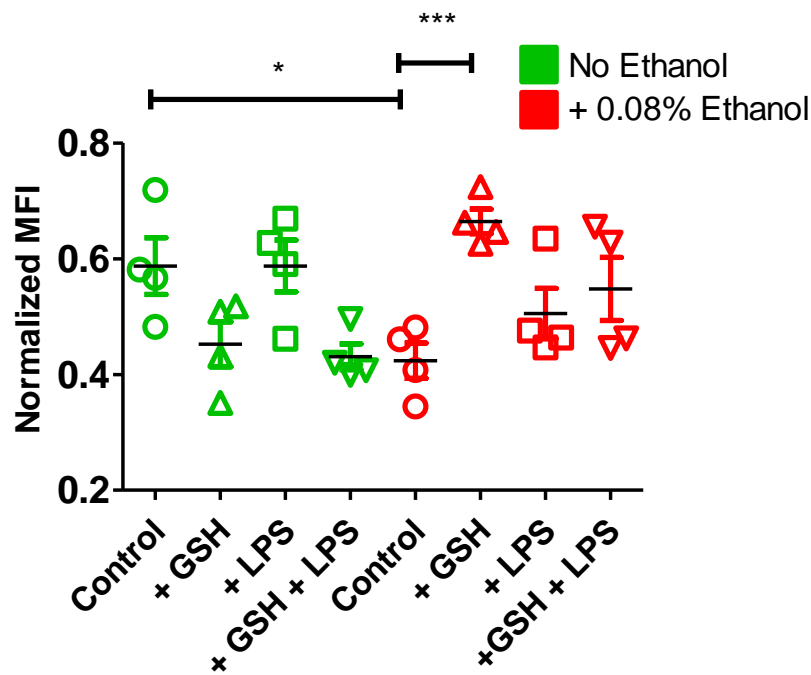


Figure 31. Extent of actin remodeling for various macrophage conditions. Plot displaying how different treatments on macrophages influence the ratio between intracellular and overall actin staining.

5.3 Discussion and conclusions

Oxidative stress and TLR4 signaling have been reported to be mutually beneficial^{186,189}. On one hand, removing Nox components which produce ROS will

diminish TLR4 signaling¹⁸⁷. The opposite will occur if endogenous antioxidant production is removed¹⁸⁷. On the other hand, inhibiting TLR4 signaling can limit the macrophage production of ROS¹⁸⁸. Furthermore, the presence of ROS can accelerate recruitment of existing TLR4 to the cell surface¹⁸⁹. It is possible that these mechanisms promote robust detection of LPS while macrophages are bombarded by a complex inflammatory milieu. After all, macrophages make up the majority of cell mass in the alveolus and therefore are present from initiation through the recession of inflammation, experiencing the effector functions of a variety of immune cells¹⁵⁶. Although, overactivation of TLR4 signaling can lead to excessive macrophage effector functions including ROS production and TGF- β secretion, which have been shown to directly contribute to injuries such as renal hypertension¹⁸⁸. At the same time, oxidative stress induced by chronic ethanol exposure has been shown to impair macrophage function and differentiation- a process directly related to TLR4 recognition of LPS¹⁸¹. These discrepant findings are reminiscent of those reported for T cells, whereby hydrogen peroxide can promote and diminish T cell effector function⁹⁶. A difference between the two systems is that ROS has been previously shown to contribute to abrogation of TCR recognition while it appears to have had the opposite effect for macrophages, at least specifically for TLR4 signaling. Additionally, there has not been as extensive of study on the effects of ROS on various macrophage signaling molecules compared to those in T cells. The lack of such information aligns well with the black box approach undertaken in aim 2 of this thesis. Accordingly, investigation of critical metrics of macrophage recognition of LPS were measured in this aim using the micropipette adhesion frequency assay while the macrophages were endogenously generating ROS in response to ethanol exposure¹⁸².

5.3.1 Novel chemotaxis of macrophages in response to LPS

Previous work using the present alveolar macrophage cell line found that differentiation and phagocytosis were impaired in response to ethanol exposure which coincided with upregulation of ROS production by Nox1 and Nox2¹⁸². However, a major axis of macrophage function tied to differentiation is TLR4 signaling¹⁶⁵. To begin exploring how TLR4 responds to the ethanol regimen applied to these macrophages, cytokine production in response to LPS was analyzed. When treated with ethanol, macrophages appeared to release more TNF α and IL-6, a finding that was observed even when cells were previously activated with LPS. Based on these functional results it was clear that oxidative stress played a role in macrophage sensing of LPS, consistent with previous studies that suggested a mutually beneficial relationship^{187,189}. The cells were then monitored under the real-time adhesion frequency assay for binding between TLR4 and LPS. It is accepted that TLR4 requires MD-2 to form a stable complex with LPS, and prior to that, CD14 is involved for lateral transfer after it extract LPS from the cell wall with the assistance of LBP¹⁹⁶. Nevertheless, binding was attempted using the present method because SPR had previously measured kinetics between purified LPS and TLR4¹⁹⁸. Despite detecting binding above a nonspecific level, the adhesion frequency was outstandingly low and did not differ between cells exposed and not exposed to ethanol. This was likely due to the fact that MD-2 was not present in the experimental chamber to form a stable complex with TLR4 and LPS, as shown in the crystal structure. It is curious, however, how these macrophages were able respond to LPS in functional assays. A likely explanation is that the macrophages secreted sufficient MD-2 over the hours-long durations necessary to induce effector functions in response to LPS, which may have not been captured in the 15 minutes duration of the adhesion frequency assay. Indeed, adhesion frequency improved if the macrophages were activated with LPS prior to testing binding, but still did not significantly correlate to macrophage dysfunction. It is also possible that the purified LPS used in this experimental system is not conducive to

binding compared to those used in other studies¹⁹⁸. Previous studies have shown that minor alterations in LPS structure have can greatly influence macrophage response^{196,240,241}.

Interestingly, morphological changes were consistently observed over the course of real-time adhesion frequency assay. Therefore, metrics describing the interaction with the aspirating micropipette and the LPS-coated RBC were developed. It was found that over the course of 15 minutes of repeated contact with high densities of LPS, macrophages moved away and crawled onto the micropipette in a uniform fashion. Since this movement did not occur with blank RBCs that were only coated with LPS, it is clear that the morphological change was specifically due to LPS. Although, it is unclear how such a low adhesion frequency had such a profound specific impact on macrophages. A possible explanation for this is that pattern recognition by TLR4 was sufficient to induce signaling but not binding. Indeed, analogous to the weak interactions between the E8 TCR with mutant TPI, binding was not detected by SPR but robust recognition between T cells and APCs was demonstrated^{198,204}. Additionally, TLR4 is well-documented to be N-terminal glycosylated when expressed on cells which may further accelerate dissociation^{207,242}. These difficulties may explain why there were no documented cases of *in situ* binding kinetics between TLR4 and LPS before the results presented in this aim¹⁹⁸. It is important to note that these cells may not necessarily be “moving away” from LPS. It is possible that upon actin reorganization, macrophages crawl onto the only solid surface available, which is the micropipette. Thus, this isolated observation may only be a reflection of the activation of actin reorganization in response to LPS, which is still a novel characterization at this time frame. A contrasting morphological change was observed for macrophages that were pre-treated with LPS for 24 hours. These activated macrophages bound to LPS with 3-fold higher adhesion frequency and after 15 minutes, moved closer to the LPS-coated RBC. This finding is consistent with previous studies that demonstrated prostaglandin-mediated chemotaxis toward LPS¹⁶⁹. However, similarly

to the prior morphological change, chemotaxis has not been previously shown to occur in such a short time frame. Furthermore, movement directly toward LPS supports the idea that macrophages are capable of morphological polarization. In other words, the bi-directional movements of the macrophage suggest that it possesses mechanisms to respond to LPS in a rapid manner. In this vein, it is reasonable to speculate that macrophages may possess a protective mechanism to evade infection by escaping excessive concentrations of LPS before it is activated to respond. To examine this phenomena in a higher throughout fashion, surfaces coated with a gradient of LPS were developed. As they arrived onto the surface, macrophages appeared to respond to the changing LPS density and navigated their adhering to the surface either away from high LPS concentrations if they were not pre-treated with LPS, or toward the high concentrations if they were pretreated.

Cellular morphological changes and mobility are mediated by acto-myosin reorganizations²⁴³. As shown in aim 2, inhibition of actin polymerization can also greatly inhibit receptor-ligand binding. Additionally, as previously discussed, components of actin are sensitive to oxidation and therefore may play a role in the macrophage impairment^{96,244}. After the three-day regimen of ethanol treatment, the amount of fully formed actin fibers was diminished compared to untreated cells as measured by fluorescently-tagged phalloidin. It is possible that membrane proximal cofilin was oxidized by the upregulation of ROS¹⁸², which prevented actin reorganization and manifested in the lack of morphological changes observed under the real-time adhesion frequency assay.

5.3.2 Implications for ethanol induced deficiencies

These actin-based deficiencies may explain the impairments in phagocytosis and differentiation in response to ethanol exposure, since those processes are related to actin reorganization. Specifically, both Fc receptor- and complement receptor-based

phagocytosis require actin reorganization to form the phagocytotic cup, which could be susceptible to oxidation¹⁷⁰. Similarly, CD14-mediated endocytosis of LPS, which represents an alternative activation pathway for macrophages, relies on actin polymerization²⁴⁵. The relation between actin reorganization and differentiation is less direct although from a lens of actin-dependent internalization, CD14 and TLR4 signaling can steer differentiation^{165,170}. Another possible mechanism actin can dictate differentiation is through selective viability. It was recently shown that perturbing nucleation of actin polymerization using chondramide A led to depletion of M2 differentiated macrophages while the M1 macrophages upregulated their effector functions²⁴⁶. Furthermore, there have been documented changes in stiffness of cells through the differentiation process, suggesting that the process may be susceptible to impairment or delaying if actin reorganization were perturbed²⁴⁷. Interestingly, when cells not treated with ethanol or LPS were supplemented with the antioxidant glutathione, actin reorganization was also slightly diminished. This was reflected in the morphological changes as well. Thus, it is possible that the excess of antioxidants may interfere with intracellular signaling processes in a redox dependent fashion²⁴⁴. This was expected in the case of TLR4 signaling, since that cascade has been strongly suggested to be mutually tied to ROS signaling¹⁸⁷. But the finding that the presence of antioxidants also led to impairment in morphological changes was not expected. It is not clear from the data whether the changes in actin due to oxidative stress directly cause less formation of actin fibers as measured by phalloidin staining, or whether it induces a different macrophage phenotype which may possess a less stiff morphology that does not require as extensive of a actin cytoskeleton network, consistent with previous studies that present profound plasticity in macrophage phenotype²⁴⁷.

Administration of glutathione to alveolar macrophages *in vitro* and *in vivo* led to downregulation of Nox expression and ROS generation, improved macrophage phagocytosis, and ultimately led to greater bacterial clearance of LPS releasing *K.*

pneumoniae^{183,248}. The results from that study provide an elegant validation of previous literature that show introduction of LPS leads to generation of ROS. However, other studies and results in this thesis suggest that other macrophage functions such as cytokine secretions may thrive in oxidative stress environments^{187,188}. First, it must be noted that the results examining actin reorganization in this thesis were not shown to be directly linked to earlier functional studies. Notwithstanding that premise, the mechanism for deranged cytokine secretion in response to ethanol treatment in this thesis is not clear. Could generation of ROS in response to LPS recognition reach a point that will be detrimental to the cellular source itself? It is clear that phagocytosis is improved when glutathione is present¹⁸³, and the results in the present work support this notion. However, the maintenance of a reduced environment may also result in collateral phenotypic changes in the macrophages which may not have an impact over the course of prolonged phagocytosis but may be worth investigating with respect to other effector functions such as pro-inflammatory cytokine secretions¹⁶⁵. Overall, the results in this thesis support a model where chronic ethanol exposure impairs macrophage phagocytosis and differentiation by oxidizing the cytoskeleton while maintaining LPS triggered TLR4 signaling.

5.3.3 Mechanosensitive macrophages

Rapid actin remodeling may be impaired under an environment of oxidative stress. Indeed, ethanol treatment prevented macrophages from crawling onto the pipette or morphologically polarize toward LPS after prior activation by LPS. While the results in this thesis were the first presentation of morphological changes occurring on such a short time scale, a recent study employed a damage associated molecular pattern, PRDX5, to specifically bind to TLR4 and ultimately found that stiffening of the macrophage occurred over the course of 40 minutes²⁰¹. The time course of stiffening presented by their work was similar to that of seen in the present study with direct

ligation of LPS to TLR4. Importantly, the LPS presented to TLR4 expressing macrophages in this study were conducted in two different fashions. One was by repeatedly contacting macrophages with LPS-coated RBCs and the other was by allowing macrophages to plate on LPS-coated glass surfaces. It has long been appreciated that substrate stiffness can influence the degree to which macrophages cooperatively with the biochemical signals it receives^{247,249}. Recently, advances in the fields of biomaterials and nanopatterning have shown that substrates can also influence function and differentiation of macrophages with applications in immune modulation and regenerative medicine (reviewed elsewhere²⁴⁷). Therefore, despite similar results observed between the rigid glass and elastic RBC presentation of LPS, it is possible that different responses not monitored in the present experiments resulted. One difference observed was the degree to which cells polarized toward LPS, which was largely attributed to the fact that cells could only change morphology to the extent of its cell volume for the case of the micropipette assay. Nevertheless, minor changes in morphology can result in drastic outcomes since it was recently shown that patterning LPS on gold nanorods of varying axis anisotropy, but equal ligand density were able to skew macrophage differentiation between M1 and M2²⁵⁰. It was suggested that polarization resulted from changes in ligand presentation geometry in an actin dependent fashion, further supporting results in this thesis where remodeling can greatly influence differentiation²⁵⁰. Overall, the results presented herein reveal potential cell regulatory mechanisms that are susceptible to oxidation in response to ethanol exposure and provide a reconciliatory concept in understanding the relationship between macrophage function and oxidative stress by considering the mechanosensitive nature of macrophages.

CHAPTER 6 CONCLUSIONS AND FUTURE DIRECTIONS

The results presented in this thesis inform how conserved and hypervariable receptor-ligand interactions navigate their highly sensitive pathogen recognition in a different environments. Investigation began with a systematic characterization of multi-molecular interactions thought to contribute to discrimination of antigen. In the case of conserved recognition of LPS found in the cell wall of gram-negative bacteria, TLR4 associates with secreted MD-2 and works in concert with CD14 to achieve sensitive recognition. For the hypervariable and adaptive recognition of abnormal antigen expressed on infected or cancer-transformed cells, the TCR may depend on intrinsic force-regulated structural alterations to ensure discrimination from self-peptides and prevention of autoimmunity. There is reason to believe that T cell activation may also rely on CD4 and CD8 coreceptors that associate to the antigen presenting pMHC simultaneously but independently from TCR, since they can recruit phosphorylation-initiating kinases¹⁹. Additionally, CD4 and CD8 coreceptors are expressed during development of T cells and the difference in their individual expression demarcates T cell effector function⁵⁴. Thus, despite their importance, evidence of a stable TCR-pMHC-CD4 trimolecular complex is scant, due to the postulated weak interaction between CD4 and MHC⁷⁵. Whereas delicate conformational changes have been shown to be important in ligand discrimination^{53,216}, cooperativity between several molecules may also play a role in specialization of these innate and adaptive immune receptors toward modulating conserved signaling cascades for appropriate cell activation and pathogen clearance.

6.1.1 Development of a mathematical model for multi-molecular interactions

A two-pronged approach was undertaken in this thesis to measure CD4-MHC binding. First, an ultra-sensitive micropipette adhesion frequency assay was employed which has previously detected binding of the CD8-MHC interaction and has enabled a

larger dynamic range of affinity measurements that correlate better to pMHC potency compared to measurements made by SPR²¹. Interestingly, the adhesion frequency assay was previously used to distinguish trimolecular TCR-pMHC-CD4 binding from TCR-pMHC binding using an antibody blockade for CD4, to no avail⁴⁹. To circumvent potential problems with limited efficacy of antibody blockade, a minimalist system of purified TCR, CD4, and pHLA was used. Additionally, the TCR used in these experiments was previously found to not bind to its cognate pHLA unless tetramerized²⁰⁴ and was therefore hypothesized herein to minimize the dominant binding of TCR to pHLA which could potentially mask any CD4-HLA binding. First, in contrast to SPR measurements, E8 TCR-TPI pHLA was readily detected by the adhesion frequency assay. Then, despite hovering close to the detection limit of the assay, CD4 binding to HLA was also detected, yielding the first documented characterization of CD4-MHC kinetics. Furthermore, when TCR and CD4 were mixed on the same surface interacting with pHLA, CD4 was observed to stabilize TCR-pHLA interactions in a synergistic fashion. By analyzing the contribution of CD4 to form observed bonds, a mass-action based analytical solution describing a trimolecular interaction was developed which reasonably fits the nonlinearities exhibited by the experimental results. This is the first instance of a mathematical model describing cooperativity exhibited by a trimolecular interaction and can be used to extend models that describe bimolecular hemoglobin cooperativity such as the Hill, Koshland-Némethy-Filmer, and Monod-Wyman-Changeux models.

A limitation of the trimolecular model is that it was built on kinetic parameters determined from the adhesion frequency assay which represent two-dimensional kinetics, and therefore may not be appropriate using kinetics determined from three-dimensional techniques such as ITC or SPR which do not always demonstrate strong correlations between cell function and binding between membrane anchored receptor-ligand pairs²¹. However, these results and mathematical model have many implications for TCR

triggering models such as kinetic proofreading and serial engagement which can broadly be applied to triggering of other cell surface receptors²⁰⁸. Specifically, detectable CD4-MHC binding and synergy suggest that CD4 contribution cannot be neglected when considering dwell-times of TCR-pMHC interactions which eventually lead to ITAM phosphorylation. In fact, functional studies in this thesis demonstrated that CD4 inclusion led to more efficient T cell activation. Importantly, enhancement found herein may only be the case since the specific TCR-pHLA pair used in these experiments is a very weak interaction, thereby amplifying the role CD4 may play. Therefore, immediate future work for this aim include testing the contribution of CD4 in synergistic stabilization for a system that uses the same TCR but a pHLA that possesses a point residue mutation which has been previously shown to greatly enhance its potency²⁰⁴. Interestingly, the 3D affinities between the wild-type and mutant peptides could not be distinguished which poses a relevant challenge for the adhesion frequency assay. Preliminary studies found in Appendix Figure 32 have shown that this assay could in fact detect binding between TCR and both peptides and can distinguish their affinities. Therefore, analysis of CD4 synergy using the mathematical framework developed in this aim could be a facile approach to understand what role TCR-pHLA bimolecular affinity plays in trimolecular bond formation. Error in the mathematical model compared to observed data seems to largely stem from nonlinearities with pHLA density. Testing a greater range of pHLA densities- from limiting to excess- could reveal an additional factor that may need to be included in the model. Specifically, this could be determined by creating an expression that relates the errors in the model directly to the pHLA densities. Beyond the aforementioned point residue mutations, additional mutations could be determined through molecular dynamic simulations which could abolish the catch-slip bond profile exhibited by the TCR-pHLA bimolecular interaction. Such mutations could pose the question of whether CD4 stabilization can occur with a TCR-pHLA interaction that exhibits a slip-bond profile, and if so, to what degree and can it change bond profile from slip to catch-slip? The same

analysis can be conducted for the CD4-HLA interaction. In fact, mutations in CD4 which greatly enhances CD4-HLA association was tested in early in this thesis. While using a mutant CD4 may not be as physiologically relevant as the naturally occurring point residue mutation in HLA, understanding even strong CD4 contribution relative to TCR-pHLA binding can inform TCR triggering and be exploited for protein engineering studies. Indeed, a recent study expressed the mutant CD4 on cell lines prone to false negative screenings and improved TCR signaling to the point of being as robust as in primary cell lines²⁵¹. Next, since Lck associates with coreceptors, the possibility of Lck inhibition in current Jurkat system abrogating bond lifetime synergy would corroborate the model describing a pseudodimer of dimers between TCR, CD3, pMHC, and coreceptor¹⁹. Finally, functional studies examining activation of membrane proximal signaling components may provide a more detailed picture of how CD4 is contributing directly to triggering compared to calcium flux. Specifically, total internal reflection microscopy can be employed to observe phosphorylation events of kinases proximal to signaling motifs on CD3. Together, these future studies would provide a more detailed understanding of how TCR, pHLA, and CD4 cooperate to afford the outstanding sensitivity and specificity exhibited by T cells in recognizing foreign antigen amid an abundance of self-antigen.

6.1.2 Reconciliation of oxidative effects on T cell function

The precise interplay between multiple molecules for signaling specialization must withstand the soluble influences between varying tissue compartments each with its own microenvironment milieu. For example, the difference in cytokine presence between circulation and tissue compartments can modulate T cell function and fate in the context of viral infections²⁵². More explicitly, ROS has been suggested to mediate T cell dysfunction by oxidizing critical signaling molecules in both activating and inhibiting fashions⁹⁶. The results presented in the second aim of this thesis are the first instance

where TCR-pMHC binding was monitored in real-time in response to ROS. In doing so, the convoluted findings of previous studies were reconciled, and a model was proposed to explain how the various effects of ROS on TCR machinery components can lead to a scenario of impaired binding, which has been shown to be a good predictor of T cell function. Early observations of this project found that mtOVA binding to TCR on primary naïve T cells was reduced in response to a pathologically representative concentration of H₂O₂. Yet, the reduction could have been due to a litany of signaling molecules associated with the TCR and shown to be sensitive to oxidation⁹⁶. The technique developed in this aim enabled *in situ* monitoring of an amalgamation of potential effects manifesting in the critical metric of binding while carefully comparing only one molecular difference between two systems. Together with the quantitative nature of the method, this approach ultimately led to parsing out which molecules were likely playing a role in the reduced binding. The model proposed has its limitations in that the activity of oxidation sensitive phosphatases were not directly analyzed. CD45 and Shp1 directly modulate Lck proximal activity¹⁰⁰ but their role in T cell function in response to oxidation is not completely understood. It is thought that inactivation of Shp1 by oxidation of critical cysteines leads to overactivation of Lck and this should represent an increase in binding based on the pseudodimer of dimers model. Although the model did indeed incorporate such an increase, examining the redox state of cysteines in these phosphatases in response to the concentrations of H₂O₂ used in the adhesion frequency experiment by mass spectrometry-based techniques developed by Hogg and colleagues¹³² could provide necessary validation.

The major limitation of these results was the in the optimization of the system. Only naïve T cells were used in this system, and immediate future studies should investigate the effect on other developmental stages of T cells^{253,254}. Effector T cells would be an instructive system to study because it has been postulated that survival of these cells is prolonged due to their increased antioxidant capacity compared to naïve T

cells. In what could be an evolutionarily conserved mechanism to survive the harsh environment of inflammatory sites, this difference could also corroborate the implication of the present results which posit that the redox state of T cells is important for sensitive and specific TCR recognition. With an appropriate level of protection afforded by endogenous antioxidants, it is hypothesized that TCR on effector cells would not experience reduced binding in response to pathological concentrations of H₂O₂. However, if binding is reduced, a more quantitative understanding for how ROS can alter TCR recognition in the tumor environment could be achieved. What must be developed to approach such a problem is a mathematical black box model that incorporates H₂O₂ concentration (which includes an initial presence of ROS, as well as consumption and generation), experimentally derived information surrounding TCR-pMHC 2D affinity, and the endogenous antioxidant capacity of a given T cell. Thus, by inputting ROS context and surface molecule expression levels while assuming constant expression signaling molecules which may or may not be ROS-sensitive, an idea for TCR recognition can be outputted.

Quantitative information like this would inform rational design of genetically modified T cells that express catalase for antioxidant protection in two ways. The first is that global expression of catalase may be optimized to determine the degree of antioxidant production that will maximize TCR binding. Once such a value is obtained, exploration of compartmentalized expression of catalase can be pursued to ensure that T cell signaling cascades known to depend on oxidation are not perturbed. Rather than use binding as a metric at this stage, T cell effector functions such as proliferation and cytokine secretion would be monitored for maximization. However, the first step in these sequence of experiments would be to test TCR-pMHC binding in the exact same manner as done in this thesis, except for surface expression of catalase as previously described²²⁹. In the case of a H₂O₂ bolus, it is hypothesized that the reduction in binding between TCR and mtOVA would be minimized or abrogated. For the case of continuous

production of ROS, it is hypothesized that the catalase generation would protect both wtOVA and mtOVA binding. To circumvent the byproducts and consequences of continuous artificial production of H₂O₂ by glucose oxidase, it would be worth exploring whether T cells can upregulate ROS production via Nox proteins as macrophages have been shown to¹⁸². While the molecular mechanism for the upregulation in macrophages has yet to be determined, it is not unreasonable to suggest the same phenomena can be exerted by T cells because they have been shown to upregulate expression and activity of Nox proteins upon TCR triggering¹²⁰. If such a mechanism exists for T cells, a system consisting of endogenously produced ROS at physiologically relevant concentrations could be implemented in the proposed mathematical framework for ROS effects. These future studies would greatly inform the convoluted nature of antioxidant therapeutics which have suffered from poor outcomes and represent a promising avenue to understanding a major facet of how tumors escape immune surveillance²³⁹.

6.1.3 Toward understanding multi-molecular interactions in macrophages

The challenges in studying the effects of ROS also plague the field of macrophage immunobiology with some studies describing detrimental effects on macrophages¹⁸² while others providing evidence for the requirement of ROS in effective TLR4 signaling¹⁸⁹. Furthermore, sensitivities of macrophage intracellular signaling molecules to ROS have not been catalogued as extensively as for T cells, which prompted using the black box approach developed in this thesis to delineate oxidation sensitives manifested in macrophage trimolecular binding. These methods resulted in the first documented *in situ* binding kinetics between macrophage cell surface molecules and LPS and description of a novel morphological polarization in response to LPS at short time scales. Supporting evidence came from the development of a gradient of LPS coated on a glass surface. Together, the findings in the third aim of this thesis suggested that actin played a role in macrophage impairment under oxidative stress induced by ethanol exposure.

Addressing this hypothesis were confocal images of actin fibers which appeared to be less prevalent when under oxidative stress. Conclusions from this aim align well with previous studies and have implications in various pathologies and regenerative medicine as macrophages are often the predominant tissue surveilling immune cell¹⁵⁶. On one hand, TLR4 signaling was indeed enhanced with ROS as measured by cytokine secretions while on the other hand they may be effectively decoupled from other functions such as phagocytosis and differentiation which rely more on the actin cytoskeleton organization¹⁷⁰. Notwithstanding the decoupling, a compelling narrative emerges from the data: TLR4 triggering by LPS generates a positively reinforcing generation of ROS which can continue in excess until inducing macrophage dysfunction which predisposes patients to infection and tissue damage. Unlike the response of T cells studied in this aim with mild concentrations of ROS, it is likely that sufficient concentrations were present to impair actin reorganization. Immediate future studies would develop a ratio between antioxidant capacity and ROS generation by macrophages to more directly compare actin susceptibility between macrophages and T cells in this thesis which were exposed to exogenous ROS and did not appear to experience actin machinery oxidation.

The major limitation of this thesis chapter was the inability to comprehensively measure binding kinetics between TLR4 and LPS. One difficulty stemmed from the expression of both CD14 and TLR4 on the surface of macrophages, which without antibody blockade of either of the receptors, specificity could not be clarified. However, due to the low baseline adhesion frequency, blockade was not immediately pursued. Since binding frequency improved after LPS mediated pre-activation of macrophages, consistent with improved MD-2 secretion, adding soluble MD-2 and LBP into the micropipette experimental chamber may assist in stabilizing bond formation according to crystal structures. The challenge of this approach is to ensure purification tags of soluble proteins do not lead to nonspecific anchoring, but this may be circumvented by antibody

blockade such as for the Fc-receptor. Once improved binding is detected, several future experiments are envisioned. The first, most relevant to the goal of this thesis, is to understand the contribution of each molecular player in formation of bonds, using the model developed in aim 1 between TLR4, MD-2, and LPS. Differences to expect between systems are the docking geometries and soluble nature of MD-2, both of which may necessitate changes in the mathematical model. Monitoring the stability of this complex in response to oxidative stress by systematically parsing through each molecular player as in aim 2 would reveal whether any of them are sensitive to ROS. This approach could serve as an initial step toward cataloging susceptibilities of macrophage surface and intracellular signaling molecules to ROS, in addition to cholesterol and actin determined through this thesis. Ultimately, an application of this work is to lay the framework for a systems-level model that encompasses ROS-sensitive signaling proximal and receptor-ligand interactions to predict the antigen recognition phase of activation for a variety of cell types.

The methods developed in this thesis can be extended to further predict downstream signaling processes. It has long been established that activation of macrophages through TLR4 requires about hours of stimulation with soluble LPS in culture²⁵⁵. However, the dynamics of binding between TLR4 and LPS through this process is unexplored and is important to understand for design of therapeutics and since the soluble environment surrounding the macrophage *in vivo* is dynamic upon initiation of inflammation. In lieu of distinct difference in adhesion frequency between naïve and activated macrophages, monitoring binding in real-time over the course of 6 hours necessary for activation could reveal the threshold of activation and the dynamics of MD-2 secretion if the surface expression of TLR4 is characterized over time (a facile task separately determined at various time points of LPS stimulation using flow cytometry). A corresponding experiment could be conducted for the chemotaxis of macrophages in response to LPS, which would reveal the temporal threshold by which macrophages

switch between polarizing away and toward LPS. A transwell system would be more effective in capturing long term migration patterns (in a digital fashion) than the gradient surface method because the latter appeared to only capture early adhering behaviors. Comparing the temporal thresholds between these two experiments could elucidate mechanisms that occur between the establishment of activation and effector functions such as migration. In other words, a difference between temporal thresholds would indicate that MD-2 secretion and migration occur in a specific sequence. Finally, throughout this thesis, oxidation of signaling molecules was inferred from binding experiments. To complement results presented herein, fluorescent reporters of ROS could be implemented in T cells and macrophages which would determine with high resolution the localization of ROS experienced by cells and further inform the rational design of compartmentalized expression of antioxidant protections.

6.1.4 Final Remarks

The overall goal of this thesis was to contextualize well-established bimolecular interactions into physiologically relevant biophysical and biochemical environments. By developing a mathematical model that predicts cooperation between many molecules, a conceptual model that explains how those interactions can be perturbed under an oxidative environment, and experimental methods to quantify binding and cell behaviors in real-time, a novel understanding of immune recognition by different cell types under pathological conditions was achieved. Results of this thesis align well with existing literature and provide inspiration for future studies that aim to more comprehensively detail early immune signaling and activation events toward rationale design of therapeutic interventions.

APPENDIX

A.1. Binding between mutant TPI and E8 TCR

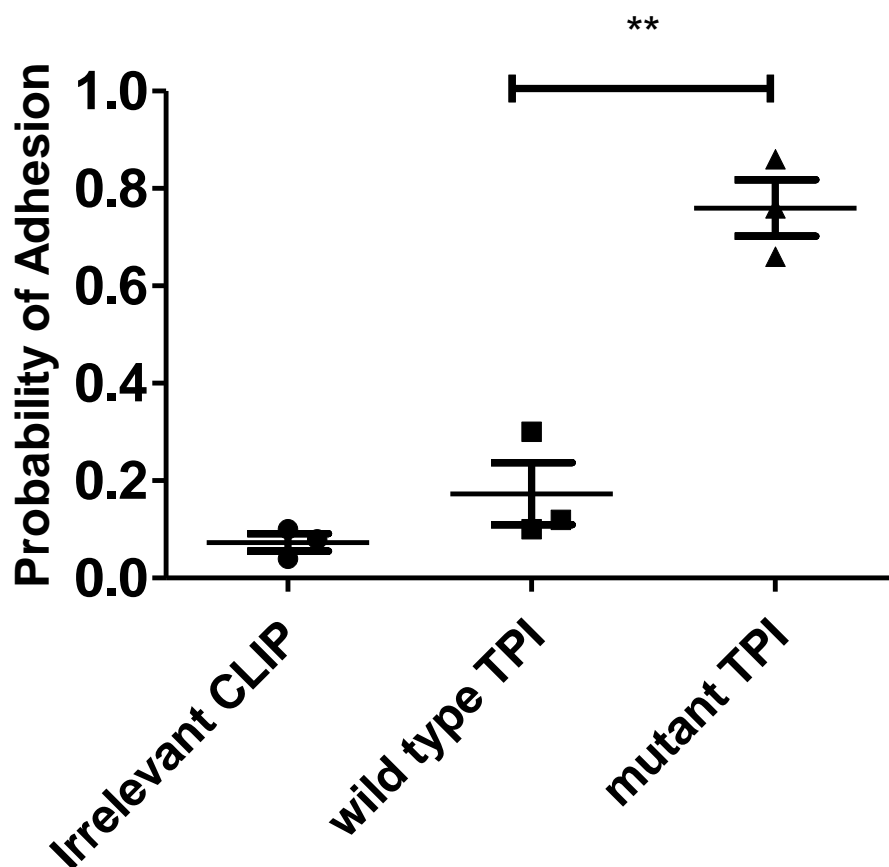
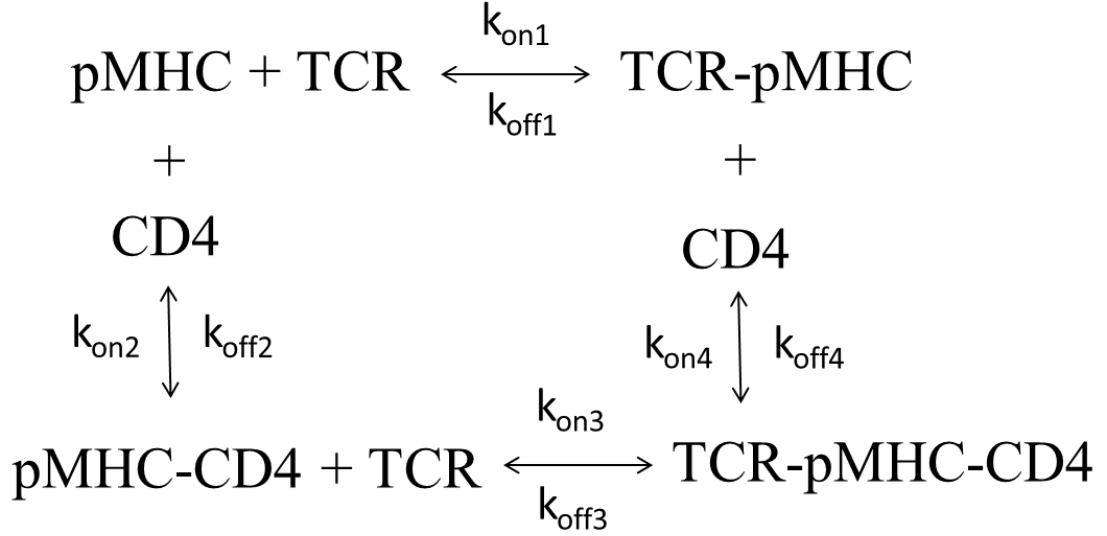


Figure 32. Mutant TPI binds to E8 TCR with much higher affinity.

The wild-type TPI pHLA is a 'cryptic peptide' in that it is capable of immune evasion. A point residue mutation in the peptide greatly enhances its immune detection, however, its binding affinity is indistinguishable from SPR when E8 is tetramerized, while neither can be detected when E8 is monomeric. Using the micropipette adhesion frequency assay, not only the wild-type TPI-TCR interactions detected with monomeric TCR, but the mutant peptide clearly demonstrated a much higher affinity value with TCR than with the wild-type counterpart, a result that correlates well with function.

A.2. Derivation of mathematical model for trimolecular interaction

The following derivation is the work of Dr. Cheng Zhu:



Kinetic equations

$$\frac{d\langle n \rangle_{\text{TCR}}}{dt} = m_{\text{TCR}} m_{\text{pMHC}} A_c k_{\text{on}1} - k_{\text{off}1} \langle n \rangle_{\text{TCR}} + k_{\text{off}4} \langle n \rangle_{\text{tri}} - m_{\text{CD4}} k_{\text{on}4} \langle n \rangle_{\text{TCR}}$$

$$\frac{d\langle n \rangle_{\text{CD4}}}{dt} = m_{\text{CD4}} m_{\text{pMHC}} A_c k_{\text{on}2} - k_{\text{off}2} \langle n \rangle_{\text{CD4}} + k_{\text{off}3} \langle n \rangle_{\text{tri}} - m_{\text{TCR}} k_{\text{on}3} \langle n \rangle_{\text{CD4}}$$

$$\frac{d\langle n \rangle_{\text{tri}}}{dt} = m_{\text{CD4}} k_{\text{on}4} \langle n \rangle_{\text{TCR}} - k_{\text{off}4} \langle n \rangle_{\text{tri}} + m_{\text{TCR}} k_{\text{on}3} \langle n \rangle_{\text{CD4}} - k_{\text{off}3} \langle n \rangle_{\text{tri}}$$

In vector form:

$$\frac{d}{dt} \begin{Bmatrix} \langle n \rangle_{\text{TCR}} \\ \langle n \rangle_{\text{CD4}} \\ \langle n \rangle_{\text{tri}} \end{Bmatrix} + \begin{bmatrix} m_{\text{CD4}} k_{\text{on}4} + k_{\text{off}1} & 0 & -k_{\text{off}4} \\ 0 & m_{\text{TCR}} k_{\text{on}3} + k_{\text{off}2} & -k_{\text{off}3} \\ -m_{\text{CD4}} k_{\text{on}4} & -m_{\text{TCR}} k_{\text{on}3} & k_{\text{off}3} + k_{\text{off}4} \end{bmatrix} \begin{Bmatrix} \langle n \rangle_{\text{TCR}} \\ \langle n \rangle_{\text{CD4}} \\ \langle n \rangle_{\text{tri}} \end{Bmatrix} = \begin{Bmatrix} m_{\text{TCR}} m_{\text{pMHC}} A_c k_{\text{on}1} \\ m_{\text{CD4}} m_{\text{pMHC}} A_c k_{\text{on}2} \\ 0 \end{Bmatrix}$$

Solving the equations:

$$\text{Let } \begin{pmatrix} x_1 \\ x_2 \\ x_3 \end{pmatrix} = \begin{pmatrix} \langle n \rangle_{\text{TCR},\infty} - \langle n \rangle_{\text{TCR}} \\ \langle n \rangle_{\text{CD4},\infty} - \langle n \rangle_{\text{CD4}} \\ \langle n \rangle_{\text{tri},\infty} - \langle n \rangle_{\text{tri}} \end{pmatrix} \text{ where } \begin{pmatrix} \langle n \rangle_{\text{TCR},\infty} \\ \langle n \rangle_{\text{CD4},\infty} \\ \langle n \rangle_{\text{tri},\infty} \end{pmatrix} \text{ is the equilibrium solution, i.e.,}$$

$$\begin{bmatrix} m_{\text{CD4}}k_{\text{on4}} + k_{\text{off1}} & 0 & -k_{\text{off4}} \\ 0 & m_{\text{TCR}}k_{\text{on3}} + k_{\text{off2}} & -k_{\text{off3}} \\ -m_{\text{CD4}}k_{\text{on4}} & -m_{\text{TCR}}k_{\text{on3}} & k_{\text{off3}} + k_{\text{off3}} \end{bmatrix} \begin{pmatrix} \langle n \rangle_{\text{TCR},\infty} \\ \langle n \rangle_{\text{CD4},\infty} \\ \langle n \rangle_{\text{tri},\infty} \end{pmatrix} = \begin{pmatrix} m_{\text{TCR}}m_{\text{pMHC}}A_c k_{\text{on1}} \\ m_{\text{CD4}}m_{\text{pMHC}}A_c k_{\text{on2}} \\ 0 \end{pmatrix}$$

The vector $\begin{pmatrix} x_1 \\ x_2 \\ x_3 \end{pmatrix}$ satisfies the homogeneous differential equation, i.e.,

$$\frac{d}{dt} \begin{pmatrix} x_1 \\ x_2 \\ x_3 \end{pmatrix} + \begin{bmatrix} m_{\text{CD4}}k_{\text{on4}} + k_{\text{off1}} & 0 & -k_{\text{off4}} \\ 0 & m_{\text{TCR}}k_{\text{on3}} + k_{\text{off2}} & -k_{\text{off3}} \\ -m_{\text{CD4}}k_{\text{on4}} & -m_{\text{TCR}}k_{\text{on3}} & k_{\text{off3}} + k_{\text{off4}} \end{bmatrix} \begin{pmatrix} x_1 \\ x_2 \\ x_3 \end{pmatrix} = \begin{pmatrix} 0 \\ 0 \\ 0 \end{pmatrix}$$

Equilibrium solution

$$\langle n \rangle_{\text{TCR},\infty} = \frac{1}{m_{\text{CD4}}k_{\text{on4}} + k_{\text{off1}}} (m_{\text{TCR}}m_{\text{pMHC}}A_c k_{\text{on1}} + k_{\text{off4}} \langle n \rangle_{\text{tri},\infty})$$

$$\langle n \rangle_{\text{CD4},\infty} = \frac{1}{m_{\text{TCR}}k_{\text{on3}} + k_{\text{off2}}} (m_{\text{CD4}}m_{\text{pMHC}}A_c k_{\text{on2}} + k_{\text{off3}} \langle n \rangle_{\text{tri},\infty})$$

$$m_{\text{CD4}}k_{\text{on4}} \langle n \rangle_{\text{TCR},\infty} + m_{\text{TCR}}k_{\text{on3}} \langle n \rangle_{\text{CD4},\infty} = (k_{\text{off3}} + k_{\text{off4}}) \langle n \rangle_{\text{tri},\infty}$$

$$\frac{m_{\text{CD4}}k_{\text{on4}}}{m_{\text{CD4}}k_{\text{on4}} + k_{\text{off1}}} (m_{\text{TCR}}m_{\text{pMHC}}A_c k_{\text{on1}} + k_{\text{off4}} \langle n \rangle_{\text{tri},\infty})$$

$$+ \frac{m_{\text{TCR}}k_{\text{on3}}}{m_{\text{TCR}}k_{\text{on3}} + k_{\text{off2}}} (m_{\text{CD4}}m_{\text{pMHC}}A_c k_{\text{on2}} + k_{\text{off3}} \langle n \rangle_{\text{tri},\infty})$$

$$= (k_{\text{off3}} + k_{\text{off4}}) \langle n \rangle_{\text{tri},\infty}$$

$$\langle n \rangle_{\text{tri},\infty} = m_{\text{TCR}}m_{\text{CD4}}m_{\text{pMHC}}A_c \frac{k_{\text{on1}}k_{\text{on4}}(m_{\text{TCR}}k_{\text{on3}} + k_{\text{off2}}) + k_{\text{on2}}k_{\text{on3}}(m_{\text{CD4}}k_{\text{on4}} + k_{\text{off1}})}{k_{\text{off1}}k_{\text{off4}}(m_{\text{TCR}}k_{\text{on3}} + k_{\text{off2}}) + k_{\text{off2}}k_{\text{off3}}(m_{\text{CD4}}k_{\text{on4}} + k_{\text{off1}})}$$

Equilibrium solution (continued)

$$\langle n \rangle_{\text{TCR},\infty} = \frac{m_{\text{TCR}}m_{\text{pMHC}}A_c k_{\text{on1}}}{m_{\text{CD4}}k_{\text{on4}} + k_{\text{off1}}} + \left(\frac{k_{\text{on1}}k_{\text{on4}}}{m_{\text{CD4}}k_{\text{on4}} + k_{\text{off1}}} + \frac{k_{\text{on2}}k_{\text{on3}}}{m_{\text{TCR}}k_{\text{on3}} + k_{\text{off2}}} \right) \times$$

$$\frac{m_{\text{TCR}}m_{\text{CD4}}m_{\text{pMHC}}A_c k_{\text{off4}}}{m_{\text{CD4}}k_{\text{on4}} + k_{\text{off1}}} / (k_{\text{off3}} + k_{\text{off4}} - \frac{m_{\text{CD4}}k_{\text{on4}}k_{\text{off4}}}{m_{\text{CD4}}k_{\text{on4}} + k_{\text{off1}}} - \frac{m_{\text{TCR}}k_{\text{on3}}k_{\text{off3}}}{m_{\text{TCR}}k_{\text{on3}} + k_{\text{off2}}})$$

$$\langle n \rangle_{\text{CD4},\infty} = \frac{m_{\text{CD4}}m_{\text{pMHC}}A_c k_{\text{on2}}}{m_{\text{TCR}}k_{\text{on3}} + k_{\text{off2}}} + \left(\frac{k_{\text{on2}}k_{\text{on3}}}{m_{\text{TCR}}k_{\text{on3}} + k_{\text{off2}}} + \frac{k_{\text{on1}}k_{\text{on4}}}{m_{\text{CD4}}k_{\text{on4}} + k_{\text{off1}}} \right) \times$$

$$\frac{m_{\text{TCR}}m_{\text{CD4}}m_{\text{pMHC}}A_c k_{\text{off3}}}{m_{\text{TCR}}k_{\text{on3}} + k_{\text{off2}}} / (k_{\text{off3}} + k_{\text{off4}} - \frac{m_{\text{CD4}}k_{\text{on4}}k_{\text{off4}}}{m_{\text{CD4}}k_{\text{on4}} + k_{\text{off1}}} - \frac{m_{\text{TCR}}k_{\text{on3}}k_{\text{off3}}}{m_{\text{TCR}}k_{\text{on3}} + k_{\text{off2}}})$$

$$\langle n \rangle_{\text{total},\infty} = \frac{m_{\text{TCR}}k_{\text{on1}}}{m_{\text{pMHC}}A_c} + \frac{m_{\text{CD4}}k_{\text{on2}}}{m_{\text{TCR}}k_{\text{on3}} + k_{\text{off2}}} + \left(1 + \frac{k_{\text{off4}}}{m_{\text{CD4}}k_{\text{on4}} + k_{\text{off1}}} + \frac{k_{\text{off3}}}{m_{\text{TCR}}k_{\text{on3}} + k_{\text{off2}}} \right) \times$$

$$\left(\frac{m_{\text{TCR}}k_{\text{on1}}m_{\text{CD4}}k_{\text{on4}}}{m_{\text{CD4}}k_{\text{on4}} + k_{\text{off1}}} + \frac{m_{\text{CD4}}k_{\text{on2}}m_{\text{TCR}}k_{\text{on3}}}{m_{\text{TCR}}k_{\text{on3}} + k_{\text{off2}}} \right) / (k_{\text{off3}} + k_{\text{off4}} - \frac{m_{\text{CD4}}k_{\text{on4}}k_{\text{off4}}}{m_{\text{CD4}}k_{\text{on4}} + k_{\text{off1}}} - \frac{m_{\text{TCR}}k_{\text{on3}}k_{\text{off3}}}{m_{\text{TCR}}k_{\text{on3}} + k_{\text{off2}}})$$

Simplified forms

$$\langle n \rangle_{\text{TCR},\infty} = \frac{m_{\text{TCR}}m_{\text{pMHC}}A_c}{m_{\text{CD4}}k_{\text{on4}} + k_{\text{off1}}} \left[k_{\text{on1}} + m_{\text{CD4}}k_{\text{off4}} \frac{k_{\text{on1}}k_{\text{on4}}(m_{\text{TCR}}k_{\text{on3}} + k_{\text{off2}}) + k_{\text{on2}}k_{\text{on3}}(m_{\text{CD4}}k_{\text{on4}} + k_{\text{off1}})}{k_{\text{off1}}k_{\text{off4}}(m_{\text{TCR}}k_{\text{on3}} + k_{\text{off2}}) + k_{\text{off2}}k_{\text{off3}}(m_{\text{CD4}}k_{\text{on4}} + k_{\text{off1}})} \right]$$

$$\langle n \rangle_{\text{CD4},\infty} = \frac{m_{\text{CD4}}m_{\text{pMHC}}A_c}{m_{\text{TCR}}k_{\text{on3}} + k_{\text{off2}}} \left[k_{\text{on2}} + m_{\text{TCR}}k_{\text{off3}} \frac{k_{\text{on1}}k_{\text{on4}}(m_{\text{TCR}}k_{\text{on3}} + k_{\text{off2}}) + k_{\text{on2}}k_{\text{on3}}(m_{\text{CD4}}k_{\text{on4}} + k_{\text{off1}})}{k_{\text{off1}}k_{\text{off4}}(m_{\text{TCR}}k_{\text{on3}} + k_{\text{off2}}) + k_{\text{off2}}k_{\text{off3}}(m_{\text{CD4}}k_{\text{on4}} + k_{\text{off1}})} \right]$$

$$\langle n \rangle_{\text{tri},\infty} = m_{\text{TCR}}m_{\text{CD4}}m_{\text{pMHC}}A_c \frac{k_{\text{on1}}k_{\text{on4}}(m_{\text{TCR}}k_{\text{on3}} + k_{\text{off2}}) + k_{\text{on2}}k_{\text{on3}}(m_{\text{CD4}}k_{\text{on4}} + k_{\text{off1}})}{k_{\text{off1}}k_{\text{off4}}(m_{\text{TCR}}k_{\text{on3}} + k_{\text{off2}}) + k_{\text{off2}}k_{\text{off3}}(m_{\text{CD4}}k_{\text{on4}} + k_{\text{off1}})}$$

$$\langle n \rangle_{\text{total},\infty} = \frac{m_{\text{TCR}}k_{\text{on1}}}{m_{\text{pMHC}}A_c} + \frac{m_{\text{CD4}}k_{\text{on2}}}{m_{\text{TCR}}k_{\text{on3}} + k_{\text{off2}}} + m_{\text{TCR}}m_{\text{CD4}} \left(1 + \frac{k_{\text{off4}}}{m_{\text{CD4}}k_{\text{on4}} + k_{\text{off1}}} + \frac{k_{\text{off3}}}{m_{\text{TCR}}k_{\text{on3}} + k_{\text{off2}}} \right)$$

$$\times \frac{k_{\text{on1}}k_{\text{on4}}(m_{\text{TCR}}k_{\text{on3}} + k_{\text{off2}}) + k_{\text{on2}}k_{\text{on3}}(m_{\text{CD4}}k_{\text{on4}} + k_{\text{off1}})}{k_{\text{off1}}k_{\text{off4}}(m_{\text{TCR}}k_{\text{on3}} + k_{\text{off2}}) + k_{\text{off2}}k_{\text{off3}}(m_{\text{CD4}}k_{\text{on4}} + k_{\text{off1}})}$$

REFERENCES

- 1 Zuniga, E. I., Macal, M., Lewis, G. M. & Harker, J. A. Innate and Adaptive Immune Regulation During Chronic Viral Infections. *Annu Rev Virol* **2**, 573-597, doi:10.1146/annurev-virology-100114-055226 (2015).
- 2 Brubaker, S. W., Bonham, K. S., Zanoni, I. & Kagan, J. C. in *Annual Review of Immunology Vol 33* Vol. 33 *Annual Review of Immunology* (eds D. R. Littman & W. M. Yokoyama) 257-290 (2015).
- 3 Kenneth Murphy, C. W. *Janeway's Immunobiology*. (W.W. Norton & Company, Inc., 2016).
- 4 Neefjes, J., Jongstra, M. L. M., Paul, P. & Bakke, O. Towards a systems understanding of MHC class I and MHC class II antigen presentation. *Nat Rev Immunol* **11**, 823-836, doi:10.1038/nri3084 (2011).
- 5 Huppa, J. B. & Davis, M. M. T-cell-antigen recognition and the immunological synapse. *Nat Rev Immunol* **3**, 973-983, doi:10.1038/nri1245 (2003).
- 6 Grakoui, A. *et al.* The immunological synapse: A molecular machine controlling T cell activation. *Science* **285**, 221-227, doi:DOI 10.1126/science.285.5425.221 (1999).
- 7 Guidotti, L. G. *et al.* Immunosurveillance of the Liver by Intravascular Effector CD8(+) T Cells. *Cell* **161**, 486-500, doi:10.1016/j.cell.2015.03.005 (2015).
- 8 DeGrendele, H. C., Estess, P. & Siegelman, M. H. Requirement for CD44 in activated T cell extravasation into an inflammatory site. *Science* **278**, 672-675, doi:DOI 10.1126/science.278.5338.672 (1997).
- 9 Hickman, H. D. *et al.* CXCR3 Chemokine Receptor Enables Local CD8(+) T Cell Migration for the Destruction of Virus-Infected Cells. *Immunity* **42**, 524-537, doi:10.1016/j.immuni.2015.02.009 (2015).
- 10 Basu, R. *et al.* Cytotoxic T Cells Use Mechanical Force to Potentiate Target Cell Killing. *Cell* **165**, 100-110, doi:10.1016/j.cell.2016.01.021 (2016).
- 11 Buchholz, V. R., Schumacher, T. N. M. & Busch, D. H. T Cell Fate at the Single-Cell Level. *Annu Rev Immunol* **34**, 65-92, doi:10.1146/annurev-immunol-032414-112014 (2016).
- 12 Masopust, D., Vezys, V., Marzo, A. L. & Lefrancois, L. Preferential localization of effector memory cells in nonlymphoid tissue. *Science* **291**, 2413-2417, doi:DOI 10.1126/science.1058867 (2001).
- 13 Kim, J. M., Rasmussen, J. P. & Rudensky, A. Y. Regulatory T cells prevent catastrophic autoimmunity throughout the lifespan of mice. *Nat Immunol* **8**, 191-197, doi:10.1038/ni1428 (2007).
- 14 Starr, T. K., Jameson, S. C. & Hogquist, K. A. Positive and negative selection of T cells. *Annual Review of Immunology* **21**, 139-176, doi:10.1146/annurev.immunol.21.120601.141107 (2003).
- 15 SloanLancaster, J. & Allen, P. M. Altered peptide ligand-induced partial T cell activation: Molecular mechanisms and role in T cell biology. *Annual Review of Immunology* **14**, 1-27, doi:10.1146/annurev.immunol.14.1.1 (1996).
- 16 Tubo, N. J. & Jenkins, M. K. TCR signal quantity and quality in CD4(+) T cell differentiation. *Trends Immunol.* **35**, 591-596, doi:10.1016/j.it.2014.09.008 (2014).

- 17 Meydan, C., Otu, H. H. & Sezerman, O. U. Prediction of peptides binding to MHC class I and II alleles by temporal motif mining. *Bmc Bioinformatics* **14**, doi:Artn S13 10.1186/1471-2105-14-S2-S13 (2013).
- 18 Veronika I. Zarnitsyna, B. D. E., Louis N. Schoettle, Joseph N. Blattman, and Rustom Antia. Estimating the Diversity, Completeness, and Cross-Reactivity of the T Cell Repertoire. *Frontiers in immunology* **4** (2013).
- 19 Hong, J. S. *et al.* A TCR mechanotransduction signaling loop induces negative selection in the thymus. *Nat Immunol* **19**, 1379-+, doi:10.1038/s41590-018-0259-z (2018).
- 20 Liu, B. Y., Chen, W., Evavold, B. D. & Zhu, C. Accumulation of Dynamic Catch Bonds between TCR and Agonist Peptide-MHC Triggers T Cell Signaling. *Cell* **157**, 357-368, doi:10.1016/j.cell.2014.02.053 (2014).
- 21 Huang, J. *et al.* The kinetics of two-dimensional TCR and pMHC interactions determine T-cell responsiveness. *Nature* **464**, 932-U156, doi:10.1038/nature08944 (2010).
- 22 Mallis, R. J. *et al.* Pre-TCR ligand binding impacts thymocyte development before alpha beta TCR expression. *P Natl Acad Sci USA* **112**, 8373-8378, doi:10.1073/pnas.1504971112 (2015).
- 23 Das, D. K. *et al.* Pre-T Cell Receptors (Pre-TCRs) Leverage V Complementarity Determining Regions (CDRs) and Hydrophobic Patch in Mechanosensing Thymic Self-ligands. *Journal of Biological Chemistry* **291**, 25292-25305, doi:10.1074/jbc.M116.752865 (2016).
- 24 Mallis, R. J., Arthanari, H., Lang, M. J., Reinherz, E. L. & Wagner, G. NMR-directed design of pre-TCR beta and pMHC molecules implies a distinct geometry for pre-TCR relative to alpha beta TCR recognition of pMHC. *Journal of Biological Chemistry* **293**, 754-766, doi:10.1074/jbc.M117.813493 (2018).
- 25 Garcia, K. C. *et al.* An alpha beta T cell receptor structure at 2.5 angstrom and its orientation in the TCR-MHC complex. *Science* **274**, 209-219, doi:DOI 10.1126/science.274.5285.209 (1996).
- 26 Reinherz, E. L. *et al.* The crystal structure of a T cell receptor in complex with peptide and MHC class II. *Science* **286**, 1913-1921, doi:10.1126/science.286.5446.1913 (1999).
- 27 Wang, J. H. & Reinherz, E. L. The structural basis of a ss T-lineage immune recognition: TCR docking topologies, mechanotransduction, and co-receptor function. *Immunol. Rev.* **250**, 102-119, doi:10.1111/j.1600-065X.2012.01161.x (2012).
- 28 Birnbaum, M. E. *et al.* Molecular architecture of the alpha beta T cell receptor-CD3 complex. *P Natl Acad Sci USA* **111**, 17576-17581, doi:10.1073/pnas.1420936111 (2014).
- 29 Davis, S. J. & van der Merwe, P. A. The kinetic-segregation model: TCR triggering and beyond. *Nat Immunol* **7**, 803-809, doi:10.1038/ni1389 (2006).
- 30 DeFord-Watts, L. M. *et al.* The Cytoplasmic Tail of the T Cell Receptor CD3 epsilon Subunit Contains a Phospholipid-Binding Motif that Regulates T Cell Functions. *Journal of Immunology* **183**, 1055-1064, doi:10.4049/jimmunol.0900404 (2009).

- 31 Xu, C. Q. *et al.* Regulation of T Cell Receptor Activation by Dynamic Membrane Binding of the CD3 epsilon Cytoplasmic Tyrosine-Based Motif. *Cell* **135**, 702-713, doi:10.1016/j.cell.2008.09.044 (2008).
- 32 Zhang, H., Cordoba, S. P., Dushek, O. & van der Merwe, P. A. Basic residues in the T-cell receptor zeta cytoplasmic domain mediate membrane association and modulate signaling. *P Natl Acad Sci USA* **108**, 19323-19328, doi:10.1073/pnas.1108052108 (2011).
- 33 Li, L. Y. *et al.* Ionic CD3-Lck interaction regulates the initiation of T-cell receptor signaling. *P Natl Acad Sci USA* **114**, E5891-E5899, doi:10.1073/pnas.1701990114 (2017).
- 34 Kim, S. T. *et al.* The alpha beta T Cell Receptor Is an Anisotropic Mechanosensor. *Journal of Biological Chemistry* **284**, 31028-31037, doi:10.1074/jbc.M109.052712 (2009).
- 35 Lee, M. S. *et al.* A Mechanical Switch Couples T Cell Receptor Triggering to the Cytoplasmic Juxtamembrane Regions of CD3 zeta zeta. *Immunity* **43**, 227-239, doi:10.1016/j.immuni.2015.06.018 (2015).
- 36 Chen, Y. F., Ju, L. N., Rushdi, M., Ge, C. H. & Zhu, C. Receptor-mediated cell mechanosensing. *Mol Biol Cell* **28**, 3134-3155, doi:10.1091/mbc.E17-04-0228 (2017).
- 37 Malissen, B. & Bongrand, P. Early T Cell Activation: integrating Biochemical, Structural, and Biophysical Cues. *Annual Review of Immunology Vol 33* **33**, 539-561, doi:10.1146/annurev-immunol-032414 (2015).
- 38 Holler, P. D., Chlewicki, L. K. & Kranz, D. M. TCRs with high affinity for foreign pMHC show self-reactivity. *Nat Immunol* **4**, 55-62, doi:10.1038/ni863 (2003).
- 39 Skokos, D. *et al.* Peptide-MHC potency governs dynamic interactions between T cells and dendritic cells in lymph nodes (vol 8, pg 835, 2007). *Nat Immunol* **8**, 1266-1266, doi:10.1038/ni1107-1266a (2007).
- 40 Hemmer, B. *et al.* Contribution of individual amino acids within MHC molecule or antigenic peptide to TCR ligand potency. *Journal of Immunology* **164**, 861-871, doi:DOI 10.4049/jimmunol.164.2.861 (2000).
- 41 Ladbury, J. E. & Chowdhry, B. Z. Sensing the heat: The application of isothermal titration calorimetry to thermodynamic studies of biomolecular interactions. *Chem Biol* **3**, 791-801, doi:Doi 10.1016/S1074-5521(96)90063-0 (1996).
- 42 Lemmon, M. A. Ligand-induced ErbB receptor dimerization. *Exp Cell Res* **315**, 638-648, doi:10.1016/j.yexcr.2008.10.024 (2009).
- 43 vanderMerwe, P. A. & Barclay, A. N. Analysis of cell-adhesion molecule interactions using surface plasmon resonance. *Curr Opin Immunol* **8**, 257-261, doi:Doi 10.1016/S0952-7915(96)80065-3 (1996).
- 44 Margulies, D. H., Plaksin, D., Khilko, S. N. & Jelonek, M. T. Studying interactions involving the T-cell antigen receptor by surface plasmon resonance. *Curr Opin Immunol* **8**, 262-270, doi:Doi 10.1016/S0952-7915(96)80066-5 (1996).
- 45 Boniface, J. J. & Davis, M. M. The kinetics of binding of peptide/MHC complexes to T-cell receptors: Application of surface plasmon resonance to a low-affinity measurement. *Methods (Orlando)* **6**, 168-176, doi:10.1006/meth.1994.1019 (1994).

- 46 Kersh, G. J., Kersh, E. N., Fremont, D. H. & Allen, P. M. High- and low-potency ligands with similar affinities for the TCR: The importance of kinetics in TCR signaling. *Immunity* **9**, 817-826, doi:Doi 10.1016/S1074-7613(00)80647-0 (1998).
- 47 Chesla, S. E., Selvaraj, P. & Zhu, C. Measuring two-dimensional receptor-ligand binding kinetics by micropipette. *Biophys J* **75**, 1553-1572, doi:Doi 10.1016/S0006-3495(98)74074-3 (1998).
- 48 Chen, W., Evans, E. A., McEver, R. P. & Zhu, C. Monitoring receptor-ligand interactions between surfaces by thermal fluctuations. *Biophys J* **94**, 694-701, doi:10.1529/biophysj.107.117895 (2008).
- 49 Hong, J. S. *et al.* Force-Regulated In Situ TCR-Peptide-Bound MHC Class II Kinetics Determine Functions of CD4(+) T Cells. *Journal of Immunology* **195**, 3557-3564, doi:10.4049/jimmunol.1501407 (2015).
- 50 Sibener, L. V. *et al.* Isolation of a Structural Mechanism for Uncoupling T Cell Receptor Signaling from Peptide-MHC Binding. *Cell* **174**, 672-+, doi:10.1016/j.cell.2018.06.017 (2018).
- 51 Evans, E. A. & Calderwood, D. A. Forces and bond dynamics in cell adhesion. *Science* **316**, 1148-1153, doi:10.1126/science.1137592 (2007).
- 52 Marshall, B. T. *et al.* Direct observation of catch bonds involving cell-adhesion molecules. *Nature* **423**, 190-193, doi:10.1038/nature01605 (2003).
- 53 Wu, P. *et al.* Mechano-regulation of Peptide-MHC Class I Conformations Determines TCR Antigen Recognition. *Molecular cell*, doi:10.1016/j.molcel.2018.12.018 (2019).
- 54 Janeway, C. A. THE T-CELL RECEPTOR AS A MULTICOMPONENT SIGNALING MACHINE - CD4/CD8 CORECEPTORS AND CD45 IN T-CELL ACTIVATION. *Annual Review of Immunology* **10**, 645-674, doi:10.1146/annurev.immunol.10.1.645 (1992).
- 55 Meuer, S. C., Schlossman, S. F. & Reinherz, E. L. CLONAL ANALYSIS OF HUMAN CYTO-TOXIC LYMPHOCYTES-T - T4+ AND T8+ EFFECTOR T-CELLS RECOGNIZE PRODUCTS OF DIFFERENT MAJOR HISTOCOMPATIBILITY COMPLEX REGIONS. *Proceedings of the National Academy of Sciences of the United States of America-Biological Sciences* **79**, 4395-4399, doi:10.1073/pnas.79.14.4395 (1982).
- 56 Weiss, A. T-CELL ANTIGEN RECEPTOR SIGNAL TRANSDUCTION - A TALE OF TAILS AND CYTOPLASMIC PROTEIN-TYROSINE KINASES. *Cell* **73**, 209-212, doi:10.1016/0092-8674(93)90221-b (1993).
- 57 Kern, P., Hussey, R. E., Spoerl, R., Reinherz, E. L. & Chang, H. C. Expression, purification, and functional analysis of murine ectodomain fragments of CD8 alpha alpha and CD8 alpha beta dimers. *Journal of Biological Chemistry* **274**, 27237-27243, doi:10.1074/jbc.274.38.27237 (1999).
- 58 Huang, J., Edwards, L. J., Evavold, B. D. & Zhu, C. Kinetics of MHC-CD8 interaction at the T cell membrane. *Journal of Immunology* **179**, 7653-7662, doi:DOI 10.4049/jimmunol.179.11.7653 (2007).
- 59 Artyomov, M. N., Lis, M., Devadas, S., Davis, M. M. & Chakraborty, A. K. CD4 and CD8 binding to MHC molecules primarily acts to enhance Lck delivery. *P Natl Acad Sci USA* **107**, 16916-16921, doi:10.1073/pnas.1010568107 (2010).

- 60 Jiang, N. *et al.* Two-Stage Cooperative T Cell Receptor-Peptide Major Histocompatibility Complex-CD8 Trimolecular Interactions Amplify Antigen Discrimination. *Immunity* **34**, 13-23, doi:10.1016/j.immuni.2010.12.017 (2011).
- 61 Garcia, K. C. *et al.* CD8 enhances formation of stable T-cell receptor MHC class I molecule complexes. *Nature* **384**, 577-581, doi:DOI 10.1038/384577a0 (1996).
- 62 Doyle, C. & Strominger, J. L. INTERACTION BETWEEN CD4 AND CLASS-II MHC MOLECULES MEDIATES CELL-ADHESION. *Nature* **330**, 256-259, doi:10.1038/330256a0 (1987).
- 63 Irvine, D. J., Purbhoo, M. A., Krogsaard, M. & Davis, M. M. Direct observation of ligand recognition by T cells. *Nature* **419**, 845-849, doi:10.1038/nature01076 (2002).
- 64 Rudolph, M. G., Stanfield, R. L. & Wilson, I. A. How TCRs bind MHCs, peptides, and coreceptors. *Annual Review of Immunology* **24**, 419-466, doi:10.1146/annurev.immunol.23.021704.115658 (2006).
- 65 Bevan, M. J. IMMUNOLOGY - STIMULATING KILLER CELLS. *Nature* **342**, 478-479, doi:10.1038/342478a0 (1989).
- 66 Sadeghnasseri, S. & Germain, R. N. A ROLE FOR PEPTIDE IN DETERMINING MHC CLASS-II STRUCTURE. *Nature* **353**, 167-170, doi:10.1038/353167a0 (1991).
- 67 Kozono, H., White, J., Clements, J., Marrack, P. & Kappler, J. PRODUCTION OF SOLUBLE MHC CLASS-II PROTEINS WITH COVALENTLY BOUND SINGLE PEPTIDES. *Nature* **369**, 151-154, doi:10.1038/369151a0 (1994).
- 68 Ryan, K. R., McNeil, L. K., Dao, C. N., Jensen, P. E. & Evavold, B. D. Modification of peptide interaction with MHC creates TCR partial agonists. *Cell Immunol* **227**, 70-78, doi:10.1016/j.cellimm.2004.01.003 (2004).
- 69 Wu, H., Kwong, P. D. & Hendrickson, W. A. Dimeric association and segmental variability in the structure of human CD4. *Nature* **387**, 527-530, doi:DOI 10.1038/387527a0 (1997).
- 70 Yin, Y. Y., Wang, X. X. & Mariuzza, R. A. Crystal structure of a complete ternary complex of T-cell receptor, peptide-MHC, and CD4. *P Natl Acad Sci USA* **109**, 5405-5410, doi:10.1073/pnas.1118801109 (2012).
- 71 Xiong, Y., Kern, P., Chang, H. C. & Reinherz, E. L. T cell receptor binding to a pMHCII ligand is kinetically distinct from and independent of CD4. *Journal of Biological Chemistry* **276**, 5659-5667, doi:DOI 10.1074/jbc.M009580200 (2001).
- 72 Davis, S. J. *et al.* The nature of molecular recognition by T cells. *Nat Immunol* **4**, 217-224, doi:10.1038/ni0303-217 (2003).
- 73 Wang, X. X. *et al.* Affinity maturation of human CD4 by yeast surface display and crystal structure of a CD4-HLA-DR1 complex. *P Natl Acad Sci USA* **108**, 15960-15965, doi:10.1073/pnas.1109438108 (2011).
- 74 Huppa, J. B. *et al.* TCR-peptide-MHC interactions in situ show accelerated kinetics and increased affinity. *Nature* **463**, 963-U143, doi:10.1038/nature08746 (2010).
- 75 Jonsson, P. *et al.* Remarkably low affinity of CD4/peptide-major histocompatibility complex class II protein interactions. *P Natl Acad Sci USA* **113**, 5682-5687, doi:10.1073/pnas.1513918113 (2016).

- 76 Zhu, D. M., Dustin, M. L., Cairo, C. W. & Golan, D. E. Analysis of two-dimensional dissociation constant of laterally mobile cell adhesion molecules. *Biophys J* **92**, 1022-1034, doi:10.1529/biophysj.106.089649 (2007).
- 77 Boggon, T. J. & Eck, M. J. Structure and regulation of Src family kinases. *Oncogene* **23**, 7918-7927, doi:10.1038/sj.onc.1208081 (2004).
- 78 Palacios, E. H. & Weiss, A. Function of the Src-family kinases, Lck and Fyn, in T-cell development and activation. *Oncogene* **23**, 7990-8000, doi:10.1038/sj.onc.1208074 (2004).
- 79 Nika, K. *et al.* Constitutively Active Lck Kinase in T Cells Drives Antigen Receptor Signal Transduction. *Immunity* **32**, 766-777, doi:10.1016/j.immuni.2010.05.011 (2010).
- 80 Krummel, M. F., Sjaastad, M. D., Wulfig, C. & Davis, M. M. Differential clustering of CD4 and CD3 zeta during T cell recognition. *Science* **289**, 1349-1352, doi:DOI 10.1126/science.289.5483.1349 (2000).
- 81 Ehrlich, L. I. R., Ebert, P. J. R., Krummel, M. F., Weiss, A. & Davis, M. M. Dynamics of p56lck translocation to the T cell immunological synapse following agonist and antagonist stimulation. *Immunity* **17**, 809-822, doi:Doi 10.1016/S1074-7613(02)00481-8 (2002).
- 82 Rossy, J., Owen, D. M., Williamson, D. J., Yang, Z. M. & Gaus, K. Conformational states of the kinase Lck regulate clustering in early T cell signaling. *Nat Immunol* **14**, 82-89, doi:10.1038/ni.2488 (2013).
- 83 Wiest, D. L. *et al.* Regulation of T-Cell Receptor Expression in Immature Cd4+Cd8+ Thymocytes by P56(Lck) Tyrosine Kinase - Basis for Differential Signaling by Cd4 and Cd8 in Immature Thymocytes Expressing Both Coreceptor Molecules. *J Exp Med* **178**, 1701-1712, doi:DOI 10.1084/jem.178.5.1701 (1993).
- 84 Stepanek, O. *et al.* Coreceptor Scanning by the T Cell Receptor Provides a Mechanism for T Cell Tolerance. *Cell* **159**, 333-345, doi:10.1016/j.cell.2014.08.042 (2014).
- 85 Babior, B. M. Oxygen-Dependent Microbial Killing by Phagocytes .1. *New Engl J Med* **298**, 659-668, doi:Doi 10.1056/Nejm197803232981205 (1978).
- 86 Winterbourn, C. C., Kettle, A. J. & Hampton, M. B. Reactive Oxygen Species and Neutrophil Function. *Annu Rev Biochem* **85**, 765-792, doi:10.1146/annurev-biochem-060815-014442 (2016).
- 87 Comhair, S. A. A. & Erzurum, S. C. Redox Control of Asthma: Molecular Mechanisms and Therapeutic Opportunities. *Antioxid Redox Sign* **12**, 93-124, doi:10.1089/ars.2008.2425 (2010).
- 88 Yu, B. P. Cellular Defenses against Damage from Reactive Oxygen Species. *Physiol Rev* **74**, 139-162 (1994).
- 89 Fitzpatrick, A. M., Jones, D. P. & Brown, L. A. S. Glutathione Redox Control of Asthma: From Molecular Mechanisms to Therapeutic Opportunities. *Antioxid Redox Sign* **17**, 375-408, doi:10.1089/ars.2011.4198 (2012).
- 90 Baynes, J. W. Role of Oxidative Stress in Development of Complications in Diabetes. *Diabetes* **40**, 405-412, doi:DOI 10.2337/diabetes.40.4.405 (1991).
- 91 Sies, H., Berndt, C. & Jones, D. P. Oxidative Stress. *Annual Review of Biochemistry, Vol 86* **86**, 715-748, doi:10.1146/annurev-biochem-061516-045037 (2017).

- 92 Rhee, S. G. H₂O₂, a necessary evil for cell signaling. *Science* **312**, 1882-1883, doi:10.1126/science.1130481 (2006).
- 93 Aust, A. E. & Eveleigh, J. F. Mechanisms of DNA oxidation. *P Soc Exp Biol Med* **222**, 246-252, doi:DOI 10.1046/j.1525-1373.1999.d01-141.x (1999).
- 94 Bienert, G. P., Schjoerring, J. K. & Jahn, T. P. Membrane transport of hydrogen peroxide. *Bba-Biomembranes* **1758**, 994-1003, doi:10.1016/j.bbamem.2006.02.015 (2006).
- 95 Davies, M. J. Protein oxidation and peroxidation. *Biochem J* **473**, 805-825, doi:10.1042/Bj20151227 (2016).
- 96 Simeoni, L. & Bogeski, I. Redox regulation of T-cell receptor signaling. *Biol Chem* **396**, 555-568, doi:10.1515/hsz-2014-0312 (2015).
- 97 Kettenhofen, N. J. & Wood, M. J. Formation, Reactivity, and Detection of Protein Sulfenic Acids. *Chem Res Toxicol* **23**, 1633-1646, doi:10.1021/tx100237w (2010).
- 98 Zorov, D. B., Juhaszova, M. & Sollott, S. J. Mitochondrial Reactive Oxygen Species (Ros) and Ros-Induced Ros Release. *Physiol Rev* **94**, 909-950, doi:10.1152/physrev.00026.2013 (2014).
- 99 Sena, L. A. *et al.* Mitochondria Are Required for Antigen-Specific T Cell Activation through Reactive Oxygen Species Signaling. *Immunity* **38**, 225-236, doi:10.1016/j.immuni.2012.10.020 (2013).
- 100 Rhee, S. G., Bae, Y. S., Lee, S. R. & Kwon, J. Hydrogen peroxide: a key messenger that modulates protein phosphorylation through cysteine oxidation. *Science's STKE : signal transduction knowledge environment* **2000**, pe1 (2000).
- 101 Sundaresan, M., Yu, Z. X., Ferrans, V. J., Irani, K. & Finkel, T. Requirement for Generation of H₂O₂ for Platelet-Derived Growth-Factor Signal-Transduction. *Science* **270**, 296-299, doi:DOI 10.1126/science.270.5234.296 (1995).
- 102 Sabroe, I., Dower, S. K. & Whyte, M. K. B. The role of toll-like receptors in the regulation of neutrophil migration, activation, and apoptosis. *Clin Infect Dis* **41**, S421-S426, doi:Doi 10.1086/431992 (2005).
- 103 Amulic, B., Cazalet, C., Hayes, G. L., Metzler, K. D. & Zychlinsky, A. Neutrophil Function: From Mechanisms to Disease. *Annual Review of Immunology, Vol 30* **30**, 459-489, doi:10.1146/annurev-immunol-020711-074942 (2012).
- 104 Antunes, F. & Cadenas, E. Estimation of H₂O₂ gradients across biomembranes. *Febs Lett* **475**, 121-126, doi:Doi 10.1016/S0014-5793(00)01638-0 (2000).
- 105 Davies, K. J. A. The broad spectrum of responses to oxidants in proliferating cells: A new paradigm for oxidative stress. *Iubmb Life* **48**, 41-47, doi:Doi 10.1080/713803463 (1999).
- 106 Gulden, M., Jess, A., Kammann, J., Maser, E. & Seibert, H. Cytotoxic potency of H₂O₂ in cell cultures: Impact of cell concentration and exposure time. *Free Radical Bio Med* **49**, 1298-1305, doi:10.1016/j.freeradbiomed.2010.07.015 (2010).
- 107 Sokol, R. J. *et al.* Extreme prematurity: An alcohol-related birth effect. *Alcohol Clin Exp Res* **31**, 1031-1037, doi:10.1111/j.1530-0277.2007.00384.x (2007).

- 108 Sabharwal, S. S. & Schumacker, P. T. Mitochondrial ROS in cancer: initiators, amplifiers or an Achilles' heel? *Nat Rev Cancer* **14**, 709-721, doi:10.1038/nrc3803 (2014).
- 109 Gao, P. *et al.* HIF-dependent antitumorigenic effect of antioxidants in vivo. *Cancer Cell* **12**, 230-238, doi:10.1016/j.ccr.2007.08.004 (2007).
- 110 Schumacker, P. T. Reactive Oxygen Species in Cancer: A Dance with the Devil. *Cancer Cell* **27**, 156-157, doi:10.1016/j.ccell.2015.01.007 (2015).
- 111 Harris, I. S. *et al.* Glutathione and Thioredoxin Antioxidant Pathways Synergize to Drive Cancer Initiation and Progression. *Cancer Cell* **27**, 211-222, doi:10.1016/j.ccell.2014.11.019 (2015).
- 112 Novogrodsky, A., Ravid, A., Rubin, A. L. & Stenzel, K. H. Hydroxyl Radical Scavengers Inhibit Lymphocyte Mitogenesis. *Proceedings of the National Academy of Sciences of the United States of America-Biological Sciences* **79**, 1171-1174, doi:DOI 10.1073/pnas.79.4.1171 (1982).
- 113 Chaudhri, G., Clark, I. A., Hunt, N. H., Cowden, W. B. & Ceredig, R. Effect of Antioxidants on Primary Alloantigen-Induced T-Cell Activation and Proliferation. *Journal of Immunology* **137**, 2646-2652 (1986).
- 114 Chaudhri, G., Hunt, N. H., Clark, I. A. & Ceredig, R. Antioxidants Inhibit Proliferation and Cell-Surface Expression of Receptors for Interleukin-2 and Transferrin in Lymphocytes-T Stimulated with Phorbol-Myristate Acetate and Ionomycin. *Cell Immunol* **115**, 204-213, doi:Doi 10.1016/0008-8749(88)90174-8 (1988).
- 115 Tatla, S., Woodhead, V., Foreman, J. C. & Chain, B. M. The role of reactive oxygen species in triggering proliferation and IL-2 secretion in T cells. *Free Radical Bio Med* **26**, 14-24, doi:Doi 10.1016/S0891-5849(98)00133-6 (1999).
- 116 Roth, S. & Droge, W. Regulation of T-Cell Activation and T-Cell Growth-Factor (Tc α 1) Production by Hydrogen-Peroxide. *Cell Immunol* **108**, 417-424, doi:Doi 10.1016/0008-8749(87)90224-3 (1987).
- 117 Los, M., Droge, W., Stricker, K., Baeuerle, P. A. & Schulzeosthoff, K. Hydrogen-Peroxide as a Potent Activator of T-Lymphocyte Functions. *Eur J Immunol* **25**, 159-165, doi:DOI 10.1002/eji.1830250127 (1995).
- 118 Devadas, S., Zaritskaya, L., Rhee, S. G., Oberley, L. & Williams, M. S. Discrete generation of superoxide and hydrogen peroxide by T cell receptor stimulation: Selective regulation of mitogen-activated protein kinase activation and Fas ligand expression. *J Exp Med* **195**, 59-70, doi:DOI 10.1084/jem.20010659 (2002).
- 119 Jackson, S. H., Devadas, S., Kwon, J., Pinto, L. A. & Williams, M. S. T cells express a phagocyte-type NADPH oxidase that is activated after T cell receptor stimulation. *Nat Immunol* **5**, 818-827, doi:10.1038/ni1096 (2004).
- 120 Belikov, A. V., Schraven, B. & Simeoni, L. TCR-triggered extracellular superoxide production is not required for T-cell activation. *Cell Commun Signal* **12**, doi:ARTN 50 10.1186/s12964-014-0050-1 (2014).
- 121 Michalek, R. D. *et al.* Estrogen-related receptor- α is a metabolic regulator of effector T-cell activation and differentiation. *P Natl Acad Sci USA* **108**, 18348-18353, doi:10.1073/pnas.1108856108 (2011).

- 122 Wang, R. N. *et al.* The Transcription Factor Myc Controls Metabolic Reprogramming upon T Lymphocyte Activation. *Immunity* **35**, 871-882, doi:10.1016/j.immuni.2011.09.021 (2011).
- 123 Baixauli, F. *et al.* The mitochondrial fission factor dynamin-related protein 1 modulates T-cell receptor signalling at the immune synapse. *Embo J* **30**, 1238-1250, doi:10.1038/emboj.2011.25 (2011).
- 124 Gill, T. & Levine, A. D. Mitochondria-derived Hydrogen Peroxide Selectively Enhances T Cell Receptor-initiated Signal Transduction. *Journal of Biological Chemistry* **288**, 26246-26255, doi:10.1074/jbc.M113.476895 (2013).
- 125 Clayton, L. K., Sieh, M., Pious, D. A. & Reinherz, E. L. Identification of Human Cd4 Residues Affecting Class-II Mhc Versus Hiv-1 Gp120 Binding. *Nature* **339**, 548-551, doi:DOI 10.1038/339548a0 (1989).
- 126 Hussey, R. E. *et al.* A Soluble Cd4 Protein Selectively Inhibits Hiv Replication and Syncytium Formation. *Nature* **331**, 78-81, doi:DOI 10.1038/331078a0 (1988).
- 127 Bleul, C. C., Wu, L. J., Hoxie, J. A., Springer, T. A. & Mackay, C. R. The HIV coreceptors CXCR4 and CCR5 are differentially expressed and regulated on human T lymphocytes. *P Natl Acad Sci USA* **94**, 1925-1930, doi:10.1073/pnas.94.5.1925 (1997).
- 128 Wilkin, T. J. & Gulick, R. M. CCR5 Antagonism in HIV Infection: Current Concepts and Future Opportunities. *Annu Rev Med* **63**, 81-93, doi:10.1146/annurev-med-052010-145454 (2012).
- 129 Naisbitt, D. J. *et al.* Plasma cysteine deficiency and decreased reduction of nitrososulfamethoxazole with HIV infection. *Aids Res Hum Retrov* **16**, 1929-1938, doi:Doi 10.1089/088922200750054657 (2000).
- 130 Aukrust, P. *et al.* Disturbed glutathione metabolism and decreased antioxidant levels in human immunodeficiency virus-infected patients during highly active antiretroviral therapy - Potential immunomodulatory effects of antioxidants. *J Infect Dis* **188**, 232-238, doi:Doi 10.1086/376459 (2003).
- 131 Cribbs, S. K., Guidot, D. M., Martin, G. S., Lennox, J. & Brown, L. A. Anti-Retroviral Therapy Is Associated with Decreased Alveolar Glutathione Levels Even in Healthy HIV-Infected Individuals. *Plos One* **9**, doi:ARTN e88630 10.1371/journal.pone.0088630 (2014).
- 132 Maekawa, A., Schmidt, B., Fazekas de St Groth, B., Sanejouand, Y. H. & Hogg, P. J. Evidence for a domain-swapped CD4 dimer as the coreceptor for binding to class II MHC. *Journal of Immunology* **176**, 6873-6878, doi:DOI 10.4049/jimmunol.176.11.6873 (2006).
- 133 Moldovan, M. C. *et al.* CD4 dimers constitute the functional component required for T cell activation. *Journal of Immunology* **169**, 6261-6268, doi:DOI 10.4049/jimmunol.169.11.6261 (2002).
- 134 Moldovan, M. C., Sabbagh, L., Breton, G., Sekaly, R. P. & Krummel, M. F. Triggering of T cell activation via CD4 dimers. *Journal of Immunology* **176**, 5438-5445, doi:DOI 10.4049/jimmunol.176.9.5438 (2006).
- 135 Matthias, L. J., Azimi, I., Tabrett, C. A. & Hogg, P. J. Reduced Monomeric CD4 Is the Preferred Receptor for HIV. *Journal of Biological Chemistry* **285**, 40793-40799, doi:10.1074/jbc.M110.190579 (2010).

- 136 Cerutti, N., Killick, M., Jugnarain, V., Papathanasopoulos, M. & Capovilla, A. Disulfide Reduction in CD4 Domain 1 or 2 Is Essential for Interaction with HIV Glycoprotein 120 (gp120), which Impairs Thioredoxin-driven CD4 Dimerization. *Journal of Biological Chemistry* **289**, 10455-10465, doi:10.1074/jbc.M113.539353 (2014).
- 137 Veillette, A., Dumont, S. & Fournel, M. Conserved Cysteine Residues Are Critical for the Enzymatic Function of the Lymphocyte-Specific Tyrosine Protein-Kinase P56lck. *Journal of Biological Chemistry* **268**, 17547-17553 (1993).
- 138 Kanner, S. B. *et al.* Sulfhydryl Oxidation down-Regulates T-Cell Signaling and Inhibits Tyrosine Phosphorylation of Phospholipase C-Gamma-1. *P Natl Acad Sci USA* **89**, 300-304, doi:DOI 10.1073/pnas.89.1.300 (1992).
- 139 Nakamura, K. *et al.* Redox Regulation of a Src Family Protein-Tyrosine Kinase P56(Lck) in T-Cells. *Oncogene* **8**, 3133-3139 (1993).
- 140 Stefanova, I. *et al.* HIV infection-induced posttranslational modification of T cell signaling molecules associated with disease progression. *J Clin Invest* **98**, 1290-1297, doi:Doi 10.1172/Jci118915 (1996).
- 141 Secrist, J. P., Burns, L. A., Karnitz, L., Koretzky, G. A. & Abraham, R. T. Stimulatory Effects of the Protein Tyrosine Phosphatase Inhibitor, Pervanadate, on T-Cell Activation Events. *Journal of Biological Chemistry* **268**, 5886-5893 (1993).
- 142 Cunnick, J. M., Dorsey, J. F., Mei, L. & Wu, J. Reversible regulation of SHP-1 tyrosine phosphatase activity by oxidation. *Biochem Mol Biol Int* **45**, 887-894 (1998).
- 143 Singer, S. J. & Nicolson, G. L. The Fluid Mosaic Model of the Structure of Cell Membranes. *Science* **175**, 720+, doi:DOI 10.1126/science.175.4023.720 (1972).
- 144 Edidin, M. The state of lipid rafts: From model membranes to cells. *Annu Rev Bioph Biom* **32**, 257-283, doi:10.1146/annurev.biophys.32.110601.142439 (2003).
- 145 Janes, P. W., Ley, S. C. & Magee, A. I. Aggregation of lipid rafts accompanies signaling via the T cell antigen receptor. *J Cell Biol* **147**, 447-461, doi:DOI 10.1083/jcb.147.2.447 (1999).
- 146 Drevot, P. *et al.* TCR signal initiation machinery is pre-assembled and activated in a subset of membrane rafts. *Embo J* **21**, 1899-1908, doi:DOI 10.1093/emboj/21.8.1899 (2002).
- 147 Schamel, W. W. A. *et al.* Coexistence of multivalent and monovalent TCRs explains high sensitivity and wide range of response. *J Exp Med* **202**, 493-503, doi:10.1084/jem.20042155 (2005).
- 148 Xavier, R., Brennan, T., Li, Q. Q., McCormack, C. & Seed, B. Membrane compartmentation is required for efficient T cell activation. *Immunity* **8**, 723-732, doi:Doi 10.1016/S1074-7613(00)80577-4 (1998).
- 149 Molnar, E. *et al.* Cholesterol and Sphingomyelin Drive Ligand-independent T-cell Antigen Receptor Nanoclustering. *Journal of Biological Chemistry* **287**, 42664-42674, doi:10.1074/jbc.M112.386045 (2012).
- 150 Murugesan, S. *et al.* Formin-generated actomyosin arcs propel T cell receptor microcluster movement at the immune synapse. *J Cell Biol* **215**, 383-399, doi:10.1083/jcb.201603080 (2016).

- 151 Chen, W. & Zhu, C. Mechanical regulation of T-cell functions. *Immunol. Rev.* **256**, 160-176, doi:10.1111/imr.12122 (2013).
- 152 Klemke, M. *et al.* Oxidation of cofilin mediates T cell hyporesponsiveness under oxidative stress conditions. *Immunity* **29**, 404-413, doi:10.1016/j.immuni.2008.06.016 (2008).
- 153 Samstag, Y., John, I. & Wabnitz, G. H. Cofilin: a redox sensitive mediator of actin dynamics during T-cell activation and migration. *Immunol. Rev.* **256**, 30-47, doi:10.1111/imr.12115 (2013).
- 154 Valensin, S. *et al.* F-actin dynamics control segregation of the TCR signaling cascade to clustered lipid rafts. *Eur J Immunol* **32**, 435-446, doi:DOI 10.1002/1521-4141(200202)32:2<435::Aid-Immu435>3.0.Co;2-H (2002).
- 155 Wang, F., Beck-Garcia, K., Zorzin, C., Schamel, W. W. A. & Davis, M. M. Inhibition of T cell receptor signaling by cholesterol sulfate, a naturally occurring derivative of membrane cholesterol. *Nat Immunol* **17**, 844+, doi:10.1038/ni.3462 (2016).
- 156 Davies, L. C., Jenkins, S. J., Allen, J. E. & Taylor, P. R. Tissue-resident macrophages. *Nat Immunol* **14**, 986-995, doi:10.1038/ni.2705 (2013).
- 157 Laskin, D. L. & Pendino, K. J. Macrophages and Inflammatory Mediators in Tissue-Injury. *Annu Rev Pharmacol* **35**, 655-677, doi:DOI 10.1146/annurev.pa.35.040195.003255 (1995).
- 158 Gordon, S., Pluddemann, A. & Estrada, F. M. Macrophage heterogeneity in tissues: phenotypic diversity and functions. *Immunol. Rev.* **262**, 36-55, doi:10.1111/imr.12223 (2014).
- 159 Morales-Nebreda, L., Misharin, A. V., Perlman, H. & Budinger, R. S. The heterogeneity of lung macrophages in the susceptibility to disease. *Eur. Respir. Rev.* **24**, 505-509, doi:10.1183/16000617.0031-2015 (2015).
- 160 Whitsett, J. A., Wert, S. E. & Weaver, T. E. Alveolar Surfactant Homeostasis and the Pathogenesis of Pulmonary Disease. *Annual Review of Medicine* **61**, 105-119, doi:10.1146/annurev.med.60.041807.123500 (2010).
- 161 Hoidal, J. R., Schmeling, D. & Peterson, P. K. Phagocytosis, Bacterial Killing, and Metabolism by Purified Human-Lung Phagocytes. *J Infect Dis* **144**, 61-71, doi:DOI 10.1093/infdis/144.1.61 (1981).
- 162 Kirby, A. C., Coles, M. C. & Kaye, P. M. Alveolar Macrophages Transport Pathogens to Lung Draining Lymph Nodes. *Journal of Immunology* **183**, 1983-1989, doi:10.4049/jimmunol.0901089 (2009).
- 163 Lipscomb, M. F. *et al.* Human Alveolar Macrophages - Hla-Dr-Positive Macrophages That Are Poor Stimulators of a Primary Mixed Leukocyte Reaction. *Journal of Immunology* **136**, 497-504 (1986).
- 164 Hussell, T. & Bell, T. J. Alveolar macrophages: plasticity in a tissue-specific context. *Nat Rev Immunol* **14**, 81-93, doi:10.1038/nri3600 (2014).
- 165 Martinez, F. O. & Gordon, S. The M1 and M2 paradigm of macrophage activation: time for reassessment. *F1000prime reports* **6**, 13, doi:10.12703/p6-13 (2014).
- 166 Murray, P. J. Macrophage Polarization. *Annu Rev Physiol* **79**, 541-566, doi:10.1146/annurev-physiol-022516-034339 (2017).

- 167 Vogel, D. Y. S. *et al.* Macrophages in inflammatory multiple sclerosis lesions have an intermediate activation status. *J Neuroinflamm* **10**, doi:Artn 35 10.1186/1742-2094-10-35 (2013).
- 168 Kopf, M., Schneider, C. & Nobs, S. P. The development and function of lung-resident macrophages and dendritic cells. *Nat Immunol* **16**, 36-44, doi:10.1038/ni.3052 (2015).
- 169 Tajima, T. *et al.* Lipopolysaccharide induces macrophage migration via prostaglandin D-2 and prostaglandin E-2. *J Pharmacol Exp Ther* **326**, 493-501, doi:10.1124/jpet.108.137992 (2008).
- 170 Aderem, A. & Underhill, D. M. Mechanisms of phagocytosis in macrophages. *Annual Review of Immunology* **17**, 593-623, doi:DOI 10.1146/annurev.immunol.17.1.593 (1999).
- 171 Allen, L. A. H. & Aderem, A. Molecular definition of distinct cytoskeletal structures involved in complement- and Fc receptor-mediated phagocytosis in macrophages. *J Exp Med* **184**, 627-637, doi:DOI 10.1084/jem.184.2.627 (1996).
- 172 Moss, M. *et al.* Chronic alcohol abuse is associated with an increased incidence of acute respiratory distress syndrome and severity of multiple organ dysfunction in patients with septic shock. *Crit Care Med* **31**, 869-877, doi:10.1097/01.Ccm.0000055389.64497.11 (2003).
- 173 Moss, M., Bucher, B., Moore, F. A., Moore, E. E. & Parsons, P. E. The role of chronic alcohol abuse in the development of acute respiratory distress syndrome in adults. *Jama-J Am Med Assoc* **275**, 50-54, doi:DOI 10.1001/jama.275.1.50 (1996).
- 174 Erickson, S. E. *et al.* Recent trends in acute lung injury mortality: 1996-2005. *Crit Care Med* **37**, 1574-1579, doi:10.1097/CCM.0b013e31819fefdf (2009).
- 175 Ware, L. B. The acute respiratory distress syndrome (vol 342, pg 1334, 2000). *New Engl J Med* **343**, 520-520 (2000).
- 176 Gauthier, T. W., Manar, M. H. & Brown, L. A. S. Is maternal alcohol use a risk factor for early-onset sepsis in premature newborns? *Alcohol* **33**, 139-145, doi:10.1016/j.alcohol.2004.06.003 (2004).
- 177 Gauthier, T. W., Drews-Botsch, C., Falek, A., Coles, C. & Brown, L. A. S. Maternal alcohol abuse and neonatal infection. *Alcohol Clin Exp Res* **29**, 1035-1043, doi:10.1097/01.Alc.0000167956.28160.5e (2005).
- 178 Gauthier, T. W. *et al.* Fetal alcohol exposure impairs alveolar macrophage function via decreased glutathione availability. *Pediatr Res* **57**, 76-81, doi:10.1203/01.Pdr.0000149108.44152.D3 (2005).
- 179 Ping, X. D., Harris, F. L., Brown, L. A. S. & Gauthier, T. W. In vivo dysfunction of the term alveolar macrophage after in utero ethanol exposure. *Alcohol Clin Exp Res* **31**, 308-316, doi:10.1111/j.1530-0277.2006.00306.x (2007).
- 180 Gauthier, T. W. *et al.* In Utero Ethanol Exposure Impairs Defenses Against Experimental Group B Streptococcus in the Term Guinea Pig Lung. *Alcohol Clin Exp Res* **33**, 300-306, doi:10.1111/j.1530-0277.2008.00833.x (2009).
- 181 Gauthier, T. W., Ping, X. D., Gabelaia, L. & Brown, L. A. S. Delayed neonatal lung macrophage differentiation in a mouse model of in utero ethanol exposure. *Am J Physiol-Lung C* **299**, L8-L16, doi:10.1152/ajplung.90609.2008 (2010).

- 182 Yeligar, S. M., Harris, F. L., Hart, C. M. & Brown, L. A. S. Ethanol Induces Oxidative Stress in Alveolar Macrophages via Upregulation of NADPH Oxidases. *Journal of Immunology* **188**, 3648-3657, doi:10.4049/jimmunol.1101278 (2012).
- 183 Yeligar, S. M., Harris, F. L., Hart, C. M. & Brown, L. A. S. Glutathione attenuates ethanol-induced alveolar macrophage oxidative stress and dysfunction by downregulating NADPH oxidases. *Am J Physiol-Lung C* **306**, L429-L441, doi:10.1152/ajplung.00159.2013 (2014).
- 184 Nagase, T. *et al.* Acute lung injury by sepsis and acid aspiration: a key role for cytosolic phospholipase A(2). *Nat Immunol* **1**, 42-46 (2000).
- 185 Imai, Y. *et al.* Angiotensin-converting enzyme 2 protects from severe acute lung failure. *Nature* **436**, 112-116, doi:10.1038/nature03712 (2005).
- 186 Imai, Y. *et al.* Identification of oxidative stress and toll-like receptor 4 signaling as a key pathway of acute lung injury. *Cell* **133**, 235-249, doi:10.1016/j.cell.2008.02.043 (2008).
- 187 Kong, X. N., Thimmulappa, R., Kombairaju, P. & Biswal, S. NADPH Oxidase-Dependent Reactive Oxygen Species Mediate Amplified TLR4 Signaling and Sepsis-Induced Mortality in Nrf2-Deficient Mice. *Journal of Immunology* **185**, 569-577, doi:10.4049/jimmunol.0902315 (2010).
- 188 Pushpakumar, S. *et al.* Toll-like Receptor 4 Deficiency Reduces Oxidative Stress and Macrophage Mediated Inflammation in Hypertensive Kidney. *Sci Rep-Uk* **7**, doi:10.1038/s41598-017-06484-6 (2017).
- 189 Powers, K. A. *et al.* Oxidative stress generated by hemorrhagic shock recruits Toll-like receptor 4 to the plasma membrane in macrophages. *J Exp Med* **203**, 1951-1961, doi:10.1084/jem.20060913 (2006).
- 190 Murdock, J. L. & Nunez, G. TLR4: The Winding Road to the Discovery of the LPS Receptor. *Journal of Immunology* **197**, 2561-2562, doi:10.4049/jimmunol.1601400 (2016).
- 191 Wright, S. D., Ramos, R. A., Tobias, P. S., Ulevitch, R. J. & Mathison, J. C. Cd14, a Receptor for Complexes of Lipopolysaccharide (Lps) and Lps Binding-Protein. *Science* **249**, 1431-1433, doi:DOI 10.1126/science.1698311 (1990).
- 192 Chow, J. C., Young, D. W., Golenbock, D. T., Christ, W. J. & Gusovsky, F. Toll-like receptor-4 mediates lipopolysaccharide-induced signal transduction. *Journal of Biological Chemistry* **274**, 10689-10692, doi:DOI 10.1074/jbc.274.16.10689 (1999).
- 193 Schumann, R. R. *et al.* Structure and Function of Lipopolysaccharide Binding-Protein. *Science* **249**, 1429-1431, doi:DOI 10.1126/science.2402637 (1990).
- 194 Shimazu, R. *et al.* MD-2, a molecule that confers lipopolysaccharide responsiveness on Toll-like receptor 4. *J Exp Med* **189**, 1777-1782, doi:DOI 10.1084/jem.189.11.1777 (1999).
- 195 Visintin, A., Mazzoni, A., Spitzer, J. A. & Segal, D. M. Secreted MD-2 is a large polymeric protein that efficiently confers lipopolysaccharide sensitivity to Toll-like receptor 4. *P Natl Acad Sci USA* **98**, 12156-12161, doi:DOI 10.1073/pnas.211445098 (2001).
- 196 Park, B. S. *et al.* The structural basis of lipopolysaccharide recognition by the TLR4-MD-2 complex. *Nature* **458**, 1191-U1130, doi:10.1038/nature07830 (2009).

- 197 Warner, N. & Nunez, G. MyD88: A Critical Adaptor Protein in Innate Immunity Signal Transduction. *Journal of Immunology* **190**, 3-4, doi:10.4049/jimmunol.1203103 (2013).
- 198 Shin, H. J. *et al.* Kinetics of binding of LPS to recombinant CD14, TLR4, and MD-2 proteins. *Mol Cells* **24**, 119-124 (2007).
- 199 Tobias, P. S., Soldau, K., Gegner, J. A., Mintz, D. & Ulevitch, R. J. Lipopolysaccharide-Binding Protein-Mediated Complexation of Lipopolysaccharide with Soluble Cd14. *Journal of Biological Chemistry* **270**, 10482-10488, doi:DOI 10.1074/jbc.270.18.10482 (1995).
- 200 Miyake, K. Roles for accessory molecules in microbial recognition by Toll-like receptors. *J Endotoxin Res* **12**, 195-204, doi:10.1179/096805106x118807 (2006).
- 201 Knoop, B. *et al.* Specific Interactions Measured by AFM on Living Cells between Peroxiredoxin-5 and TLR4: Relevance for Mechanisms of Innate Immunity. *Cell Chem Biol* **25**, 550+, doi:10.1016/j.chembiol.2018.02.006 (2018).
- 202 Ju, L. N. & Zhu, C. Benchmarks of Biomembrane Force Probe Spring Constant Models. *Biophys J* **113**, 2842-2845, doi:10.1016/j.bpj.2017.10.013 (2017).
- 203 Evans, E., Ritchie, K. & Merkel, R. Sensitive Force Technique to Probe Molecular Adhesion and Structural Linkages at Biological Interfaces. *Biophys J* **68**, 2580-2587, doi:Doi 10.1016/S0006-3495(95)80441-8 (1995).
- 204 Deng, L. *et al.* Structural basis for the recognition of mutant self by a tumor-specific, MHC class II-restricted T cell receptor. *Nat Immunol* **8**, 398-408, doi:10.1038/ni1447 (2007).
- 205 Moody, A. M. *et al.* Developmentally regulated glycosylation of the CD8 alpha beta coreceptor stalk modulates ligand binding. *Cell* **107**, 501-512, doi:Doi 10.1016/S0092-8674(01)00577-3 (2001).
- 206 Daniels, M. A. *et al.* CD8 binding to MHC class I molecules is influenced by maturation and T cell glycosylation. *Immunity* **15**, 1051-1061, doi:Doi 10.1016/S1074-7613(01)00252-7 (2001).
- 207 Kuball, J. *et al.* Increasing functional avidity of TCR-redirectioned T cells by removing defined N-glycosylation sites in the TCR constant domain. *J Exp Med* **206**, 463-475, doi:10.1084/jem.20082487 (2009).
- 208 van der Merwe, P. A. & Dushek, O. Mechanisms for T cell receptor triggering. *Nat Rev Immunol* **11**, 47-55, doi:10.1038/nri2887 (2011).
- 209 Hopfield, J. J. KINETIC PROOFREADING - NEW MECHANISM FOR REDUCING ERRORS IN BIOSYNTHETIC PROCESSES REQUIRING HIGH SPECIFICITY. *P Natl Acad Sci USA* **71**, 4135-4139, doi:10.1073/pnas.71.10.4135 (1974).
- 210 Bernardi, F., Saghi, M., Dorizzi, M. & Ninio, J. NEW APPROACH TO DNA-POLYMERASE KINETICS. *J. Mol. Biol.* **129**, 93-112, doi:10.1016/0022-2836(79)90062-7 (1979).
- 211 Mckeithan, T. W. Kinetic Proofreading in T-Cell Receptor Signal-Transduction. *P Natl Acad Sci USA* **92**, 5042-5046, doi:DOI 10.1073/pnas.92.11.5042 (1995).
- 212 Liu, Y. *et al.* DNA-based nanoparticle tension sensors reveal that T-cell receptors transmit defined pN forces to their antigens for enhanced fidelity. *P Natl Acad Sci USA* **113**, 5610-5615, doi:10.1073/pnas.1600163113 (2016).

- 213 Brodovitch, A. *et al.* T lymphocytes need less than 3 min to discriminate between peptide MHCs with similar TCR-binding parameters. *Eur J Immunol* **45**, 1635-1642, doi:10.1002/eji.201445214 (2015).
- 214 Krogsgaard, M. *et al.* Agonist/endogenous peptide-MHC heterodimers drive T cell activation and sensitivity. *Nature* **434**, 238-243, doi:10.1038/nature03391 (2005).
- 215 Hoerter, J. A. H. *et al.* Coreceptor affinity for MHC defines peptide specificity requirements for TCR interaction with coagonist peptide-MHC. *J Exp Med* **210**, 1807-1821, doi:10.1084/jem.20122528 (2013).
- 216 Nagaraj, S. *et al.* Altered recognition of antigen is a mechanism of CD8(+) T cell tolerance in cancer. *Nature Medicine* **13**, 828-835, doi:10.1038/nm1609 (2007).
- 217 Kniss-James, A. S., Rivet, C. A., Chingozha, L., Lua, H. & Kemp, M. L. Single-cell resolution of intracellular T cell Ca²⁺ dynamics in response to frequency-based H₂O₂ stimulation. *Integr Biol-Uk* **9**, 238-247, doi:10.1039/c6ib00186f (2017).
- 218 Zarnitsyna, V. I. *et al.* Memory in receptor-ligand-mediated cell adhesion. *P Natl Acad Sci USA* **104**, 18037-18042, doi:10.1073/pnas.0704811104 (2007).
- 219 Liu, B. Y. *et al.* The cellular environment regulates in situ kinetics of T-cell receptor interaction with peptide major histocompatibility complex. *Eur J Immunol* **45**, 2099-2110, doi:10.1002/eji.201445358 (2015).
- 220 Serafini, P., Borrello, I. & Bronte, V. Myeloid suppressor cells in cancer: Recruitment, phenotype, properties, and mechanisms of immune suppression. *Seminars in Cancer Biology* **16**, 53-65, doi:10.1016/j.semcancer.2005.07.005 (2006).
- 221 Swamy, M. *et al.* A Cholesterol-Based Allosteric Model of T Cell Receptor Phosphorylation. *Immunity* **44**, 1091-1101, doi:10.1016/j.immuni.2016.04.011 (2016).
- 222 Ge, C. H., Rushdi, M. N. & Zhu, C. T cells exert force for pMHC pull-ups. *Transl Cancer Res* **5**, S855-S857, doi:10.21037/tcr.2016.10.21 (2016).
- 223 Kusmartsev, S., Nagaraj, S. & Gabilovich, D. I. Tumor-associated CD8(+) T cell tolerance induced by bone marrow-derived immature myeloid cells. *Journal of Immunology* **175**, 4583-4592 (2005).
- 224 Huang, B. *et al.* Gr-1(+)CD115(+) immature myeloid suppressor cells mediate the development of tumor-induced T regulatory cells and T-cell anergy in tumor-bearing host. *Cancer Res.* **66**, 1123-1131, doi:10.1158/0008-5472can-05-1299 (2006).
- 225 Kusmartsev, S. & Gabilovich, D. I. Role of immature myeloid cells in mechanisms of immune evasion in cancer. *Cancer Immunol Immun* **55**, 237-245, doi:10.1007/s00262-005-0048-z (2006).
- 226 Kusmartsev, S., Nefedova, Y., Yoder, D. & Gabilovich, D. I. Antigen-specific inhibition of CD8(+) T cell response by immature myeloid cells in cancer is mediated by reactive oxygen species. *Journal of Immunology* **172**, 989-999 (2004).
- 227 Haqqani, A. S., Kelly, J. F. & Birnboim, H. C. Selective nitration of histone tyrosine residues in vivo in mutatact tumors. *J. Biol. Chem.* **277**, 3614-3621, doi:10.1074/jbc.M105730200 (2002).

- 228 Quint, P., Reutzel, R., Mikulski, R., McKenna, R. & Silverman, D. N. Crystal structure of nitrated human manganese superoxide dismutase: Mechanism of inactivation. *Free Radic. Biol. Med.* **40**, 453-458, doi:10.1016/j.freeradbiomed.2005.08.045 (2006).
- 229 Ando, T. *et al.* Transduction with the Antioxidant Enzyme Catalase Protects Human T Cells against Oxidative Stress. *Journal of Immunology* **181**, 8382-8390 (2008).
- 230 Ligtenberg, M. A. *et al.* Coexpressed Catalase Protects Chimeric Antigen Receptor-Redirected T Cells as well as Bystander Cells from Oxidative Stress-Induced Loss of Antitumor Activity. *Journal of Immunology* **196**, 759-766, doi:10.4049/jimmunol.1401710 (2016).
- 231 Willcox, J. K., Ash, S. L. & Catignani, G. L. Antioxidants and prevention of chronic disease. *Crit Rev Food Sci* **44**, 275-295, doi:10.1080/1008690490468489 (2004).
- 232 Westerlund, A. *et al.* Dietary supplement use patterns in men with prostate cancer: the Cancer Prostate Sweden Study. *Ann Oncol* **22**, 967-972, doi:10.1093/annonc/mdq456 (2011).
- 233 Godic, A., Poljsak, B., Adamic, M. & Dahmane, R. The Role of Antioxidants in Skin Cancer Prevention and Treatment. *Oxid Med Cell Longev*, doi:Artn 860479 10.1155/2014/860479 (2014).
- 234 The alpha-tocopherol, beta-carotene lung cancer prevention study: design, methods, participant characteristics, and compliance. The ATBC Cancer Prevention Study Group. *Annals of epidemiology* **4**, 1-10 (1994).
- 235 Omenn, G. S. *et al.* Risk factors for lung cancer and for intervention effects in CARET, the beta-carotene and retinol efficacy trial. *J Natl Cancer I* **88**, 1550-1559, doi:DOI 10.1093/jnci/88.21.1550 (1996).
- 236 Goodman, M., Bostick, R. M., Kucuk, O. & Jones, D. P. Clinical trials of antioxidants as cancer prevention agents: Past, present, and future. *Free Radical Bio Med* **51**, 1068-1084, doi:10.1016/j.freeradbiomed.2011.05.018 (2011).
- 237 Sayin, V. I. *et al.* Antioxidants Accelerate Lung Cancer Progression in Mice. *Sci Transl Med* **6**, doi:ARTN 221ra15 10.1126/scitranslmed.3007653 (2014).
- 238 Le Gal, K. *et al.* Antioxidants can increase melanoma metastasis in mice. *Sci Transl Med* **7**, doi:ARTN 308re8 10.1126/scitranslmed.aad3740 (2015).
- 239 Wang, H. *et al.* NRF2 activation by antioxidant antidiabetic agents accelerates tumor metastasis. *Sci Transl Med* **8**, doi:ARTN 334ra51 10.1126/scitranslmed.aad6095 (2016).
- 240 Teghanemt, A., Zhang, D. S., Levis, E. N., Weiss, J. P. & Gioannini, T. L. Molecular basis of reduced potency of underacylated endotoxins. *Journal of Immunology* **175**, 4669-4676, doi:10.4049/jimmunol.175.7.4669 (2005).
- 241 Park, B. S. & Lee, J. O. Recognition of lipopolysaccharide pattern by TLR4 complexes. *Exp. Mol. Med.* **45**, 9, doi:10.1038/emm.2013.97 (2013).
- 242 Correia, J. D. & Ulevitch, R. J. MD-2 and TLR4 N-linked glycosylations are important for a functional lipopolysaccharide receptor. *Journal of Biological Chemistry* **277**, 1845-1854, doi:10.1074/jbc.M109910200 (2002).

- 243 Pollard, T. D. & Cooper, J. A. Actin, a Central Player in Cell Shape and Movement. *Science* **326**, 1208-1212, doi:10.1126/science.1175862 (2009).
- 244 Hung, R. J., Pak, C. W. & Terman, J. R. Direct Redox Regulation of F-Actin Assembly and Disassembly by Mical. *Science* **334**, 1710-1713, doi:10.1126/science.1211956 (2011).
- 245 Rajaiah, R., Perkins, D. J., Ireland, D. D. C. & Vogel, S. N. CD14 dependence of TLR4 endocytosis and TRIF signaling displays ligand specificity and is dissociable in endotoxin tolerance. *P Natl Acad Sci USA* **112**, 8391-8396, doi:10.1073/pnas.1424980112 (2015).
- 246 Pergola, C. *et al.* Modulation of actin dynamics as potential macrophage subtype-targeting anti-tumour strategy. *Sci Rep-Uk* **7**, doi:ARTN 41434 10.1038/srep41434 (2017).
- 247 Sridharan, R., Cameron, A. R., Kelly, D. J., Kearney, C. J. & O'Brien, F. J. Biomaterial based modulation of macrophage polarization: a review and suggested design principles. *Mater Today* **18**, 313-325, doi:10.1016/j.mattod.2015.01.019 (2015).
- 248 Vinogradov, E. *et al.* Structures of lipopolysaccharides from *Klebsiella pneumoniae* - Elucidation of the structure of the linkage region between core and polysaccharide O chain and identification of the residues at the non-reducing termini of the O chains. *Journal of Biological Chemistry* **277**, 25070-25081, doi:10.1074/jbc.M202683200 (2002).
- 249 Patel, N. R. *et al.* Cell Elasticity Determines Macrophage Function. *Plos One* **7**, doi:ARTN e41024 10.1371/journal.pone.0041024 (2012).
- 250 Kang, H., Wong, S. H. D., Pan, Q., Li, G. & Bian, L. Anisotropic Ligand Nanogeometry Modulates the Adhesion and Polarization State of Macrophages. *Nano letters*, doi:10.1021/acs.nanolett.8b05150 (2019).
- 251 Williams, T. *et al.* Development of T cell lines sensitive to antigen stimulation. *J Immunol Methods* **462**, 65-73, doi:10.1016/j.jim.2018.08.011 (2018).
- 252 Seo, Y. J., Jothikumar, P., Suthar, M. S., Zhu, C. & Grakoui, A. Local Cellular and Cytokine Cues in the Spleen Regulate In Situ T Cell Receptor Affinity, Function, and Fate of CD8(+) T Cells. *Immunity* **45**, 988-998, doi:10.1016/j.immuni.2016.10.024 (2016).
- 253 Takahashi, A. *et al.* Preferential cell death of CD8(+) effector memory (CCR7(-)CD45RA(-)) T cells by hydrogen peroxide-induced oxidative stress. *Journal of Immunology* **174**, 6080-6087, doi:DOI 10.4049/jimmunol.174.10.6080 (2005).
- 254 Mougiakakos, D., Johansson, C. C. & Kiessling, R. Naturally occurring regulatory T cells show reduced sensitivity toward oxidative stress-induced cell death. *Blood* **113**, 3542-3545, doi:10.1182/blood-2008-09-181040 (2009).
- 255 Fitzgerald, K. A. *et al.* LPS-TLR4 signaling to IRF-3/7 and NF-kappa B involves the toll adapters TRAM and TRIF. *J Exp Med* **198**, 1043-1055, doi:10.1084/jem.20031023 (2003).